

JTC1 2017

First JTC1 Workshop on Advances in Landslide Understanding

24 – 26 May 2017, Barcelona, Spain

Eduardo Alonso & Núria Pinyol (Eds.)



First JTC1 Workshop

Advances in Landslide Understanding

Proceedings of the
First JTC1 Workshop
Advances in Landslide Understanding
Barcelona, Spain
May 24th - 26th, 2017

Edited by: Eduardo Alonso & Núria Pinyol

A publication of:

**International Center for Numerical
Methods in Engineering (CIMNE)**

Barcelona, Spain

ISBN: 978-84-946909-1-4



Printed by: Artes Gráficas Torres S.L., Huelva 9, 08940 Cornellà de Llobregat, Spain

FOREWORD

The terms of reference of the Joint Technical Committee 1 on Natural Slopes and Landslides (www.isrm.net/gca/index.php?id=307) include the organization of Workshops, which typically are expected to address and discuss specific issues in a format which favours discussion in relaxed ambient. The Committee is also expected to advance the science and engineering behind the extremely wide range of aspects involved in landslides.

The format selected for the Workshop highlights a relatively large number of keynote lectures and invited presentations, including the presentation of the Hutchinson Lecture.

The time allocated to special lectures and regular presentation is generous so that discussions are facilitated.

Paper accepted for presentation fall, in general terms, in three wide categories which are often related: physics, mechanisms and modelling; rainfall-landslides interactions; and case records. The papers reflect also the variety of circumstances to be found in practice. This is the inherent nature of a discipline which deals with virtually any geologic environment and a variety of man-induced situations. This electronic book includes all the Extended Abstracts accepted for presentation to the Workshop.

Eduardo Alonso
Chair of the JTC1 2017 Workshop
Barcelona, May 15th 2017

TABLE OF CONTENTS

Index of Papers	5
Hutchinson Lecture	9
Keynote Lectures.....	13
Invited Lectures	28
Papers	77
Annex - Field Trip	153
Index of Authors	158

INDEX OF PAPERS

Hutchinson Lecture

Effects of layering on the hydrological and mechanical response of unsaturated granular sloping covers

E. Damiano 9

Keynote Lectures

Interaction of debris flow with rigid and flexible barriers: centrifuge and numerical simulations

C.W.W. Ng, C.E. Choi and D. Song 13

Stability of submarine slopes

A.M. Puzrin 21

Soil-atmosphere interaction in landslide triggering

L. Pagano, A. Reder and G. Rianna 24

Invited Lectures

Model calibration of landslide boundary value problems by inverse analysis

M. Calvello 28

Effect of unsaturated conditions on disasters due to landslides

M.M. Futai 32

Development of numerical models for landslide mitigation works

J.S.H. Kwan 36

Rock avalanches: constitutive and numerical modelling

D.G. Manzanal, M. Pastor, M. Stickle and A. Yague 40

Geomechanical models for shallow rainfall-induced landslides at the catchment scale built in feedback-loop from geological-geomorphological investigation

M. Nicotera, A. Tarantino, A. Santo, B. Balzano, M. De Falco and G. Forte 44

Soil-atmosphere interactions. Comprehensive modelling and practical rules

J. Vaunat, D. Ruiz, S. Samat, M. Saaltink and D. Virely 48

Effect of shear band thickness on the termo-hydro-mechanical coupled analysis of landslides

N.M. Pinyol, M. Alvarado and E.E. Alonso 52

Tailings dam post-failure flow dynamics: analysis of the rheological behaviour

M. Pirulli 56

Hysteresis processes and effective rainfall histories

G. Rianna, A. Reder, L. Pagano and L. Comegna 60

Effect of variability in soil properties on stability of residual soil slope <i>A. Satyanaga and H. Rahardjo</i>	64
Landslide generated waves: new insights from physical models <i>W.A. Take and R.P. Mulligan</i>	69
Fludized landsliding phenomena during earthquakes <i>G. Wang</i>	73

Papers

Unstable zone of sand-silt mixture using static triaxial tests <i>R.S. Dalvi and N. Choudhari</i>	77
Evolution of safety in weathered infinite slopes <i>G. De la Morena, L. Asensio and V. Navarro</i>	81
Analysis of tailings dam failure based on historical documents: the case study of "La Luciana", Spain <i>F.J. Fernández, V. Rodríguez, R. Rodríguez, M.E. Alberruche, J.C. Arranz, R.M. Mateos, G. Herrera, L. Vadillo and R. Sarro</i>	85
Clay minerals effects in shallow landslide at Takadake area, Aso mountain, Kumamoto, Japan <i>M.L. Istiyanti and S. Goto</i>	89
Application of the hydraulic gradient method for physical modeling of rainfall induced landslide <i>M. Jamei, F. Hamrouni and H. Trabelsi</i>	93
Understanding spreads in Canadian sensitive clays <i>A. Locat, S. Leroueil and D. Demers</i>	97
Twenty years of continuous monitoring of the Vallcebre landslide (Eastern Pyrenees): lessons learned <i>J. Moya, J. Corominas, J.A. Gili, A. Ledesma and A. Lloret</i>	101
In-situ monitoring of slope mass-wasting, examples from the Pyrenees <i>R. Oorthuis, M. Hürlimann, J. Moya and J. Vaunat</i>	105
Preliminary estimation of Aubeta Debris flow deposition and erosion volumes using Lidar data <i>J. Pinyol, M. González and M. Moysset</i>	109
Stability of residual soil slopes based on spatial distribution of soil properties <i>H. Rahardjo and A. Satyanaga</i>	113
The use of InSAR in landslide monitoring <i>J. Raventós and M. Arroyo</i>	118
Wetting collapse and failure of an slope tested in centrifuge machine <i>A. Ruiz, M. Alvarado, N.M. Pinyol and B. Caicedo</i>	122

Landslides and its relation with faults and hidden fractures zones - results from the lidar-based dem and structural analysis (silesian beskid, outer carpathians)	
<i>R. Sikora</i>	126
Bipartite rockslides: geomorphic evidence of partial extreme mobility	
<i>A.L. Strom</i>	130
Long-term slope instability after gigantic earth-quakes and their causes with emphasis on rock fracturing	
<i>I. Towhata and K. Gunji</i>	134
Analysis, evaluation and zoning of the susceptibility due to landslides in the aloag - Santo Domingo Road (Ecuador)	
<i>F.J. Torrijo, J. Garzón and V. Capa</i>	138
Coupled distinct element method computational fluid dynamics analyses for reservoir landslide modelling	
<i>S. Utili and T. Zhao</i>	141
Three-dimensional simulation of the Hongshiyuan landslide with the material point method	
<i>X.R. Xu, Q.C. Sun, F. Jin and K. Soga</i>	145
Runout evaluation of the Oso landslide with the material point method	
<i>A. Yerro, K. Soga and J. Bray</i>	149
ANNEX - FIELD TRIP	153
INDEX OF AUTHORS	158

EFFECTS OF LAYERING ON THE HYDROLOGICAL AND MECHANICAL RESPONSE OF UNSATURATED GRANULAR SLOPING COVERS

Emilia Damiano*

* DiCDEA Università degli studi della Campania “L. Vanvitelli”, Aversa, Italy

Rainfall-induced landslides are widespread in shallow layered granular soil deposits. In many cases, slope instability is related to the loss of suction during rainwater infiltration. However, the contrasts in the unsaturated hydraulic properties of the soils deeply affect the infiltration process, thus influencing slope failure. Coarse-textured soil layers embedded between finer ones may initially confine the process within the uppermost finer layers, delaying the infiltration and eventually inducing lateral flow diversion. Nonetheless, depending on the state variables at the beginning of rain as well as on rainfall characteristics, the coarser layers may have or not a positive effect on stability. The results of a research based on advanced geotechnical characterization, physical and numerical modeling and in-situ monitoring have been analyzed to address the effects of layering on slope stability.

Keywords: soil layering, capillary barrier, rainwater infiltration, slope stability

INTRODUCTION

Rainfall-induced landslides in granular soils are experiencing a growing attention due to their frequency and, now even more, to climate changes. Sloping deposits are often characterized by a layered soil profile. In some cases, as in residual soils, the layering is characterized by a increasingly weathered profile with a continuous variation of the hydraulic and mechanical soil properties. In other cases, as in air-fall pyroclastic covers, the soil profile is more complex, being often characterized by finer and coarser layers which alternating within the stratigraphic sequence.

This is the case of a large hilly and densely urbanized area around the Somma-Vesuvius volcanic complex (South Italy) which, after prolonged rainfall periods, periodically experiences fast slope movements involving deposits of ashes and pumices, a few meters thick (Fig. 1a). The stability of these slopes relies on the positive effect of matric suction on soil shear strength, as the slope angles (up to 50°) are even much greater than the soil friction angles. During rainfall, the progressive decrease in suction may lead to slope failure. Soil layering, affecting the infiltration process, potentially influences both the depth of the sliding surface and the degree of saturation of soil at failure which, in these loose granular covers, is one of the key factors for the assessment of the post-failure evolution of the landslide (Damiano and Olivares, 2010). Indeed, coarse-grained materials, due to their low hydraulic conductivity at low degrees of saturation, may initially act as “capillary barriers” to the propagation of the wetting front (Shackelford et al., 1994, Stormont & Anderson, 1999), promoting lateral water diversion. This effect has been investigated to realize cover systems for slope stabilization and

for remediation in waste disposal sites (Tami et al., 2004, Aubertin et al., 2009, Rahardjo et al., 2013, Zhan et al., 2014) and seems to work well in semi-arid environments. However, few studies are still available for natural slopes in humid climatic conditions. To this aim, physical and mathematical modeling was conducted in order to evaluate the effect of rainfall intensity and of initial soil-moisture condition on the infiltration and water redistribution processes in layered sloping deposits.

MATERIALS AND METHODS

A series of infiltration tests were performed on layered small-scale slope models (0.2m thick, 0.5m wide and 1.75m long), reconstituted in an instrumented flume (Fig. 1c). The deposits, constituted by a pumices layer embedded between two finer ash layers of different inclinations ($0^{\circ}\div 38^{\circ}$), were subjected to various rainfall intensities ($18\div 83\text{mm/h}$). The investigated soils were sampled at the Cervinara slope (Damiano et al., 2012). The ash is a silty sand, the pumice is a gravel with sand, both characterized by a very low dry unit weight ($13\text{-}14\text{kN/m}^3$). Under the mean field effective stress the saturated conductivity (k_{sat}) of undisturbed ash samples is about 10^{-6} m/s, while the one of reconstituted pumices is around $5\cdot 10^{-6}$ m/s. In unsaturated conditions the hydraulic conductivity of ashes decreases of more than two orders of magnitude.

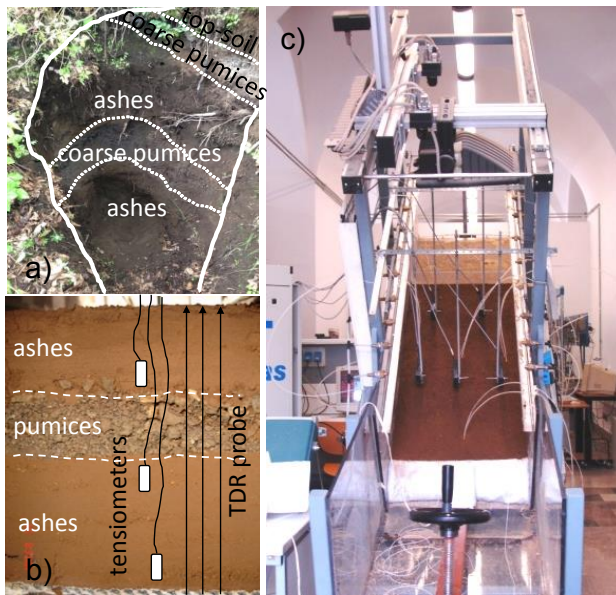


Fig. 1 Views of: (a) natural, (b) reconstituted layered profiles, and (c) the instrumented flume

During the tests, the suction and the volumetric water content (θ_w) were respectively monitored by minitensiometers located at three depths within the ashes, and a TDR probe inserted orthogonally to the deposit, throughout its entire thickness (Fig. 1b), to retrieve the θ_w profile (Greco, 2006). This allowed determining the Soil Water Retention Curves (SWRC) that soils experienced during the infiltration stages (Fig. 2). Both SWRCs show the typical features of granular materials being characterized by a very low value of the air-entry points and a steep slope in the transition zone.

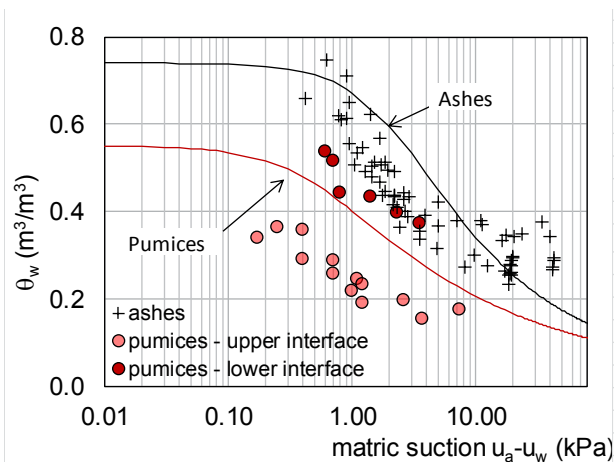


Fig 2 SWRCs of the investigated soils

A mathematical model of water flow, based on the 2D Richards' equation and formulated under the hypothesis of rigid soil skeleton and isothermal conditions was calibrated and validated on the basis of the test results (Damiano et al., 2017), and then used for the interpretation of the phenomena also in conditions far from the experimental ones.

During the tests, the suction and the volumetric water content (θ_w) were respectively monitored by minitensiometers located at three depths within the ashes, and a TDR probe inserted orthogonally to the deposit, throughout its entire thickness (Fig. 1b), to retrieve the θ_w profile (Greco, 2006). This allowed determining the Soil Water Retention Curves (SWRC) that soils experienced during the infiltration stages (Fig. 2). Both SWRCs show the typical features of granular materials being characterized by a very low value of the air-entry points and a steep slope in the transition zone.

RESULTS

A synthesis of the experimental results is reported in Figs. 3 and 4. The influence of the initial condition of the soil and of the rainfall intensity on the infiltration is highlighted in Fig. 3, which shows the advance of the wetting front. The labels indicate the mean suction values of the soil at the beginning of rainfall.

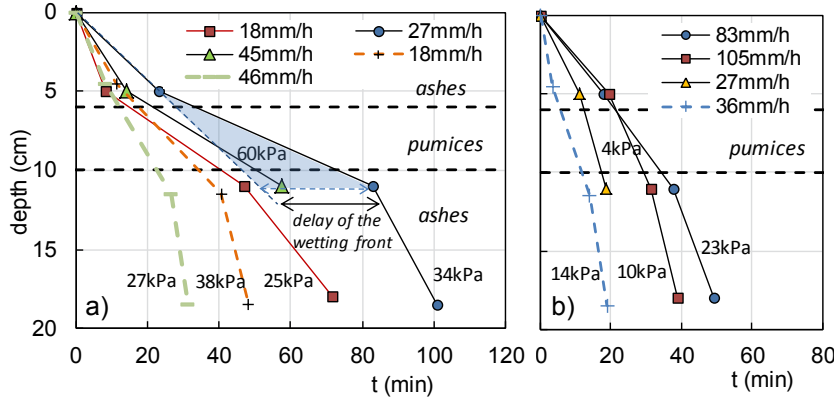


Fig 3 Arrival times of the wetting front at various depths during the tests

The pumices slow down the advance of the wetting front for an initially dry soil profile (Fig. 3a), whereas this effect is not so clear for wetter, but still far from saturation, soil profiles (Fig. 3b): as a matter of fact, with wetting, the difference between the unsaturated hydraulic conductivities of finer and coarser layer decreases, the capillary barrier effect vanishes and the layered-soil profile behaves in an opposite way. Nonetheless, depending on the rainfall intensity, a water flow diversion occurs in the upper finer layer when it approaches saturation. This can be inferred by the plot in Fig.4 which shows the trend of the cumulative infiltration, as retrieved by water content measurements, compared to the cumulated rainfall height during one of the tests characterized by an initial quite dry soil moisture profile.

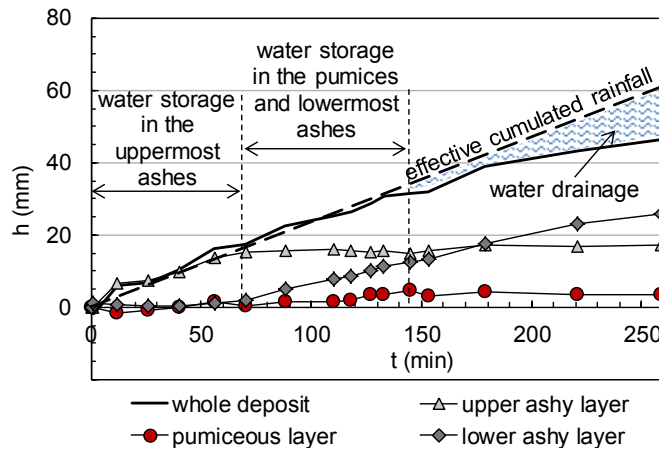


Fig 4 Cumulative water storage in the layered deposit

Initially the entire rainwater amount is stored in the uppermost layer which soon reaches and remains in a practically saturated condition ($\theta_w \leq 0.7$). Once the wetting front enters the pumice layer, water quickly starts to accumulate within the lowermost part of the deposit. It has to be noted that the cumulative infiltration in the whole deposit gradually diverges from the cumulated rainfall height (Fig. 4), indicating that part of the water is drained out of the slope. As no significant surface runoff occurred, this means that a subsurface drainage establishes in the uppermost finer soil layer. During this last stage, the rate of water stored in the lower ashes exceeds that stored in pumices: even remaining unsaturated, the coarse-textured soil is not capable of retaining water, which quickly passes through it.

The numerical analysis confirms the main features of the process, indicating that the water flow direction in the uppermost layer, initially orthogonal to the soil surface due to the high capillarity gradient, first becomes vertical, as soon as the gravitational gradient prevails, then deviates toward the slope direction through the entire layer. For high rainfall intensities, such

a subsurface flow occurs only at the interface between the uppermost ashes and the pumices. When the ash layer reaches complete saturation, the water flow becomes again vertical: consequently the amount of water drained downslope reduces.

CONCLUSIONS

Rainwater infiltration into unsaturated layered deposits is a very complex process and it is still a challenging task for the prediction of the slope behavior. Depending on the initial suction distribution within the soil profile and on rainfall characteristics, the presence of coarser soil layers in the stratigraphic sequence may slow down the propagation of the wetting front, confining the water in the uppermost soil layers and causing a lateral diversion of the water flow. In sloping pyroclastic covers, characterized by alternating layers of ashes and pumices, during high intensity storms occurring at the beginning of rainy season, when the soil profile is still quite dry, the establishment of a subsurface runoff through the topsoil prevents the storage of all the infiltrating rainfall into the soil cover, thus favoring the slope stability.

During long-lasting rainfall periods, the pumices layer cannot prevent water from infiltrating into the underlying finer soil layer, even before its full saturation. In soil covers presenting another coarser layer at a greater depth, soil rupture may likely occur at the interface between ashes and the lowermost pumices, where a highest degree of saturation is expected and other stabilizing factors such as pedogenized soils, roots reinforcement and water uptake, typically acting in top soils, are scarcely effective.

Obviously, these simplified considerations hold for idealized regular and continuous layered soil covers. Along real slopes, characterized by complex morphologies, lateral redistribution of water (3D effects), lacks in layers continuity and other minor effects may induce flow concentration, locally leading to unexpected failures.

REFERENCES

- Aubertin M, Cifuentes E, Apithy SA, Bussi re B, Molson J & Chapuis RP (2009). Analyses of water diversion along inclined covers with capillary barrier effects. *Can Geotech J* 46: 1146-1164.
- Damiano E, Olivares L (2010) The role of infiltration processes in steep slope stability of pyroclastic granular soils: laboratory and numerical investigation. *Nat Haz* 52:329–350.
- Damiano E, Olivares L & Picarelli L (2012) Steep-slope monitoring in unsaturated pyroclastic soils. *Eng Geol* 137-138, 1-12.
- Damiano E, Greco R, Guida G, Olivares L & Picarelli L (2017) Investigation on rainwater infiltration into layered shallow covers in pyroclastic soils and its effect on slope stability. *Eng Geol* 220: 208-218.
- Greco R (2006). Soil water content inverse profiling from single TDR waveforms. *J Hydrol* 317: 325–339.
- Rahardjo H, Santoso VA, Leong EC, Ng YS, Tam CPH & Satyanaga A (2013) Use of recycled crushed concrete and Secudrain in capillary barriers for slope stabilization. *Can Geotech J* 50: 662-673.
- Shackelford CD, Chang C-K & Chiu T-F (1994) The capillary barrier effect in unsaturated flow through soil barriers. Proc. of the First International Congress on Environmental Geotechnics. Edited by WD Carrier. ISSMFE-CGS ISSMFE-CGS, Edmonton, Canada, 789–793 (July 10–15, 1994).
- Stormont JC & Anderson CE (1999) Capillary barrier effect from underlying coarser soil layer. *J. Geotech. Geoenviron. Eng.* 125: 641-648
- Tami D, Rahardjo H, Leong EC & Fredlund DG (2004) Design and laboratory verification of a physical model of sloping capillary barrier. *Can Geotech J* 41(5): 814-830.
- Zhan TLT, Li H, Jia GW, Chen YM & Fredlund DG (2014) Physical and numerical study of lateral diversion by three-layer inclined capillary barrier covers under humid climatic conditions. *Can Geotech J* 51, 1438-1448.

INTERACTION OF DEBRIS FLOW WITH RIGID AND FLEXIBLE BARRIERS: CENTRIFUGE AND NUMERICAL SIMULATIONS

Charles W. W. Ng¹, Clarence E. Choi^{1,2}, Dongri Song³

Department of Civil and Environmental Engineering, the Hong Kong University of Science and Technology, Hong Kong SAR¹
The HKUST Jockey Club Institute for Advanced Study, Hong Kong SAR²
Institute of Mountain Hazards and Environment, Chinese Academy of Sciences, China³

Abstract: The dynamics of debris flow are governed by the interaction between its solid grains and the viscous interstitial fluid. However, understanding the effect of solid-fluid interaction for impact problems has proven to be quite the challenge since debris flows have poor temporal predictability and are scale-dependent. Existing frameworks characterising impact adopts macroscopic variables such as the Froude number without considering solid-fluid interaction. This has resulted in design approaches that rely much on empiricism and have also led to international recommendations, specifically pressure coefficients (α) that are mutually inconsistent. In this extended abstract, a series of centrifuge tests modelling the impact between debris flow and model rigid and a novel model flexible barrier are discussed. The solid-fluid interaction was investigated by varying the solid volume fraction of the flow to change the degree of grain contact stress. A large-nonlinear finite element model was then adopted to back-analyse centrifuge experiments to study the effects of the fluid viscosity on the dynamic response of a new model flexible barrier.

keywords: debris flow impact; rigid and flexible barriers; centrifuge modelling; finite element modelling

INTRODUCTION

Debris flows are distinct compared to other geophysical flows, such as mud flows and debris floods, because of their strong dependence on the interaction between incompressible grains of soil and the viscous pore fluid (Iverson 2015). Solid-fluid interaction has profound effects on changes in pore pressures which in turn controls the mobility of the flow (Iverson 2003). For impact-related problems, solid-fluid interaction governs the degree of contact stresses between grains, which in turn dictates the impact mechanism (Choi *et al.* 2015a; Ng *et al.* 2016a) and loading distribution on a barrier (Song *et al.* 2017). Despite the importance of solid-fluid interaction, it is not considered in existing frameworks which characterise impact. The main challenges in understanding the fundamental mechanisms of impact of two-phase flows is the scale-dependency of debris flow. For instance, shallower flow depths that develop in bench-top experiments exhibit disproportionalities in viscous shearing and the ability to sustain pore pressures (Iverson 2015).

Existing frameworks characterising the impact of debris flow simply treat the flow as an equivalent fluid and do not consider solid-fluid interaction. Instead, impact is characterised macroscopically using the Froude number and the conservation of momentum (Cui *et al.* 2015).

The most commonly adopted momentum-based equation for estimating debris impact (WSL 2009; Kwan 2012) is given as follows:

$$F_d = \alpha \rho v^2 \sin \beta h w \quad (1)$$

where F_d is the bulk debris impact force, α is the pressure coefficient, ρ is the debris density, v is the debris velocity, β is the angle between the barrier and impact orientation, h is the debris thickness and w is the channel width. However, it is clear from Eqn. (1) that the effects of solid-fluid interaction are not fundamentally considered.

To tackle this challenge and to enable a fundamental understanding of solid-fluid interaction and scale-effects in a systematic manner, the geotechnical centrifuge provides a suitable means. The centrifuge correctly captures the absolute stress state (Schofield 1980; Ng 2014) of a granular assembly and ensures the correct response in pore pressures. Also, by varying the particle diameter and fluid viscosity (Bowman *et al.* 2010), stress ratios in key dimensionless groups which describe the dynamics of debris flow can be systematically controlled (Iverson 1997).

In this extended abstract, a series of centrifuge experiments studying the impact of two-phase flows on rigid and flexible barriers are discussed. Numerical back-analyses using a large-nonlinear finite element model was then used to back analyse centrifuge experiments to bear further insight on the influence of fluid viscosity on the dynamic response of a flexible barrier.

CENTRIFUGE MODEL TESTS AND FINITE ELEMENT MODELLING

Centrifuge modelling

The 400 g-ton Geotechnical Centrifuge Facility (GCF) at the Hong Kong University of Science and Technology was used to carry out the experiments. The beam centrifuge has an arm radius of 4.2 m (Ng 2014). All tests were conducted at a g-level of 22.4g inside a model container with plan dimensions of 1245 mm × 350 mm and a height of 851 mm. A 25° slope with a width of 233 mm and a length of 1000 mm was installed inside the model container. A storage container was mounted at the top of the model container to contain the debris material. Inside the storage container a helical ribbon mixer was installed to prevent the consolidation of the debris mixture in-flight. A hinged door is installed at its base of the storage container which is released in-flight by controlling a hydraulic actuator.

On the model slope, either a rigid or a novel model flexible barrier, both 200 mm (model dimensions) in height, can be installed perpendicularly to study the interaction between different flow and barrier types. Figures 1a and 1b show the front view of the novel model flexible barrier and spring elements mounted used to replicate prototype cable load-displacement, respectively. Details of the novel model flexible barrier and the spring elements are discussed in Ng *et al.* (2016a). Load cells and laser sensors were installed to measure the axial load and cable displacement in each model flexible barrier cable. The rigid barrier was modelled as a 10 mm thick (model dimension) cantilevered steel plate. The rigid barrier was instrumented with load cells to study the distribution of impact pressure along the height of the barrier. Furthermore, impact kinematics for each test were captured using a high-speed camera capable of

capturing a resolution of 1300×1600 pixels at a sampling rate of 640 frames per second. Images were then used to carry out Particle Image Velocimetry (White *et al.* 2003) analysis to understand the impact kinematics.

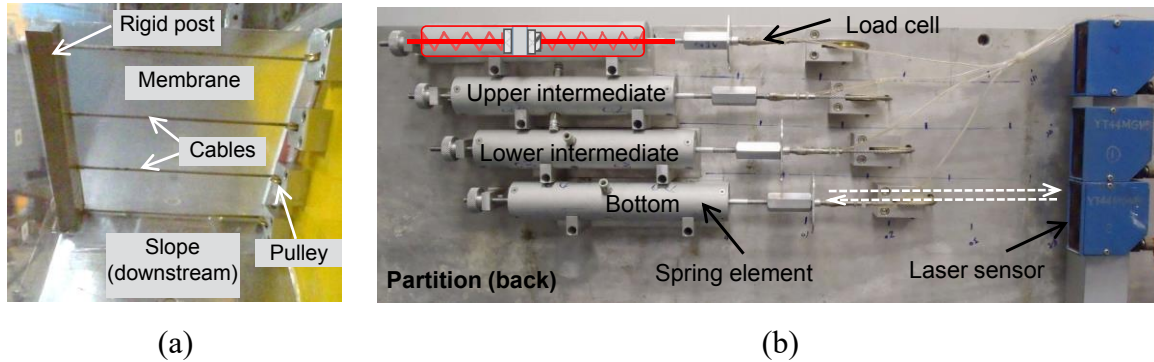


Fig. 1. Model flexible barrier (Ng *et al.* 2016 b): (a) front view of barrier; (b) spring elements at the back of the partition

Leighton Buzzard (LB) fraction C sand, with a particle diameter of about 0.6 mm, was used in the tests. The internal and interface friction angles of the sand are 31° and 22.6° , respectively. The viscous liquid has a specific viscosity of 11.3 Pa·s and a density similar to that of the LB sand (Ng *et al.* 2016a). A summary of the tests discussed in this extended abstract is given in Table 1.

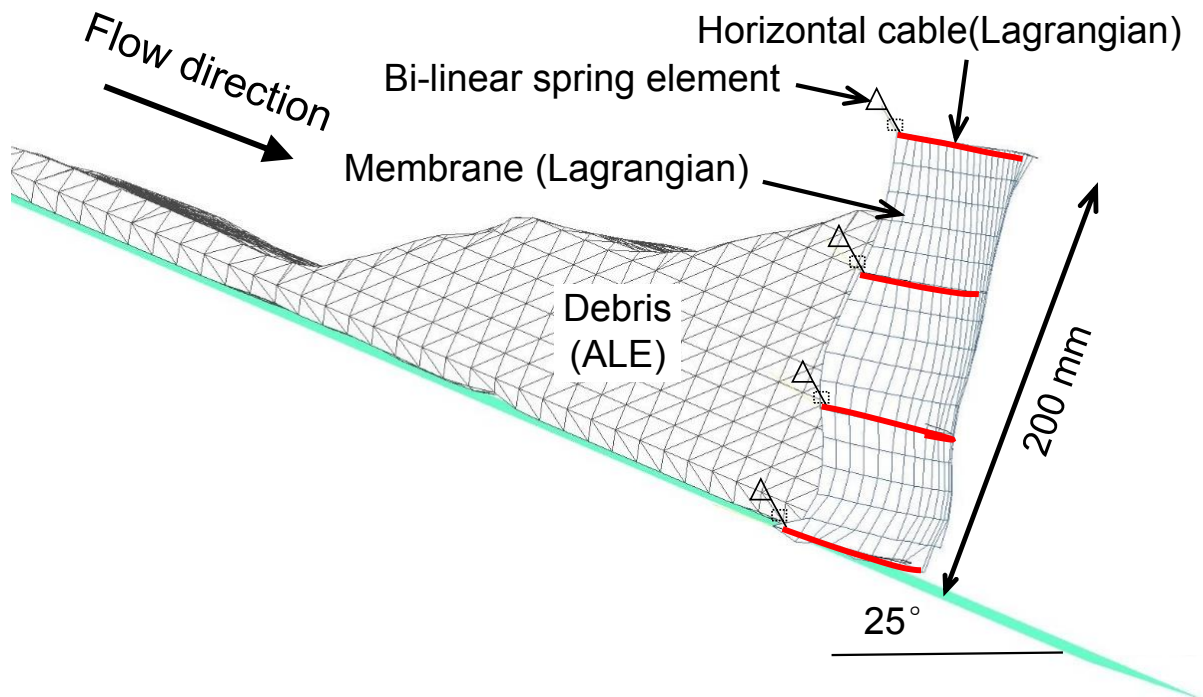


Fig. 3. Large-nonlinear finite element model (LS-DYNA)

Large-nonlinear finite element modelling

A large-nonlinear finite element model software package in three-dimensions, LS-DYNA, was used to study the influence of flow viscosity on the dynamic response of a flexible barrier. LS-DYNA uses explicit time integration to study nonlinear flow problems and has been applied widely for stress and deformation analysis of structures subjected to impact. This approach provides a continuum numerical solution based on the conservation of energy and Newton’s laws of motion. The Arbitrary Lagrangian-Eulerian (ALE) formulation discretises the computational domain into a mesh of elements, which can move arbitrarily and optimise the shape of the elements, enabling large deformation of the debris flow.

The numerical model is shown in Fig. 3. The interaction of debris flow with a barrier requires a coupling technique to take into account the material internal stress changes and structural deformation upon impact. The interaction between the debris flow (ALE-based elements) and barrier and the channel (shell and beam elements) is modelled using finite-element contacts following the approach of Olovsson and Souli (2000 & 2001) and Hallquist (2006). Any penetration of the flow material into the barrier or channel results in a normal reaction force with the interface which is distributed evenly to both the flow and the barrier or channel base.

This LS-DYNA model has been benchmarked against several well-documented laboratory flows and field studies (Hallquist 2006; Koo 2015; Kwan *et al.* 2015). Test FL in this extended abstract was adopted to carry out numerical back-analysis and a parametric study to investigate the influence of fluid viscosity on the dynamic response of the flexible barrier. The flow viscosity was varied according to measurements of field debris flows (Iverson 1997), 0.001 Pa·s to 0.1 Pa·s. A summary of the numerical parameters adopted in the simulations are summarized in Table 2.

Table. 1 Test programme for rigid and flexible barriers (dimensions in model)

Test ID	Description	Material
RL	Rigid barrier + sand-liquid mixture	Viscous liquid (Solid fraction 0%)
RSL20		Solid fraction 20%
RSL40		Solid fraction 40%
RSL50		Solid fraction 50%
FL	Flexible barrier + liquid	Viscous liquid, viscosity 11.3 Pas

Table. 2. Input parameters

Component	Parameter	Value	Unit
Viscous flow	Density ρ	1580	kg/m ³
	Viscosity η	11.3	Pas
Flexible cable	Stiffness K_1	1.8*10 ⁶	N/m
	Stiffness K_2 (1 k_c)	2.0*10 ⁵	N/m

INTERPRETATION OF RESULTS

Impact pressure distribution

Figure 4 shows a comparison of the measured peak impact pressure distributions along the rigid barrier for flows with varying solid fraction. The solid fraction by volume was varied as 0 (test RL), 0.2 (test RSL20), 0.4 (test RSL40), and 0.5 (test RSL50). Reference lines are shown for

comparison with existing design recommendations from China (SWCB 2005; MLR 2006), Canada (Hung *et al.* 1984; VanDine 1996), and Japan (Watanabe 1981; NILIM 2007). The peak pressure shown as the pressure coefficient (α) from Eqn. 1. A horizontal reference line is also shown to highlight the uniform impact distribution with flow thickness h that is generally assumed in international guidelines.

Results reveal that the measured pressure distributions can be characterised using triangular pressure distributions. It is also evident that α is dependent on the solid fraction of the flow. With an increasing solid fraction, a triangular distribution is more pronounced and α increases. The increase in α is attributed to static loading at the base of the barrier from granular deposits during the impact process. The wedge-like granular deposit is called a dead zone (Fig. 5). This dead zone serves two purposes, firstly it contributes a static loading concurrently with dynamic loading. Secondly, the dead zone redirects the momentum of subsequent flow vertically along the barrier face. The redirection of momentum is crucial for reducing the impact loading on the rigid barrier.

A comparison of measured pressure profiles show differences with design recommendations from around the world. Most obviously, the shape of the pressure distributions are quite different. The triangular distribution measured from the centrifuge tests are quite different compared to the uniform distribution assumed in Eqn. 1. More importantly, the formation of a dead zone for debris flows is a key aspect of solid-fluid interaction with the barrier that cannot be captured using Eqn. 1. Another key difference between the measured results and existing design recommendations is that α values can exhibit a disparity of up to 2 times. Most concerning of all is that there is a very wide range of α , although generally on the conservative end of the spectrum, that appear to be mutually inconsistent with each other. It is clear that the further research is warranted to improve the characterisation of impact with the consideration of solid-fluid interaction.

Influence of fluid viscosity on impact

Figure 6 shows the influence of viscosity on the peak impact pressure. The peak impact pressure is represented using α from Eqn. 1. The target Fr range, 3 to 4.5, in this parametric study is for the most part dynamically similar. The typical range of viscosity for natural debris flows ranges from 0.001 to 0.1 Pa·s (Iverson 1997). Simulations clearly show that viscous shearing effects for debris flows have an insignificant effect on the macroscopic flow dynamics. The insignificant contribution of viscous shearing in altering the flow dynamics is consistent with that reported by Choi *et al.* (2015b) for small-scale flume tests studying the mobility of single-phased flows. Furthermore, results demonstrate that the pressure coefficient of each viscous flow falls around unity. By contrast to the two-phase flows (Fig. 5), viscous flows lack a solid component, and thus their pressure coefficients are generally quite similar. It can also be deduced that effect of viscous shearing alone has little influence on the dynamic response of a flexible barrier.

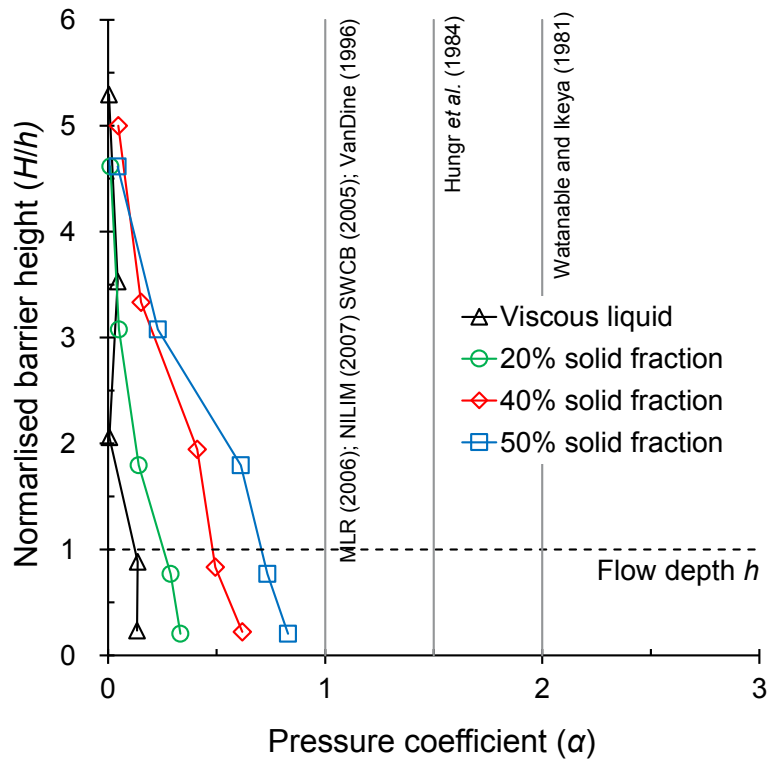


Fig. 4. Peak impact pressure profiles

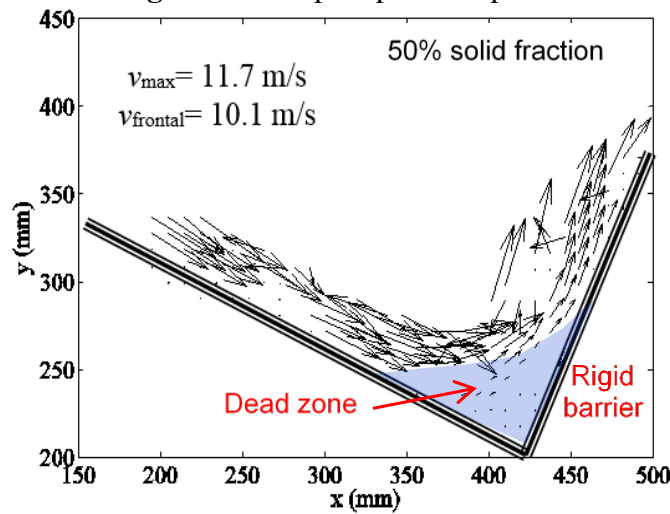


Fig. 5. Impact kinematics analysed using PIV (test RSL50)

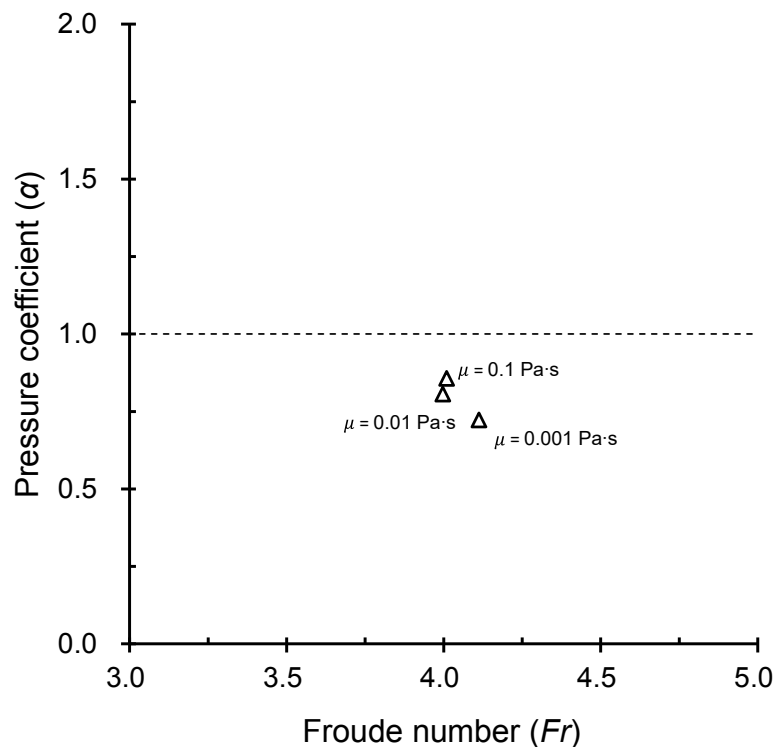


Fig. 6. Influence of viscosity on impact pressure coefficient

SUMMARY

Centrifuge experiments and numerical simulations modelling the interaction between debris flow and barriers were discussed in this extended abstract. Contrary to existing design approaches, which treats the flow macroscopically, it is imperative to consider the interaction between the solid and fluid phases to properly estimate the impact pressure distribution acting on the barrier. The pressure coefficient (α) used in momentum-based design approaches is dependent on the solid fraction of the flow. It is also evident that the wide range of recommended α values in literature is not only mutually inconsistent but highly-conservative. In some guidelines, the recommended α values are almost twice as large as that measured from the centrifuge experiments. Furthermore, the effect of viscous shearing alone has negligible influence on α . This further corroborates that the design on barriers against debris flows, more specifically α , is fundamentally dependent on the solid volume fraction of the flow.

ACKNOWLEDGEMENTS

The work described in this abstract is supported by the Research Grants Council of the Hong Kong Special Administrative Region, China (T22-603/15-N). The authors are grateful for the support of the HKUST Jockey Club Institute for Advanced Study.

REFERENCES

- Bowman ET, Laue J, Imre B & Springman SM (2010) Experimental modelling of debris flow behaviour using a geotechnical centrifuge. *Canadian Geotechnical Journal* 47(7), 742-762.
- Choi CE, Au-Yeung SCH, Ng CWW & Song D (2015a) Flume investigation of landslide granular debris and water runup mechanisms. *Géotechnique Letters* 5(1), 28-32.

- Choi CE, Ng CWW, Au-Yeung, SCH & Goodwin G (2015b) Froude scaling of landslide debris in flume modeling. *Landslides* 12(6), 1197-1206.
- Cui P, Zeng C, & Lei Y (2015) Experimental analysis on the impact force of viscous debris flow. *Earth Surface Processes and Landforms* 40(12), 1644-1655.
- Hallquist JO (2006) LS-DYNA theory manual. *Livermore Software Technology Corporation*.
- Hungri O, Morgan GC & Kellerhals R (1984) Quantitative analysis of debris torrent hazards for design of remedial measures. *Canadian Geotechnical Journal* 21(4), 663-677.
- Iverson RM (1997) The physics of debris flows. *Reviews of Geophysics* 35(3), 245-296.
- Iverson RM (2003) How should mathematical models of geomorphic processes be judged? In *Prediction in Geomorphology*, P. R. Wilcock and R. M. Iverson (eds. American Geophysical Union, Washington, USA.
- Iverson RM & Ouyang C (2015) Entrainment of bed material by earth surface mass flows: review and reformulation of depth-integrated theory. *Reviews of Geophysics* 53(1), 27-58.
- Koo RCH (2015) 3D debris mobility assessment using LS-DYNA, *special project report 4/2015*. Geotechnical Engineering Office, Hong Kong, SAR.
- Kwan JSH (2012) Supplementary technical guidance on design of rigid debris-resisting barriers. *GEO Report No. 270*. Geotechnical Engineering Office, Hong Kong, SAR.
- Kwan JSH, Koo RCH & Ng CWW (2015) Landslide mobility analysis for design of multiple debris-resisting barriers. *Canadian Geotechnical Journal* 52(9), 1345-1359.
- Major JJ (1997) Depositional processes in large-scale debris-flow experiments. *The Journal of Geology* 105(3), 345-366
- MLR (2006) *Specification of geological investigation for debris flow stabilization*. DZ/T 0220-2006. National Land Resources Department, China.
- Ng CWW, Song D, Choi CE, Koo RCH & Kwan JSH (2016a) A novel flexible barrier for landslide impact in centrifuge. *Géotechnique Letters* 6(3), 221-225.
- Ng CWW, Song D, Choi CE, Liu LHD, Kwan JSH, Koo RCH & Pun W (2016b) Impact mechanisms of granular and viscous flows on rigid and flexible barriers. *Canadian Geotechnical Journal* 54(2), 188-206.
- Ng CWW (2014) The state-of-the-art centrifuge modelling of geotechnical problems at HKUST. *Journal of Zhejiang University SCIENCE A* 15(1), 1-21.
- NILIM (2007) Manual of Technical Standard for Designing Sabo Facilities against Debris Flow and Driftwood. *Technical Note of NILIM No. 365*, Natural Institute for Land and Infrastructure Management, Ministry of Land, Infrastructure and Transport, Japan.
- Olovsson L & Souli MH (2000) ALE and fluid-structure interaction capabilities in LS-DYNA. *ASME-PUBLICATIONS-PVP* 414(1), 71-78.
- Olovsson L & Souli M (2001) Improved fluid-structure capabilities in LSDYNA. *Proceedings of 3rd European LS-DYNA conference*. Paris, France.
- Schofield AN (1980) Cambridge geotechnical centrifuge operations. *Geotechnique* 30(3), 227-268.
- Song D, Ng CWW, Choi CE, Kwan JSH & Koo RCH (2017) Influence of debris flow solid fraction on rigid barrier impact. (submitted to *Canadian Geotechnical Journal*)
- SWCB (2005) Manual of soil and water conservation. *Soil and Water Conservation Bureau, Taiwan*.
- VanDine DF (1996) Debris flow control structures for forest engineering. *Res. Br., BC Min. For., Victoria, BC, Work. Pap8*, 1996.
- Watanabe M & Ikeya H (1981) Investigation and analysis of volcanic mud flows on Mount Sakurajima Japan. *Erosion sediment transport measurement. International Association on Hydrology, Florence. Science Publication* 133, 245-256.
- White DJ, Take WA & Bolton MD (2003) Soil deformation measurement using particle image velocimetry (PIV) and photogrammetry. *Géotechnique* 53(7) 619-631
- WSL (2009) Full-scale Testing and Dimensioning of flexible debris flow barriers. *Technical report 1-22*. WSL, Birmensdorf, Swiss Federal Institute for Forest, Snow and Landscape Research

STABILITY OF SUBMARINE SLOPES

Alexander M. Puzrin*

* ETH Zurich, Switzerland

As oil and gas developments move into deeper waters, geohazards becomes an important risk driver. Landslide deposits and features observed on the seabed in the vicinity of potential future development indicate processes that were active in the geological past and can be expected to continue in the future. Shear band propagation is an effective mechanism to explain large landslides observed in the sediment record. The simple form of the SBP criteria enables their incorporation into deterministic and probabilistic slope stability analysis of offshore developments within the Geographical Information System. In contrast to conventional limiting equilibrium approaches used in such analysis, the shear band propagation approach was capable of explaining enormous dimensions of observed palaeo-landslides and predicting orders of magnitude higher annual probabilities of failure validated by historical frequencies.

Keywords: submarine landslides; shear band propagation; slope stability analysis

INTRODUCTION

A Geographical Informational System (GIS)-based deterministic and probabilistic slope stability analysis (PSSA) for offshore developments requires slope stability calculations to be repeated millions of times, excluding possible use of finite element methods and relying mainly on analytical limiting equilibrium (LE) slope failure criteria. In strain softening soils, however, LE approach assumes that the failure takes place simultaneously along the portion of the sliding surface where the shear stress exceeds the peak shear strength. It cannot explain the failure of the parts of the slope, where the shear stress is lower than the peak shear strength, frequently observed in gigantic submarine landslides. It also cannot distinguish between different landslide failure modes, such as slab failures, spreadings, ploughings and runouts (Figure 1). There is a clear need in an alternative approach, which would allow for overcoming this limitation while maintaining the simplicity of the LE analysis.

SHEAR BAND PROPAGATION APPROACH

A potential candidate to fill this gap is the shear band propagation (SBP) approach (e.g., Palmer and Rice 1973; Puzrin and Germanovich 2005), which in contrast to the LE provides criteria for an initial slip surface, in which the shear stress exceeds the peak shear strength, to propagate into “quasi-stable” portions of the slope, where the gravitational shear stress τ_g is lower than the peak shear strength τ_p but exceeds the residual strength τ_r . This helps to explain observed enormous dimensions of submarine landslides.

Puzrin et al. (2016) proposed a novel approach to modelling different stages of the submarine landslide evolution as a single continuous process driven by catastrophic and progressive shear band propagation, summarizing the recent advances in the SBP approach addressing the existing limitations, and providing analytical criteria for the shear band propagation and arrest in a 2D slope geometry. These simple criteria, validated against physical model experiments,

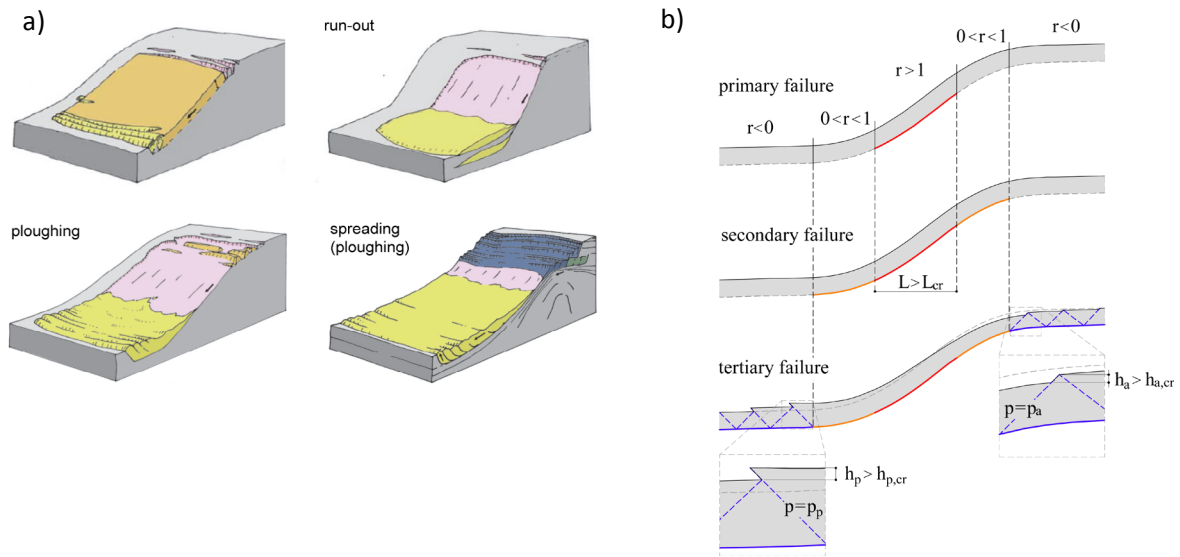


Fig. 1 Submarine landslides: (a) typical failure modes in translational (courtesy of Dr. Andy Mills); (b) shear band propagation mechanisms of landslide evolution.

numerical analysis and paleo-landslide data, allowed for the SBP approach to be incorporated into GIS based deterministic and probabilistic slope stability analysis, confirming the non-conservative nature of limiting equilibrium calculations.

For 2D and 3D slope geometry, Puzrin et al. (2016) proposed to treat the submarine landslide evolution as a continuous sequence of catastrophic and progressive SBP mechanisms (Fig. 1b). Conventional slope stability analysis assumes that slopes fail simultaneously along their entire length. In contrast, the SBP mechanism is capable of explaining the failure evolution from a relatively short initial shear band, triggered (*e.g.*, by an earthquake) in the steepest part of the slope, where gravitational τ_g and seismic τ_h forces exceed the peak shear strength (shear stress ratio $r = (\tau_g + \tau_h - \tau_r) / (\tau_p - \tau_r) > 1$, primary failure in Fig. 1b). If this initial shear band becomes sufficiently long, it can propagate catastrophically parallel to the slope surface into those parts of the slope, where gravitational and seismic forces exceed the residual shear strength ($0 < r < 1$), triggering a slab failure (secondary failure in Fig. 1b). Once the slab fails in active or passive failure at its ends, this causes changes in the seabed level, driving progressive propagation of the shear band into those parts of the slope where gravitational and seismic forces are smaller than the residual shear strength ($r < 0$) and triggering spreadings, ploughings and runouts (tertiary failure in Fig. 1b).

Puzrin et al (2016) demonstrated the ability of the SBP approach to formulate quantitative criteria for these post-failure evolution scenarios in Figures 1a and 1b and to explain the dimensions of some large submarine palaeo-landslides and the resulting geomorphological features. Rushton et al. (2015) incorporated the SBP approach, into the GIS based deterministic and probabilistic stability analysis and applied it to an area of the Caspian seafloor. The resulting annual probability of failure predicted by the SBP approach (Fig. 2) is an order of magnitude higher than the one predicted by the LE approach, approaching the observed historical landslide frequencies and contributing to the landslide risk assessment.

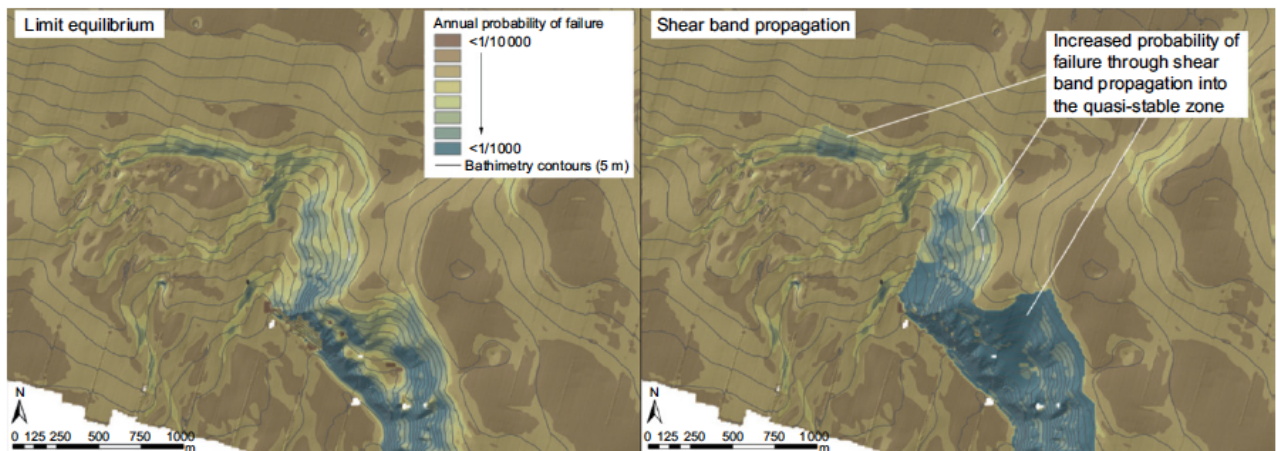


Fig 2. Annual probabilities of failure predicted using: LE (left) and SBP (right) approaches (after Rushton *et al.*, 2015), with permission of OTC.

CONCLUSIONS

Various components of the SBP approach to submarine slope stability have been validated experimentally, numerically and against historical field data. The energy balance approach used for the derivation of the proposed analytical criteria is, however, based on rather restricting assumptions and may not necessarily produce the most accurate results. Several studies have been recently devoted to refining the criteria (Puzrin 2016; Puzrin *et al.* 2015, 2017; Zhang *et al.* 2015, 2016), but much more work is still required. It is, however, hoped that the proposed framework of the SBP analysis of the submarine slope stability will serve as guidance for the future developments in this area.

REFERENCES

- Palmer, A. C., and J. R. Rice (1973). The Growth of Slip Surfaces in the Progressive Failure of Overconsolidated Clay, *Proceedings of the Royal Society of London*, A 332, 527-548.
- Puzrin, A. M., and L. N. Germanovich (2005). The growth of shear bands in the catastrophic failure of soils, *Proceedings of the Royal Society of London*, A 461(2056), 1199–1228.
- Puzrin, A.M., Germanovich, L.N. & Friedli, B. (2016). Shear band propagation analysis of submarine slope stability. *Géotechnique*, 66(3), 188-201.
- Puzrin, A.M. (2016). Simple criteria for ploughing and runout in post-failure evolution of submarine landslides. *Canadian Geotechnical Journal*, 53(8): 1305-1314.
- Puzrin, A.M., Gray, T. and Hill, A.J. (2015). Significance of the true non-linear slope geometry for catastrophic failure in submarine landslides. *Proceedings of the Royal Society, Series A: Mathematics, Physics and Engineering Science*, 471 (2175): 20140722.
- Puzrin, A.M., Gray, T.E. and Hill, A.J. (2017). Retrogressive shear band propagation and spreading failure criteria for submarine landslides. *Géotechnique*, 67(2): 95-105.
- Rushton, D., Gray, T.E., Puzrin, A.M., and Hill, A.J. (2015) GIS-Based Probabilistic Slope Stability Assessment Using Shear Band Propagation. In *OTC 2015*, Houston, USA: paper OTC 25871-MS.
- Zhang, W., Wang, D., Randolph, M.F. and Puzrin, A.M. (2015). Catastrophic failure in planar landslides with a fully softened weak zone. *Géotechnique*, 65(9): 755-769.
- Zhang, W., Wang, D., Randolph, M.F. and Puzrin, A.M. (2016). Dynamic propagation criteria for catastrophic failure in planar landslides. *International Journal for Numerical and Analytical Methods in Geomechanics*, 40: 2312-2338.

SOIL-ATMOSPHERE INTERACTION IN LANDSLIDE TRIGGERING

L. Pagano*, A. Reder *[†], G. Rianna [†]

* University of Naples Federico II, Naples, Italy

[†] CMCC Foundation, Euromediterranean Center on Climate Change

This work describes the role of evaporation and evapotranspiration phenomena on the evolution of the hydrological condition of soil on slopes made of silty volcanic soils.

The investigation was carried out by first empirically identifying the characteristics of the hydrological behavior of a silty volcanic layer in a lysimeter under both bare and vegetated conditions. The experimental dataset was then used to interpret a landslide case history, also in bare and vegetated contexts. The results provided by the tested layer and yielded by the studies indicate that evapotranspiration fluxes are a major influence in the reliable interpretation or forecasting of a rainfall-induced landslide, and suggest that vegetation is likely to result in limiting landslide occurrence.

Keywords: pyroclastic soil, landslide, evaporation, evapotranspiration, lysimeter

INTRODUCTION

In a rainfall-induced landslide, an exceptional rainfall event triggering the landslide phenomenon typically acts in synergy with a soil state that, in terms of high water content or low suction levels, predisposes to instability. The relative role of these two components is strictly related to a number of factors pertaining to soil properties, slope geometry and boundary conditions. The predisposing soil state results from the complex interaction between the soil and the atmosphere that occurs over the antecedent periods; it results from the balance of water flux exchanges, governed by atmospheric forcing and the state of the topsoil. Entering fluxes correspond to rainfall events of different intensity and duration, while exiting fluxes are due to evapotranspiration, deep drainage and lateral diversion. The effects of antecedent rainfall have been widely recognized in both past and recent literature (e.g., Rahardjo et al., 2001; Pagano et al., 2010). Several experimental and theoretical geotechnical works have also recently investigated evaporation or evapotranspiration issues, highlighting the key role of these fluxes in slope stability and other geotechnical issues (Rianna et al., 2014, Rahardjo et al., 2013; Calabresi et al., 2013; Hazra et al., 2017).

This work describes the role of evaporation and evapotranspiration phenomena on the evolution of the hydrological condition of silty volcanic slopes. The main aim is to gain a better understanding of the role of these phenomena in delaying or preventing landslide initiation and, consequently, individuating procedures suitable to interpret or forecast reliably landslide.

The first step was to examine the hydrological behavior of a silty volcanic layer placed in a lysimeter exposed to the elements for a period of 6 years (2010-2016). The experiment was carried out initially in bare soil conditions (2010-2014) and, subsequently, with vegetation on the surface of the layer. This approach made it possible to observe and compare the response

of the layer under two different surface conditions. Since the soil placed in the lysimeter is of the same type as that involved in the 2005 Nocera Inferiore landslide (Campania region, Southern Italy), the rich experimental dataset delivered by the experiment may be used to interpret this case history. To do so, the lysimeter data were used to calibrate model parameters for two thermo-hydraulic approaches, suitable for analyzing slope behavior in both bare and vegetated conditions. The meteorological variables recorded for this case history were converted into predictions of hydrological slope behavior in the two situations mentioned of bare and vegetated slopes. A comparison and discussion of the predictions yielded by the studies then follows.

AN EXPERIMENT IN BARE AND VEGETATED CONDITIONS

The physical model (Rianna et al., 2014) consists of a wooden tank containing the volcanic soil made up of sandy silt, that was involved in the Nocera Inferiore flowslide of 2005, put in place at a high field porosity of around 70%, using the pluvial deposition technique. About 1 m³ of material was exposed to the elements to investigate the interaction between the soil and the atmosphere in one-dimensional flow conditions. The material was extensively monitored to collect hydraulic, thermal and energetic variables. It was also weighted continuously over time by placing it on three load cells, to measure water storage changes easily and directly and to estimate entering and exiting water fluxes.

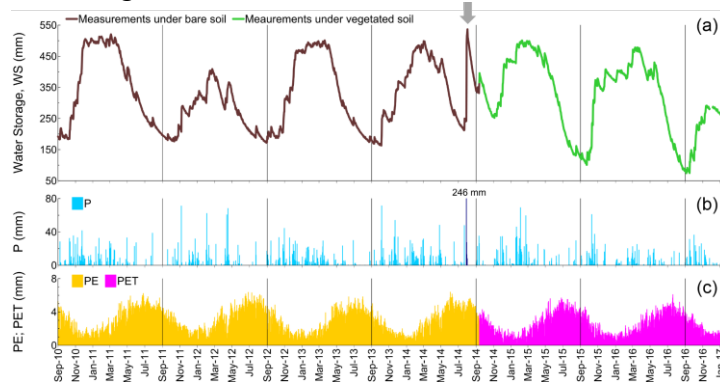


Fig. 1 Lysimeter data for bare (brown line, first 4 years) and vegetated (green line, last two years) surfaces: (a) water storage, (b) daily rainfall, (c) potential evaporation or evapotranspiration

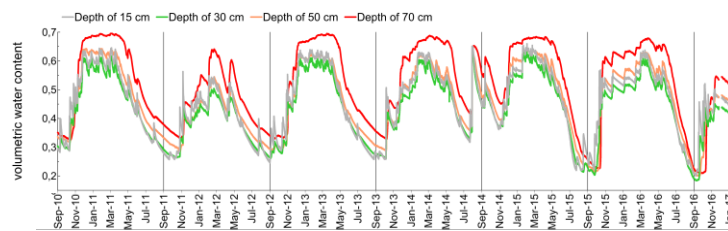


Fig. 2 Evolution of volumetric water content at four depths under bare (first 4 years) and vegetated (last two years) surfaces

The measured changes in water storage (Figure 1a), volumetric water content (Figure 2) and suction (Figure 3) detected in bare conditions fluctuate for each hydrological year following a fairly regular pattern. This is regulated by increases in layer imbibition during autumn and winter due to precipitation, and decrements during late spring and the hot season due to evaporation. At the end of the fourth hydrological year, a saturation test was performed to identify the precise level of water storage at full saturation (grey arrow in Figure 1a).

At the beginning of the fifth hydrological year, graminaceous vegetation was added to the surface of the layer. Dynamics similar to those observed for bare conditions were also observed under vegetated conditions. The main difference was the minimum value of water storage for

the layer, gradually reducing during the summer seasons due to the action of the roots, which progressively deepened within the layer. The roots extracted water from the lower part of the layer, a result that can clearly be seen from a comparison of the deepest volumetric water content in bare and vegetated conditions during the warm-dry seasons. In bare conditions, volumetric water content measured at a depth of 70 cm is distinctly higher than the shallower water content, while in vegetated conditions it reduces significantly, matching the trends at shallower measuring points (Figure 2). Thanks to root extraction, the soil layer is able to meet atmospheric demand (actual evapotranspiration constantly at the potential value), for a longer part of the year, up to the first part of the summer season (Figure 3a, last two years). Conversely, in bare conditions, actual evaporation significantly departs from potential evaporation (Figure 3a, first four years), as it is difficult for deep water to come out of the layer.

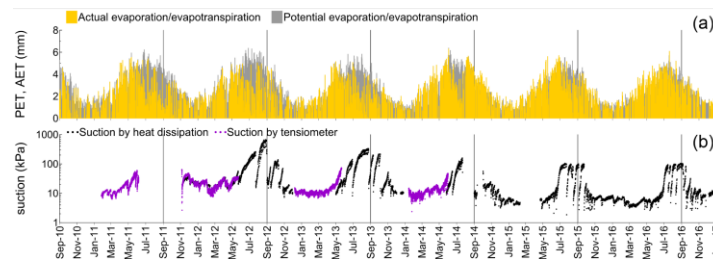


Fig. 3 a) estimated actual (yellow) and potential (grey) evaporation/evapotranspiration throughout the entire monitoring period; b) suction at a depth of 5cm monitored using a tensiometer (black), and heat dissipation probes (purple line)

The suction changes detected show how the presence of vegetation and water transport that they cause in the shallow zones significantly lowers the maximum suction levels during the summer season (Figure 3b).

LANDSLIDE CASE HISTORY ANALYSIS

The layer placed in the lysimeter was 0.75 m thick, and the meteorological conditions were normal for the area under consideration. In order to extend the pattern to the thicker layers often encountered in natural slopes, and to investigate the effects of exceptional meteorological conditions resulting in landslides, the experimental data presented here were adopted to interpret the Nocera Inferiore landslide of 2005. This event involved a 2-meter thick volcanic deposit tilting to approximately 40° and resting on fractured bedrock. The intrinsic properties and porosity level were comparable to those of the tested layer.

Hourly records for different meteorological variables taken near the landslide over a period of ten years, including the time of the landslide, were converted into hydrological soil variables for the slope stability conditions (suction and water storage) using two different models. The first model schematizes the (liquid water)-(vapour water) flow via hydrothermal coupling, and reproduces internal evaporation (Wilson et al., 1994). It was adopted in order to interpret the case history in bare soil conditions. The second model represents an extension of the first one adding a “sink” term to simulate the transpiration component (Tratch et al., 1995). This model was adopted to interpret the case history in vegetated conditions. The equations governing both models were solved using the FEM code VADOSE/W 2007 (GeoStudio, 2007).

Features shared by both models are the assumption of a one-dimensional flow through a 2-meter-thick unsaturated rigid layer (domain), the precipitation history applied to the top-boundary at hourly resolution, and a seepage surface applied to the bottom boundary.

The soil parameters required by both numerical models were quantified by referring to the data provided by the tested layer in bare and vegetated conditions.

The changes in water storage yielded by the simulations for the bare and vegetated surfaces reproduce the regular seasonal patterns observed for the tested layer. In both cases, a peak at record is yielded by the analyses at the landslide time, so both predictions recognize a hydrological peculiarity for the time of the landslide.

However, under vegetated conditions, soil water content was systematically lower than that predicted in the bare conditions also during the months more prone to landslide triggering (November-May). Results suggest that the effectiveness of roots in extracting deep water are likely to result in limiting landslide occurrence and that predictions carried out without accounting for vegetation may overestimate the occurrence of conditions potentially entailing slope instability events.

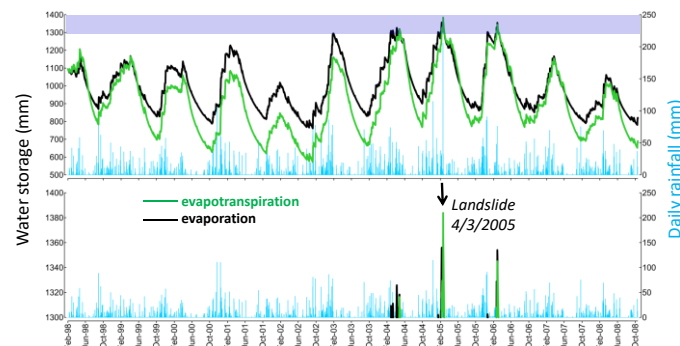


Fig. 5 Computed evolution of water storage under the effects of meteorological conditions resulting in the Nocera Inferiore landslide (4th March 2005) for bare and vegetated slopes

CONCLUSIONS

Following an approach that extrapolates the behavior of a control layer of silty volcanic soil tested in fully controlled or monitored conditions from the field environment of a landslide case-history, the study shows that evapotranspiration fluxes are a major influence in the reliable interpretation or forecasting of rainfall-induced landslides. Both empirically and theoretically, comparison between the bare and vegetated conditions resulted in similar behavioural patterns followed by hydrological variables, under the effects of either typical or exceptional meteorological conditions. Significant differences arose, however, regarding imbibition levels over time, even during months when landslide events typically occur.

REFERENCES

- Calabresi G, Colleselli F, Danese D, Giani GP., Mancuso C, Montrasio L, Nocilla A, Pagano L, Reali E & Sciotti A (2013) A research study of the hydraulic behaviour of the Po river embankments. *Canadian Geotechnical Journal* 50, 947–960.
- Hazra B, Gadi V, Garg A, Ng CWW & Das GK (2017) Probabilistic analysis of suction in homogeneously vegetated soils. *Catena* 149, 394–401.
- Pagano L, Picarelli L, Rianna G & Urciuoli G (2010) A simplified approach for timely prediction of precipitation-induced landslides in unsaturated pyroclastic soils. *Landslides* 7(3), 273–289.
- Rahardjo H, Li XW, Toll DG & Leong EC (2001) The effect of antecedent rainfall on slope stability. *Geotechnical and Geological Engineering* 19(3), 371–399.
- Rahardjo H, Satyanaga A & Leong EC (2013) Effects of flux boundary conditions on pore water pressure distribution in slope. *Engineering Geology* 165, 133–142.
- Rianna G, Pagano L & Urciuoli G (2014) Investigation of soil-atmosphere interaction in pyroclastic soils. *Journal of Hydrology* 510, 480–492.
- Tratch DJ, Wilson GW & Fredlund DG (1995) An introduction to analytical modeling of plant transpiration for geotechnical engineers. *Proceedings of the 48th Canadian Geotechnical Conference* 2, 771–780.
- Wilson GW, Fredlund DG & Barbour SL (1994) Coupled soil-atmosphere modelling for soil evaporation. *Canadian Geotechnical Journal* 31(2), 151–161.

MODEL CALIBRATION OF LANDSLIDE BOUNDARY VALUE PROBLEMS BY INVERSE ANALYSIS

Michele Calvello

Department of Civil Engineering, University of Salerno, Fisciano, Italy

The paper presents an inverse analysis procedure used as a tool to calibrate the numerical models of two very different landslides: a slow moving active slide characterized by very slow movements occurring within a narrow band of weathered bedrock; and a fast moving debris flow characterized by a relatively short propagation distance. In the first case, the procedure is used to update, with time, the landslide model using available groundwater and displacements monitoring data. In the second case, the study focuses on the key role played by the field observations used to set up the inverse analysis and to assess the reliability of the numerical simulations. In both cases, results already published by the Author are presented alongside with more recent research findings.

Keywords: inverse analysis, landslide, modelling, field observations

INTRODUCTION

Landslide boundary value problems are often difficult to model. The accuracy of the model predictions are related to factors such as: the boundary value problem schematization (e.g., geometry, stratigraphy, soil constitutive laws); the estimates of the model input parameters; the initial and boundary conditions. To improve the reliability of landslide models, calibration is often conducted performing back-analyses of landslide case studies for which monitoring data are available. Inverse analysis techniques may be very helpful to this purpose. The major advantage of inverse analysis approaches to calibrate model input parameters is the automatic and objective calculation of the parameter values that produce the best fit between measured data and computed results. The paper presents the case studies of two very different landslides, for which a versatile inverse analysis algorithm, based on a multiparametric linear regression method, is effectively used to calibrate the numerical models of the phenomena.

ADOPTED INVERSE ANALYSIS PROCEDURE

Inverse analysis works in the same way as a non-automated calibration approach: parameter values and other aspects of the model are adjusted until the model's computed results match the observed behavior of the system. In this study, model calibration is conducted adopting a procedure (Calvello, 2014) based on a modified Gauss-Newton regression method (Poeter and Hill, 1998) that minimizes a weighted least-squares objective function, $S(\underline{b})$:

$$S(\underline{b}) = [\underline{y} - \underline{y}'(\underline{b})]^T \underline{\omega} [\underline{y} - \underline{y}'(\underline{b})] = \underline{e}^T \underline{\omega} \underline{e} \quad (1)$$

where: \underline{b} is the vector of the parameters being estimated; \underline{y} is the vector of the observations being matched by the regression; $\underline{y}'(\underline{b})$ is the vector of the corresponding computed values; $\underline{\omega}$ is the weight matrix, being the weight of every observation taken as the inverse of its error variance; \underline{e} is the vector of residuals.

The regression needs, at any given iteration, the computation of a sensitivity matrix using a perturbation method and, thus, multiple runs of the numerical model. Two convergence criteria are used to end the optimization. Weights are assigned to the observations for two purposes: to reduce or increase the influence of some observations; to produce weighted residuals that have the same units. A commonly used indicator of the overall magnitude of the weighted residuals is the model error variance, s^2 :

$$s^2 = \frac{S(\underline{b})}{ND - NP} \quad (2)$$

where: $S(\underline{b})$ is the objective function; ND is the number of observations; NP is the number of estimated parameters. More details on the procedure adopted herein can be found in Calvello (2014).

SLOW-MOVING LANDSLIDE CASE STUDY

The case study is a well-studied active landslide located in central Italy characterized by a soil profile consisting of three overlying layers: a marly clay bedrock, a weathered band of the bedrock, wherein most of the landslide movements occur, and a clayey silt colluvial cover (Bertini et al., 1984). In situ data include observations from one pluviometric station, 12 piezometric cells and six inclinometers. Calvello et al. (2008) analyzed this case study proposing an inverse analysis procedure comprising a seepage model and a kinematic model relating landslide movements along pre-existing slip surfaces to rainfall data. They were able to adequately simulate, for the 3-year long period under study, both the pore pressure fluctuations in all installed piezometers and the kinematics of the movement along the slip surface. As an example of the obtained results, Fig. 1 presents the head contour lines of the calibrated seepage model at the end of the numerical simulation and the comparison between recorded and computed piezometric levels. For some of the piezometers (A2, B3, B4, C7, G11, G12) the fit is almost perfect, but even for the rest of them the fit is satisfactory. The adopted modelling approach, which combines the observational method and inverse analysis techniques to update, with time, the model of a boundary value problem using available monitoring data, may be called “observational modelling” (Calvello, 2017).

FAST-MOVING LANDSLIDE CASE STUDY

The case study is a debris flow characterized by a relatively short propagation distance which occurred in Hong Kong in 2005 (Knill 2006). Following up on a previous study by Cuomo et al. (2015), this study focuses on the role played by the field observations used to set up the inverse analysis and to evaluate the reliability of the numerical simulations. Several sets of observation are herein used. They all refer to soil thickness values at the end of the propagation stage, yet they differ in the both location and number of the adopted values. The numerical analysis is performed using GeoFlow_SPH (Pastor et al., 2009) and schematizing slope

topography through a regular grid of 2 m spaced nodes and the propagating mass through a set of 1 m spaced particles. Two rheological laws are used to simulate the behaviour of the propagating mass: a simple frictional law based on a single input parameter (ϕ'_b); a complex rheological law, modelling the propagating mass as a solid skeleton saturated with water, depending on four input parameters (ϕ'_b , H_{rw} , P_{rw} , B_{fact}). The calibration procedure employed is based on a series of back-analyses—i.e. parametric and optimization analyses—organized in two sequential steps, one for each rheology. During the first step, many observation sets are tested with the aim of defining the ones that are most suitable to be used for the back-analysis of the considered debris flow. Those sets are then used, in the second step, to calibrate the model parameters of the complex rheological law. The points used to define the different sets of observation in the analyses are shown in Fig. 2a. The results reported herein refer to the two parametric analyses performed, respectively during the first (Fig. 2b) and the second (Fig. 2c) step of the procedure. In both cases the analyses employ a set of observations along the main cross section of the deposited mass, i.e. 15 soil height data. In the first case, 11 simulations are run to evaluate the effect of an assumed range of values for $\tan \phi'_b$. As expected, when the friction angle increases the soil height in the deposition zone decreases; yet, at the top of the section the height values estimated by numerical modeling are always higher than the observations. In the second case, the variation in error variance, for different pairwise combinations of the four parameters' values, is used to define the parameters playing a relevant role in the performance of the model. In this case, it is evident that only two parameters, ϕ'_b (basal frictional angle) and P_{rw} (ratio between initial basal pore-water pressure and liquefaction pressure), significantly influence the numerical results of the model.

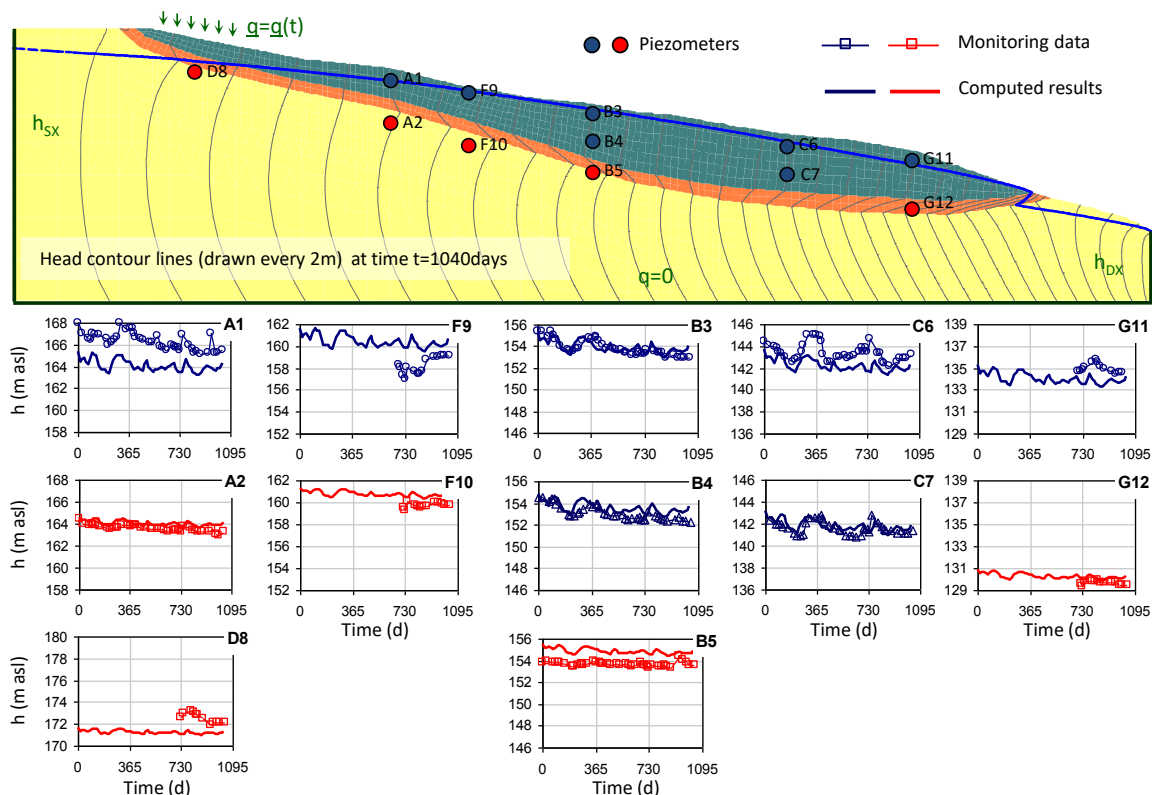


Fig. 1 Comparison between computed and measured head (m a.s.l.) at the location of the piezometers (modified from Calvello et al., 2008).

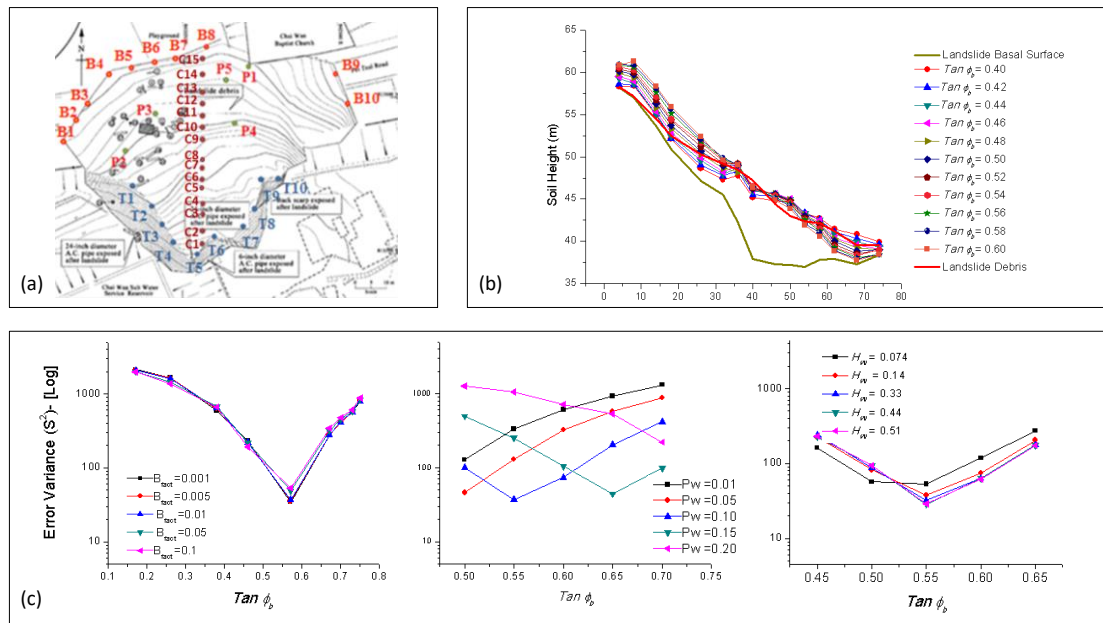


Fig. 2 Observations (a) and results of the parametric analyses employing 15 soil height data along the main cross section of the landslide (C1-C15) when one-parameter rheology (b) or four-parameter rheology (c) are used.

CONCLUSION

A versatile inverse analysis algorithm has been effectively used to calibrate the numerical models of the two landslide boundary value problems: a slow moving active slide and a fast moving debris flow. In the first case, observational modelling is possible, i.e. inverse analysis techniques can be used to update, with time, the landslide model using available monitoring data. Indeed, as time passes and more monitoring data are available, the update of the numerical model allows more reliable model predictions of the future landslide behavior. In the second case, the adopted calibration procedure proved successful in calibrating the model parameters of a complex rheological law once the most suitable observation sets were selected based on a simpler rheological law adopting a single input parameter.

REFERENCES

- Bertini T, D’Elia B, Grisolia M, Olivero S & Rossi-Doria M (1984). Climatic conditions and slow movements of colluvial covers in central Italy. *Proc. IV Int. Symp. on Landslides*. Vol. 1, pp. 367–376.
- Calvello M (2014). Calibration of soil constitutive laws by inverse analysis. *ALERT Doctoral School 2014 - Stochastic Analysis and Inverse Modelling*. Hicks MA & Jommi C (eds.). pp. 239-262.
- Calvello M (2017). From the observational method to “observational modelling” of geotechnical engineering boundary value problems. *ASCE Geotechnical Special Publication*. In press.
- Calvello M, Cascini L & Sorbino G (2008) A numerical procedure for predicting rainfall-induced movements of active landslides along pre-existing slip surfaces. *Int. J. Numer. Anal. Meth. Geomech.* 32, 327-351.
- Cuomo S, Calvello M, Villari V (2015). Inverse analysis for rheology calibration in SPH analysis of landslide run-out. *Proc. XII Int. IAEG Congress*. Vol. 2, pp. 1635-1639.
- Knill J (2006). Report on the Fei Tsui Road Landslide of 13 August 1995. *GEO Report No. 188*. Geotechnical Engineering Office, Hong Kong Special Administration Region.
- Pastor M, Haddad B, Sorbino G, Cuomo S & Drempetic V (2009). A depth-integrated, coupled SPH model for flow-like landslides and related phenomena. *Int. J. Numer. Anal. Meth. Geomech.* 33, 143-172.
- Poeter EE & Hill MC (1998). Documentation of UCODE, a computer code for universal inverse modeling. *Investigations Report 98-4080*. U.S. Geological Survey Water-Resources.

EFFECT OF UNSATURATED CONDITIONS ON DISASTERS DUE TO LANDSLIDES

Marcos Massao Futai*

* School of Engineering – University of Sao Paulo, Sao Paulo, Brazil

Keywords: landslides, natural disaster, unsaturated, tropical soil

INTRODUCTION

The economic losses and deaths caused by natural disasters are growing worldwide. Earthquake, which can be considered the most damaging natural disaster, do not occur in Brazil; In fact, flood is the most common disaster, although landslides are responsible for disasters with the most victims and economic losses. The tropical climate contributes to forming thick soils and heavy rainstorms, which is why landslide disasters are very common in countries such as Brazil.

Rainfall may act as a preparatory agent to trigger landslides and is the main cause of slope failure in Brazil. Water commands the instability process, and this may occur in unsaturated or saturated soils. Reduced suction, soil saturation or increased water table depend on the interaction of the soil with the climate conditions. In normal conditions, rainfall infiltration is the main source of water from the slopes. On occupied hillsides, there may be outflow of wastewater, and other cases may involve leakages from water or sewage pipes, which may also contribute to infiltration.

Some examples of natural disaster caused by landslides in Brazil are: 1948 – Vale do Paraíba do Sul approximately 250 fatal victims; 1966 – Rio de Janeiro city – approximately 100 fatal victims; 1967 – Caraguatatuba – Sao Paulo State – approximately 120 fatal victims; 1985 - Cubatão Mountain – 1500 landslides, no deaths were registered; 1988 – Petrópolis – Rio de Janeiro State – 171 fatal victims; 2008 – Vale do Jataí –Santa Catarina State – 135 people died and 2011 - Mountain Region of Rio de Janeiro – 1500 fatal victims. All the disasters mentioned occurred in the Serra do Mar, a mountain range extending for about 1,500 km along the southeast coast of Brazil. Disasters related with landslides in the Serra do Mar were observed to happen in less than ten years and to depend on climate conditions.

INSTABILITY MECHANISMS

The different systems for classifications of mass movements include studies by Wolle (1988) who distinguished mechanisms in the coastal mountain range of Serra do Mar, which can generally be considered for most Brazilian hillsides. Wolle (1988) divided the instability phenomena into landslides (translational, rotational or caused by spreading), rock falls (falls, roll-

ing boulders, block slides, structured failure) and soil creeps. Wolle (1988) indicated two types of possible mechanisms of instability associated with translational landslides in the Serra do Mar: classic and alternative.

The *Classic Mechanism* consists of a rise in the pre-existing water level due to the flow of water infiltration; a landslide is determined by an almost instant rise in the water table, which may occur when the wetting front reaches the groundwater. This creates a sharp rise in neutral pressures in the soil profile, leading to landslides due to the reduction in effective confining stresses. The gradual rise in water level can also be caused by the formation of a flow network parallel or sub-parallel to the slope, sustained by a less permeable horizon than the surface horizon.

The *Alternative Mechanism* consists of infiltration, forming a wetting front on hillsides without a pre-existing water level, and was proposed by Terzaghi (1950). According to Wolle (1988), his first finding was in the Serra do Mar, on the hillsides next to the Imigrantes Highway. In unsaturated soils, the elimination or even the reduction in suction due to rainfall infiltration causes a considerable decrease and possibly no cohesion intercept at all. Failure occurs when the wetting front reaches a critical depth at which the strength parameters no longer guarantee slope stability.

Shallow landslides in colluvial and residual soils are very common in tropical regions, mainly associated with periods of heavy rainfall. Many of these cases can be interpreted by infinite slopes. After defining the distribution of suction and strength parameters, the safety factor is easily calculated. However, to represent the actual conditions, it is necessary to know the spatial and the time distribution of the suction. Calculating stability is no longer a single analysis of a slope. It also depends on the interaction of the slope with climate conditions associated with rainfall infiltration, variation in the water table or another mechanism that alters the suction distribution in the soil, given the importance of infiltration to the stability of unsaturated soils. Landslides in unsaturated conditions occur on hillsides formed by thick soils with a deep water table, without the presence of geological-geotechnical conditioning factors to develop a perched water table. Some examples are the excavation of slopes for some highways. Another possible condition occurs on very steep hillsides, which have a much higher gradient than the angle of friction and remain stable due to the suction effect.

CASES OF DISASTERS

Two historical disaster cases were selected to understand the mechanisms of the instabilization of shallow landslides during extreme rainfall associated with the disaster of the Cubatão Mountain and of the Mountain Region of Rio de Janeiro.

On the 22th and 23th of January 1985, 1500 shallow landslides devastated the Cubatão Mountain located in the State of Sao Paulo (Lopes et al, 2007). Then, it rained more in this region than on any other site of Serra do Mar. The annual precipitation for this site can be higher than 3000mm. The panoramic view is presented in Figure 1a.

The latest serious disaster occurred in the Mountain Region of Rio de Janeiro on the 11th and 12th of January 2011. According to Avelar et al. (2012), more than 3,500 landslides cause

1,500 fatal victims. Most movements were shallow landslides along with debris flow, mud-flow, flew rotational landslides and rock fall. The geomorphological difference between the Mountain Region of Rio de Janeiro (Figure 1b) and the Cubatão Mountain can be compared in Figure 1. The main characteristics of this region and of the landslides are summarized in Table 1.



Figure 1 – Panoramic Picture of Shallow landslides: (a) Cubatão Mountain (IPT) and (b) Nova Friburgo – Mountain Region of RJ (Coelho Neto, 2012)

Table 1 – Characteristics of Cubatão Mountain and the Mountain Region of Rio de Janeiro

Parameter	Cubatão Mountain	Mountain Region of Rio de Janeiro
State	São Paulo	Rio de Janeiro
Annual precipitation	3500mm	2500mm
Average declivity	40°	19°
Date of disaster	22 th and 23 th do January of 1985	11 th and 12 th January of 2011
Number of landslides	1500	3500
Soil	Colluvium	Colluvium and saprolitic soil
Main movement	Shallow landslides	Shallow landslides

Data estimated from Avelar et al (2012), Coelho Neto (2012), Wolle (1988), Lopes et al (2007)

There are no major differences among the type of landslides, the soil and the specifics regarding shear strength. However, in the Cubatão Mountain, the slope inclination and annual rainfall are higher than in the Mountain Region of Rio de Janeiro (Table 1). The average slope inclination from the Mountain Region of Rio de Janeiro, where landslides were observed, is half that for the Cubatão Mountain. Even the type of landslides being the same, the mechanisms of instabilization are quite different. Both cases are unsaturated in normal climate conditions because no water level has been measure near the slide surface. Futai (2014) explains, using Duñes (2014) numerical analysis data, which geological condition and direction of flow are different. The soil profile of the Cubatão Mountain is composed of colluvium, which is less permeable than the saprolitic soil, and the rock is very fractured, reason why it cannot develop water level and the saturated pore-water pressure remains zero (Figure 2a). In the Mountain Region of Rio de Janeiro, the saturated permeability decreases with depth and the soil-rock contact can be considered impermeable in many cases. In normal conditions, there is no water table; however, when the intense rain period occurs just before an extreme rainfall, the water table can be formed and the pore-water pressure should be positive (Figure 2b). These instability mechanisms (Figure 2) were identified by Wolle (1988) and now they can be used to explain disaster along the Serra do Mar Mountain Range supported by numerical simulations (Duñes, 2014).

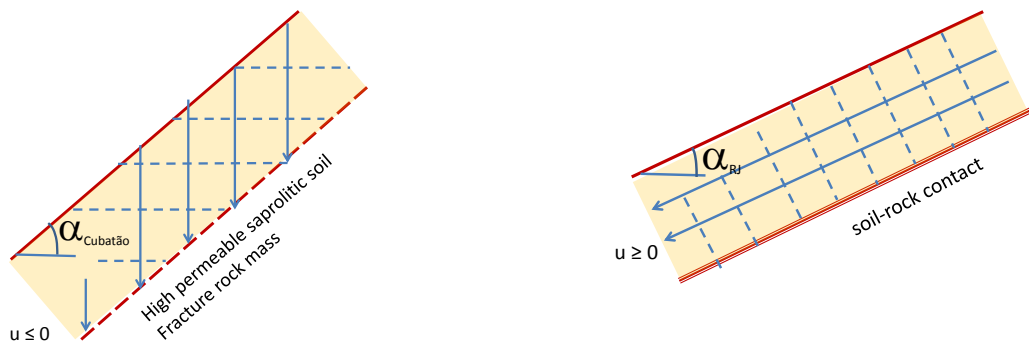


Figure 2 - Model of net flow and stability model for (a) the Cubatão Mountain and (b) the Mountain Region of Rio de Janeiro

CONCLUSIONS

The Serra Mar Mountain extends along 1,500 km and disasters associated with landslides have been observed in less than a ten-year period associated with extreme rainfall. The instability mechanisms in tropical soil depend on climate and geological conditions. Two cases were presented and compared to clarify the influence of the flow condition and of the unsaturated condition. In both cases, infiltration is defined by the unsaturated condition (soil water retention curve, conductivity function, unsaturated shear strength) because the surface always remains unsaturated. However, in the Cubatão Mountain, the landslides were triggered near the saturation, and in the Mountain Region of Rio de Janeiro had to have occurred positive pore-water-pressure. This conclusion was presented by Futai (2014) after analyzing the numerical simulation.

ACKNOWLEDGE: CAPES, CNPq, FAPESP and Proalerta-CEPED

REFERENCES

- Avelar, A.S., Coelho Neto, A.L, Lacerda, W.L., Becker, L.B. E Mendonça, M.B. (2011) Mechanisms of the Recent Catastrophic Landslides in the Mountainous Range of Rio de Janeiro, Brazil. Proc. Of the Second World Landslides Forum, Roma.
- Coelho Neto, A.S., Sato, A.M, A.L, Avelar, Vianna, G.G., Araujo, I.S., Ferreira, D.L.C, Lima, P.H., Silva, A.P. E Soilva, R.P.(2011). January 2011: the Extreme Landslide disaster in Brazil. Proc. Of the Second World Landslides Forum, Roma.
- Duñes, V.Z. (2014) Numerical analysis of extremely rainfall in the slope stability. Master Thesis, Escola Politécnica da Universidade de São Paulo, São Paulo. (in Portuguese)
- Futai, M.M. (2014) Mechanisms of shallow landslides associated with the natural disaster. Keynote lecture. Brazilian Conference of Soil Mechanics and Geotechnical Engineering. Belo Horizonte, Brazil.
- Lopes, E.S.S., Riedel, P.S., Bentz, C.M., Ferreira, M.V. and Naletto, J.L.C. (2007) Inventory of natural landslides in a geographic database - analysis of Conditioning factors in the region of Serra de Cubatão – SP. Brazilian Symposium on Remote Sensing, 2785-2796 (in Portuguese)
- Terzaghi, K. (1950). Mechanism of Landslides. *In: Application of Geology to Engineering Practice*, Geological Society of America, Berkeley, p.83-123.
- Wolle, C.M. (1988). Analysis of translational landslides in the Serra do Mar in the context of a classification of mechanisms of slope instability. PhD Thesis, Escola Politécnica da Universidade de São Paulo, São Paulo. (in Portuguese)

DEVELOPMENT OF NUMERICAL MODELS FOR LANDSLIDE MITIGATION WORKS

Julian S. H. Kwan*

* Geotechnical Engineering Office, Civil Engineering and Development Department, the Government of the Hong Kong Special Administrative Region, Hong Kong, China

The Geotechnical Engineering Office (GEO) has launched a Landslip Prevention and Mitigation Programme (LPMitP) to systemically deal with landslide risks in Hong Kong. Through the Programme, risks arising from natural hillside landslides are mitigated using appropriate measures including debris-resisting barriers. To achieve design optimisation of these barriers, the GEO has implemented a structured R&D study, and one of the initiatives of the study is to develop numerical models to study the dynamics of landslide debris and its interaction with barriers. The finite-element program LS-DYNA was used to conduct the numerical analyses. This paper discusses the modelling techniques and some of the verification cases. The developed models are being used to obtain a better understanding of the mechanism of debris-barrier interactions and to facilitate the development of design guidelines.

Keywords: finite-element method, landslide debris mobility, debris-resisting barriers

INTRODUCTION

Hong Kong is located in a subtropical region with average annual rainfall of around 2300 mm. About 60% of the total land area in Hong Kong is hilly terrain. The rapid population growth since the 1950s has resulted in a high concentration of urban development on steep terrain in close proximity to man-made slopes and natural hillsides, which are susceptible to landslides during high seasonal rainfall. The Geotechnical Engineering Office (GEO) has launched a Landslip Prevention and Mitigation Programme (LPMitP) to systemically deal with landslide risks. Through the Programme, risks arising from natural hillside landslides are mitigated using appropriate measures including landslide debris-resisting barriers. To achieve design optimisation and enhancement of robustness of these barriers, the GEO has initiated a structured R&D study, which includes laboratory tests and numerical modelling as well as large-scale physical testing. This paper briefly discusses the development of numerical models to predict the mobility of landslide debris and its dynamic interactions with flexible steel barriers.

INVESTIGATION APPROACH

Although the prediction of landslide debris mobility and the structural modelling of flexible barriers have been successfully carried out in the past (e.g. Hungr, 1995; Kwan & Sun, 2006; Kwan et al., 2014), their coupled modelling remains a challenge in the landslide community. Over the last several years, the GEO has been using the general-purpose finite-element program LS-DYNA for advanced numerical analyses. The automated contact algorithm and a

wide range of material models available in LS-DYNA permit the analyses of many complex real-world problems such as automotive crash analysis, metal forming, and blast simulation. This program has also been used for solving a range of static and dynamic problems in civil engineering. Therefore, this program was chosen to investigate the interaction between landslide debris and structural countermeasures. The investigation was divided into three phases: 1) simulation of landslide debris mobility, 2) structural modelling of flexible steel barrier, and 3) coupled analyses of debris-barrier interaction. Each of them is briefly described below.

LANDSLIDE DEBRIS MOBILITY

Landslide debris was modelled as a continuum using solid elements. Since the debris undergoes very large deformations during the flow process, the arbitrary Lagrangian-Eulerian (ALE) formulation was used to model the debris. In order to justify the appropriateness of this modelling technique, a simulation model was first set up and verified against field observations made during the Yu Tung Road debris flow in Hong Kong. This debris flow was triggered by a rainstorm on 7 June 2008. Over 3000 m³ of landslide debris ran down the hillside as a channelised flow down to Yu Tung Road. The debris travelled a total distance of over 600 m. A detailed account of the event has been documented in AECOM (2012).

To simulate the landslide debris, the Drucker-Prager failure criterion was used and a damping force was applied to replicate the Voellmy-type damping of the debris. Fig. 1 shows the simulations at three different times, and Fig. 2 compares the observed and back-calculated frontal velocities of the debris at different chainage along the flow path. The result from the two-dimensional debris mobility modelling program 2d-DMM (Kwan & Sun, 2006) is also included in Fig. 2 for comparison. The results show that the numerical model in LS-DYNA can reproduce results close to field observations. Further details about the simulation of this event in LS-DYNA can be found in Kwan et al. (2015). Back-analyses of other historical landslides in Hong Kong have been conducted using the same approach and the results are documented in Koo et al. (2017a).

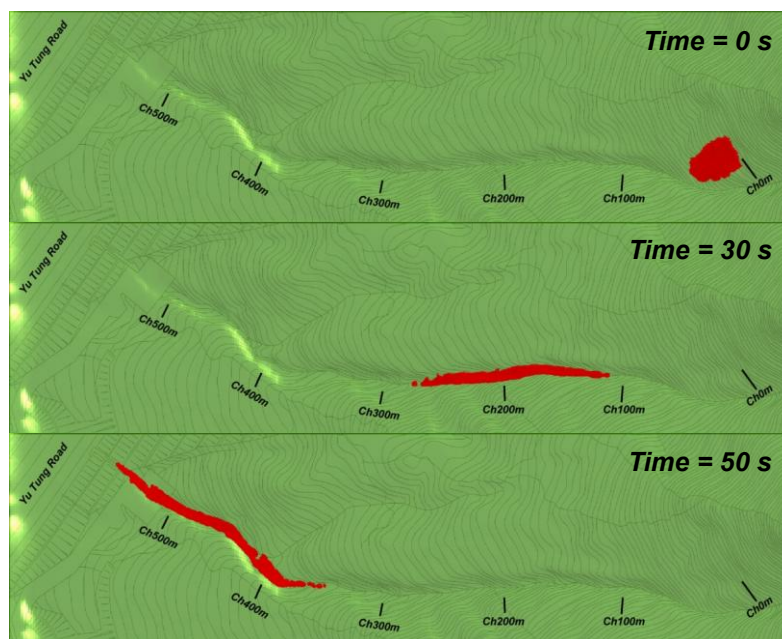


Fig. 1 Finite-element simulation of the Yu Tung Road debris flow

It is worthwhile to emphasise that at present landslide debris is modelled as a single-phase continuum material using suitable rheological model parameters. Further work will be required to simulate debris flows carrying large boulders.

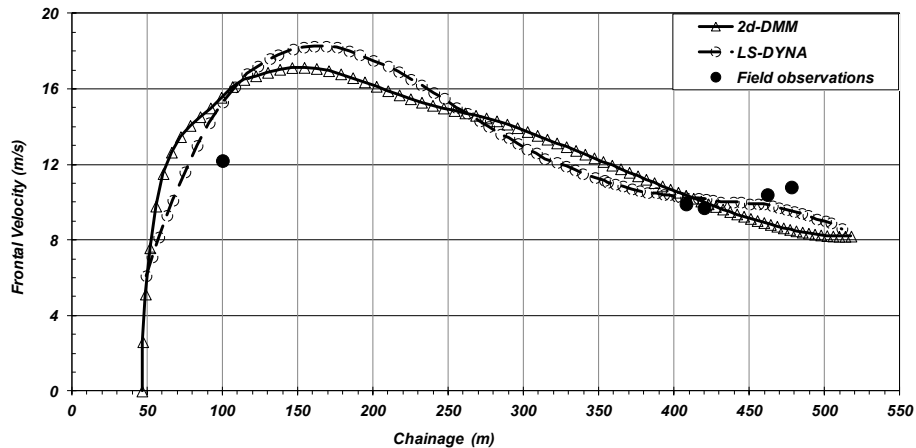


Fig. 2 Comparison between observed and back-calculated frontal velocities of the Yu Tung Road debris flow

STRUCTURAL MODELLING OF FLEXIBLE STEEL BARRIERS

Because of the highly flexible nature of steel barriers, it is crucial that the adopted simulation methodology can handle the material and geometrical nonlinearities of individual barrier components. A benchmarking exercise was thus carried out using the rockfall test results reported in Volkwein (2004). In LS-DYNA, all structural components were modelled using beam elements, whereas the impactor (a concrete ball) was modelled as a rigid sphere. Inelastic material models were assigned to steel rings where plasticity may develop under impact loading. The interactions between the rings, shackles and cables were simulated explicitly using the beam-to-beam contact algorithm available in LS-DYNA. Fig. 3 shows the simulated movement of one of the steel barriers tested by Volkwein (2004). A good agreement was obtained between the simulated and observed behaviour of the barrier. Further details about this verification case are given in Koo et al. (2017b).

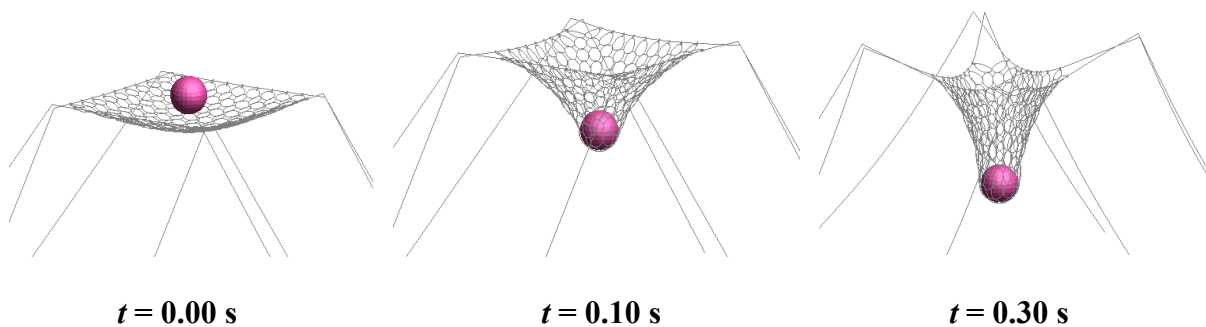


Fig. 3 Simulated behaviour of a flexible barrier impacted by a rigid sphere

DEBRIS-BARRIER INTERACTION

The simulation methodologies for flexible barriers and landslide debris assessed in previous sections are coupled to investigate the debris-barrier interaction. The results of the field tests

conducted at Illgraben in Switzerland were used for further assessment of the LS-DYNA simulation. Details about the field tests have been reported in Wendeler (2008) and are not repeated here. Fig. 4 shows the simulated barrier just before and after the barrier is overtopped. Many salient features observed in the field are also captured in the simulation. Further details are available in Huang et al. (2014).

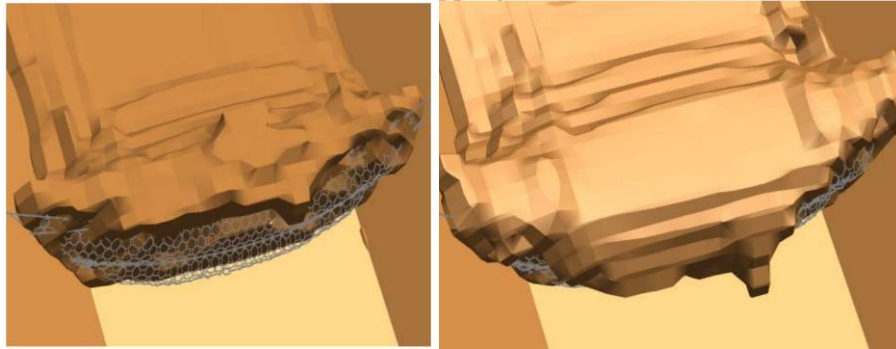


Fig. 4 Simulated behaviour of a flexible steel barrier impacted by a debris flow

CONCLUSIONS

Driven by the need to manage the landslide risk in Hong Kong, the GEO has developed numerical models to simulate the dynamics of landslide debris and its interaction with flexible steel barriers. The modelling techniques and some of the verification cases are discussed in this paper. The developed models are being used to better understand the mechanism of debris-barrier interactions. The findings will be used to formulate optimised guidelines for the design of debris-resisting barriers.

REFERENCES

- AECOM (2012) Detailed study of the 7 June 2008 landslide on the hillside above Yu Tung Road, Tung Chung. *GEO Report No. 271*. Geotechnical Engineering Office, Hong Kong, 124 p.
- Huang Y, Yiu J, Pappin J, Sturt R, Kwan JSH, Ho KKS (2014) Numerical investigation of landslide mobility and debris-resistant flexible barrier with LS-DYNA. *Proceedings of the 13th International LS-DYNA Users Conference*. Dearborn, Michigan. Livermore Software Technology Corporation, pp. 1-12.
- Hung O (1995) A model for the runout analysis of rapid flow slides, debris flows, and avalanches. *Canadian Geotechnical Journal* 32, 610-623.
- Koo RCH, Kwan JSH, Lam C, Choi CE, Ng CWW, Yiu J, Goodwin GR, Ho KKS & Pun WK (2017a) Dynamic analysis of notable landslide case histories in Hong Kong using a three-dimensional debris mobility model. *Canadian Geotechnical Journal*, under review.
- Koo RCH, Kwan JSH, Lam C, Ng CWW, Yiu J, Choi CE, Ng AKL, Ho KKS & Pun WK (2017b) Dynamic response of flexible rockfall barriers under different loading geometries. *Landslides*, published online.
- Kwan JSH, Chan SL, Cheuk JCY & Koo RCH (2014) A case study on an open hillside landslide impacting on a flexible rockfall barrier at Jordan Valley, Hong Kong. *Landslides* 11, 1037-1050.
- Kwan JSH, Koo RCH & Ng CWW (2015) Landslide mobility analysis for design of multiple debris-resisting barriers. *Canadian Geotechnical Journal* 52, 1345-1359.
- Kwan JSH & Sun HW (2006) An improved landslide mobility model. *Canadian Geotechnical Journal* 43, 531-539.
- Volkwein A (2004) *Numerische Simulation von flexible Steinschlagschutzsystemen*. Doctoral thesis, ETH Zürich (in German).
- Wendeler C (2008) *Murgangrückhalt in Wildbächen – Grundlagen zu Planung und Berechnung von flexible Barrieren*. Doctoral thesis, ETH Zürich (in German).

ROCK AVALANCHES: CONSTITUTIVE AND NUMERICAL MODEL- LING

Diego G. Manzanal*[†], Manuel Pastor*, Miguel M. Stickle*, Angel Yagüe*

* ETSI de Caminos, Canales y Puertos, Universidad Politecnica de Madrid, Spain

[†]CONICET-UBA-UNPSJB, Argentina

Rock avalanches present high velocities of propagation, and large volume of materials that generate extremely mobility capable of travelling long distance and spreading over large areas causing high destructive power. The accurate prediction of runout, depth and velocity of rock avalanches is of paramount importance since, in general, preventing it is not possible.

The purpose of this paper is to assess the influence of the rheology on the avalanche properties using a depth integrated, SPH model. The paper compares the performance of different rheological models to reproduce the track, runout and depth of the final deposit for two real events such as Thurwieser and Frank rock avalanches. The paper provides information on the proposed model accuracy and limitations

Keywords: rheology, depth integrated, propagation, landslide, SPH

INTRODUCTION

A fundamental ingredient for modelling propagation of landslide is the model used to describe the behaviour of the fluidized material. Most of the approaches used so far are based on rheological laws relating effective stress and rate of deformation tensors. On the other hand, triggering is usually described using constitutive models where the increments of the stress and strain tensors are given by a suitable constitutive law. This makes the whole process difficult to model, because at a certain moment one has to switch from a constitutive law to a rheological model. A possible alternative has been to use viscoplasticity of Perzyna type, because it can provide suitable laws both for the solid and the fluidized behaviours (Pastor et al. 2010). One most interesting conclusion is that from Perzyna's viscoplasticity, it is possible to derive simple rheological laws, which can be used for frictional fluids.

The approach we propose in this work is based on continuum mechanics, and consists in a depth integrated mathematical model, which is discretized by using the SPH method. Depth integrated models present a reasonable compromise between computational cost and accuracy (Savage and Hutter, 1991, Pastor et al. 2009). Different rheological laws are applied to a special case of rock avalanches: Thurwieser Avalanche (Sossio and Crosta, 2007) and Frank Avalanche (Cruden and Hungr, 1986), comparing the results obtained with them and with other more classical approximations based on Voellmy or frictional fluid laws, such as those presented in Manzanal et al. (2016).

GENERAL FRAMEWORK: MATHEMATICAL AND NUMERICAL MODEL

Depth integrated models are a convenient simplification of 3D models, providing an acceptable compromise between computational cost and accuracy. Savage and Hutter (1991) pro-

posed their 1D lagrangian model for the case of avalanche dynamics, where a simple Mohr-Coulomb model allowed a description of the granular material behaviour. Depth averaged models are obtained by integrating along depth the balance of mass and momentum equations. Details of the general framework can be found in Pastor et al. (2009).

Smoothed particle hydrodynamics (SPH) is a meshless method introduced independently by Lucy (1977) and Gingold and Monaghan (1977). It has been applied to a large variety of problems. For avalanches propagation we can mention the recent work of Rodriguez-Paz and Bonet, 2005; McDougall and Hungr, 2004; Pastor et al 2009, 2013. Fast landslides is treated as fluidized masses of either soil or rock blocks to simulate their propagation. SPH is a numerical technique able to describe these phenomena. The method is based on the approximation of given properties and its spatial derivatives by integral approximation defined in term of the smoothed function or kernel function. An interpolation process calculates the relevant properties on each “particle” over neighbouring “particles”. Therefore, SPH is based on introducing a set of nodes $\{x_k\}$ with $K=1..N$ and the nodal variables on landslide problem are: height of the landslide at node I, depth averaged, 2D velocity, surface force vector at the bottom and pore pressure at the basal surface. Details of the formulation can be found in Pastor et al 2009a, Manzanal et al 2016.

CONSTITUTIVE AND RHEOLOGICAL MODELS

Rock avalanches, at large scale, behave as fluidized granular materials. At small scales we can observe phenomena such as inverse grading and crushing of rock blocks, which results into a change in granulometry and in dilatance properties. The behaviour of this granular fluid can be modelled using either discrete element methods or continuum based rheological models. The former presents the advantage of reproducing in a natural manner crushing and inverse grading phenomena, but the computational cost of modelling a real avalanche is still difficult to afford. On the other hand, the latter reduces the cost, but suitable models have to be used to describe the constitutive/rheological behaviour of the granular fluid. And it is because of this fluid like behaviour that rheological models have been used traditionally to model rock avalanches, as in other types of avalanches. While mudflows, lahars, and some cases of debris flows have been approximated using models such as Bingham or Herschel-Bulkley (Coussot 2005), rock avalanches present a dominant frictional behaviour requiring a different approach.

Simple shear infinite landslide models are on of the simplest, which can be used to describe the behaviour of a landslide. The main assumptions are the following: (i) flow is steady, (ii) all variables are independent on the position along the landslide, which is assumed to have an infinite length. We will use here x as the abscissa along the infinite plane and z the axis perpendicular to x within the plane. A general approach can be defined as:

$$\tau = s + \mu \left(\frac{\partial v}{\partial z} \right)^m$$

where s is the basal shear strength, μ is the viscosity, m is a model parameter and v is depth average velocity. From here, it is possible to derive simple cases as: (i) newtonian fluids with $s = 0$ and $m = 1$; (ii) Bingham fluids with $s = \tau_y$ and $m = 1$ where τ_y is the cohesive strength of the fluid; (iii) $s = 0$ and $m = 2$ (Bagnold, 1954) (iv) Visco-Frictional $s = \sigma_n \tan \phi$ where σ_n is the effective stress normal to the basal plane, and ϕ the friction angle, $m=2$ (Chen et al.

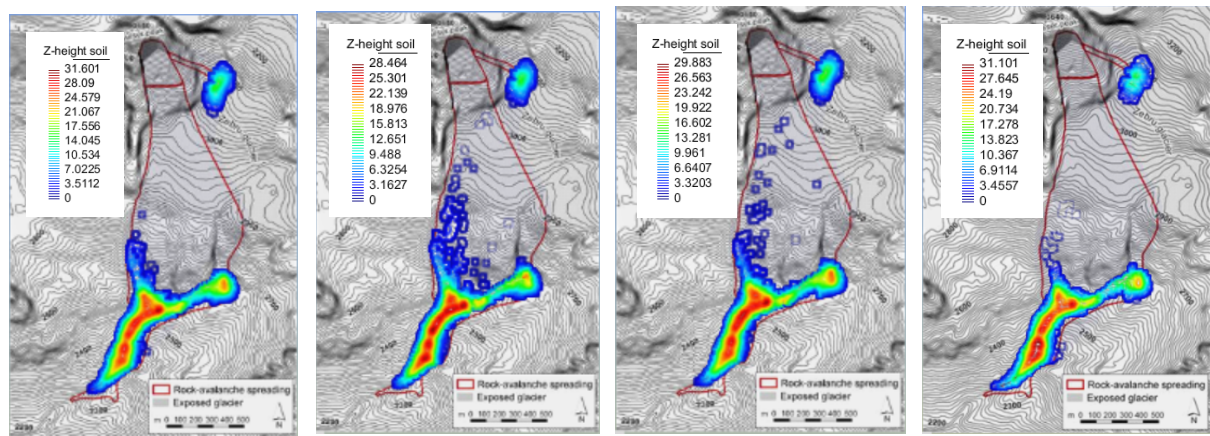
1988, Pastor et al 2009) and for the velocity profile given in Manzanal et al, (2016). It is interesting to note the similarity with Voellmy’s law (Voellmy 1955).

There exists an interesting similitude between simple shear rheological laws of the type of above equation and Perzyna elasto-viscoplastic models in 1D (Perzyna, 1963), where the rate of viscoplastic shear strain which can be used for frictional fluids. By neglecting the elastic components, the shear strain rate is given by:

$$\tau_b = s_b \left(1 + \left(2\mu_{pZ} \bar{v} / h \right)^{1/N} s_b^{\frac{n2-N}{N}} \right)$$

where $N = n1 + n2$ and p_{atm} is the atmospheric pressure or an alternative reference pressure. The velocity profiles depend now on $n1$, being given by $v = v_{max}(1 - (1 - z/h)^{n1+1})$, where v_{max} is the velocity at the top ($z = h$). It is important to note that the curvature of the velocity profile depends on $n1$.

Thurwieser and Frank rock avalanches have been studied with four rheological models (i) the simple frictional rheology, (ii) the Voellmy rheology (Voellmy, 1955), (iii) cohesive-frictional viscous rheology (Chen 1988, Pastor et al. 2009) and viscoplastic- Perzyna rheology given by proposed equation. These laws have been implemented in a SPH depth integrated code, and they will be applied to simulate real rock avalanches and to assess the influence of the rheology on the avalanche properties. The constitutive parameters have been obtained from analysis. Since the material involved is mostly dry fragmented rock, the simulations have been carried out with zero pore pressure ratio. Figure 1 provides the comparison of computed results and field measurements as example of Thurwieser avalanche. Detailed comparisons of both avalanches are in Manzanal et al 2016.



a) Frictional rheology b) Voellmy rheology c) Viscous Frictional Rheol. d) Viscoplastic-Perzyna rheol.

Fig. 1. Thurwieser avalanche after 90s. for different rheological models: Computed results (colour isolines and deposit height) versus field measurements (black isolines and red line for the spreading).

CONCLUSIONS

The model presented combines a depth-integrated model with basal friction laws obtained from different rheological models to reproduce the propagation of rock avalanches with GEOFLOW-SPH code (Pastor et al 2009). The real cases of Thurwieser and Frank rock avalanches are analysed. The validation presents accurate prediction of runout, depth and velocity of both rock avalanches. The viscoplastic constitutive model presented derives from the continuum mechanics rather than empirical results as previous rheological laws. This approach

allows reproducing the transition between initiation and propagation of the failure in a consistent manner and represents a generalization of the previous rheological law.

ACKNOWLEDGEMENTS

The authors gratefully acknowledge the economic support provided by the Spanish Ministry MINECO (Projects GEOFLOW and ALAS). The first author gratefully acknowledges the support of CONICET and UNPSJB.

REFERENCES

- Bagnold, R.A.: Experiments on a Gravity-Free Dispersion of Large Solid Spheres in a Newtonian Fluid under Shear. *Proc. R. Soc. A Math. Phys. Eng. Sci.* 225, 49–63 (1954).
- Chen, C.L (1988), Generalized viscoplastic modeling of debris flows. *J.Hyd.Eng. ASCE* 114, 3, 237-258
- Coussot, P.: *Rheometry of pastes, suspensions and granular matter*. Wiley&Sons Inc (2005).
- Gingold R. A. and Monaghan J. J., "Smoothed Particle Hydrodynamics - Theory and Application to Non-Spherical Stars." *Mont. Not. of the Royal Astron. Soc.*, 1977, 375-389
- Hungr, O. (1995). A model for the run-out analysis of rapid flow slides, debris flows, and avalanches. *Canadian Geotechnical Journal*, 32: 610–623.
- Lucy L. B., Numerical Approach to Testing of Fission Hypothesis. *Astron. J.*, 1977, 1013-1024
- Manzanal, D; Dremptic, V.; Haddad, B.; Pastor, M.; Martin Stickle, M.; Mira, P. (2016). Application of a new rheological model to rock avalanches: an SPH approach. *J. of Rock Mechanics and Rock Engineering*. DOI: 10.1007/s00603-015-0909-5.
- McDougall, S., and Hungr,O. (2004). "A model for the analysis of rapid landslide motion across three-dimensional terrain." *Canadian Geotechnical Journal* 41.6 (2004): 1084-1097.
- Pastor M., Haddad B., Sorbino G., Cuomo S. and Dremptic V. (2009a), "A depth-integrated, coupled SPH model for flow-like landslides and related phenomena." *International Journal for Numerical and Analytical Methods in Geomechanics*, (2009a), 143-172.
- Pastor M., Manzanal D., Fernandez Merodo J.A., Mira P., Blanc T., Dremptic V., Pastor Elizade M.J., Haddad B., Sanchez M., 2010, From solid to fluidized soils: Diffuse failure mechanisms in geostructures with applications to fast catastrophic landslides, *Granular Matter* , Vol. 12, Number 3, pp. 211-228, ISSN: 1434-7636
- Pastor, M., Stickle, M. M., Dutto, P., Mira, P., Merodo, J. F., Blanc, T., & Benítez, A. S. (2013). A viscoplastic approach to the behaviour of fluidized geomaterials with application to fast landslides. *Continuum Mechanics and Thermodynamics*, 1-27.
- Perzyna, P. (1963).: The constitutive equations for rate sensitive plastic materials. *Q.Appl. Math.* 20, 321–332.
- Rodríguez Paz, M.X. and Bonet, J. (2005). "A corrected smooth particle hydrodynamics formulation of the shallow-water equations". *Computers and Structures* 83, pp.1396– 1410.
- Savage, S.B. and Hutter, K. (1991). "The dynamics of avalanches of granular materials from initiation to runout. Part I: Analysis", *Acta Mechanica* 86, pp 201-223.
- Sossio, R. and Crosta,G (2007)., "Thurwieser Rock avalanche", in the Information package, Geotechnical Engineering Office, Civil Engineering and Development Department, The Government of the Hong Kong Special Administrative Region.
- Voellmy, A.: Über die Zerstörungskraft von Lawinen. (1955).

GEOMECHANICAL MODELS FOR SHALLOW RAINFALL-INDUCED LANDSLIDES AT THE CATCHMENT SCALE BUILT IN FEEDBACK-LOOP FROM GEOLOGICAL-GEOMORPHOLOGICAL INVESTIGATION

Marco Nicotera*, Alessandro Tarantino[†], Antonio Santo*, Brunella Balzano[†],
Melania De Falco*, Giovanni Forte*

* Università degli Studi di Napoli Federico II, Napoli, Italy

[†] University of Strathclyde, Glasgow, United Kingdom

The 1997 winter season recorded prolonged and intense rainfalls all over the Campania region in Italy. As a result, a large number of extremely rapid debris-earth flow-like landslides were triggered. These phenomena occurred in the late Quaternary volcanoclastic deposits, mantling the carbonate slopes of Campania region. The Sorrento Peninsula- Lattari Mts. was the most affected area by this catastrophic event: some hundreds of shallow mass movements took place during January 1997.

These phenomena have been studied and monitored for several years since then, and many models have been proposed to explain the mechanisms of slope failures. Several field campaigns and investigations have been conducted in order to gain information about the stratigraphical setting of the areas affected by the slope instabilities and laboratory tests have been performed in order to characterize the hydro-mechanical behavior of the soils involved in the landslides.

The aim of this work is to build reliable physically-based numerical models for a number of landslides events recognized from the past geological surveys. These models were built and validated against well characterized slope failures and, therefore, used to investigate the geometrical factors making the slopes more prone to failure. Potential geo-physical methods to characterize the slope geometry and their practical implementations are finally discussed.

Keywords: early-warning system, flow-like landslide, numerical models, debris-flow, slope stability.

INTRODUCTION

In the last 20 years, several flowslides involving pyroclastic unsaturated soils affected the carbonate ridges of the Campania region (South of Italy). They represent a main source of risk for the community as already many victims and economic damages have been counted over the years. Rainwater infiltration is considered the main mechanism that lead or predispose the whole slope to failure by reducing matric suction in unsaturated soils or causing an increase in pore water pressure in the saturated slope, thus reducing the shear strength (Pirone et al., 2015 and referenced papers). These landslides are characterized by high velocity and fluidity, they

were initially triggered by small falls or slides and subsequently evolved through an amplification phase, with an avalanche effect (Di Crescenzo and Santo 1999; 2005).

Winter 1996/97 is remembered for its high intense rainfalls. After a 4-month period of prolonged low intensity rainfall events, a very high intensity rainfall occurred on the 10th of January, triggering hundreds of landslides along the slopes of the Sorrento Peninsula – Lattari Mts. This work aims to understand and model the failure mechanisms behind landslide events, involving geotechnical and geomorphological/geological studies interacting in feedback loop. The results are adopted to validate the landslides occurrences at the catchment scale.

GEOLOGICAL SETTING AND TRIGGERING RAINFALL EVENTS

The study area is located on the Tyrrhenian coast of Campania where, during Plio-Quaternary times, as consequence of several tectonic movements, many carbonate ridges were originated in the area: the Sorrento Peninsula–Lattari, the Partenio, the Caserta, of Pizzo D’Alvano and Maggiore Mts. They are made of more than 1500-m-thick Mesozoic dolomites and limestones. The most recent deposits on the limestone peaks are continental detritus and pyroclastic deposits; the latter are a few metres thick and linked to Late Pleistocene–Holocene eruptions of the Campi Flegrei and Somma-Vesuvio volcanic centers.

From 1997 to 1999, many landslides, often turning into extremely rapid flow-like phenomena, repeatedly affected the carbonate slopes of Campania region. In particular, the Sorrento Peninsula was the most affected area of the 1997 regional slope-instability crisis. Some hundreds of shallow mass movements took place during January 1997. The most important mass movement occurred during the January 9–11, 1997, regional event. In fact days prior the event, an intense precipitation occurred in Campania. Rainfall was especially heavy in the western portions of the region, namely, the Sorrento Peninsula and the Lattari Mountains. A maximum 3-day cumulative rainfall of about 280 mm was recorded in these locations, following a 4-month period of particularly high rainfall values. In the same days, many hundreds of landslides were triggered in other areas of the region. Most of the landslides (about 400) occurred in the Sorrento Peninsula–Lattari Mountains.

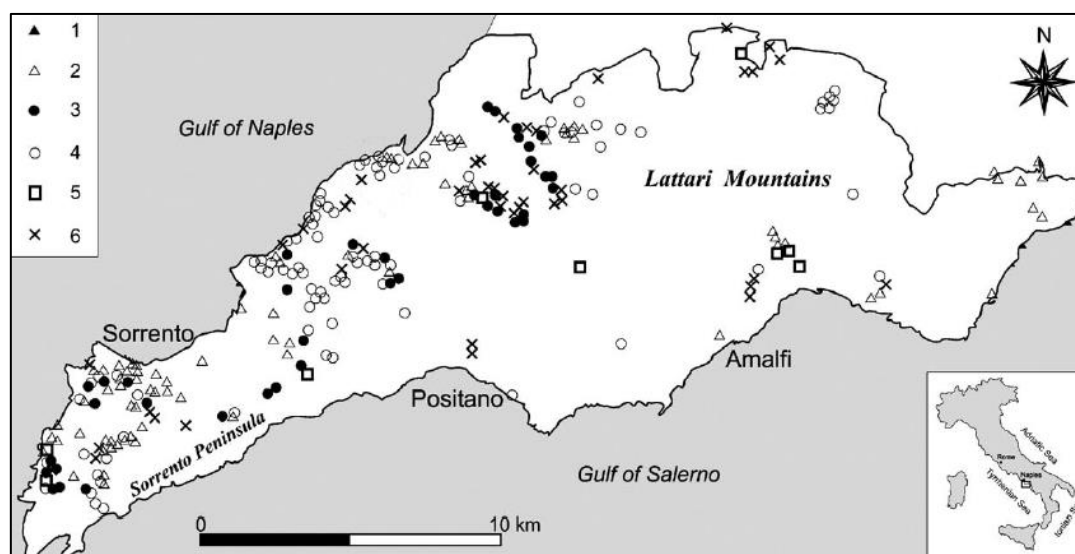


Fig.1 Inventory map of the January 1997 landslides in the Sorrento Peninsula. (1) Debris or earth fall; (2) rock fall; (3) rotational landslide; (4) translational slide; (5) flow; (6) complex landslide.(Calcaterra and Santo, 2004)

GEOLOGICAL AND GEOTECHNICAL CHARACTERIZATION

Although most of the landslides activated across the peninsula involved moderate volumes of soil, a number of catastrophic events occurred, which were associated with landslides evolving in debris flows.

The catastrophic nature of these events led the local authorities to commission studies to assess landslide hazard and develop early warning systems. As a result, several field campaigns took place after the landslide events, all over the region, in order to acquire information about stratigraphy, geomorphology, landslides geometry and collect soil samples for the geotechnical characterization.

Geological surveying campaigns allowed characterizing the geometry of the landslides bodies, estimating their volumes and locating the possible failure surfaces.

Soil samples were taken from the pyroclastic deposits to characterize the hydro-mechanic behaviour of the materials forming the different pyroclastic layers. The surveying has shown that all the areas affected by shallow landslides are characterized by the presence of 3 main soil layers:

- A) an upper layer of pyroclastic soils, made of ash and reworked pumices (A2). Its upper part have been modified by pedogenetic processes (A1). It comes from the 79 AD Vesuvius eruption. The action of vegetation and micro-organisms has affected the hydraulic and mechanical behavior of this layer;
- B) an intermediate layer of white pumices, of 1-6 cm of diameter, related to the 79 AD Vesuvius eruption;
- C) a bottom layer of ashes deposits coming from an older eruption, with significant clay fraction.

Figure 2 shows a schematic stratigraphy for the area under study. It is worth noticing that the layer of white pumices or compacted ashes may be missing in some areas.

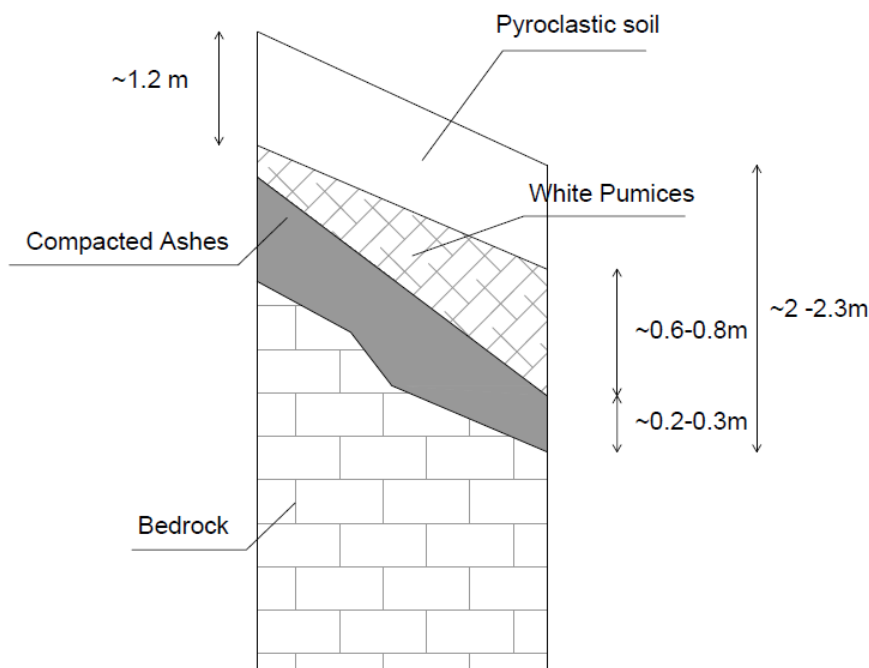


Fig. 2 Typical stratigraphy of the areas affected by landslide events.

Laboratory tests have been carried out on these soils. The main average hydraulic and mechanical properties are reported in the Table 1.

Tab. 1 Soils properties

Property/ Soil type	Ashes(C)	Pumices(B)	Pyroclastic cover(A)
Dry density γ_d [kN/m ³]	9.012	5	9.056
Void Ratio e [-]	1.8	2.8	2.5
Friction Angle φ' [°]	36	37	38
Saturated hydraulic conductivity k_{sat} [m/s]	4.07 e-9	1.3 e-4	5.5e-7
Volumetric Water Content at saturation θ_s	0.672	0.8	0.653
Residual Volumetric Water Content θ_r	0.196	0.1	0.001

Due to the presence of vegetation the pedogenized upper layer is assumed to have shear strength higher than unrooted soil due to the root reinforcement.

CONCLUSIONS

This work has focused on 2 landslides case studies where the effect of the stratigraphy appears to be predominant. The soil profile has been characterized based on the geological survey after the landslides event. The hydro-mechanical models for the chosen case studies have been validated with respect to their ability to reproduce failure conditions when subjected to the same antecedent and triggering rainfall events. The hydro-mechanical models were then exploited to investigate the geometrical factors that are making the slopes more likely to fail upon a rainfall event. These factors need to be measured to quantify the susceptibility to failure of given area. We finally propose a range of possible technologies for diffuse measurements of soil profiles that might be practically deployed in the field.

REFERENCES

- Di Crescenzo G., Santo A. (1999) Analisi geomorfologica delle frane da scorrimento- colata rapida in depositi piroclastici della penisola Sorrentina. *Geografia Fisica e Dinamica Quaternaria* 22, 57-72.
- Di Crescenzo G., Santo A. (2005) Debris slides-rapid earth flows in the carbonate massifs of the Campania region (Southern Italy): morphological and morphometric data for evaluating triggering susceptibility. *Geomorphology* 66, 255-276.
- Calcaterra D., Santo A. (2004) The January 10, 1997 Pozzano Landslide, Sorrento Peninsula, Italy. *Engineering Geology* 75 (2004), 181-200.
- Pirone M., Papa R., Nicotera M.V., Urciuoli G. (2015) In situ monitoring of the groundwater field in an unsaturated pyroclastic slope for slope stability evaluation. *Landslides*, 12, 259–276

SOIL-ATMOSPHERE INTERACTIONS. COMPREHENSIVE MODELLING AND PRACTICAL RULES

Vaunat, J*, Ruiz, D.*, Samat, S.*, Saaltink M.* & Virely, D.†

* Universitat Politècnica de Catalunya (UPC), Barcelona, Spain

† CEREMA, Toulouse, France

The paper presents a framework to model the response of slopes under climatic actions, based on the consideration of a non-linear, time variable boundary condition which retrieves the different thermo-hydraulic fluxes crossing soil-atmosphere interface. Model is validated on several cases of slopes in soils and rocks and hints provided for an effective use of the model.

Keywords: Climatic action, Natural slope, Numerical modelling, Finite Elements, Field cases

INTRODUCTION

The interactions between the ground and the atmosphere play a central role in the analysis of natural risks associated to slope movements. As pointed by Leroueil (2002), slopes respond often to changes in pore pressure whose relationship to rainfall is complex. It depends, on the one hand, on material properties such as permeability and consolidation coefficients and, on the other hand, on the interactions with atmosphere, including infiltration, runoff, evaporation and evapotranspiration. Vegetation plays often a non-negligible role by intercepting part of the rainfall, limiting the runoff, releasing back vapour to the atmosphere and providing the soil with root reinforcement, when not creating settlements or increasing soil permeability by desiccation. Details in stratigraphy and three-dimensional slope geometry are moreover important factors that determine zones of run-off concentration and preferential infiltration.

The objective of the paper is to present a modelling framework suitable to be implemented in numerical tools for geotechnical analysis and aiming at simulating the effect of climate on slopes. After a brief description of the physical processes acting at the interface between ground and atmosphere and of the equations used to model them, emphasis is put on the practical use of this kind of models through the analysis of several real cases.

PHYSICAL PROCESSES AND MODELLING FRAMEWORK

The processes controlling atmosphere conditions include solar radiation, heat and moist exchange (controlling clouds and precipitation), air mass motion as well as their interactions with earth surface, including outcropping soils and rocks, free water surfaces and vegetation canopies. All these processes are coupled and form complex, turbulent and instable systems whose modelling is far beyond the scope of the geomechanical modelling of slope response under climatic actions. A suitable alternative consists in representing the effect of the atmosphere by a special boundary condition prescribed at soil surface. This condition retrieves all the fluxes crossing the surface (solar short wave and long wave radiation,

sensible heat, water infiltration, evaporation) and the state of the atmosphere above the ground (temperature, relative humidity and air pressure) (Blight, 1997). In the same spirit, vegetation effect can be simplified into nonlinear sink terms of water mass applied in the root zone (Noilhan & Mahfouf, 1996).

The atmosphere/vegetation boundary condition defined in that way must be consistent with the continuum formulation considered to model the underlying ground. Particularly, all the fluxes crossing the boundary must be balanced by ground internal fluxes of the same nature (see Tab. 1). Their modelling in deformation problems like slope analysis requires the consideration of fully coupled thermo-hydro-mechanical models. The THM formulation used is based on the work by Olivella et al. (1996) and includes the solution of the mass balance of water and air, the energy balance and the stress equilibrium, supplemented by constitutive laws and restrictions. Thermo-hydraulic laws are summarized in Tab. 2 in case in which local thermal equilibrium is considered between air, water and solid phase. They are completed by the stress-strain-temperature-suction law of the soil matrix.

Tab. 1 Soil-atmosphere fluxes and their counterpart within the ground.

Fluxes at ground-atmosphere interface	Fluxes within the ground
Infiltration and ponding	Liquid water filtration (Darcy's law)
Sensible heat	Heat conduction (Fourier's law)
Evaporation	Vapour diffusion (Fick's law)
Heat convected by liquid and gas fluxes	Heat convection by liquid and gas fluxes
Vapour convection by gas flow	Vapour convection by gas flow

Tab. 2 Constitutive laws and restrictions used in thermo-hydro-mechanical models.

Terms	Hydraulic laws and restrictions	Thermal laws and restrictions
Storage term	Soil-water retention curve	Heat capacity for water, air and solid phase
	State equations of liquid water and vapour	State equation for solid phase
	Psychrometric law	Latent heat for water vaporization
Flow term	Darcy's law	Fourier's law
	Variation of hydraulic conductivity with degree of saturation, temperature and porosity	Variation of thermal conductivity with degree of saturation, temperature and porosity

The numerical analysis of slope response under climatic action would thus ideally require solving thermo-hydro-mechanical boundary value problems where a time-variable atmospheric condition is applied at ground-atmosphere interface. Variation period must be generally small in order to include daily atmospheric variations and short events rainfall. On the other hand, the need for a realistic representation of infiltration and run-off would often induce to consider three-dimensional geometry. These aspects generally lead to models requiring large computational resources and the identification of a significant number of parameters. In this context, model validation and reduction are essential issues for the effective use of numerical models in the study of soil and rock slopes under climatic actions.

MODEL VALIDATION

The strategy used to model soil-atmosphere interactions has been validated by benchmarking numerical results with measurements obtained in several experimental fields. The case reported here corresponds to an experimental field located at "Le Fauga", France (Calvet et al., 2007). It is a flat ground composed by quaternary deposits of gravels relying on a substratum of yellow marl and topped with 0.5 m thick layer of silt. Precipitation, atmospheric pressure, incoming solar (short wave) and atmospheric (long wave) radiation, air

temperature, relative humidity, wind speed and direction were monitored on a half-hour basis. Sensible and latent heat have been also estimated using both the eddy-covariant and the aerodynamic methods. Vegetation parameters (height, biomass, dry matter, water content and Leaf Area Index) were measured weekly on samples of size 25 x 25 cm² randomly taken in the fallow area. Soil moisture and temperature profiles are automatically measured each 30 minutes by impedance sensors installed at depths: 5, 10, 20, 30, 50, 60, 70, 80 and 90 cm.

Fig. 1 shows the comparison between computed values and measurements for several variables: surface evapotranspiration flux, temperature below the surface and volumetric water contents at different depths. They evidence on the one hand an acceptable representativeness and accuracy of the model. On the other hand, they highlight typical patterns of water content variations in soils. At ground surface, fluctuations respond both to daily and seasonal atmospheric actions. In depth, the amplitude of variations decreases progressively and the daily signature gradually borrowed. This response is consistent with the diffusive character of the water mass balance equation and provides hints to reduce computational costs by removing part of the frequency spectrum of meteorological records according to the depth at which pore pressure variations are relevant for the mechanical problem.

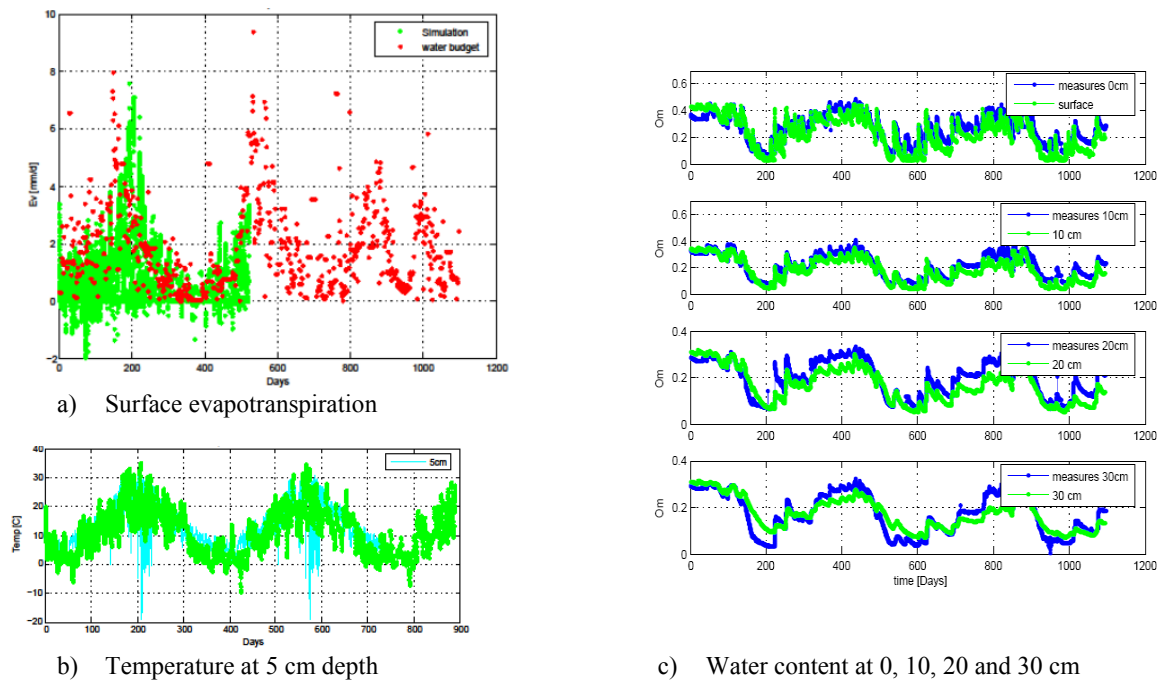


Fig. 1 Comparison between numerical results and measurements at “Le Fauga” experimental field.

APPLICATION TO SLOPES

Model has been applied to different cases of slopes in slope and rocks. A first case corresponds to a rock fall what occurred in a calcareous cliff above the village of La Roque Gageac, France (see Fig. 2.a). To estimate the risk of a larger failure, several extensometers have been installed to monitor displacements (and temperatures) in the massif. Numerical model evidences the strong relationship existing between strain and temperature variations in the massif, in turn controlled by atmosphere temperature and incoming solar radiation, which

allows defining scenarios of rock falls. Sensitivity analysis highlights moreover the robustness of the model against parameters controlling soil-atmosphere heat exchanges.

Two other cases (Fig. 2) refer to shallow landslides in essentially granular materials (Cervinara, Italy; Damiano et al., 2017; and Senet, Spain; Oorthuis et al, this issue). In both cases, failure is clearly related to suction and pore pressure values, whose variations are strongly controlled by the retention curve of the materials and the presence of preferential water paths at some depths. Monitoring should thus ideally include measurements of both water contents and suctions at close points in depth, in order to correctly identify the retention curve in the field. Numerical model appears to exhibit a good predictability of hydraulic changes in the slope, provided that the ratio between run-off and infiltration is well-estimated. In order to capture it, a special layer has been introduced in the model on top of the ground surface. Discussion on the estimation of the initial state in the slope is also reported.



a) Rock fall at La Roque Gageac, France



b) Debris flows and floods at Senet, Spain

Fig. 2 Two cases of slope failure induced by atmospheric actions and modelled within the present framework

ACKNOWLEDGEMENT

The financial support of the Spanish Ministry for Economy and Competiveness through the research grant BIA2015-67500-R is acknowledged.

REFERENCES

- Blight, GE (1971) Interactions between the atmosphere and the Earth. *Géotechnique* 47, 715–767.
- Calvet JC, Fritz N, Froissard F, Suquia D, Petitpa B, Piguet B (2007) In situ soil moisture observations for the CAL/VAL of SMOS: the SMOSMANIA network. *International geoscience and remote sensing symposium, IGARSS*, Barcelona, Spain. doi: 10.1109/IGARSS.2007.4423019
- Damiano E, Greco R., Guida A., Olivares L, & Picarelli L. (2017) Investigation on rainwater infiltration into layered shallow covers in pyroclastic soils and its effect on slope stability. *Eng. Geol.*, pp. 208–218
- Leroueil S (2001) Natural slopes and cuts: movement and failure mechanisms. *Géotechnique* 51, 197–243.
- Noilhan, J. & Mahfouf, J.F. (1996). The ISBA land surface parameterization scheme. *Global and Planetary Change* 13, 145–159.
- Olivella S, Carrera J, Gens A & Alonso EE (1994) Non-isothermal Multiphase Flow of Brine and Gas through Saline media. *Transport in Porous Media*, 15, 271–293.
- Oorthuis R, Hürliman M, Moya J & Vaunat J (2017) In situ-monitoring of slope mass-wasting. Examples from the Pyrenees. *This issue*.

EFFECT OF SHEAR BAND THICKNESS ON THE TERMO-HYDRO-MECHANICAL COUPLED ANALYSIS OF LANDSLIDES

Núria M. Pinyol*[†], Mauricio Alvarado*[†], Eduardo E. Alonso*[†]

* Centre de Metodes Numerics en Enginyeria, Barcelona, Spain

[†] Universitat Politècnica de Catalunya, Barcelona, Spain

Thermal effects induced by the own motion of an unstable mass have been included in the analysis of the post-failure behavior in early works, most of them with the aim of looking for the causes of the rapid acceleration of Vajont landslide (Italy, 1963). Some limitations of these contributions, including recently published papers, lies in the fact that (a) the analyzed landslide geometries are simple and (b) the plastic work dissipation, inducing heat, is concentrated in a shear band defined by the contacts between rigid bodies. This contribution generalizes previous ideas and presents a numerical approach capable of including thermally induced pore water pressure in landslide analyses. Special attention is given to the effect of the shear band thickness, which becomes relevant in numerical simulations.

Keywords: rapid landslides, material point method, THM coupling, shear band thickness.

INTRODUCTION

Starting at the early contribution of Voight & Faust (1982), several authors have explained the acceleration of landslides invoking the frictional heating of the slip zone. By formulating mass, energy and momentum balances in the shear band the following phenomena are accounted for: once a soil mass becomes unstable, the pore water pressure in shear bands increases because of the frictional heat generated and the thermal expansion of the saturated soil. The associated decrease in effective stress leads to a loss of frictional resistance at the slip zone and, consequently, the acceleration of the sliding mass. A summary table on contributions to the analysis of thermally-induced catastrophic landslides is presented in Alonso et al. (2016). In all of these contributions simple geometries are analyzed and the approach followed consists of combining the dynamic equilibrium of the entire unstable mass with the coupled thermo-hydro-mechanical (THM) phenomena occurring in the shear band and the surrounding soil. These approaches imply that the application of the described phenomena cannot be generally applied. Note that in the prediction of a slope behavior, the position of the basal sliding surface is not known a priori and shear bands can be distributed inside sliding mass and not only in the assumed “basal” surface. The THM phenomena eventually develops in the entire domain. With the aim of overcoming such limitations, Pinyol et al. (2017) have recently presented a numerical approach capable of modelling the thermal pressurization effects on landslides in a general way.

A key aspect of the motion lies in the thickness of the shear band. This aspect is analyzed in detail here. To do that, analytical solutions for simple cases, under particular assumptions, are discussed. A planar landslide analyzed by means of the finite differences method (Alonso et al., 2016) is considered to take advantage of the fact that, in this approach, the shear band

thickness is imposed and it does not depend on the numerical discretization. Finally, the consequences of shear band thickness in the numerical modelling in MPM is highlighted.

EFFECT OF SHEAR BAND THICKNESS

The effect of shear band thickness can be derived explicitly for the case of a block sliding on a horizontal surface at an imposed constant velocity (v) assuming adiabatic conditions and impervious material. The following differential equation (Eq. 1) can be obtained by formulating the governing equations (mass, heat and momentum balance equations and the Mohr-Coulomb failure criterion) and assuming that the source term in the heat balance equation is equal to the frictional work dissipated in the shear band where plastic strains localize:

$$\frac{du_w(t)}{dt} = \frac{\beta \tan \phi' v}{(m_v + n\alpha_w)(\rho c)_m 2e} [\sigma_n - u_w(t)] \quad (1)$$

where the unknown variable is the thermally induced excess pore water pressure in time, $u_w(t)$, σ_n is the total normal stress, $2e$ is the thickness of the shear band, m_v is the oedometric compressibility coefficient, n is the porosity, ϕ' is the effective frictional angle, $\beta = (1-n)\beta_s + n\beta_w$ is the volumetric thermal expansion coefficient for the mixture computed as a weighted average of the volumetric thermal expansion coefficients of solid particles (s) and water (w). The parameter $(\rho c)_m = (n\rho_w c_w + (1-n)\rho_s c_s)$ is the specific heat of the soil where ρ is the soil density and c indicates the specific heat.

Equation (1) can be solved analytically and the thermally induced excess pore water pressure is given by:

$$u_w(t) = \sigma_n \left[1 - \exp\left(-\frac{\beta \tan \phi' v}{(m_v + n\alpha_w) \rho c_m 2e} t\right) \right] \quad (2)$$

Figure 1 shows the effect of the shear band thickness on the excess pore water pressure for the particular case defined in the figure. The effect of the shear band thickness is significant. Given a displacement rate, the shear band thickness determines the magnitude of the dissipated work per unit of volume which, in turn, determines the temperature increments. In this sense, highest increments of temperature and pore water pressure are expected inside the thinnest shear bands.

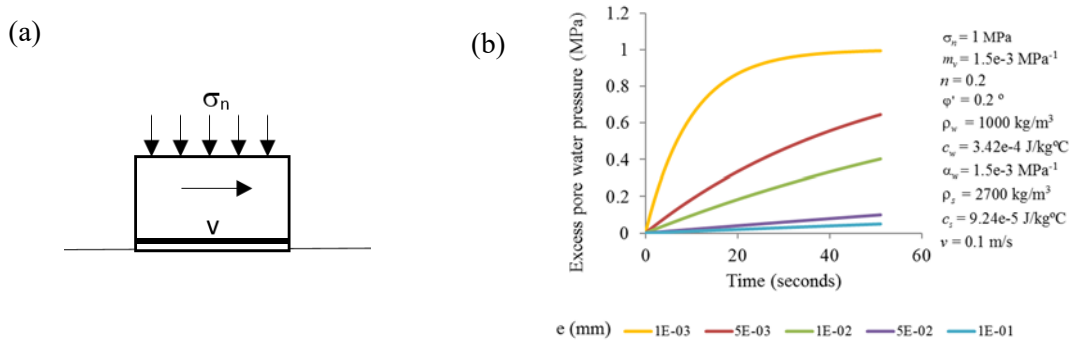


Fig. 1 (a) Sliding block at imposed constant velocity; (b) Effect of the shear band thickness.

Similar results are obtained when a more general case is analyzed in which temperature and pore water pressure dissipation is allowed. This is the case of the planar landslide shown in Figure 2 for two values of permeability ($k=10^{-7}$ and 10^{-11} m/s). These results have been

computed following the procedure presented in Alonso et al. (2016). The low dissipation of the excess pore water pressure for permeability $k=10^{-11}$ m/s leads to higher velocities if compared with the case in which the excess pore water pressure dissipation is stronger (for $k=10^{-7}$ m/s). Notice that the isothermal case is also plotted in Figure 2a. It is observed that the effect of the shear band thickness becomes relevant for values higher than 1 cm. This result suggests that it is not necessary to specify the exact thickness of the shear band (always difficult to identify in the field) when it is very thin (say in the order of mm or fraction of mm).

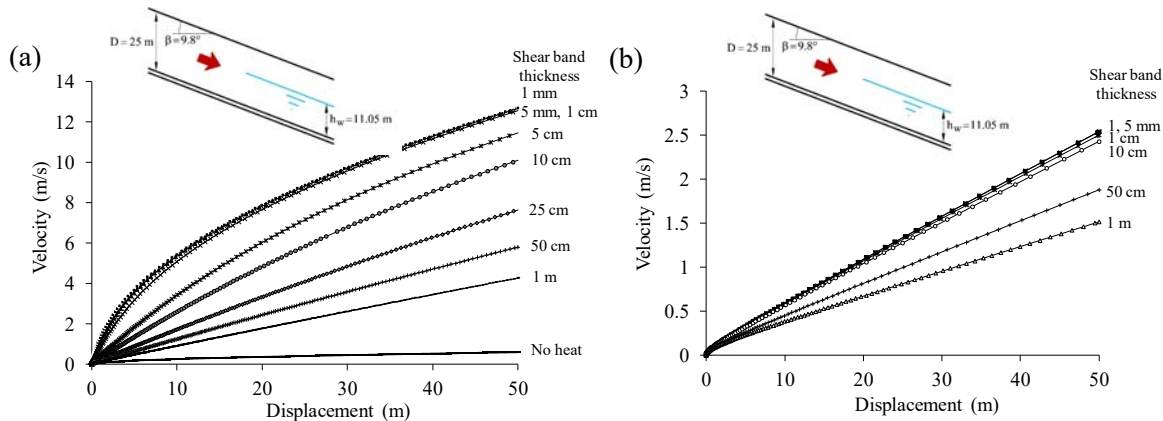


Fig. 2 Planar landslide. Effect of the shear band thickness on the velocity. (a) $k=10^{-11}$ m/s and (b) $k=10^{-7}$ m/s.

MPM NUMERICAL MODELLING

The thermo-hydro-mechanical dynamic behaviour of saturated porous media has been integrated into the framework of the material point method (MPM) (Sulsky et al. 1994) with the aim of providing a general numerical tool to simulate thermal interaction in landslide (Pinyol et al., 2017). The u - p formulation (Zienkiewicz et al. 1980) was extended to non-isothermal conditions by including the energy balance equation and assuming that the plastic mechanical work dissipates in heat.

The thickness of the shear band mainly depends on the grain size distributions of soils (Vardoulakis 1980; Scarpelli & Wood 1982; Alshibli & Hasan 2008). However, in numerical approaches such as FEM, FDM and MPM, the size of the shear bands developed depends on the element size and on the inclination of the band with respect to the mesh. The effect of the shear band is evaluated here for the case of a homogeneous slope 6 m high, inclined 36.9° and characterized with the Mohr-Coulomb failure criteria (28° of friction angle and 2 kPa of cohesion) and a permeability equal to 10^{-11} m/s. The motion is triggered by reducing the cohesion to 1 kPa. In order to evaluate the dependence on the size of mesh elements, the domain has been discretized using three alternative elements size: 0.5x0.5 m, 0.25x0.25 m and 0.125x0.125 m. In all the cases, four material points have been initially distributed per element.

The results in terms of displacement and excess pore water pressure are plotted in Figure 3. The motion observed in case of the coarse mesh is similar to the motion observed without including the heating effects (not plotted in the figure). The shear band thickness associated with the element size is too large to induce a significant generation of excess pore water pressure capable of accelerating the slope. On the contrary, the strength reduces significantly due to the accumulation of the excess pore water pressure in the case of the finest mesh and consequently the acceleration and the run-out increase.

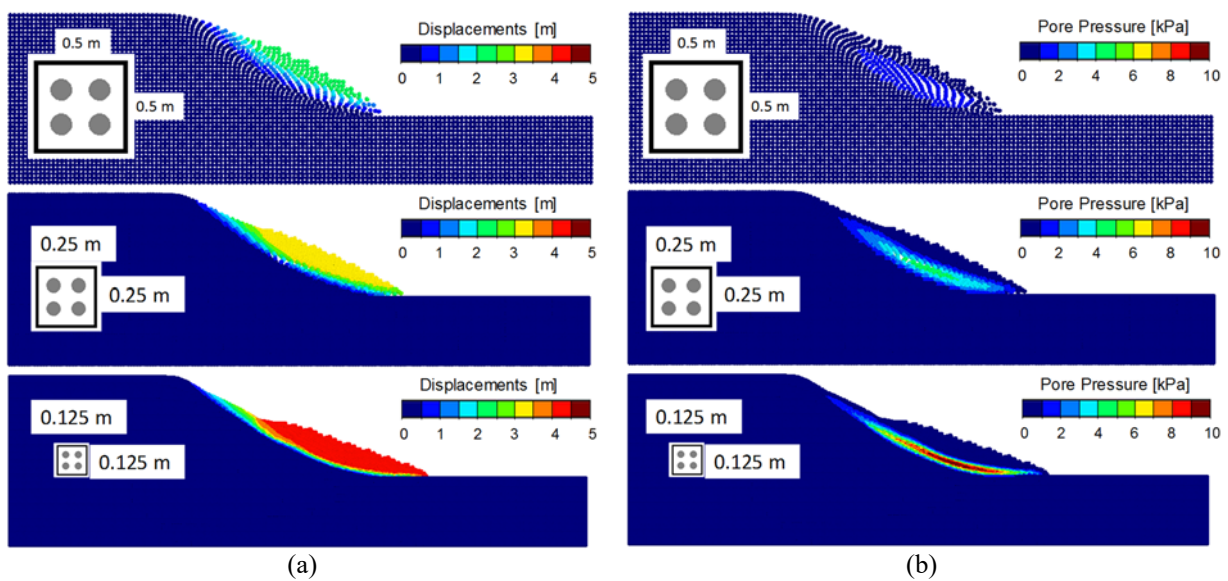


Fig. 2 MPM results. Effect of the mesh element size.

CONCLUSIONS

The shear band thickness is a key parameter in the motion of landslides when thermal effects take a relevant role. The effect of the shear band thickness is negligible when it lies in the millimeter range. However, larger changes in the magnitude of the shear band thickness lead to highly different landslide responses (the thicker the shear band, the smaller the landslides acceleration). This feature is important in numerical simulations of slope motions in which the shear band thickness depends on the mesh size. A proper simulation using standard continuous numerical methods as FEM, DFM or MPM require the discretization of the domain where shear bands will be generated using an element size similar in size to the expected shear band thickness.

ACKNOWLEDGMENT

The authors acknowledge the financial support to CIMNE via the CERCA Programme/ Generalitat de Catalunya and to the Spanish Government for the research fellowships awarded to the first and second authors.

REFERENCES

- Alonso EE, Zervos A & Pinyol NM (2016) Thermo-poro-mechanical analysis of landslides: from creeping behaviour to catastrophic failure. *Géotechnique* 66(3), 202–219.
- Alshibli KA & Hasan A (2008) Spatial variation of void ratio and shear band thickness in sand using X-ray computed tomography. *Géotechnique* 58(4), 249–257.
- Pinyol NM, Alvarado M, Alonso EE & Zabala F (2017) Thermal effects in landslide mobility. A MPM approach. *Géotechnique* (sent to publish)
- Scarpelli G & Wood DM (1982) Experimental observations of shear band patterns in direct shear tests. In *Proceedings of the IUTAM Conference on Deformation and Failure of Granular Materials*. Delft, Holland: Balkema, pp. 473–484.
- Sulsky D, Chen Z & Schreyer HL (1994) A particle method for history-dependent materials. *Computer Methods in Applied Mechanics and Engineering* 118(1–2), 179–196.
- Vardoulakis I (1980) Shear band inclination and shear modulus of sand in biaxial tests. *International Journal for Numerical and Analytical Methods in Geomechanics* 4, 113–119.
- Voight B & Faust (1982) Frictional heat and strength loss in some rapid landslides. *Géotechnique* 32, 43–54.
- Zienkiewicz O, Chang C & Bettess P (1980) Drained, undrained, consolidating and dynamic behaviour assumptions in soils. *Géotechnique* 30(4), 385–395.

TAILINGS DAM POST-FAILURE FLOW DYNAMICS: ANALYSIS OF THE RHEOLOGICAL BEHAVIOUR

M. Pirulli*

* Politecnico di Torino, Department of Structural, Geotechnical and Building Engineering, Torino, Italy

With the intent to investigate the complex rheological behaviour of tailings flows released following a dam failure, a new version of the one-phase continuum-mechanics-based RASH^{3D} code has been implemented and applied to simulate the 1985 Stava (Italy) tailings dam collapse. Four alternative rheologies were tried: Frictional, Bingham, Turbulent and Voellmy. The two-parameter Voellmy rheology gave the best results in terms of debris runout, velocity and super-elevation on banks and of minimum changes of rheological values along the runout path.

Keywords: tailings dams, flow dynamics, numerical modelling, rheology

INTRODUCTION

Tailings are the wastes resulting from the chemical and mechanical processes of mining extraction. Some several thousand million tonnes of mining wastes are produced each year worldwide, that are often stored in upstream/downstream valleys, or in ring impoundments and, in all these cases, are retained by a dam. Guaranteeing the stability of such impoundments is one of the most challenging tasks in mine waste management, proof of which is the fact that mining industry to date has experienced significant dam failures (Rico et al., 2008a). The liquefied material that originates from the failure of tailings is usually composed of highly water-saturated, oozy sediments, which can exhibit various kinds of fluid behaviour, ranging from debris flows to hyper-concentrated flows (Rico et al., 2008b), and is characterized by a high energy content. In most cases the flow is laminar in nature, and the liquefied tailings behave approximately like a Bingham plastic fluid, exhibiting both a yield stress and viscous flow characteristics, once this stress has been exceeded.

However, the entrainment of large quantity of free water, the confinement of the run-out path and the mass entering an active flowing watercourse can significantly alter the flow properties of the fluid. A turbulent behaviour can result and the description of the flowing mass can be then obtained adopting a Manning resistance relation. The Hanks & Pratt (1967) or the Takahashi (2007) criteria can however help to determine whether a flow will be laminar or turbulent.

Because of the wide range of rheological behaviour that tailings flows can assume, a new version of the single-phase continuum-mechanics based RASH^{3D} code (Pirulli 2005), which was designed to study flow-like landslide run-outs, has been implemented and is here used to simulate the well documented case of a pair of tailings dams whose failure, on 19 July 1985, generated a catastrophic flood in the area of Stava, Northern Italy (Berti et al., 1988; Chandler

& Tosatti, 1995). The upgraded code integrates the existing rheological kernel (Frictional, Voellmy) with two new rheological laws (Bingham and Turbulent), and adds the possibility of changing, in a GIS (geographic information system) environment, the rheological parameters of the flowing mass during the propagation process.

In an attempt to understand whether a single rheology is able to simulate the whole process, from triggering to deposition, without any changes in its rheological values along the run-out path, or with a minimum number of changes, numerical analyses with Frictional, Bingham, Turbulent and Voellmy rheologies have been carried. The obtained results are discussed and compared with Takahashi's (1991) 1) velocity estimates of the flowing mass attained at various points along its path, and 2) physical measurements of flow super-elevations measured in channel bends.

TAILINGS DAMS AT STAVA

The Stava Creek is located in the North-Eastern Italian Alps, in the upper valley of the Avisio River (Fig. 1).

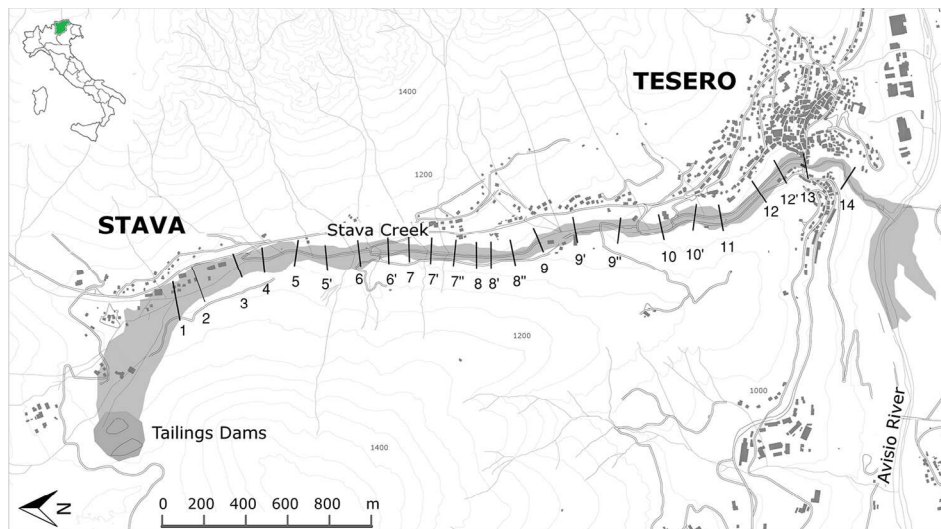


Fig. 1 Location of the Stava tailings dams with reconstruction of the area impacted by the 1985 flowing event (shaded area). Numbered sections identify sectional reaches used in Tab. 1 and Fig. 2.

On July 19, 1985, the Stava two-basins tailings dams of fluorite, located at an elevation ranging from 1330 to 1380 m a.s.l., failed (Genevois & Tecca, 1993). The villages of Stava and Tesero, located along the creek and at its end, respectively, were completely wiped out or buried. The released mass, estimated in about 185.000 m³ of mud debris, surged down the 600 m long 10° mountain slope, which was covered by grass in the upper part and by forest in the lower part, clashed into the cliff on the left side of the Stava Creek and changed its flow direction perpendicularly, by channeling along the Stava Creek. After weaving right and left for about 3800 m along the creek, it finally stopped at the junction with the Avisio River (Fig. 1). Although the flowing mass had an intensive destructive power, as well as a high fluidity, the Stava Creek channel itself did not suffer from much erosion or deposition (Berti et al., 1997). Furthermore, Takahashi (1991) underlined that the involved material was so fine that it had a relative depth of about 10⁵. In this condition, the resistance to flow is similar to that of a plain water flow, and the Manning equation can be applied. The Manning roughness coefficients to use along the Stava Creek were determined by Takahashi (1991) through reverse calculation from flow velocity data, which in their turn were obtained with the Lenau formula (1979) at the flow super-elevations on bends (Tab. 1).

Tab. 1 Mean velocity and Manning's roughness coefficient defined by Takahashi (1991). Sectional reaches are indicated in Fig. 1

Sectional Reach	2-3	3-5	6'-7	7'-8	8-9	9-9"	9"-10	10-10'	10'-12	12'-13
Mean Velocity (m/s)	18	23	31	25	22	22	18	11	6.2	6.8
Manning Coefficient, n (-)	0.04	0.04	0.04	0.04	0.04	0.04	0.04	0.08	0.13	0.12

ANALYSIS OF RASH^{3D} NUMERICAL RESULTS

Four rheologies were tested: Turbulent, T (Manning coefficient, n , varied between 0.02 and 0.13); Frictional, F (bulk friction angle, ϕ , varied between 7° and 10°); Bingham, B (yield stress, τ_B , varied between 1 and 2 kPa; viscosity, μ_B , varied between 0.05 kPa·s and 0.1 kPa·s) and Voellmy, V (friction coefficient, μ , varied between 0.03 and 0.05; turbulence coefficient, ξ , varied between 100 m/s² and 2000 m/s²). Taking advantage of the GIS function that has also been implemented in RASH^{3D}, some of the analyses were run changing the rheological parameter values along the run-out path.

A first set of analyses was run with a Frictional rheology but it was not possible to identify a combination of parameters able to reproduce the overall trend of the flow velocity along the propagation path, even using the different values of friction angle along the runout path.

Moving to the Bingham rheology, it was evidenced, according with the literature that interprets the Stava event as turbulent, that this rheology cannot reproduce the flowing process in a satisfactory way, as well. This aspect is further underlined in Fig. 2a by the impossibility of matching the best fit results ($\tau_B = 1$ kPa; $\mu_B = 0.1$ kPa·s) to Takahashi on-site estimated velocities.

Changing to the Turbulent rheology, one of the analyses was then carried using the Manning coefficient values suggested by Takahashi (1991) (Tab. 1). Obtained results are quoted in Fig. 2 in terms of both velocity (Fig. 2a) and flow super-elevation on left and right side banks (Fig. 2b and 2c, respectively). A comparison with Takahashi's on-site measured super-elevations and estimated velocities evidences a rather good agreement between the RASH^{3D} computed values and Takahashi's estimated values, along the whole propagation path.

To overcome the impossibility of this rheology to reproduce the cessation of motion on gently sloping surfaces and trying to limit the number of rheological value changes along the runout path, the last set of analyses was carried out with a Voellmy rheology. The best fit results in terms of runout, flow velocity (Fig. 2a) and super-elevation on banks (Figs. 2b and 2c) were obtained with the combination of rheological parameters 0.05-2000 m/s² up to Sectional reach 10 (Fig.1) and 0.03-100m/s² from here to the final deposition of the mass. Even if this rheology needs a change of the rheological values along the runou path, it largely reduces the number of changes with respect to the others rheology and to the Turbulent rheology in particular.

CONCLUSION

With the intent to investigate the complex rheological behaviour of tailings flows released following a dam failure, a new version of the one-phase continuum-mechanics-based RASH^{3D} code, which integrates the existing rheological kernel (Frictional, Voellmy) with two new rheological laws (Bingham and Turbulent), and adds the possibility of changing the rheological properties of the flowing mass during the propagation process, using an integrated GIS function, has been applied to simulate the 1985 Stava tailings dams collapse.

Comparison between obtained results and Takahashi (1991) interpretation of the event has identified the Voellmy rheology as the law that better simulates the study case in terms of runout, velocity, depth distribution, by also reducing the changes in rheological values along the runout path.

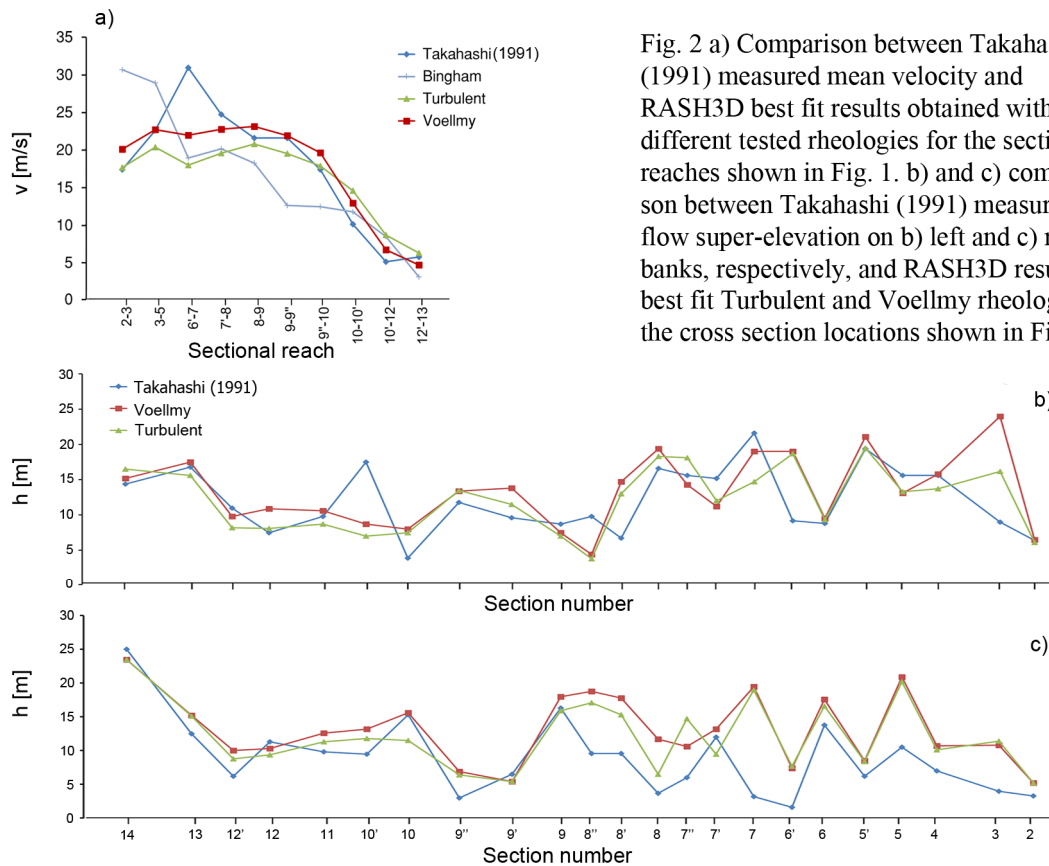


Fig. 2 a) Comparison between Takahashi (1991) measured mean velocity and RASH3D best fit results obtained with the different tested rheologies for the sectional reaches shown in Fig. 1. b) and c) comparison between Takahashi (1991) measured flow super-elevation on b) left and c) right banks, respectively, and RASH3D results for best fit Turbulent and Voellmy rheologies at the cross section locations shown in Fig. 1.

REFERENCES

- Rico M, Benito G, Díez-Herrero A (2008a) Floods from tailings dam failures. *J Hazard Mater* 154: 79-87.
- Rico M, Benito G, Salgueiro AR, Díez-Herrero A & Pereira HG (2008b) Reported tailings dam failures: a review of the European incidents in the worldwide context. *J Hazard Mater* 152: 846-852.
- Hanks RW & Pratt DR (1967) On the flow of Bingham plastic slurries in pipes and between parallel plates. *Journal of Society of Petroleum Engineers*, December, 342-346.
- Takahashi T (2007) *Debris flows: Mechanics, prediction and countermeasures*. Balkema, Rotterdam.
- Pirulli M (2005) *Numerical modelling of landslide runout: A continuum mechanics approach*. Ph.D. thesis, Politecnico di Torino, Italy.
- Berti G, Villa F, Dovera D, Genevois R & Grauns J (1988) The disaster of Stava. *Proceedings of the Spec. Conf. on Hydraulic Fill Structures*, New York, ASCE SP21: 492-509.
- Chandler RL & Tosatti G (1995) The Stava tailings dams failure, Italy, July 1985. *Proc. Instn. Civ. Engrs. Geotech. Engng*, 133: 67-79.
- Takahashi T (1991) *Debris flows*. IAHR Monograph, Balkema, Rotterdam.
- Genevois R & Tecca PR (1993) The tailings dams of Stava (northern Italy): an analysis of the disaster. *Environmental Management Geo-water and Engineering Aspects*. R.N. Chowdhury & M. Sivakumar (eds.). Rotterdam, Balkema, pp. 23-36.
- Berti M, Genevois R & Tecca PR (1997) The 1985 flow slide and debris flow at Stava (Italy). *Proceedings of the 1st Internat. Conf. on "Debris Flow Hazard Mitigation: Mechanics, Prediction and Assessment"*. Cheng-lung Chen (eds). 7-9 August 1997, San Francisco (Cal.), Am. Soc. Civ. Engrs, New York, pp. 309-321.
- Lenau CW (1979) Super critical flow in bends of trapezoidal section. *J. Eng. Mech. Div.*, ASCE, 105: 43-54.

HYSTERESIS PROCESSES AND EFFECTIVE RAINFALL HISTORIES

Guido Rianna*, Alfredo Reder*[†], Luca Pagano[†], Luca Comegna[°]

* CMCC Foundation, Capua (CE), Italy

[†]Università degli Studi di Napoli, Napoli, Italy

[°]Università degli Studi della Campania, Aversa (CE), Italy

The research is aimed to investigate how accounting for (or not) hydraulic hysteresis could influence the prediction of pore water pressures in partially saturated pyroclastic soils of Campania Region. The issue is particularly interesting as, in last years, they have been frequently affected by rainfall induced landslides. The analysis is based on i) deep investigations performed on such soils through field monitoring, laboratory test and physical models allowing to calibrate and validate a widely adopted literature model and ii) numerical analysis designed to detect the main features distinguishing the predictions of pore water pressures carried out taken into account hydraulic hysteresis.

Keywords: pyroclastic covers, hysteresis, Soil-water characteristic curve, landslide triggering weather patterns

1. INTRODUCTION

In last years, weather-induced landslides largely affected pyroclastic covers of Campanian Region, Southern Italy (Sarno, 1998; Cervinara, 1999; Nocera, 1997 and 2005; Ischia, 2006). Under usual conditions, the partially saturated state of the soil and then the contribution provided by suction to soil tightening can significantly increase soil shear strength permitting them to be stable also on very steep relieves. Wetting phenomena (primarily precipitation), increasing soil water content, can remarkably reduce such contributions up to attain local slope failure conditions (Pagano et al., 2010).

Due to the complexity of the investigated issues, the investigations about hydraulic soil state conditions inducing the events require the adoption of numerical methods. To this aim, the soil hydraulic behavior of an unsaturated soil is usually modelled by assigning two main functions: i) soil–water characteristic curve (SWCC) and ii) hydraulic conductivity function. However, many researches proved how both relationships exhibit a hysteretic behavior (e.g. Poulouvasilis, 1962) while different studies have widely demonstrated in the laboratory, field and numerical investigations the relevance of the hysteresis for both soil hydraulic (Lenhard and Parker, 1987b) and mechanical response (Likos et al., 2014). The main goal of our research is to deepen the role of hydraulic hysteresis on the triggering of landslide events involving silty pyroclastic soils. It is accomplished by first studying the hysteretic behavior of the soils in hand, basing it on experimental results coming from laboratory tests and a physical model (Rianna et al., 2014) interpreted by suitable hysteretic model. Subsequently, through numerical analysis aimed to evaluate the hydrological behavior of a silty pyroclastic cover under the action of virtual atmospheric conditions. Finally, by comparing these theoretical results with ones obtained in the hypothesis of non-hysteretic behavior.

2. METHODS AND DATA

Among the several approaches proposed in literature (Iwata et al., 1995), the Lenhard-Parker (LP) approach (1987a,b) is adopted. It predicts the wetting and drying scanning curves scaled from the respective main wetting (w) and drying (d) curves defined through the Mualem-van Genuchten approach (1980):

$$\frac{\theta - \theta_r}{\theta_s - \theta_r} = \theta = (1 + (\alpha s)^n)^{-m} \quad k = k_s \theta^\lambda \left(1 - (1 - \theta^{1/m})^m\right)^2 \quad (1)$$

where θ_r (θ_s) represents residual (saturated) volumetric water content; k (k_s) hydraulic conductivity (saturated hydraulic conductivity); n , $m(=1-1/n)$, and α [kPa^{-1}] and $\lambda(=0.5)$ are empirical parameters. The definition of the functions for the two branches (subscript d for drying and w for wetting) entails the assessment of 5x2 parameters. However, the LP approach requires two simplifying assumptions: $\theta_r = \theta_r^d = \theta_r^w$ and $n = n^d = n^w$. Furthermore, it prevents the non-closure of moisture retention scanning loops in simulations of cyclic paths (artificial pumping errors, APE), and permits considering the air entrapment effects employing the algorithm proposed by Land (1968) also in terms of differences in relative permeability.

In this work, the approach has been calibrated and validated for a pyroclastic soil (Table 1), a silty sand part of stratigraphic series found on Monteforte Irpino (Avellino Province, Campania Region) relieves and deeply investigated through laboratory tests (Nicotera et al., 2010) and field monitoring by Pirone et al. (2015). The main drying curve ($\theta_r, n, \theta_s^d, \alpha^d$) is obtained from ku-pF apparatus while the remaining parameters are estimated through an inverse analysis (Hopmans et al., 2002) carried out using suction and volumetric water content measurements collected during an entire hydrological year through the physical model developed by Rianna et al. (2014).

In Figure 1a, the values, observed and returned after calibration and the related estimated main wetting curve are reported. The matching appears quite satisfying on the entire range. Nevertheless, also for validation periods (Figure 1b-c), the paths are recognized well reproduced by the LP approach. The parameters are listed in Table 1.

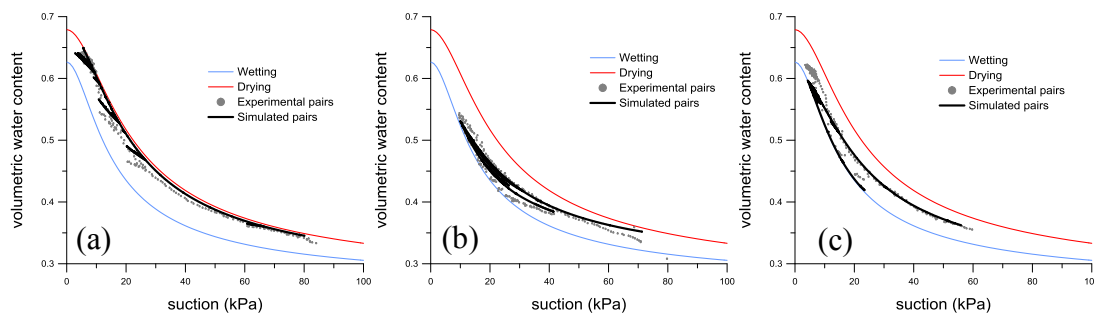


Fig. 1 Experimental (grey) and findings (black) returned on calibration hydrological year period 2010-2011(a) and validation: 2011-2012 (b); 2012-2013 (c). Main drying (red) and wetting (blue) curves are also reported

Tab. 1 Main soil parameters for investigated pyroclastic soil

Field average thickness	0.6m	α^w / α^d	0.07/0.1 (kPa^{-1})
Field porosity	0.7	θ_s^w / θ_s^d	0.69/0.63
Gs	2.57	θ_r	0.26
n	1.9	k_s	1e-6 m/s

3. RESULTS

The evaluation on the effects of accounting (or not) hysteretic dynamics for landslide triggering in pyroclastic soils is carried out investigating how they can impact the prediction of pore water pressures, on short time scale, under the effect of heavy rainfall events (potential triggering event) and on longer time scales (seasonal) to provide a frame of differences in terms of potential antecedent conditions.

In this perspective, several sets of numerical analysis have been carried out in Hydrus 1D code (Simunek et al.,2005) on a homogeneous soil column 2m long. At the bottom, a capillary barrier condition is used (consistently with field conditions usually retrieved on field) while at the ground surface soil atmosphere dynamics are reproduced following the Feddes et al. (1974) approach. By way of example, the results concerning the application at ground surface of a constant ingoing flux equal to saturated permeability are displayed. Four different SWCC sand related permeability functions are considered: i) hysteretic, taking into account (HAE) or not (H) air entrapment; ii) non-hysteretic main drying (D);iii) non-hysteretic mean curve (M). In this perspective, it is worth noting that, if air entrapment is taken into account, the van Genuchten parameters regulating a hypothetical “non-hysteretic” wetting curve cannot be analytically retrieved.

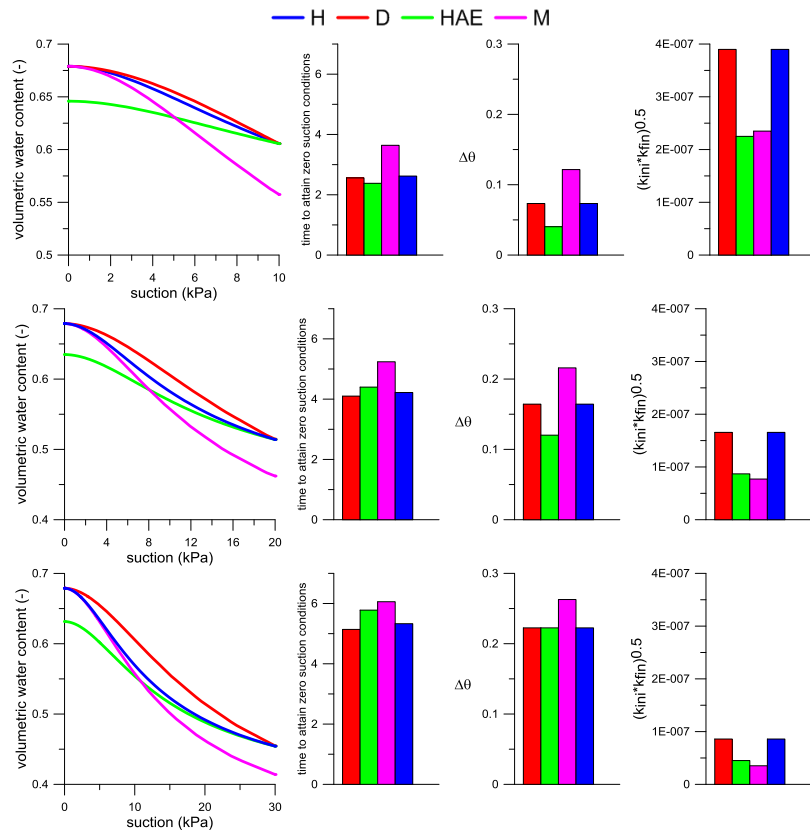


Fig. 2 suction-water content paths leading to a zero suction value (first column), the time required to attain such conditions (second column), the difference between final and initial water content (third column) and geometric average between initial and final hydraulic conductivity (fourth column). The three rows refer to three different initial conditions, respectively 10, 20 and 30 kPa at 1.5 m depth

Three initial hydrostatic conditions are assumed with water table respectively posed at 2.5, 3.5 and 4.5 m below the ground surface. A reference depth of 1.5m is considered. For HAE and H, the paths start from point located on main drying curve. For the lower initial suction value (10kPa at 1.5m), HAE approach permits firstly reaching the zero suction condition (slightly

more than 2 days), after drying and mean curve, finally hysteretic not considering air entrapment approach (H) require longer times to attain the condition (about 3.5 days). The behavior appears mainly regulated by the required variation in volumetric water content (from about 0.04 for HAE to 0.12 for M); indeed, according to the assumptions, D, H and M are required to attain θ_s^d while HAE reaches an intermediate water content value (about 0.65). Such dynamics significantly change for higher initial suction values. Indeed, for both 20 and 30 kPa, the D and H paths reach the target suction with a substantial advance respect to the other ones. However, in these cases, the higher mean values of hydraulic conductivity (more than $\Delta\theta$) regulate the processes: therefore, for D and H, around twice values are retrievable.

4. CONCLUSIONS

Under the availability of field and laboratory data, a framework to calibrate and validate the widely adopted approach proposed by Parker and Lenhard (1987) is provided. The results, for a typical pyroclastic soil present on Campanian slopes (South Italy), are then employed to assess how the different approaches for estimating soil hydraulic behavior could influence the prediction of pore water pressures under persistent rainfall histories, recognized in wet season as trigger for slope instability phenomena. An example clearly displays how arisen differences could be particularly significant and they should be considered, for example, in developing predictive approaches for early warning systems.

REFERENCES

- Feddes RA, Bresler E, Neuman SP (1974) Field test of a modified numerical model for water uptake by root systems. *Water Resources Research* 10(6): 1199-1206.
- Haines WB (1930) Studies in the physical properties of soil. V. The hysteresis effect in capillary properties, and the modes of moisture distribution associated therewith. *The Journal of Agricultural Science* 20(1), 97-116.
- Hopmans, JW, Šimůnek J, Romano N, Durner W (2002) Inverse Modeling of Transient Water Flow. *Methods of Soil Analysis, Part 1, Physical Methods, Chapter 3.6.2*. J. H. Dane and G. C. Topp (eds.). SSSA, Madison, WI, pp. 963-1008.
- Iwata S, Tabuchi T, Warkentin B P (1995) *Soil-water interactions*. Marcel Dekker, New York.
- Land CS (1968) Calculation of Imbibition Relative Permeability for Two- and Three-Phase Flow From Rock Properties. *Society of Petroleum Engineers Journal* 8(2):149-156.
- Lenhard, R J; Parker JC (1987b). A Model for Hysteretic Constitutive Relations Governing Multiphase Flow 2. Permeability-Saturation Relations. *Water Resources Research* 23(12):2197-2206.
- Likos WJ, Lu N, Godt JW (2014) Hysteresis and Uncertainty in Soil Water-Retention Curve Parameters. *Journal of Geotechnical and Geoenvironmental Engineering* 140(4).
- Nicotera MV, Papa R, Urciuoli G (2010) An experimental technique for determining the hydraulic properties of unsaturated pyroclastic soils. *Geotechnical Testing Journal* 33(4), 263-285.
- Pagano L, Picarelli L, Rianna G & Urciuoli G (2010) A simplified approach for timely prediction of precipitation-induced landslides in unsaturated pyroclastic soils. *Landslides* 7(3), 273-289.
- Parker JC, Lenhard RJ (1987a). A Model for Hysteretic Constitutive Relations Governing Multiphase Flow 1. Saturation-Pressure Relations. *Water Resources Research* 23(12):2187-2196.
- Pirone M, Papa R, Nicotera MV, Urciuoli G (2015) In situ monitoring of the groundwater field in an unsaturated pyroclastic slope for slope stability evaluation. *Landslides* 12(2), 259-276 .
- Rianna G, Pagano L & Urciuoli G (2014) Investigation of soil-atmosphere interaction in pyroclastic soils. *Journal of Hydrology* 510, 480-492.
- Simunek J, van Genuchten MT, Sejna M (2005) The HYDRUS-1D Software Package for Simulating the Movement of Water, Heat, and Multiple Solutes in Variably Saturated Media, Version 3.0, *HYDRUS Software Series 1*, Department of Environmental Sciences, University of California Riverside, Riverside, California, USA, 270 pp.
- van Genuchten MT (1980) A closed-form equation for predicting the hydraulic conductivity of unsaturated soils. *Soil Science Society of America Journal* 44, 892–898.

EFFECT OF VARIABILITY IN SOIL PROPERTIES ON STABILITY OF RESIDUAL SOIL SLOPE

Alfredo Satyanaga*, Harianto Rahardjo†

* Research Fellow, School of Civil and Environmental Engineering, Nanyang Technological University, Singapore, alfredo@ntu.edu.sg

† Professor, School of Civil and Environmental Engineering, Nanyang Technological University, Singapore, chrahardjo@ntu.edu.sg

The characteristics of residual soil tend to vary with depths due to the different degrees of weathering. The variability of soil properties causes difficulty in slope stability analyses where soil data are limited. In this study, statistical analyses were carried out to establish the range of factor of safety variations due to the most severe rainfall for residual soil slopes in different rock formations in Singapore. The variations considered was mainly due to the variability of residual soil properties.

Keywords: residual soil, variability, soil-water characteristic curve, shear strength

INTRODUCTION

Residual soil is the final product of the in-situ mechanical and chemical weathering of underlying rocks, which have lost their original rock fabrics (Wesley, 1990). Thick layers of residual soil are commonly found in tropical regions with warm to hot climate. In Singapore, residual soils are also characterized based on rock formation and degree of weathering (Winn et al., 2001). The geology of Singapore consists essentially of three formations (see Fig 1): (i) igneous rocks of granite (Bukit Timah Granite or BTG) in the centre and northwest, (ii) sedimentary rocks (Jurong Formation or JF) in the west, and (iii) a semi-hardened alluvium (Old Alluvium or OA) which covers older rocks beneath in the east of Singapore (PWD, 1976). Residual soils from Bukit Timah Granite are made up of mainly silt particles with some clay contents and they are usually medium to highly plastic. On the other hand, residual soils from sedimentary Jurong formation have mainly clay contents with sands or silts and they are usually medium to highly plastic (Leong et al., 2002).

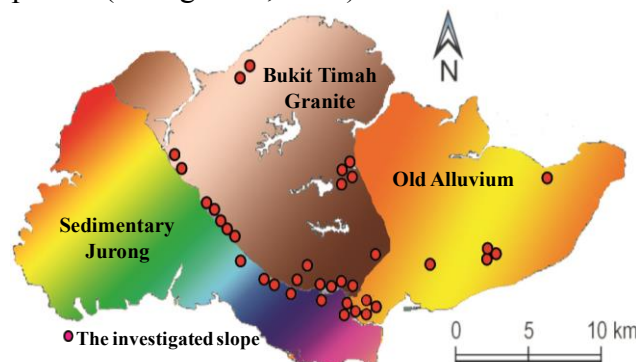


Fig. 1 Location of soil investigations in different rock formations in Singapore

Residual soils are usually found unsaturated, since they are often observed above the ground water table where the pore water pressures are negative (Rahardjo et al., 2013). During rainfall, water flows into the unsaturated zone, causing the pore-water pressure to increase and the shear strength of residual soil to decrease. As a result, rainfall-induced slope failures frequently happen in the tropical areas which mainly covered with residual soils (Rahardjo et al., 2012b, Ng et al., 2003). Brand (1985) observed that residual soils were difficult to test due to their heterogeneity. Therefore, it is desirable to have tools to estimate soil heterogeneity in a quantitative scheme which is appropriate for engineering design. The main objective of this paper is to investigate the effect of the variability of saturated and unsaturated residual soil properties on slope stability in Singapore.

SOIL INVESTIGATION

Soil samples were collected from 36 slopes which were located in different rock formations in Singapore (see Fig. 1). Soil samples were collected using Mazier sampler. The drillings of each borehole were carried out by rotary boring with foam to obtain the high quality Mazier samples. Index and engineering property tests were carried out. Index properties consisted of specific gravity (ASTM D854-02), Atterberg limits (ASTM D4318-00), and grain size distribution tests (ASTM D422-63). The engineering properties consisted of saturated and unsaturated properties, such as: soil-water characteristic curve (SWCC) and saturated and unsaturated shear strength parameters. Consolidated undrained triaxial tests with pore-water pressure measurement were conducted for saturated triaxial tests (ASTM D4767-04). SWCC tests were performed using Tempe cell and pressure plate (ASTM D6838-02) apparatuses. Consolidated drained triaxial tests on unsaturated soil specimens were carried out using a modified triaxial equipment (Fredlund and Rahardjo, 1993).

METHODOLOGY

One factor that causes the uncertainty of soil variability is the inherent soil variability. The probable range of soil properties with depth can be obtained by calculating the standard deviation of the inherent soil variability (SD_w) for every depth. In this study, the inherent soil variability was obtained by calculating the mean of soil properties for every depth. Then standard deviation of the inherent soil variability (SD_w) for every depth was calculated using the mathematical equation proposed by Phoon and Kulhawy (1999). In this paper, the inherent soil variability is also called typical soil properties. The upper and lower bound of soil properties (i.e. index properties, SWCC variables, unsaturated permeability, saturated and unsaturated shear strengths) were obtained using the confidence interval approach proposed by Harr (1987). The selection of design parameters associated with a 90 % level of confidence are commonly used in practice (Elkateb et al., 2003). Therefore, this approach was also used in this study. The lower and upper bounds of the soil properties were associated with a 90% level of confidence from typical soil properties with depth for residual soils in Singapore. The upper and lower bounds of soil-water characteristic curve and permeability function were used in seepage analyses to obtain the variations of pore-water pressures during and after rainfall for different residual soils in Singapore. The upper and lower bounds of saturated and unsaturated shear strengths (effective cohesion, c' , effective friction angle, ϕ' and ϕ^b angle) and pore-water pressure changes from seepage analyses were used in slope stability analyses

to obtain the variations of factor of safety during and after rainfall for different residual soils in Singapore.

VARIABILITY OF SOIL PROPERTIES

Figs. 2 to 4 present the typical, upper and lower bounds of the c' and ϕ' , respectively. The c' of residual soils from JF, BTG and OA decreases with depth (Fig. 2). This occurs since the percentages of fine particles for residual soil from JF, BTG and OA also decrease with depth. The typical c' of residual soil from BTG is lower than that of residual soil from JF since the residual soil from BTG is coarser than that from JF. The ϕ' and ϕ^b of residual soils from JF, BTG and OA increase with depth (Figs. 3 and 4) as the percentage of sand increases with depth. The typical ϕ' and ϕ^b of residual soil from JF is lower than that for residual soils from BTG and OA. This suggests that the particle size of residual soils from JF is finer than that of residual soils from BTG and OA.

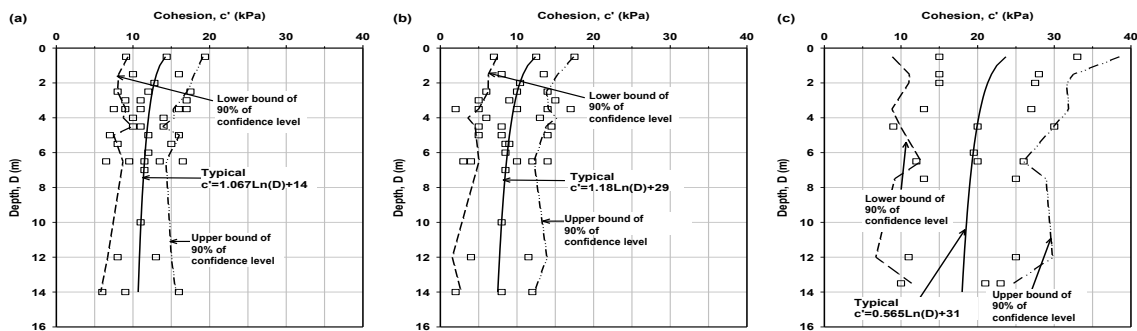


Fig. 2 Distribution of effective cohesion with depth for residual soils from (a) JF, (b) BTG and (c) OA

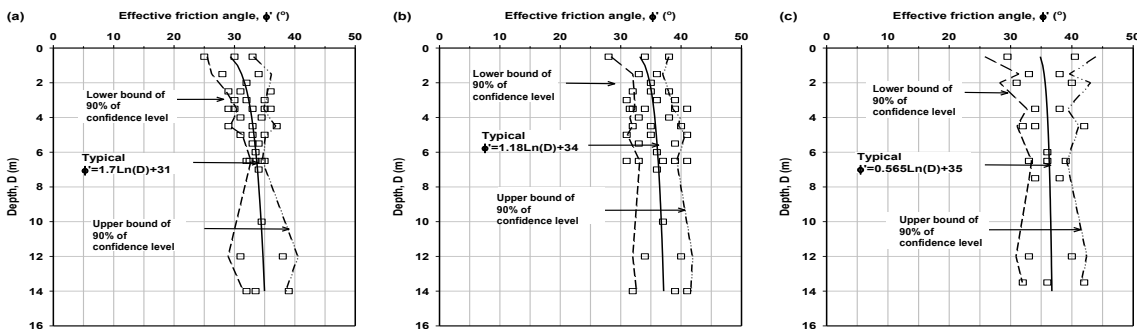


Fig. 3 Distribution of effective friction angle with depth for residual soils from (a) JF, (b) BTG and (c) OA

The SWCCs of residual soils from JF, BTG and OA were compiled and the upper and lower bounds of the SWCC for each formation were subsequently drawn on the graphs based on Fredlund and Xing (1994) equation with a correction factor = 1 as suggested by Leong and Rahardjo (1997) (see Fig. 4). It can be observed that the ranges of AEV for residual soils from BTG and OA are wider than those for residual soils from JF. This can be attributed to the greater variation of pore sizes of residual soils from BTG and OA as compared to that of residual soil from JF. Typical AEVs of residual soils from BTG and OA are lower than that of residual soil from JF indicating the pore size of residual soils from BTG and OA is larger than that observed in residual soil from JF. This is also supported by the steeper slope of SWCCs of residual soils from BTG and OA than that of residual soil from JF. The permeability func-

tions were determined indirectly using the saturated permeability and SWCC from each residual soil (see Fig. 5).

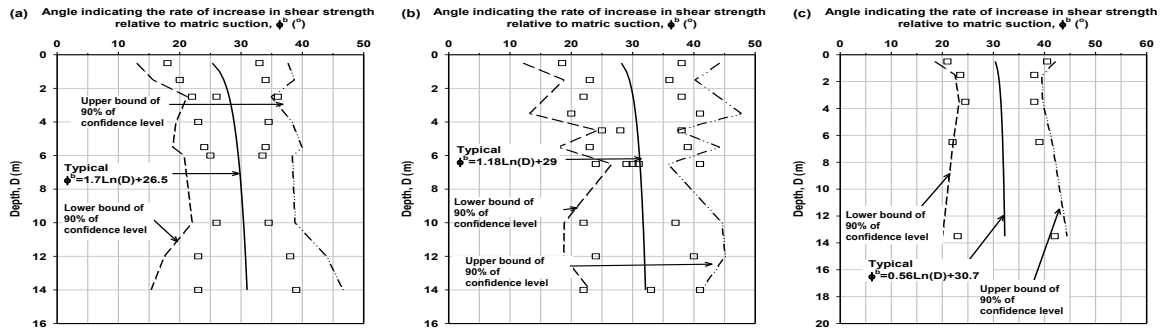


Fig. 4 Distribution of ϕ^b angle with depth for residual soils from (a) JF, (b) BTG and (c) OA

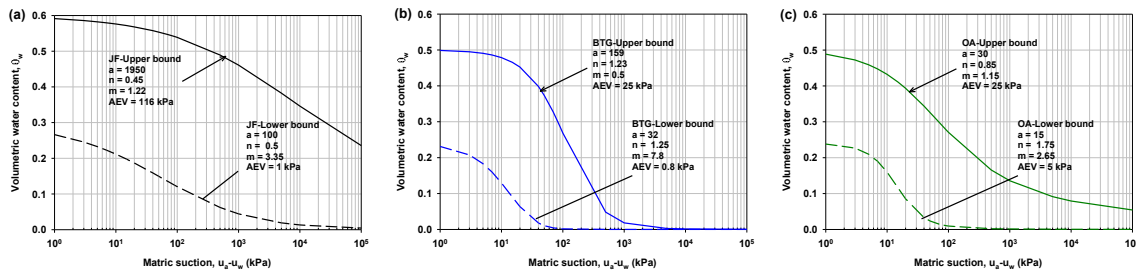


Fig. 4 SWCCs of residual soils from (a) JF, (b) BTG and (c) OA

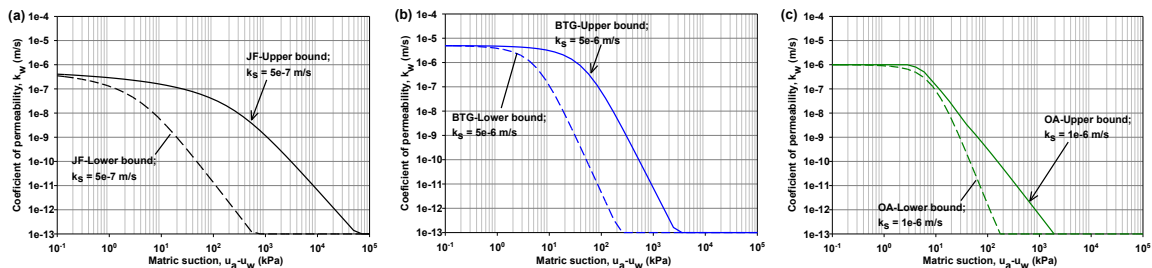


Fig. 5 Permeability functions of residual soils from (a) JF, (b) BTG and (c) OA

SLOPE STABILITY ANALYSES

Transient finite element seepage analyses were carried out to obtain the variations of pore-water pressures during and after rainfall. A most severe rainfall intensity of 22 mm/h for 24 hours was applied on the ground surface. The typical slope geometry, boundary conditions and location of groundwater table used in the numerical analyses carried out in this study are presented in Fig. 6. The slope had a height of 5 m with a slope angle of 35°. The upper and lower bounds of SWCC and permeability function for different residual soils in Singapore were used in the seepage analyses. The pore-water pressures from the seepage analyses as well as the upper and lower bounds of c' , ϕ' and ϕ^b angle from different residual soils were used as input in the slope stability analyses. Fig. 7 presents the variations of factor of safety during and after rainfall for different soil formations in Singapore. The results of analyses demonstrated that the factor of safety of residual soil slope from JF varied during rainfall in similar magnitude as that of residual soil slope from OA. On the other hand, the rate of

change in factor of safety for residual soil slope from BTG was much higher than those for residual soil slopes from JF and OA.

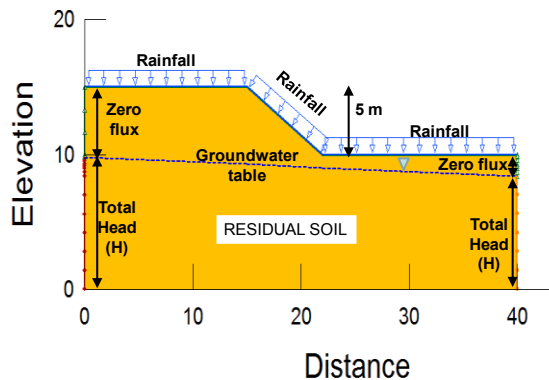


Fig. 6 Typical geometry of residual soil slope for seepage and slope stability analyses (Rahardjo et al., 2010)

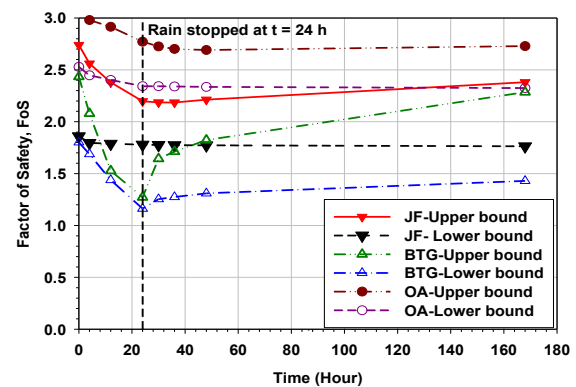


Fig. 7 Variations of factor of safety during and after rainfall

REFERENCES

- ASTM D422-63 (2002) Standard test method for particle size analysis of soils.
- ASTM D4318-00 (2000) Standard test methods for liquid limit, plastic limit, and plasticity index of soils.
- ASTM D4767-04 (2004) Standard test method for consolidated undrained triaxial compression for cohesive soil.
- ASTM D6838-02 (2008) Standard test methods for the soil–water characteristic curve for desorption using hanging column, pressure extractor, chilled mirror hygrometer, or centrifuge.
- ASTM D854-02 (2002) Standard test methods for specific gravity of soil solids by water pycnometer.
- Brand EW (1985) Geotechnical engineering in tropical residual soils. *Proc. 1st International conference Geomechanics in Tropical Lateritic and Saprolitic Soils*, Brazil, 3, 23–91.
- Elkateb T, Chalaturnyk R, Robertson PK (2003) An overview of soil heterogeneity: quantification and implications on geotechnical field problems. *Canadian Geotechnical Journal*, 40, 1–15.
- Fredlund DG & Xing A (1994) Equations for the soil–water characteristic curve. *Canadian Geotechnical Journal* 31, 533–546.
- Fredlund DG & Rahardjo H (1993) *Soil mechanics for unsaturated soils*. John Wiley & Sons Inc, New York, 517 pp.
- Harr ME (1987) *Reliability-based design in civil engineering*. McGraw-Hill Book Company, New York, N.Y.
- Leong EC & Rahardjo H (1997) Review of soil–water characteristic curve equations. *Journal of Geotechnical and Geoenvironmental Engineering* 123 (12), 1106–1117.
- Leong EC, Rahardjo H & Tang SK (2002) Characterisation and engineering properties of Singapore residual soils. *Proc. International Workshop on Characterisation and Engineering Properties of Natural Soils*, Singapore, 2, 1279–1304.
- Ng CWW, Zhan LT, Bao CG, Fredlund DG & Gong BW (2003) Performance of an unsaturated expansive soil slope subjected to artificial rainfall infiltration. *Géotechnique*, 53(2), 143–157.
- Phoon KK, Kulhawy FH (1999) Characterization of geotechnical variability. *Canadian Geotechnical Journal*, 36(4), 612–624.
- PWD (1976) *Geology of the Republic of Singapore*. Public Works Department, Singapore.
- Rahardjo H, Satyanaga A & Leong EC (2013) Effects of flux boundary conditions on pore-water pressure distribution in slope. *Journal of Engineering Geology, Special Issue on Unsaturated Soils: Theory and Applications*, 165, 133–142.
- Rahardjo H, Satyanaga A, Leong EC & Ng YS (2012a) Variability of residual soil properties. *Journal of Engineering Geology*, 141–142(124–140)
- Rahardjo H, Satyanaga A and Leong EC (2012b) Unsaturated soil mechanics for slope stabilization. *Southeast Asian Geotechnical Journal*, 43(1), 48–58.
- Wesley LD (1990) Influence of structure and composition on residual soils. *Journal of Geotechnical Engineering* 116, 589–603.
- Winn KK, Rahardjo H, Peng SC (2001) Characterization of residual soils in Singapore. *Journal of the Southeast Asian Geotechnical Society* 1, 1–13.

LANDSLIDE GENERATED WAVES: NEW INSIGHTS FROM PHYSICAL MODELS

W. Andy Take*, Ryan P. Mulligan†

* Canada Research Chair, Queen's University, Kingston, Canada

† Associate Professor, Queen's University, Kingston, Canada

Landslide tsunamis are waves created by the impact of a landslide into a body of water and represent a significant hazard in coastal areas, lakes, and dam reservoirs. The objective of this invited lecture is to describe the development of a new large scale landslide tsunami test facility and present the team's latest findings on the "effective mass" of a landslide involved in the generation of the leading wave, new theoretical advances on the momentum transfer involved with particular reference to the derivation of possible limiting conditions for the maximum wave amplitude, and new insights on the shape and evolution of waves generated by landslide impact under a range of different landslide and reservoir conditions.

Keywords: landslide, tsunami, impulse wave, reservoir

INTRODUCTION

Landslide tsunamis are waves created by the impact of a landslide into a body of water and represent a significant hazard in coastal areas, lakes, and dam reservoirs. The potential magnitude of infrastructure damage and loss of life posed by these events is clearly illustrated through the 1963 Vajont Dam disaster in which a landslide generated wave overtopped the dam and caused over 2,000 deaths in the valley downstream (Panizzo et al., 2005; Genevois and Ghirotti, 2005); historical records of the 1792 Unzen-Mayuyama landslide tsunami that resulted in 15,153 fatalities near Kumamoto, Japan (Sassa et al., 2016); and the 1958 Lituya Bay Alaska event which generated a wave that ran up the opposite slope to an elevation of 524 m above sea level (Miller, 1960; Fritz et al., 2001; Weiss et al., 2009).

CURRENT PROGRESS AND ONGOING RESEARCH QUESTIONS

A consideration of the factors involved in an assessment of the hazard posed by a potential sliding mass entering a body of water is illustrated schematically in Figure 1. Once a slip surface, geometry, and volume of the sliding mass has been identified, dynamic analyses of the mobility of the landslide debris (e.g., shallow flow dynamic models) can yield estimates of landslide velocity, v_s , and thickness, s , at the point of impact with the reservoir. These parameters, along with the density of the debris and reservoir depth, h , are key factors defining the size of the wave generated by a landslide in physical model tests defined by the slide Froude number, $F = v_s/(gh)^{1/2}$, and relative landslide thickness, $S = s/h$.

In particular, flume tests conducted by Fritz et al. (2004) led to an empirical relationship for the relative maximum near-field wave amplitude, $A_M = a_m/h$, as a function of the Froude number and the relative landslide thickness, S , given by

$$A_M = 0.25 F^{1.4} S^{0.8} \quad (1)$$

Based on a consideration of momentum transfer during the wave generation process, Heller and Hager (2010) developed an impulse product parameter, P , which extended this work to include the relative mass of the slide, $M = m_s/(\rho_w b h^2)$ where m_s is the landslide mass, ρ_w is the density of water, and b is the width of the flume. This impulse product parameter is defined as

$$P = F S^{1/2} M^{1/4} \{\cos[(6/7) \alpha]\}^{1/2} \quad (2)$$

which is dependent on the slide impact angle, α .

The near-field relationship between P and A_m was found empirically by Heller and Hager (2010) for $P < 9$ as

$$A_M = \frac{4}{9} P^{4/5} \quad (3)$$

As uncertainties in landslide volume will influence the calculated thickness and velocity of the predicted landslide mass, a range of scenarios are typically investigated to understand the sensitivity of the amplitude of the wave generated under various landslide scenarios with the largest credible potential landslide mass often defining the maximum possible hazard. However, it is currently unclear whether the entire landslide mass should be included in the calculation of impulse product. An explanation for this uncertainty is illustrated in Figure 1, in which a wave generated by a long and thin landslide will likely form and leave the near-field wave generation zone before the full volume of the landslide enters the reservoir. In this case, what fraction of the landslide mass should be used within a consideration of the momentum transfer (i.e. impulse product parameter) to calculate the amplitude of the wave in the near-field? Further physical model test data is therefore required within a new large-scale experimental facility that permits the generation of long and thin landslides to investigate this question.

A consideration of a range of landslide scenarios conducted to define the hazard posed by landslide generated waves often results in predictions of very large waves for cases in which the landslide is very large with respect to the reservoir depth. In this case, a question arises – is there a sufficient volume of water to form such a large wave? These questions illustrate that additional theoretical consideration of momentum transfer supported by new experimental research is required to explore this parameter space. However, as proposed by Heller et al. (2008), scale effects are thought to influence physical model tests at reservoir depths below 0.2 m. A consequence of this assertion is that a very large flume would be required, as large physical model landslides would be required to investigate this phenomena while keeping water depths greater than 0.2 m.

While the majority of the research on landslide wave generation has naturally focussed on the maximum amplitude of wave, the shape of the wave generated in the near-field also has significant implications for assessing landslide wave hazards. In deeper water the near-field wave behaves as a stable solitary-like wave, while in shallower water the wave behaves as a breaking dissipative bore. In the latter case, the amplitude of the wave diminishes rapidly with distance from the point of impact, while the wave formed in the former case is considerably

more stable. Additional research is therefore required to quantitatively describe the spectrum of wave shapes generated in the near field, and for data to be collected in a large physical modelling flume facility which features a long horizontal reservoir to permit the evolution of wave amplitude and shape to be quantified.

The objective of this invited lecture is to describe the development of a new large scale landslide tsunami test facility and present the team's latest findings on the "effective mass" of a landslide involved in the generation of the leading wave, new theoretical advances on the momentum transfer involved with particular reference to the derivation of possible limiting conditions for the maximum wave amplitude, and new insights on the shape and evolution of waves generated by landslide impact.

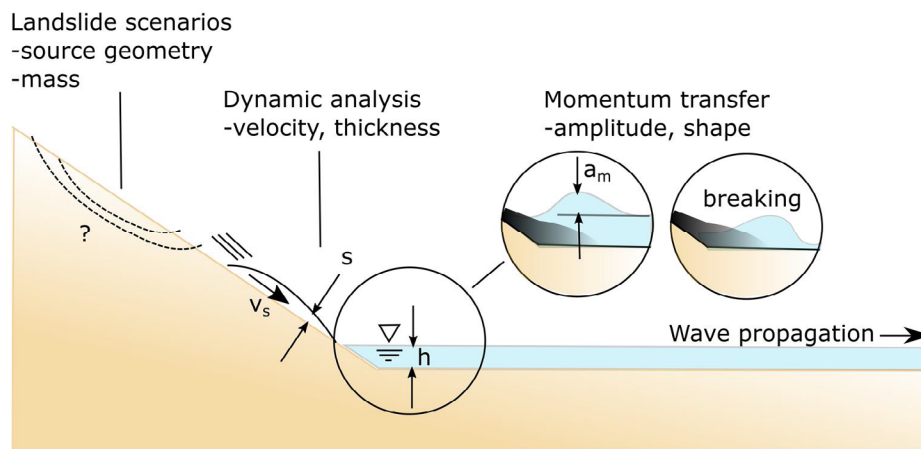


Fig. 1 Generation of tsunamis by landslides

QUEEN'S UNIVERSITY LANDSLIDE FLUME

A schematic of the Queen's University landslide tsunami flume is presented in Figure 2 (Miller et al., 2017). This large scale flume has been designed to vary the landslide source mass up to a value of 2500 kg while permitting the generation of long and thin landslides as the material is released from a source box located 6.7 m distance up a 30° incline above the reservoir water surface. High-speed imaging at 1000 frames per second is used to quantify the velocity and thickness of the granular landslide immediately prior to impact with the water reservoir. The process of wave generation is captured using video and a series of capacitance wave gauges to quantify the evolution of the amplitude, shape, and evolution of waves from the near-field for a distance of 33 m. With minimum side wall height of 1.2 m, the flume permits the testing of up to 1 m reservoir depths, while a width of 2.09 m is used to minimize the effect of sidewall friction. Granular material consisting of nominally spherical 3 mm ceramic particles was selected as this size of particle is sufficiently large to avoid significant capillarity effects on landslide mobility if the material is reused in a slightly damp moisture condition (Take et al., 2016).

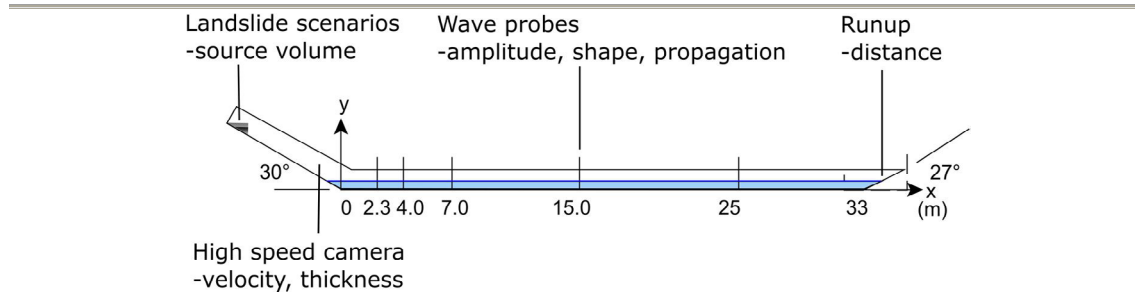


Fig. 2 Large-scale landslide test flume

CONCLUSIONS

Landslide tsunamis are waves created by the impact of a landslide into a body of water and represent a significant hazard in coastal areas, lakes, and dam reservoirs. This extended abstract provided an outline of current semi-empirical methods to predict the maximum wave amplitude, and highlighted areas requiring future research as context for the presentation of the latest findings during the workshop. This work highlights the challenges involved in the physical modelling of these events, with the purpose of stimulating discussion on the research needs for information exchange between the physical and numerical modelling communities.

REFERENCES

- Fritz HM, Hager WH & Minor H-E (2001) Lituya Bay case: rockslide impact and wave run-up. *Sci. Tsunami Hazards*, 19(1), 3–22.
- Fritz HM, Hager, WH & Minor H-E (2004) Near field characteristics of landslide generated impulse waves. *Journal of Waterway, Port, Coastal, Ocean Engineering*, 130(6), 287–302.
- Genevois R & Ghirotti M (2005) The 1963 Vaiont Landslide. *Giornale di Geologia Applicata*, 1, 41-52.
- Heller V & Hager WH (2010). Impulse product parameter in landslide generated impulse waves. *Journal of Waterway, Port, Coastal, Ocean Engineering*, 136(3), 145–155.
- Heller V, Hager WH & Minor HE (2008) Scale effects in subaerial landslide generated impulse waves, *Experiments in Fluids*, 44(5), 691-703.
- Miller DJ (1960) Giant waves in Lituya Bay Alaska. Shorter Contributions to General Geology. *Geological Survey Professional Paper 354-C*. United States Government Printing Office, Washington.
- Miller, GS, Take, WA, Mulligan, RP, McDougall, S (2017). Tsunamis generated by long and thin granular landslides in a large flume. *Journal of Geophysical Research: Oceans*, 122, 653–668.
- Panizzo A, De Girolamo P, Di Risio M, Maistri A & Petaccia A (2005) Great landslide events in Italian artificial reservoirs. *Natural Hazards and Earth System Sciences*, 5, 733-740.
- Sassa K, Dang K, Yanagisawa H, He B. A new landslide-induced tsunami simulation model and its application to the 1792 Unzen-Mayuyama landslide-and-tsunami disaster. *Landslides* 13(6):1405-19.
- Take WA, Mulligan RP, Stevenson EP & Miller GA (2016) Physical modelling of landslides into reservoirs: effect of capillarity on rheology of granular landslide at impact. *Proceedings of the 12th International Symposium on Landslides*, Napoli, Italy.
- Weiss R, Fritz HM & Wünnemann K (2009) Hybrid modeling of the mega-tsunami runup in Lituya Bay after half a century. *Geophysical Research Letters*, 36, L09602, doi:10.1029/2009GL037814.

FLUIDIZED LANDSLIDING PHENOMENA DURING EARTHQUAKES

Gonghui Wang

Disaster Prevention Research Institute, Kyoto University, Uji, Kyoto, Japan

Earthquake-induced landslides in tephra deposits are among the most hazardous geological processes; they are very catastrophic in some cases, because they can be triggered on gentle slopes with rapid and long movement. Many studies had been performed on this kind of landslides from the point of geological, geomorphological, geophysical, and geotechnical views, but much concerning the prediction of such kind of landslide remains unclear. In this study, we introduce two typical fluidized landslides triggered by the 2011 Tohoku Earthquake and the 2016 Kumamoto earthquake, respectively, in Japan. We examined the geological features of these fluidized landslides occurring on gentle slopes, and performed both in-situ direct shear tests and drained/undrained dynamic ring shear tests on the soils taken from the sliding surface. During the tests, the samples were prepared at different initial water contents, and sheared by applying static or cyclic loadings. Based on these results, we analyzed the possible initiation and movement mechanisms of these fluidized landslides.

Keywords: fluidized landslide, the 2011 Tohoku earthquake, the 2016 Kumamoto earthquake, pore-water pressure, partially saturated soils, tephra

INTRODUCTION

Earthquake-induced landslides in tephra deposits are among the most hazardous geological processes. Although in most cases they are in small size, they can be very catastrophic in some cases, because they can be triggered on gentle slopes, and the displaced landslide materials can travel long distance with rapid movement, and then become great threaten especially to these urban areas (Chigira and Suzuki, 2016). For example, the Las Colinas landslide triggered by the 2001 El Salvador earthquake flushed many houses and result in the death of more than 585 people in a residential area of Santa Tecla (Evans and Bent, 2004). By now many studies have been performed on this kind of landslides from the point of geological, geomorphological, geophysical, and geotechnical views, but it is not rare to find that many landslides triggered by the same earthquake showed relatively slow speed over short distance in the same location. Namaly, concerning the initiation and movement of such kind of coseismic landslides on tephra deposits, much remains unclear, and further study will be necessary to elevate our ability to predict their occurrence during earthquake.

Recently two large earthquakes triggered numerous landslides in tephra deposits in Japan. One is the 2011 Tohoku Earthquake, during which many landslides occurred in the wider Tohoku Region, with some concentrated in the southern part of Fukushima Prefecture, in hilly residential areas of Miyagi and Fukushima Prefectures, and on island areas of the Matsushima coast. The second one is the 2016 Kumamoto Earthquake, which triggered numerous landslides

in and around Minamiaso Village locating at the western part of Aso caldera, Kumamoto Prefecture. Although with some exceptions, the landslides triggered by these two earthquakes were basically small for the magnitude of the earthquake, many showed very high mobility, with features typical of fluidized landslides. Among these fluidized landslides, two grim cases could be exemplified by the Hanokidaira landslide and the Takanodai landslide that were triggered by the 2011 Tohoku earthquake and the 2016 Kumamoto Earthquake, respectively. To better understand the initiation and movement mechanisms of these landslides, after the earthquakes we undertook reconnaissance field examinations of the landslides, and also performed detailed investigation on some fluidized landslides. We examined the geological features of these fluidized landslides occurring on gentle slopes, and performed both in-situ direct shear tests and drained/undrained dynamic ring shear tests on the soils taken from the sliding surface. During the tests, the samples were prepared at different initial water contents, and sheared by applying static or cyclic loadings. Based on these results, we analyzed the possible initiation and movement mechanisms of these fluidized landslides.

TWO FLUIDIZED LANDSLIDES IN TEPHRA AREA IN JAPAN

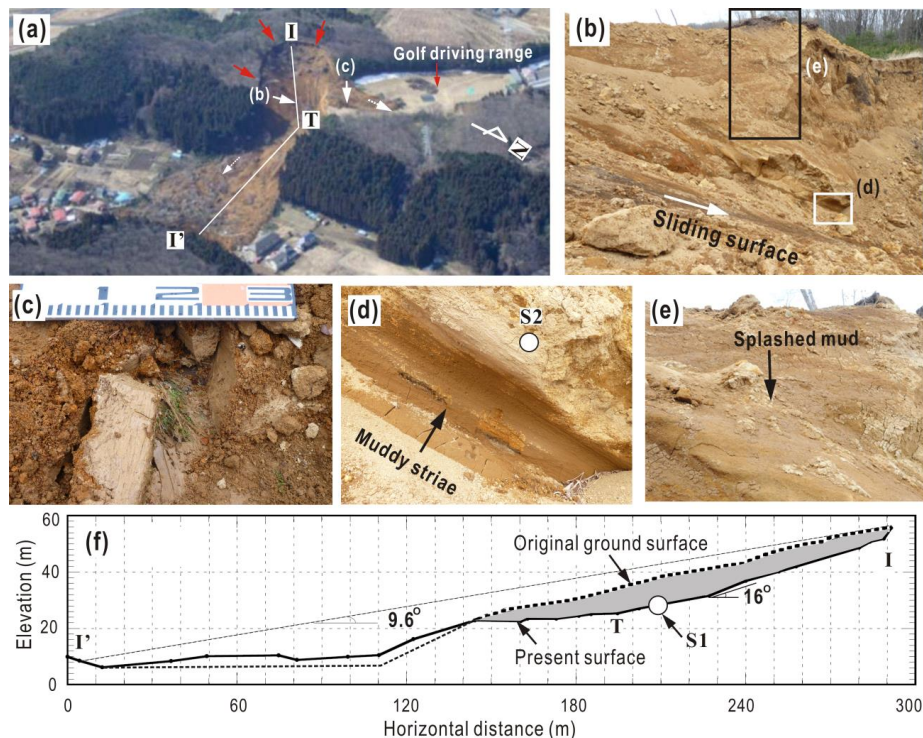


Fig. 1. Hanokidaira landslide. (a) Oblique view (after Takeshi 2011); (b) view of the left side margin and sliding surface; (c) buried grass on the golf driving range and palaeosol layer above the grass; (d) muddy striae on the left-side margin; (e) splashed mud on left-side margin; (f) longitudinal section along line I–I’.

The Hanokidaira landslide (Fig. 1a) was triggered by the 2011 Tohoku earthquake in Japan. It originated on a southeast-facing slope of a hill located about 1 km north of JR Shirakawa Station in Shirakawa City. Thirteen people were killed and 10 houses were destroyed by the debris of the landslide. A small portion of the displaced material spilled into a golf driving range, forming a thin deposit. Stratigraphically from bottom to top, the slope consists of a basal deeply weathered welded tuff, a paleosol, weathered pumice and scoria partly with paleosols, and forest soil. The bedded texture is approximately parallel to the slope surface. The primary paleosol, which overlies the welded tuff, outcropped, and had striations on its surface (Fig. 1b). We dug

into the deposits on the golf driving range and found that grass was flattened and buried by the displaced materials, but not cut or displaced from its original place (Fig. 1c). Above the grass was a displaced ~10 cm thick palaeosol layer overlain by loose pumice. Many trees had stood almost vertically while being transported. There were muddy striae on the left flank of the landslide (Fig. 1d) and also splashes of mud on the high position above the sliding surface (Fig. 1e), indicating that the displaced mass experienced slide at first and then liquefaction, and the liquefied materials (mud) were splashed during downslope movement. Fig. 1f presents a longitudinal section. The main part of the displaced materials spread into a residential area at the foot of the hill, exhibiting substantial fluid-like flow. The apparent mobilized friction angle of the slide was about 9.6° , measured from point I to I' in Fig. 1a. The volume of the displaced material was about $100,000 \text{ m}^3$.

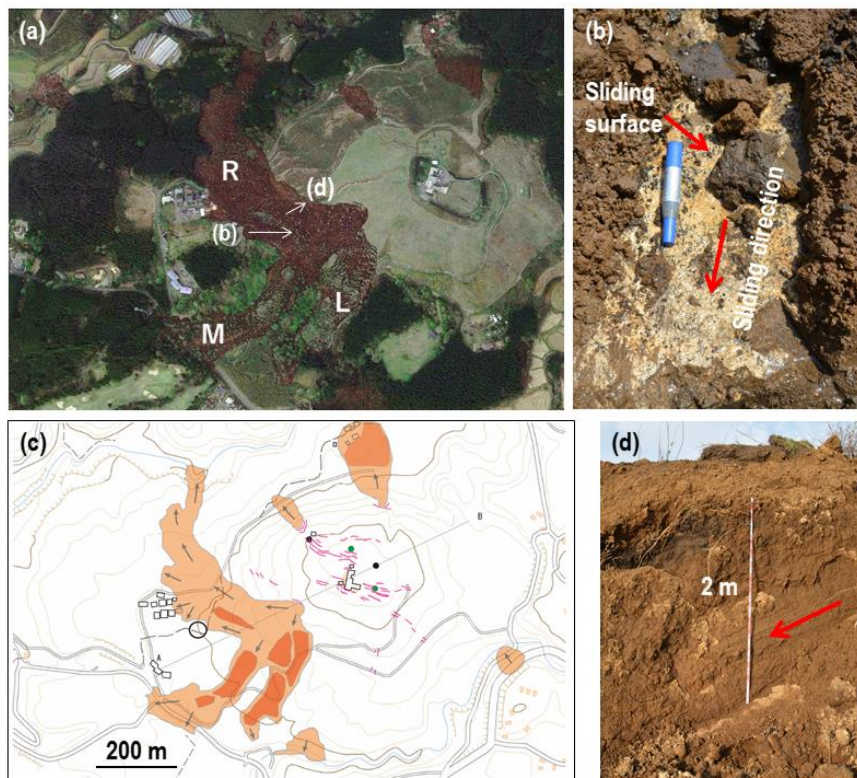


Fig. 2. Takanodai landslide. (a) Google Earth image (taken on 16 April 2016); (b) Outcropped sliding surface in location of (b) shown in Fig. 1a; (c) plan of the landslide area; (d) muddy striae on the right-side margin.

During the 2016 Kumamoto earthquake, some hundreds of landslides had been triggered, and among them the landslide occurred in Takanodai area was the most catastrophic (Fig. 2). The outcropped soil layers on the scarp is about 8 m thick and consist of tephra deposits with several layers of andosol between them. The displaced landslide materials divided into different parts (called R, M and L parts, respectively, hereinafter) and moved along three different directions (Fig. 2c). The materials in the R part were greatly scattered and fluidized with long and rapid movement, and resulted in 5 fatalities and severe damage to houses locating on the downstream. The materials in M part also fluidized and traveled long distance with the distal toe being rested on a gentle slope. Nevertheless, the L part showed less mobility: the travel distances are relatively shorter, the displaced landslide materials were not completely scattered, and a lot of blocks (about $1\sim5 \text{ m}^2$) with original lawn on its surface could be seen near the source area. Therefore, the L part could be regarded as spread flow. The sliding surface outcropped on the middle part of the source area has a thin layer of whitish soil that is underlain by scoriaceous

tephra (Fig. 2c). Investigation through trial pits and trenches immediately below the scarp revealed that above this whitish soil layer is yellow pumice that was deposited about 26ka ago. We inferred that the sliding surface was formed among the boundary between this pumice layer and underlain scoriaceous tephra. The mobilized friction angles for R, M and L parts are 6.1, 6.5, and 7.2, respectively.

TEST RESULTS AND CONCLUSIONS

To examine the initiation and movement mechanisms of these fluidized landslides, we performed direct shear tests on intact samples on the landslide fields, and also took samples from different soil layers and performed drained/undrained shear tests on them in natural water content or fully saturated state by applying different types of loading (static or dynamic).

The paleosol and pumice with scoria taken from Hanokidaira had their natural moisture contents being 94~160% and 94~151%, dry densities 0.48~0.66 and 0.51–0.64 g/cm³, respectively. Tests on these samples showed that: (1) the sliding surface could be along the boundary between a paleosol and the overlying layer of pumice and scoria. Shear failure might have occurred at first on the palaeosol layer, but liquefaction might have triggered in both the palaeosol layer and the overlaying pumice layer, resulting in the high mobility of displaced landslide materials. These soil layers are highly liquefiable in saturated condition when subjected to cyclic shear loading. High pore-water pressure can also be generated even when the soil layers are not fully saturated. (2) The shear resistance of the basal palaeosol markedly decreased with increasing shear rate, indicating that in the case of a shear failure within the palaeosol, the shear resistance of the sliding surface might become smaller with an increase of sliding velocity, thus allowing accelerating movement of the displaced landslide materials.

The samples taken from the pumice layer from Takanodai landslide had their natural moisture contents being 133~178%, and dry densities 0.44~0.56 g/cm³. The tests on these samples showed that when the moisture content was high enough (close to fully saturated state), the sample was every prone to suffer from liquefaction failure behavior when subjected to cyclic loading, and high pore-water pressure could also be generated within those sample with lower saturation degree after the shear failure was triggered. The in-situ direct shear box tests on intact samples revealed that the whitish pumice layer on the bottom of the yellowish pumice has very small peak shear strength, showing that shear failure might have been at first triggered within this layer during the earthquake. Therefore, it is inferred that liquefaction behavior within the yellowish pumice layer might have been triggered with progress of shear failure, and then resulted in the rapid movement with long travel distance. The possible coseismic loading due to the introduction of earthquake had been analyzed by using the seismic records obtained in a nearby earthquake observation station, and applied to the samples with different initial densities and moisture contents, and the results implied that the coseismic response of the slope might have been greatly enlarged due to the site effect.

REFERENCES

- Chigira M & Suzuki T (2016) Prediction of earthquake-induced landslides of pyroclastic fall deposits. In: Landslides and Engineered Slopes. Experience, Theory and Practice. S. Aversa, L. Cascini, L. Picarelli and C. Scavia (eds.), CRC Press, pp. 93-100.
- Evans SG & Bent AL (2004) The Las Colinas landslide, Santa Tecla: A highly destructive flowslide triggered by the January 13, 2001, El Salvador earthquake. Geological Society of America Special Papers, 375, p. 25-38.

Unstable zone of sand-silt mixture using static triaxial tests

Rupa S. Dalvi*, Nikita Choudhari[†]

* Associate Professor, Civil Engineering Department, College of Engineering, Pune, India.

[†]M.Tech (Civil-Geotech), College of Engineering, Pune, India.

Flow liquefaction in which large deformation produces can occur when the shear stress required for static equilibrium of soil mass is greater than the shear strength of soil in its liquified state. Flow slides triggered by monotonic loading have been observed by natural soil deposits and man made fields. Present work deals with the identification of unstable zone of sand with fines content using static triaxial tests. A series of undrained monotonic triaxial compression tests were conducted on reconstituted saturated samples of clean sand with variation in silt content as 0 %, 15 %, 25 % and 35 %. The influence of different parameters such as relative density, confining pressure and fines content on deviator stress and excess pore pressure was investigated. It was observed that the limiting fines content and relative density played a vital role in deciding the undrained behavior of a mixture of sand and silt. The zone between effective stress failure line and peak pore pressure line was regarded as an unstable zone which increased with fines content up to the limiting fines content.

Keywords: triaxial test, unstable zone, sand silt mixture, undrained.

INTRODUCTION

Instability has been observed to occur for saturated loose sand under undrained conditions and for saturated medium to dense sand under strain-controlled conditions. The term instability refers to a behaviour in which large plastic strains are generated rapidly owing to the inability of a soil element to sustain a given load or stress. In recent years, instability has been considered as one of the failure mechanisms that lead to flow slides or collapse of granular soil slopes in a number of case studies (Sheffield dam and Lower San Fernando Dam). The behavior of silty sandy soils such as hydraulic fills, landfills or alluvial deposits not clearly known during earthquake. Therefore, a thorough understanding of unstable behavior of silty sand is needed. the objective of the this work is to investigate the effect of fines on the unstable zone.

EXPERIMENTAL INVESTIGATION

The clean sand used in these experiments was silica sand obtained locally and has been classified as SP according to the unified soil classification system (USCS). Silt used in this study is non plastic and obtained from quarry dust. Fig. 1 indicates grain size distribution curves of clean sand ,silt and various sand silt mixture. The index properties of clean sand and silt are shown in Tab. 1.

Tab. 1. Index properties of sand and silt

	G	D ₅₀	γ_{max}	γ_{min}	e_{max}	e_{min}	C _u	C _c
Sand	2.416	0.28	15.16	13.98	0.745	0.609	2.24	0.85
Silt	2.751	0.042	15.70	11.91	1.175	0.753	3.6714	1.1633

The tests were conducted on clean sand and mixture of sand-silt at 30 % and 50 % relative densities for three confining pressures of 60 kPa, 120 kPa and 240 kPa with varying silt content as 15 %, 25 % and 35 %. Total twenty four tests were conducted on 50 mm diameter and 100 mm height cylindrical sample ($H/D = 2$) using moist placement method of sample preparation.

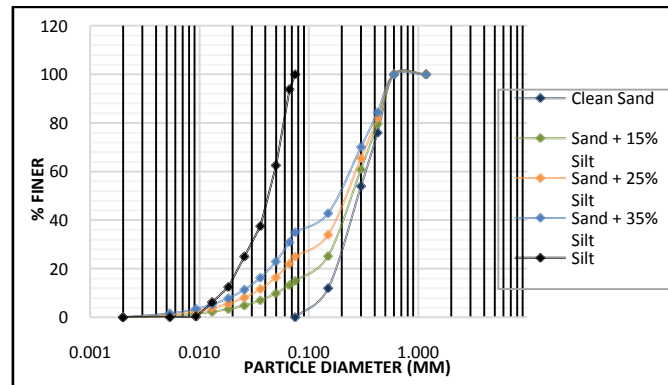


Fig.1 Grain size distribution curve

TESTING PROCEDURE

After specimens were prepared, their caps were placed and sealed with ‘O’ rings. A negative pressure of 10 kPa was applied to the specimens to reduce disturbance during removal of split mould and triaxial cell installation. When the cell was filled with water a confining pressure of 50 kPa was applied to the samples. The saturation of the specimen was done by applying CO_2 and back pressure technique. The control of saturation is done by means of Skempton’s pore pressure parameter B , $(\Delta\mu/\Delta\sigma)$. After completion of saturation process, the confining pressure was slowly increased to provide desired effective confining pressure (i.e. 60 kPa, 120 kPa, 240 kPa). All the samples were isotropically consolidated and loaded at the strain rate of 1.25 mm/min. For each confining pressure load, displacement, pore pressure and volume change were recorded using data acquisition system during the test after every 5 second. All the tests were conducted up to maximum axial strain of 20 %.

RESULTS AND DISCUSSION

Effect of confining pressure

The variations in peak deviator stress and excess pore pressure generation with increase in confining pressure for clean sand as well as sand with silt content of 15 %, 25 % and 35 % is shown in Figs. 2 and 3. It is observed that as the confining pressure increases deviator stress as well as peak pore pressure increases for all the cases studied. It is also seen that maximum value of deviator stress has been observed for clean sand. Similar behaviour is observed for specimens prepared with 50 % relative density.

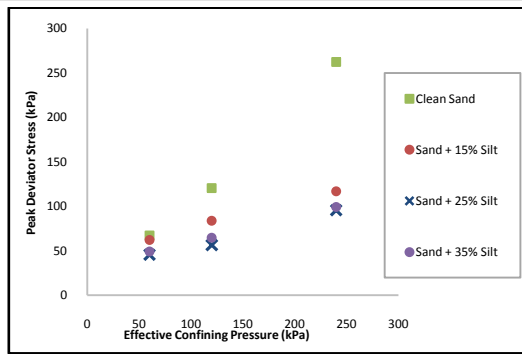


Fig. 2 Peak deviator stress vs effective confining pressure (Relative density = 30%)

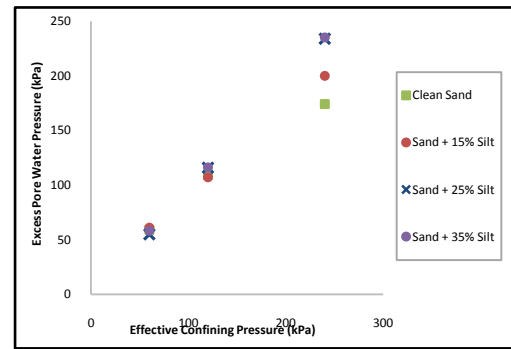


Fig. 3 Excess pore water pressure vs effective confining pressure (Relative density = 30%)

Effect of silt content

The effect of fines content on peak deviator stress of specimens prepared at 30 % and 50 % relative density with increase in silt content from 15 %, 25 % and 35 % at various effective confining pressures is as shown in Figs. 4 and 5.

As the fines content increase, peak deviator stress decreases up to limiting fines content after that peak deviator stress increases. Addition of fines reduces value of peak deviator stress before limiting fines content because fines do not participate in capacity of carrying load. Addition of fines beyond the point of limiting fines content changes behaviour of soil from sand dominated to silt dominated. For maintaining same relative density, soil needs to be compacted densely in specimen with fines content more than limiting fines content. So, load carrying capacity increases for sand with 35% silt content. Similar behaviour is observed for specimens prepared at medium dense state (50 %). (Fig. 5).

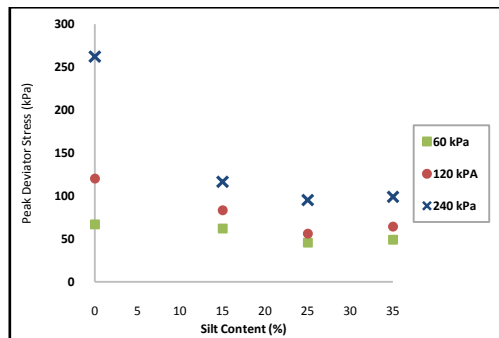


Fig. 4 Peak deviator stress vs silt content (Relative density = 30%)

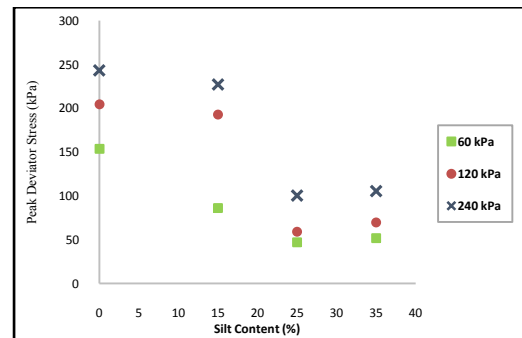


Fig. 5 Peak deviator stress vs silt content (Relative density = 50%)

UNSTABLE ZONE

In order to classify the liquefaction behavior of soil, Pathak and Dalvi (2011) have established unstable zone plotted between K_f line and peak pore pressure line on effective stress path plot. Unstable zone has been obtained by plotting effective stress path for all three confining pressures for each relative density for each percentage of fines content. K_f line is plotted based on the maximum shear stress value for each of the test. Peak pore pressure line is plotted using p' and q values corresponding to peak pore pressure point.

Unstable zone for clean sand and clean sand with 25 % silt is shown in Figs. 6 (a) and (b) It is observed that as fines content increase upto limiting fines content, unstable zone becomes wider. Further increase in fines content beyond limiting fines content, narrows down the unstable zone. This may be an effect of excess pore water pressure, as fines content increased to limiting fines content (25 %) excess pore water pressure increases.

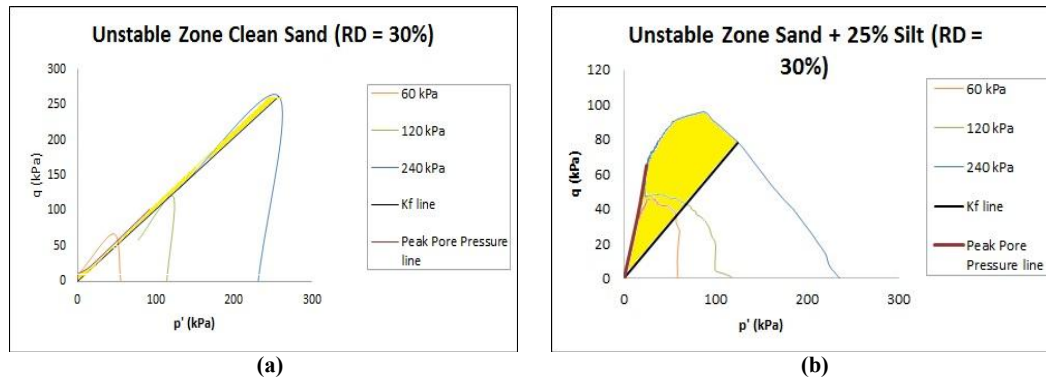


Fig. 6 Variation of unstable zone with increase in fines content at relative density RD=30 %

Similar trend of unstable zone obtained for specimen prepared at relative density 50 % as that at relative density 30%.

CONCLUSION

From the present study following conclusions are made:

1. As the confining pressure increases peak deviator stress and excess pore water pressure increases for clean sand and sand silt mixture.
2. For both loose and medium dense specimens, peak deviator stress decreases as fines content increases up to limiting fines content. Further increase in fines content increases the peak deviator stress value.
3. Unstable zone of sand-silt mixture widens as fines content increases up to limiting fines content. Further increase in fines content narrows down the unstable zone for relative density 30 % and 50 %.

REFERENCES

- ASTM Standard D4767 (2007) Standard Test Method for Consolidated Undrained Triaxial Compression Test for Cohesive Soil. ASTM International, West Conshohocken, PA. www.astm.org.
- Chu J and Leong WK (2002). Effect of fines on instability behaviour of loose sand. *Geotechnique* 52(10), 751 – 755.
- Pathak SR and Dalvi RS (2011). Static liquefaction of clean sand using triaxial test. 14th Pan-American conference on Soil Mechanics and Geotechnical Engg., 64th Canadian Geotechnical Conference, Toronto, Ontario, Canada. Paper No 452.
- Pathak SR and Dalvi RS (2014). Liquefaction Behaviour of Clean Sand for Various Sample Sizes Using Triaxial Tests. *Recent Trends in Civil Engineering & Technology*, 4(2), 1-8
- Sitharam TG, Dash HK, and Jakka RS (2013). Postliquefaction Undrained Shear Behaviour of Sand-Silt Mixtures at Constant Void Ratio. *Int. J. Geomech.* 10.1061/(ASCE)GM.1943-5622.0000225.
- Yang SL, Sandven R and Grande L (2006). Instability of Sand-Silt Mixture. *J. Soil Dynamics and Earthquake Eng.* 26, 183–190.

EVOLUTION OF SAFETY IN WEATHERED INFINITE SLOPES

Gema De la Morena*, Laura Asensio*, Vicente Navarro*

* Geoenvironmental Group, University of Castilla-La Mancha, Avda. Camilo José Cela s/n,
13071 Ciudad Real, Spain

The evolution of safety in weathered slopes is analysed, accounting for unsaturated and saturated conditions. Considering limit analysis theory and limit equilibrium methods, it is known that, when the soil is assumed to be homogeneous with constant strength parameters, and a stable bedrock in depth is considered, the critical configuration of the failure mechanism corresponds to the maximum depth (weathered soil thickness) and length (infinite slope) of the weathered soil. However, if the variability of those parameters with depth is not negligible, more shallow instabilities may occur when the slope is saturated. A silty soil with a variable cohesion in depth has been analysed. Although in this particular case the slope can be considered stable assuming unsaturated conditions, when saturated, the minimum Factor of Safety is not located at the maximum depth. Therefore, saturation could cause the failure of the slope if the design does not take this fact into account.

Keywords: safety, weathered slope, infinite slope, shallow slope failure

INTRODUCTION

Due to climatic actions, many slopes have a weathered band on surface. This weathered band has a lower strength than the unaltered soil or rock in depth. Therefore, slope instabilities are common problems in weathered slopes (Gökceogly & Aksoy, 1996; Kim et al., 2004; Cascini et al., 2010). In most cases, the slope failure occurs after rainfall, which causes the saturation of the soil because of infiltration and the rise of the groundwater table (Aleotti, 2004). The increase of water content and the reduction of suction result in a decrease in the strength of soil and may cause the failure.

The typical failure mechanism that may occur is represented in Fig. 1. If the weathered soil is considered perfectly homogeneous, and its mechanical parameters (density, friction angle and cohesion) are assumed constant, limit analysis theory demonstrate that, considering a stable bedrock in depth, the critical failure mechanism corresponds to the maximum volume mobilised, i.e. maximum depth and length of the weathered soil. However, when those parameters depend on depth, a shallower failure may occur. In this study, the effect of the variability of cohesion with depth on the security of an infinite slope is analysed, accounting for unsaturated and saturated conditions.

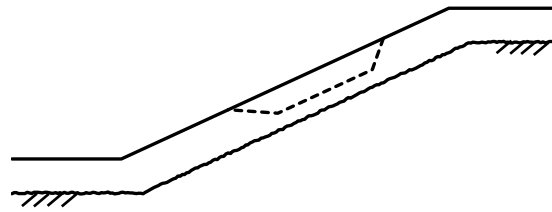


Fig. 1 Failure mechanism in a weathered slope

MATERIALS AND METHODS

Because the largest impact when a mobilisation occurs is associated with long slopes, an infinite slope was analysed in this study. Moreover, given that, in these systems, the length of the landslide is significantly greater than the thickness of the mobilised soil, the hypothesis of infinite slope is reasonable. By assuming a Mohr-Coulomb failure criterion (characterised by the friction angle, ϕ' , and the cohesion, c') for saturated conditions, the ultimate shear stress, τ_u , can be calculated as:

$$\tau_u = \sigma_n' \tan(\phi') + c' \tag{1}$$

where σ_n' is the effective normal stress. Applying the limit equilibrium method, the Factor of Safety (FS) is, for saturated conditions:

$$FS_{sat} = \frac{\tau_u}{\tau_m} = \frac{\gamma' \tan(\phi')}{\gamma_{sat} \tan(i)} + \frac{1}{\gamma_{sat}} \frac{c'}{\sin(i) h} \tag{2}$$

where τ_m is the mobilised shear stress, γ' is the submerged specific weight, γ_{sat} is the saturated specific weight, i is the slope angle, and h is the depth according to Fig. 2.

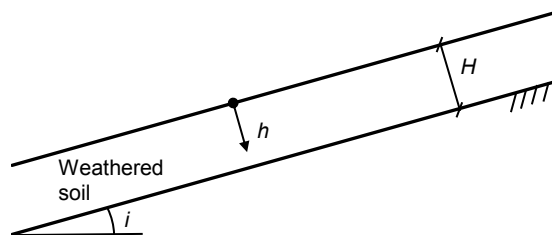


Fig. 2 Geometry of the slope considered in this study

In the case of a partially saturated soil, the ultimate shear stress can be modified taking into account the effect of suction according to the linear expression proposed by Fredlund et al. (1978):

$$\tau_u = \sigma_n'' \tan(\phi') + s \tan(\phi_b) + c' \tag{3}$$

where σ_n'' is the net normal stress, calculated as the difference between the total normal stress and the atmospheric pressure ($\sigma_n'' = \sigma_n - P_{atm}$), s is the suction, and ϕ_b is the parameter that accounts for the increase of shear strength due to suction. The Factor of Safety can be calculated as:

$$FS_{\text{unsat}} = \frac{\tau_u}{\tau_m} = FS_{\text{sat}} + \frac{\tan(\phi')}{\tan(i)} \left(\frac{\gamma_w}{\gamma_{\text{sat}}} + \frac{\tan(\phi_b)}{\tan(\phi')} \frac{1}{\gamma_d \cos(i)} \frac{s}{h} \right) + \frac{1}{\sin(i)} \frac{c'}{h} \left(\frac{1}{\gamma_d} - \frac{1}{\gamma_{\text{sat}}} \right) \quad (4)$$

where γ_w is the specific weight of water, and γ_d is the dry specific weight. The bulk density in unsaturated conditions is assumed to be equal to the dry density.

In this study, a silty soil was considered for the application case presented. Table 1 shows the geometrical and soil parameters. The cohesion was assumed to depend on depth, so that the cohesion is maximum ($c_M=20$ kPa) for the maximum depth ($H=1.5$ m), and it decreases linearly until $h=0.5$ m, where the cohesion was considered to reach a residual value equal to a 10 % of the maximum value, i.e. $c_m=2$ kPa. From this point to the surface, the cohesion was assumed constant. The suction also depended on depth, varying linearly from a minimal value of $s_m=33$ kPa at the maximum depth to a maximum value of $s_M=100$ kPa at $h=0.5$ m. From this depth to the surface, it was considered to be constant. Fig. 3 shows the variation of cohesion and suction with depth.

Tab. 1 Geometrical and soil parameters of the case study

Parameter	Symbol	Value
Saturated specific weight (kN/m ³)	γ_{sat}	18
Dry specific weight (kN/m ³)	γ_d	15
Friction angle (°)	ϕ	25
Parameter of suction (°)	ϕ_b	15
Thickness of the weathered band (m)	H	1.5
Slope angle (°)	i	30

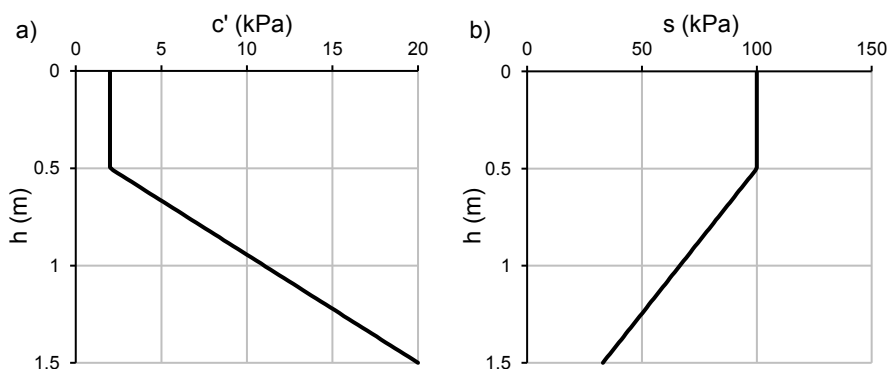


Fig. 3 Variation of (a) cohesion and (b) suction with depth

RESULTS AND DISCUSSION

Fig. 4 shows the evolution of the FS with depth for the studied case, for both saturated and unsaturated conditions. When the slope is unsaturated, the FS decreases as expected (as explained in the Introduction), until a minimum value of $FS=3.4$ is achieved at the maximum depth of the weathered soil, which is much higher than the instability limit ($FS=1$). The value $FS=1$ was assumed as a reference in this inspection exercise, because no uncertainty was considered in the soil properties. Therefore, for unsaturated conditions, the slope analysed can be considered safe. However, if the soil is saturated, for instance due to a rainfall event, the behaviour of the FS is different. Although the value of the FS is 1.8 at the maximum depth (even higher than the classical $FS=1.5$ for design), it reaches a minimum value at a shallower

position, being $FS=0.8$ at $h=0.5$ m. This value implies that, according to the considered assumptions and the model used in this study, the slope would not be stable and its failure may occur ($FS<1$).

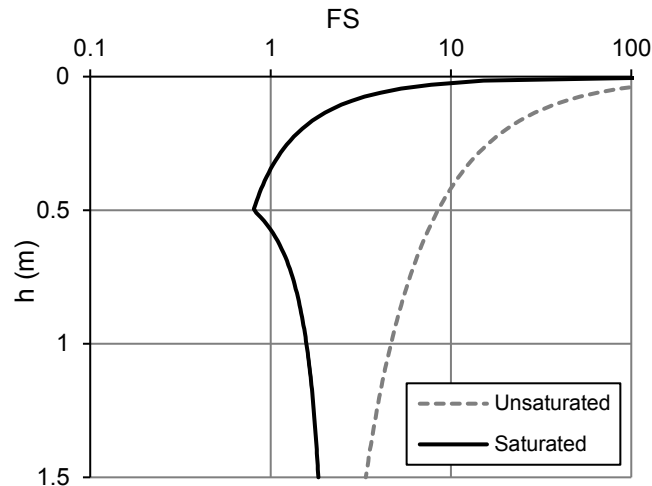


Fig. 4 Evolution of the Factor of Safety (log scale) with depth for saturated and unsaturated conditions for the case study

Therefore, the influence of the dependence of the strength parameters on depth must be taken into account, because it may change the position of the critical failure mechanism. According to these results, when the variability of the strength parameters, such as the cohesion, is not negligible, the assumption of a homogenous soil with constant values may result in an unsafe stability analysis and an inappropriate slope design for saturated conditions.

CONCLUSIONS

In this study, the influence of the variability of the strength parameters with depth in the stability of weathered infinite slopes was analysed, considering unsaturated and saturated conditions. An example that accounted for a cohesion increase with depth was studied. In that case, the minimum Factor of Safety when the slope is saturated was not located at the maximum weathered depth, unlike the results of an analysis assuming a constant cohesion. Therefore, it is important to take this fact into account and, at least, to consider that the critical failure mechanism may not be located at the maximum depth. The omission of that dependence may result in an inappropriate slope design, below the required safety level.

REFERENCES

- Aleotti P (2004) A warning system for rainfall-induced shallow failures. *Engineering Geology* 73 (3-4), 247-265.
- Cascini L, Cuomo S, Pastor M & Sorbino G (2010) Modeling of rainfall-induced shallow landslides of the flow-type. *Journal of Geotechnical and Geoenvironmental Engineering* 136 (1), 85-98.
- Fredlund DG, Morgenstern NR & Widger RA (1978) The shear strength of unsaturated soils. *Canadian Geotechnical Journal* 15, 313-321.
- Gökçeoglu C & Aksoy H (1996) Landslide susceptibility mapping of the slopes in the residual soils of the Mengen region (Turkey) by deterministic stability analyses and image processing techniques. *Engineering Geology* 44 (1-4), 147-161.
- Kim J, Jeong S, Park S & Sharma J (2004) Influence of rainfall-induced wetting on the stability of slopes in weathered soils. *Engineering Geology* 75 (3-4), 251-262.

ANALYSIS OF TAILINGS DAM FAILURE BASED ON HISTORICAL DOCUMENTS: THE CASE STUDY OF “LA LUCIANA”, SPAIN

F.J. Fernández-Naranjo*, V. Rodríguez*, R. Rodríguez*, M.E. Alberruche*,
J.C. Arranz*, R. Sarro[†], R.M. Mateos[†], G. Herrera[†], L. Vadillo*

* Department of Research on Geological Resources, Geological Survey of Spain (IGME), Ríos Rosas, 23, Madrid, Spain.

[†] Geohazard InSAR Laboratory and Modelling Group, Geological Survey of Spain (IGME), Ríos Rosas, 23, Madrid, Spain.

On 17 August 1960 the biggest disaster by death toll in Spain, related with a tailings dam failure, took place in Reocín (Santander). The tailings dam “La Luciana” failed causing the death of eighteen people, most of them children. The mining company carried out several geotechnical tests in the remaining materials of the tailings dam to understand the failure. In addition, thematic cartography related to the break was elaborated. The results are available to be consulted in the Reocín Mines Documentary Collection, from which we have obtained mechanical Cone Penetration Test (CPT) data near the fault area as well as diverse maps of the dam pre-failure and post-failure. The processing of such data through current analysis techniques has revealed the relationship between the fault of the tailings dam and static liquefaction phenomena.

Keywords: Tailings dam failure, Cone Penetration Test (CPT), Liquefaction, La Luciana

INTRODUCTION

The tailings dam called “La Luciana” is located in Reocín (Santander) in the North of Spain. It was built in 1951 (Berzal, 1976) and was active until its collapse in 1960 (Fig. 1). Due to the destruction caused and the long period of time from the disaster, there have been serious difficulties to identify the constituent parts of the deposit and there is not much technical information related the failure. Nor seismic events or heavy rainfall periods could have been associated to the failure. There were several testimonials which include additional information, like the appearance of cracks in the right side of the dike some days before the failure highlighted the explosive character of the break and noted the existence of at least two big landslides during the break (Saiz, 2008).

The technical assessment of that period concluded that the failure was triggered by the percolation of water in a 3-levels basal heap placed under the tailings, but the documents which lead at that conclusion have been lost. Several photos of that period showed a high grade of destruction of both structures the dike and the 3-levels of basal heaps.

Some evidences of liquefaction (san dikes) close to the break zone have been found at present. Due to this find, the involvement of a static liquefaction process related to the failure is suspected.



Fig. 1 Photos of La Luciana area before and after the disaster

A few technical reports which make mention to an “explosive liquefaction” phenomena usually relate the process to a seismic event (Rydelek & Tuttle, 2004). However there are several cases of tailings dam breaks around the world, for example the case in Stava on 1985 or Merriespruit on 1994, in which a static liquefaction phenomena has been related to an explosive event (Fourie et al., 2001, Davies et al. 2002).

Following the first explosive failure, there are evidences of several landslides of the tailings (several victims of the first failure died because they were trapped when a second landslide buried them, before the rescue works were concluded). The material reached distances over 500 m until have been channeled to the Besaya River. The Besaya River’s level raised 1.5 m. The area affected was more than 11 ha.

METHODOLOGY

After consulting the Reocín Mines Documentary Collection, the results of 14 old Cone Penetration Test (CPT), made between November 1960 and March 1961 in the area around the break, were acquired. In addition, old topography of the La Luciana tailings dam deposit (after and before the break) was collected, digitalized and georeferenced.

The CPT data was interpreted applying modern methodologies in order to assess the susceptibility to liquefaction (Fig. 2). The Relative Density (%) and the contractive behavior of the material were analyzed (Bolton & Gui, 1993, Ishikara, 1993). Based on the results, the origin point of the failure was located in the half level heap, in the west side of the dike (matching with the appearance place of the cracks before the failure).

On the other hand, according to the documentary information, the failure set in motion between 50.000 and 100.000 m³ of material, exposing the medium and upper levels of the basal embankments. The run-out movement may be produced in at least two events based on the testimonial information.

The cartographical information has allowed the development of several DEM of the basal embankments and the lateral heightening materials. The application of Boolean differences

arithmetic has made it possible to estimate the volume of the slid materials, as well as the establishment of an additional explanation of the origin of the liquefaction.

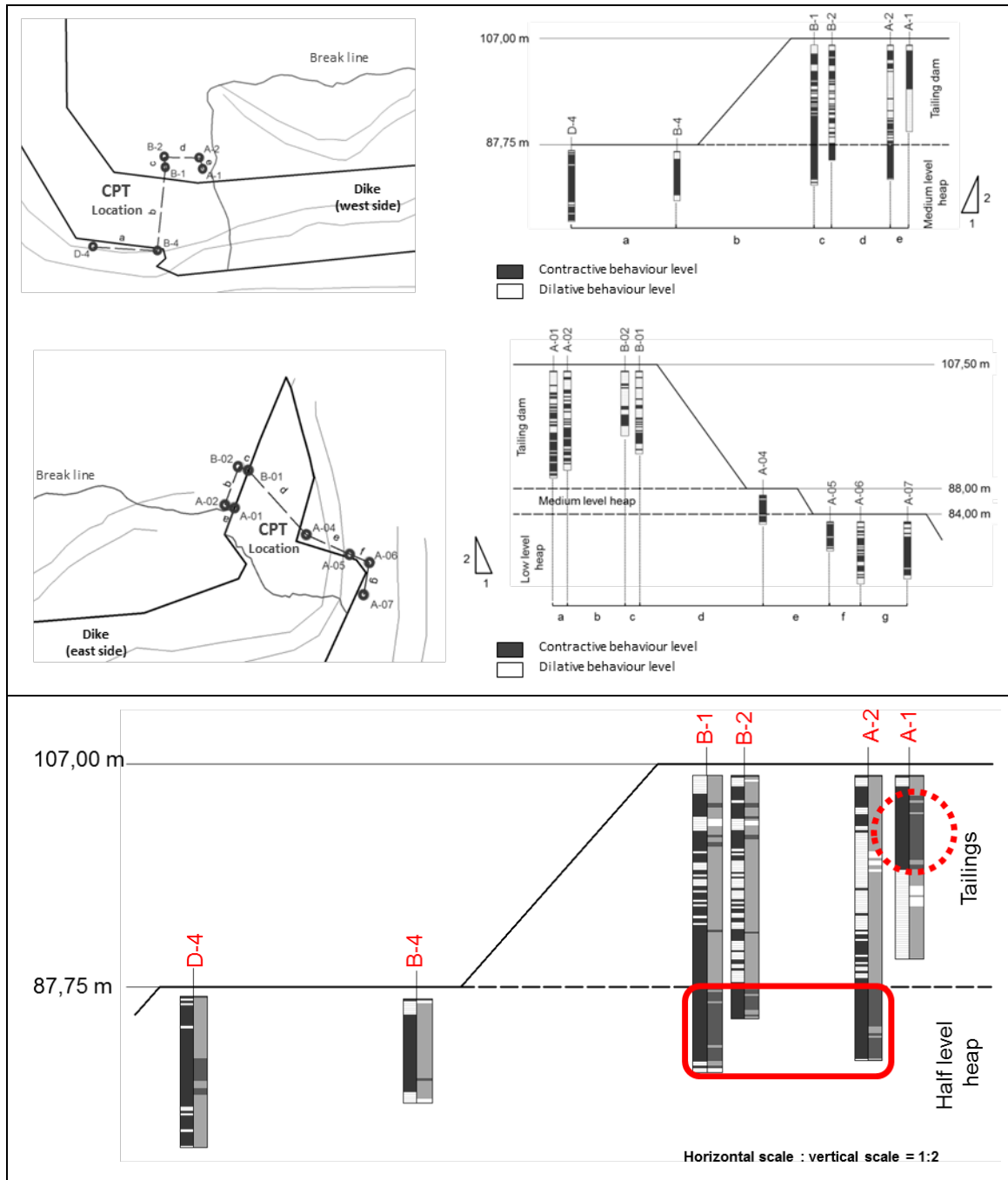


Fig. 2 Assessment of the susceptibility of liquefaction through the CPT analysis.

CONCLUSIONS

The results obtained show that the run out volume was of 300.000 m³, a volume significantly higher than estimated. More than a half of this volume corresponds to the basal embankments. The cartography shows two kind of associated sedimentation deposits: first one, a deposit of great thickness located next to the failure area; and the second one, a deposit of lower thick-

ness that flows in direction to the Besaya River and whose path that could shows an erosion sign over the previous deposit. This fact matches with the several landslide event hypothesis. Two possible scenarios about the origin point of the liquefaction event have been considered (Fig. 3): A Scenario that implies that the origin of the break is associated with the tailings and B Scenario that implies that the origin of the break is related to the basal embankments. A geometrical analysis of the topographical profile has been developed (the geometrical analysis developed consists of comparing the resulting geometry, the original slopes and location of the different elements of the reservoir in order to obtain the most plausible origin of the failure taking into account the different failure hypotheses established). It has been concluded that, based on the slope configuration and the existence of several run out events, the B Scenario is the most probably. This conclusion seems to match with the results obtained from the old CPT.

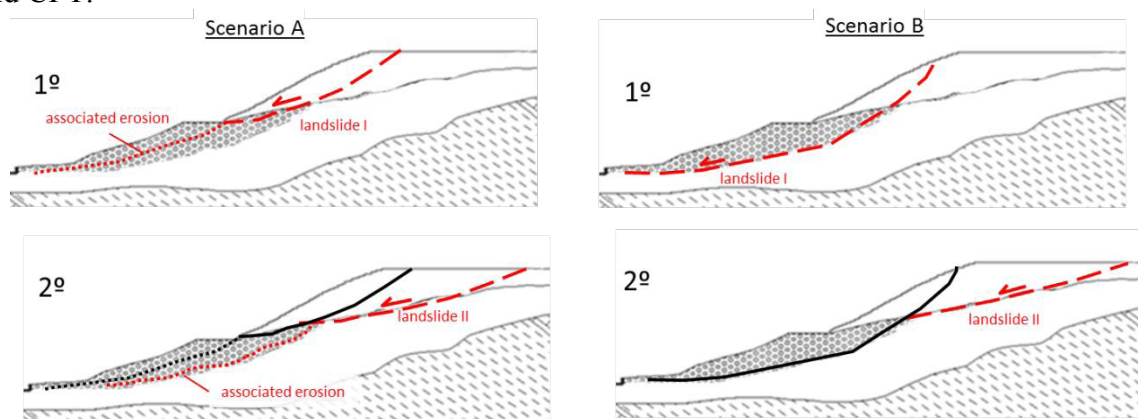


Fig. 3 Alternatives scenarios for the “La Luciana” tailing dam failure.

REFERENCES

- Berzal JL (1976) Presas de residuos mineros. *Revista de Obras Públicas* 123 (3131), 301-333
- Bolton MD & Gui MW (1993) The study of relative density and boundary effects of cone penetration tests in centrifuge. University of Cambridge, Department of Engineering, Cambridge, United Kingdom, CUED/D-SOILS/TR256
- Davies MP, McRoberts E & Martin T (2002) Static liquefaction of tailings: fundamentals and case histories. *Proceedings Tailings Dams ASDSO/USCOLD*, pp. 233-255.
- Fourie AB, Blight GE & Papageorgiou G (2001) Static liquefaction as a possible explanation for the Merriespruit tailings dam failure. *Canadian Geotechnical Journal* 38 (4), 707-719.
- Ishikara K (1993) Liquefaction and flow failure during earthquakes. *Geotechnique* 43 (3), 351-415.
- Rydelek PA & Tuttle M (2004) Explosive craters and soil liquefaction. *Nature* 427, 115-116.
- Saiz JR (2008) *Torre la Vega siglo XX. 1950-1962: Crónica ilustrada de una ciudad. Tomo III*. Ediciones Los Cántabros. Santander. pp. 251-262

CLAY MINERALS EFFECTS IN SHALLOW LANDSLIDE AT TAKADAKE AREA, ASO MOUNTAIN, KUMAMOTO, JAPAN

Mega Lia Istiyanti¹, Satoshi Goto²

¹Integrated Graduate School of Medicine, Engineering, and Agricultural Sciences, University of Yamanashi, Yamanashi, Japan

²Graduate Faculty of Interdisciplinary Research, University of Yamanashi, Yamanashi, Japan

Aso Mountain located at the Southwest Japan. Shallow landslides occurred frequently in this area due to the heavy rainfall. Furthermore, clay minerals have played a key role in this shallow landslide. The slippage plane has higher clay minerals content than other soil layers. Montmorillonite was found at the slippage plane of this shallow landslide. The slippage plane is easier to swell related with the montmorillonite characteristics.

Keywords: shallow landslide, clay minerals, slippage plane

INTRODUCTION

Aso Mountain is located in Southwest Japan. In 2012, the shallow landslides occurred in this area due to the heavy rainfall. Though it was triggered by the heavy rainfall, clay minerals have played a key role in these landslide. Clay minerals at lower part of the landslide are mostly unfavourable and often determine the stability of location (Benac et al., 2014).

Clay minerals are *hydrous aluminium silicates* plus other metallic ions, and also can form as either primary or secondary minerals (Lancellota, 2007). Clay minerals have an affinity with water and also have a negative behaviour which can be a key role in landslides (Meade, 1964).

RESEARCH AREA

The research area is located (see Fig. 1) at Takadake area in Aso Mountain's caldera, Kumamoto, Japan. Those shallow landslides were occurred at grassy hillslopes. In 2012, rainfall at research area is 459.5 mm (see Tab. 1) which triggered shallow landslide (Shimizu & Ono, 2015).

Tab. 1 Data precipitation at Aso Mountain in 2012 (Shimizu & Ono, 2015)

Date	Maximum 1-h rainfall (mm)	Maximum 3-h rainfall (mm)	Maximum 6-h rainfall (mm)
July 12, 2012	108	288.5	459.5
June 29, 2001	81	179	201
July 2, 1990	67	189	296

METHODS

The sample of the soil in the landslide was taken from landslide zone in Takadake. The soils scraped off from the surface of the scarp using shovels to expose the fresh layer of the soils. Soils were sampled for laboratory analysis to determine the soils characteristics from density

of soil particle (ρ_s), grain size distribution, water content (w), ignition loss (L_i) and Atterberg limits analysis. Soil characteristics will represent the slippage plane in landslide area.

This research will be conducted with X-ray diffraction (XRD) and Scanning Electron Microscope (SEM) for understanding the role of clay minerals in the soil layer at the landslide area. These clay minerals were separated from the soil samples. Those clay minerals will be examined by using X-ray diffraction and Scanning Electron Microscope.

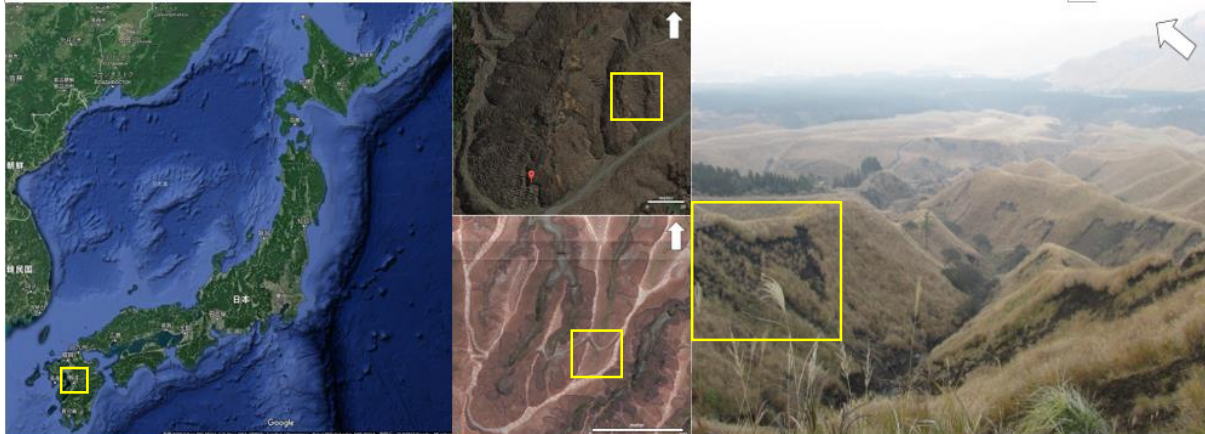


Fig. 1 Location of shallow landslide at research area

SHALLOW LANDSLIDES

Shallow landslides occurred especially on grassy hillslopes of post-caldera central cones of Aso Volcano (Shimizu & Ono, 2015). High velocity and high impact energy, typically involving a small volume of earth and/or debris, are characteristics from shallow landslides (Giannecchini et al., 2012). Soils layers in shallow landslide area divided into 11 layers from the ground to 1850 mm depth (that is sketched in Fig. 2). Generally, the layers consist of top soil, loam, Kuroboku, scoria and volcanic ash. Kuroboku is the black soil which was made by human activity. Scoria and volcanic ash is the eruption product which occurred forth times at Aso Mountain (Miyabuchi, 2012). From 11 soil layers, we took 7 soil layers for analysis (see Fig.2).

DISCUSSION

FACTORS DETERMINING SLIPPAGE PLANE BASED ON SOILS CHARACTERISTICS

The high water level is indication of stability analyses which can influence the landslide instability (Benac et al., 2014). Lower part of N3-4 Kuroboku and N2 Kuroboku has high water content in soil layers. Furthermore, clay minerals have an affinity with water. Dry clay will adsorb the water vapour from the atmosphere and will soak up large quantities of liquid water. If available, those can make swell to many times its dry volume (Meade, 1964). From plasticity index (PI) and water content (w), lower part of N3-4 Kuroboku has a higher value (see Fig. 2). Clay minerals concentration also increase an organic carbon concentration, and that pattern reflects both variations in sedimentation rates as well as the physical protection of organic matter by clay inferred for soil of modern steppes (Sanborn et al., 2006). From the ignition loss analysis, lower part of N3-4 Kuroboku has a higher organic carbon concentration (see Fig. 2), which also means that the clay minerals concentration is higher.

Basic soil property influenced by some soil physical and chemical properties is density of soil particle. The density of soil particle is in contrast with the organic carbon content. Increasing in organic matter means decreasing in the density of soil particle (Chaudhari et al., 2013). From the graphic of soil layers (see Fig. 2), the lower part of N3-4 Kuroboku has a higher organic carbon and also has a lower density of soil particle value.

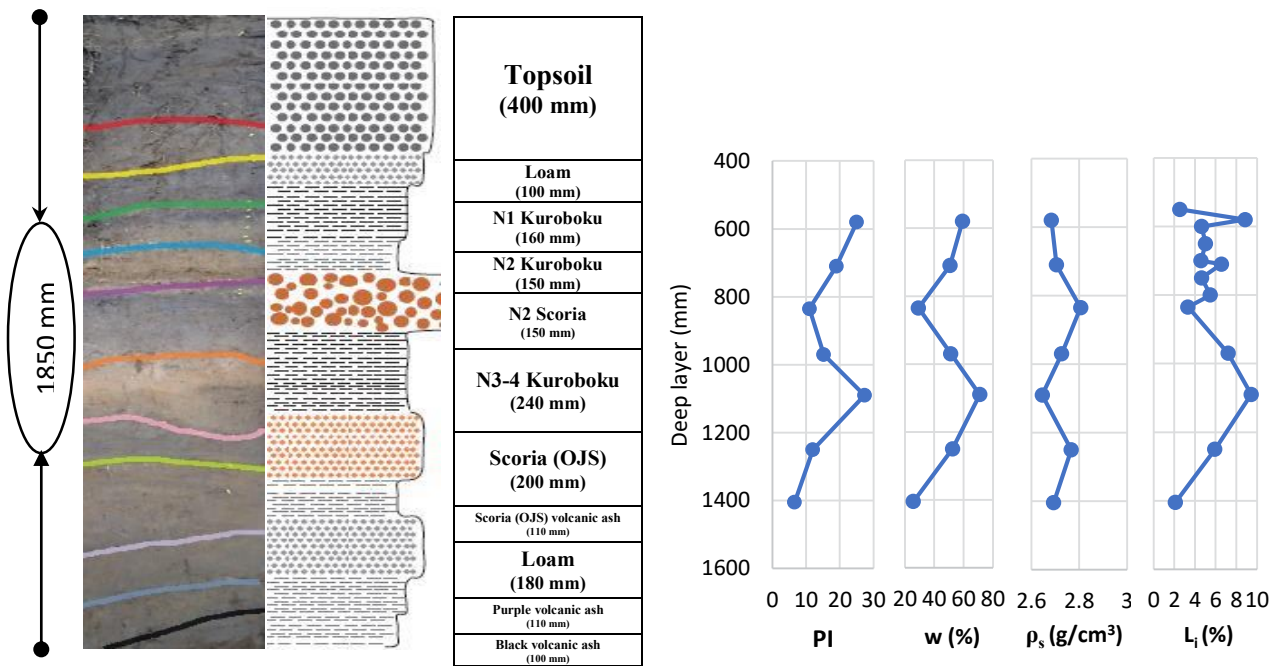


Fig. 2 Graphics of soil layer and soil properties profile at research area

Soils characteristics in soil layers at shallow landslides have different characteristics even those have almost same clay fraction percentage. The lower part of N3-4 Kuroboku has a little more clay content than other soil layers.

FACTORS DETERMINING SLIPPAGE PLANE BASED ON CLAY MINERALS CHARACTERISTICS

From 7 soil layers with clay minerals sample analysis method, we got 4 soil layers which contain clay minerals (see Tab. 2).

Tab.2 XRD and SEM analysis result (Slatt and O’Brien., 2013)

Soil layers name	N2 Kuroboku	N3-4 Kuroboku (U)	N3-4 Kuroboku (L)	OJS
Clay minerals	Smectite Kaolinite Montmorillonite	Illite	Montmorillonite	Illite
Structure	Flocculated clay	Porous flocculated	Porous flocculated	Porous flocculated
Photos				

The result of XRD and SEM analysis showed that slippage plane of this shallow landslide is lower part of N3-4 Kuroboku. Lower part of N3-4 Kuroboku content montmorillonite. Montmorillonite is a swelling clay minerals which have a negative behaviour. Water and ions which is exchangeable can enter and separate the layers. At the same time, montmorillonite have a very strong attraction for water (Holtz, R.D and Kovacs, W.D., 1981). Furthermore, montmorillonite is possibility for changing their volume, therefore induce the soil to collapse (Bell, F.G., 2007).

CONCLUSION

Based on laboratory analysis result, slippage plane on this shallow landslide is the lower part of N3-4 Kuroboku. From the soil analysis, the lower part of N3-4 Kuroboku has a high water content with high plasticity index and also high organic content. The density of soil particle is in contrast with others that have a small value. The soil layer of the lower part of N3-4 Kuroboku characteristics can trigger the shallow landslide. The result of XRD and SEM analysis also espouse that the lower part of N3-4 Kuroboku contain montmorillonite, which have a negative behaviour. Montmorillonite can induce the soil to collapse because of the ability for changing the volume, high swelling ability and strong attraction for water.

ACKNOWLEDGMENT

The completion of this paper could not have been possible without the participation and assistance of many people whose names may not all be enumerated. Especially for support from Kikibunseki Center Laboratorium at University of Yamanashi. Part of this study was carried out by the cooperation of the river and erosion control research grant (Ministry of Land, Infrastructure and Transport). We would like to express our acknowledgments to the members concerned.

REFERENCES

- Bell FG (2007) *Engineering Geology*, Second Edition. Elsevier: United States of America.
- Benac C, Ostric M, & Jovancevic SD (2014) Geotechnical properties in relation to grain-size and mineral composition. The Grohovo Landslide Case Study (Croatia), *Geologia Croatica* 67/2 127-136.
- Chaudhari PR, Ahire DV, Ahire VD, Chkravarty M, & Maity S (2013) Soil bulk density as related to soil texture, organic matter content and available total nutrients of coimbatore soil. *International Journal of Scientific and Research Publication*, Vol. Issues 2, ISSN 2250-3153.
- Giannecchini R, Galanti Y, & Avanzi GDA (2012) Critical rainfall thresholds for triggering shallow landslides in the serchio river valley (Tuscany, Italia). *Copernicus Publication: European Geosciences Union*.
- Holtz RD and Kovacs WD (2011) *An introduction to Geotechnical Engineering (Prentice-Hall civil engineering and engineering mechanics series)*. Prentice-Hall: University of Michigan.
- http://www.data.jma.go.jp/svd/vois/data/tokyo/STOCK/souran_eng/volcanoes/084_asosan.pdf
- Lancellota R (2007) *Geotechnical Engineering*, Second Edition. Taylor & Francis Group: London and New York.
- Meade RH (1964) Removal of water and rearrangement of particle during the compaction of clayey sediments-review. *Geological Survey Professional Paper 479-B: Washington*.
- Miyabuchi Y (2012) Landslides triggered by the July 2012 torrential rain in Aso Caldera, Southwestern Japan. *Journal of Geography (Chigaku Zasshi)*, 121 (6) 1073-1080 2012.
- Sanborn PT, Smith CAS, Froese DG, Zazula GD, Westgate JA (2006) *Full-glacial paleosols in perennially frozen loes sequences, Klondike Goldfields, Yukkon territory, Canada*, www.sciencedirect.com
- Shimizu O & Ono M (2015) Relationship of tephra stratigraphy and hydraulic conductivity with slide depth in rainfall-induced shallow landslides in Aso volcano, Japan. *Landslides*, Springer-Verlag Berlin Heidelberg, DOI 10.007/s10346-015-0666-2.
- Slatt RM and O'Brien N (2013) Variations in shale pore types and networks. *Geoscience Technology Workshop, Revisiting Reservoir Quality Issues in Unconventional and Conventional Resources: Technique, Technologies and Case Studies, Austin, Texas 12-13 November 2013*.

APPLICATION OF THE HYDRAULIC GRADIENT METHOD FOR PHYSICAL MODELING OF RAINFALL INDUCED LANDSLIDE: THE OPTIMAL DESIGN FOR A PHYSICAL LABORATORY MODEL

Mehrez. Jamei^(1,2), Fakher. Hamrouni⁽²⁾, Houcem. Trabelsi⁽²⁾

⁽¹⁾ Northern Border University, Engineering College, Saudi Arabia

⁽²⁾ Tunis El Manar University, National Engineering School of Tunis, Tunisia

In the last years, the researchers were focused on the modeling of rainfall-induced failure basing of the unsaturated soil mechanics approaches. Because the high cost of field tests especially for landslides study, the monitoring of a landslide on the site remains difficult and too expensive. In addition, the difficulty to conduct the laboratory and the field tests to determine the behavior law's parameters induces some added problems for the numerical modeling. For these reasons, a preference is given for the physical modeling in order to study some geotechnical problems at a smaller scale. The limitation of the last method is to respect the similarity rules which link the physical model and its corresponding field case.

The objectives of the presented work are in the first part, the validation of the proposed mechanical and hydraulic constitutive models by numerical simulations of laboratory tests on small-scale slope models and the identification of the failure mechanism for slope failure through a parametric study especially through the permeability. The aim of the second part is the study of the capability of the hydraulic gradient method to resolve the problem linked to the non-similarity rules. In this paper, we propose a procedure to optimize the physical model in order to be able to simulate the real slope behavior. Numerical analysis has been conducted using the CODE-BRIGHT software.

Keywords: rainfall, small-scale slope model, hydraulic gradient method, numerical modeling, permeability.

INTRODUCTION

The rainfall-induced landslides events are currently more frequent in many regions in the world. That is why, the rainfall is now considered as one of the most significant triggering factors for slope failures. In fact, many landslides have been occurred during or immediately after the rainfall, such as landslides that they had placed on Béja area situated in the North West of Tunisia (Jamei. M et al., 2008 and M. Jamei et al., 2015). However, the main factors that influence the initiation of rainfall-induced slope failures are still not adequately clarified. The incorporation of unsaturated soil mechanics in slope stability analysis is consequently a key requirement to identify conditions for slope failure. In fact, different methods were used to study landslide as a result of change in saturation degree such as equilibrium limit analyses and the elasto-plastic method such as the c-phi reduction method. The limitation of this approaches is that to consider the hydro-mechanical characteristics as constant and do not depend on water content evolution. In the sense that the coupling between the water content increase and the skeleton deformations, was not considered by these approaches. In contrast,

the increase of the soil water content (decrease of suction) in critical zone which generally near the toe of the slope is described as the main factor that induced slope failure. That's why for shallow landslides study, many numerical approaches take account the change of soil mechanical characteristics due to the water content evolution (or suction evolution) for the unsaturated zone. In the same context, some experimental results of infiltration and rainfall tests on small-scale slope models showed that the rainwater infiltration alone does not cause slope failure but the increase of pore water pressure due to the increase of water table level in the lower part of the slope, was described as a main condition leading to slope failure (R. P. Orense et al., 2004). In these cases, an instable zone can be developed and the landslide can occur. Based on the effective stress concept, the reduction of the effective stress due to the increase of the pore water pressure leads to the reduction of shear stress. In the unsaturated soil, the state of stress is defined by two variables: the effective stress ($\sigma - u_w$) and the suction ($u_a - u_w$) as stress acting on the mechanical parameters, which are used to explain the unsaturated soil behavior. However, for unsaturated soils the measure of the effective stress remains not accessible. For this reason, it was necessary to use an additional assumption on the effective stress definition (Bishop A W., 1959 and Laloui L. et al., 2009). An elastoplastic formulations used the effective stresses were given. In fact, by comparing the numerical results obtained thus far for landslide problems modeling to the field-measured results, we improve the capability of these models to simulate the unsaturated soils behavior especially for slope failure analysis. However, because the complexity of the associated physical problem, many landslide cases remain not completely explained and not yet deeply investigated. The effort to evaluate the effect of the environmental conditions is in line with prevailing sustainability considerations and concerns.

Due to the high cost of field tests and the difficulty to conduct a parametric study in the landslide site, the physical modeling is now one of the methods used in geotechnical science to study the real behavior of several phenomena like the rainfall-induced slope failure. By using this method, it may be possible to study the effect of the environmental conditions and evaluate its associate role degree. The parameters that were varied are the rainfall intensity, the initial groundwater level, the duration of the rainfall, the evaporation flux, the temperature rate, and all the hydro-mechanical of soil as the permeability and the shear characteristics dependency on suction.

However the 1g scale model may not completely represent field conditions as soil behavior is different within a natural slope because of stress confinement. For this reason, the proposal is to assure macro-gravity condition to make the physical model under the same stress and strains as the real slope. In order to satisfy the similarity rules, we used the hydraulic gradient method which is the main scope of the proposal study.

NUMERICAL PROGRAM

In this paper, we present some numerical simulation results of rainfall induced landslide tests on a small-scale slope model. The Figure 1 and Figure 2 show the design of the physical models used in the experimental tests developed by R. P. Orense et al., 2004 and E. Damiano et al, respectively. The goal is firstly a parametric study in order to study the effect of factors influencing slope stability such us: precipitation intensity and soil properties, principally, the permeability. Our interest in this part is the effects of the spatial variability of permeability on rainfall-induced landslides. Secondly, basing on the hydraulic gradient method, the main objective of the second part is to solve the problem due to the limits of gravity modeling in landslide studies. Based on the extension of effective stress concept to unsaturated soils a modi-

fied Mohr-Coulomb model taking into account the suction variation, has been used to simulate the shear failure of the experimental slope physical models. The proposed elastoplastic formulation takes into account the reduction of cohesion under humidification. The numerical program is reported in the following table.

Tab. 1 Numerical program

Type of test	Model type	I (mm/h)	D _r (%)	k(m/s)	Slope (°)	Objective
Rainfall	B	42-72	50%	1.8 10 ⁻⁴	40	*
Rainfall	B	Variable	5%-95%	Variable	40	**
Seepage	A	---	50%	1.8 10 ⁻⁴	40	*
Rainfall	A	Constant	Constant	10 ⁻⁴ -10 ⁻⁷	16	***
Rainfall	C	45	55%-76%	≈10 ⁻⁶	0	*
Rainfall	C	83	55%-76%	≈10 ⁻⁶	40	*

*: The objective is the validation of the proposed mechanical and hydraulic constitutive models

**: Variation of hydraulic boundary conditions and relative density D_r. The objective is to increase the hydraulic gradient and therefore the model scale based on the hydraulic gradient method.

***: The aim is to study the effects of the spatial variability of permeability on slope stability

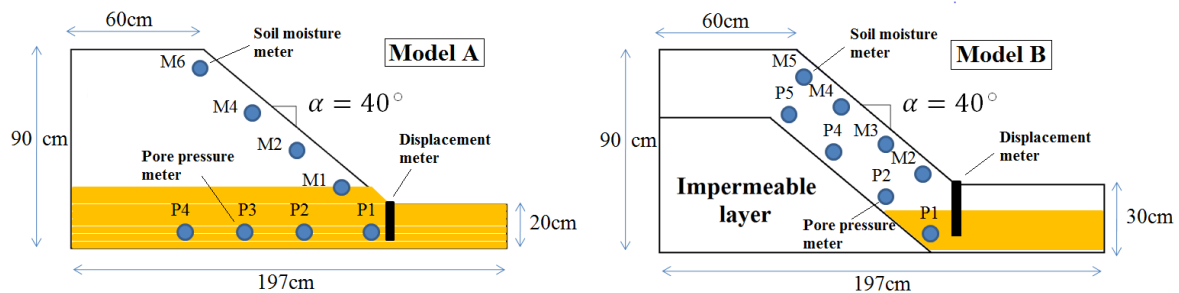


Fig. 1 The design of the small-scale slope model type A&B used in the experimental tests (R. P. Orense et al., 2004)

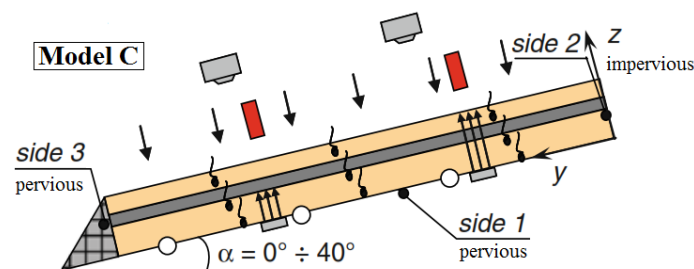


Fig. 2 The design of the small-scale slope model type C used in the experimental tests (E. Damiano et al.)

CONCLUSION

For landslide study case, laboratory test on small scale slope model is one of the methods used to study the phenomena of rainfall-triggered landslides. In the first part, the numerical simulations of rainfall and seepage tests were performed to validate the proposed numerical

approach. From experimental and numerical results, landslide occurred when the region near the toe of the slope becomes nearly full saturated and the failure process involved only the superficial portion of the slopes. The obtained results confirm the capability of the numerical approach proposed to reproduce the experimental slope behavior. On the other side, the effect of permeability is detected for fine soils (low permeability) which prevented the rainwater to infiltrate inside the soil and plays an important role on slope stability occurring. In the second part, the numerical results show an increase of laboratory model scale as long as the hydraulic gradient becomes more and more important. By exploiting the obtained results, the optimum slope model dimensions are defined making hence possible the perfect validity of the similitude's rules.

REFERENCES

- Alonso E E, Gens A, and Josa A (1990) A constitutive model for partially saturated soils. *Geotechnique*, 40, pp. 405-430.
- Bishop AW (1959) The principle of effective stress. *Tecnisk Ukeblad*, 39, pp. 859-863.
- Chales W. W. Ng, Jian Liu, Rui Chen, and Jie Xu (2015) Physical and numerical modeling of an inclined three-layer (silty/gravelly sand/ clay) capillary barrier cover system under extreme rainfall. *Waste Management*.
- Emilia Damiano, and Lucio Olivares The role of infiltration processes in steep slope stability of pyroclastic granular soils: laboratory and numerical investigation. *Nat Hazards*, 52, pp.329-350.
- Fredlund, D. G., N. R. Morgenstern, and R. A. Widger (1978) Shear strength of unsaturated soils. *Can. Geotech.J* 15, pp. 313-321.
- Henry Ling, Hoe I Ling, and M. ASCE (2012) Centrifuge Model Simulations of Rainfall-Induced Slope instability. *Journal of Geotechnical and Geoenvironmental Engineering*, 138, pp. 1151-1157.
- Hong-Hu Zhu, Bin Shi, Jun-Fan Yan, Jie Zhang, and Jing Wang (2015) Investigation of the evolutionary process of a reinforced model slope using a fiber-optic monitoring network. *Engineering, Geology*, 186, pp. 34-43.
- H. Rahardjo, D. G. Fredlund and S.K. Vanapalli (1992) Use of linear and nonlinear shear strength versus matric suction relations in slope stability analyses. *Sixth International symposium on landslides Christchurch*, pp. 531-537.
- Jamei. M, Guiras. H, Ben Hamouda. K, Hatira, M, and Olivella. S (2008) A study of the slope stability in unsaturated marly clay soil. *Studia Geotechnica et Mechanica*, XXX.
- L. Montrasio, and R. Valentino (2008) A model for triggering mechanisms of shallow landslides. *Natural Hazards and Earth System Sciences*, 8, pp. 1149-1159.
- Lorella Montrasio, Roberto Valentino, and Andrea Terrone (2014) Application of the SLIP model. *Procedia Earth and Planetary Science*, pp. 206-213.
- Lyesse Laloui, Mathieu Nuth (2009) On the use of the Generalized effective stress in the constitutive Modeling of unsaturated soils. *Computers and Geotechnics*, 36, pp. 20-23.
- Mathieu Nuth and Lyesse Laloui (2008) Effective stress concept in unsaturated soils: Clarification and validation of a unified framework. *International Journal for numerical and analytical methods in Geomechanics*, 32, pp. 771-801.
- M. Jamei, H. Guiras, and S. Olivella (2015) Analyse of slope movement initiation induced by rainfall using the Elastoplastic Barcelone Basic Model. *European journal of environmental and civil Engineering*.
- M R Hakro and I S H Harahap (2015) Laboratory experiments on rainfall-induced flowslide from pore pressure and moisture content measurements. *Natural Hazards and Earth System Sciences*, 3, pp. 1575-1613.
- Rolando P Orense, Suguru Shimoma, Kengo Maeda and Ikuo Towhata (2004) Instrumented Model Slope Failure due to water seepage. *Journal of Natural Disaster Science*, 26, pp. 15-26.
- R. I. Borja, and J. A. White (2010) Conservation laws for coupled Hydro-mechanical processes in unsaturated porous Media: Theory and Implementation. *Mechanics of Unsaturated Geomaterials*.
- Sasahara, k and Sakai, N (2014) Development of shear deformation due to the increase of pore pressure in a sandy model slope during rainfall. *Eng. Geol*, 170, pp. 43-51.
- Suguru Shimoma, Rolando P. Orense, Tsuyoshi Honda, Kengo Maeda and Ikuo Towhata (2002) Model tests on slope failures caused by heavy rainfall. *Congress publication*, 2, pp. 547-557.
- Trabelsi. H, Jamei. M, Zenzri. H, and Olivella, S, (2012) Crack patterns in clayey soils Experiments and modeling. *International Journal for Numerical and Analytical methods in geomechanics*, 36, pp. 1410-1433.
- Yechezkel Mualem A New Model for Predicting the hydraulic Conductivity of Unsaturated Porous Media. *Water Resources Research.J.* 12, pp. 513-522.

UNDERSTANDING SPREADS IN CANADIAN SENSITIVE CLAYS

Ariane Locat*, Serge Leroueil* and Denis Demers[†]

* Université Laval, Quebec, Canada

[†] Ministère des transports, de la mobilité durable et de l'électrification des transports, Quebec, Canada

For the past decades, Université Laval and Ministère des Transports, de la Mobilité durable et de l'électrification des transports du Québec have worked together in order to answer the following questions: how can we develop tools to evaluate the danger regarding spreads?; what are the geotechnical and morphological parameters controlling the initiation, propagation and extent of spreads in sensitive clays? This work portrays the latest advancement of the research program put in place with the objective to answer these questions by integrating detailed field investigation, advanced laboratory work and numerical modeling.

Keywords: Spread, progressive failure, sensitive clays.

INTRODUCTION

Spreads result from the extension and dislocation of the soil mass above a shear zone, forming horsts and grabens moving and subsiding in the underlying remoulded soil forming the shear zone (Fig. 1). They may cover large area (> 1 ha), occurred rapidly with no warning signs, and regular stability analysis do not apply, as they give too large factor of safety when back calculating actual spreads. In addition, they constitute 37% of the 108 large landslides inventoried by the Ministère des Transports, de la Mobilité durable et de l'électrification des transports du Québec (MTMDET) in Quebec (Demers et al. 2014). Spreads are therefore a major threat to population living in areas prone to sensitive clays. This work presents the advancement in our understanding of spreads in Canadian sensitive clays, focusing on the research performed on two aspects: (i) synthesis of spreads in Eastern Canada, and (ii) application of progressive failure to spreads.

SYNTHESIS OF SPREADS IN EASTERN CANADA

Combination of 7 cases of spread described in detailed with additional cases from literature and MTMDET data base gives a total of 12 cases of spread that were used to depict spreads in Canadian sensitive clays. Information gathered on these landslides is as follows: topographic data from conditions before and after each landslides from aerial photographs, Lidar data in order to interpret the morphology of the slope before the event and the debris; field investigation including boreholes, CPTU, vane shear tests, piezometers, detailed cross-sections and trenches; and laboratory testing including usual geotechnical tests, triaxial tests, direct simple shear (DSS) tests and direct shear (DS). Constant volume ring shear tests (RS) have also been done on a few samples.

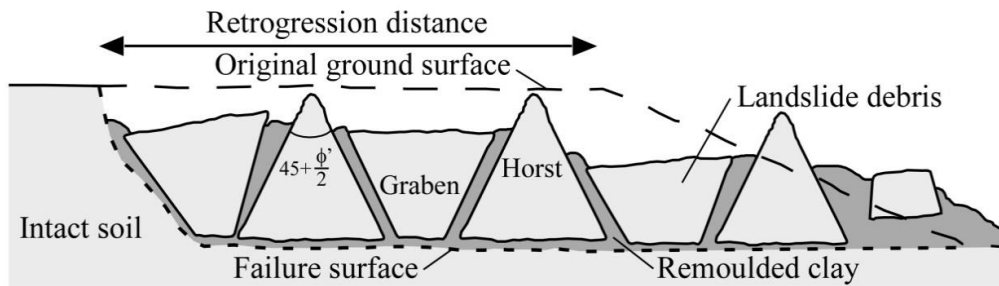


Fig. 1 Schematic representation of a spread in sensitive clays (A. Locat et al. 2016).

Compilation of information from the study of these landslides shows that spreads may concern areas larger than 1 ha. Their retrogression distance varies from 80 to 580 m and their width varies from 140 to 1045 m (Fig. 1). Their width is generally larger than their retrogression distance. Their shape is typically rectangular or half-circular. However, their shape can somewhat vary if they are constrained by topographic barriers (ex: deep gullies or older landslide scar). Craters of spreads are filled with several ridges created by horsts separated by grabens, as can be seen on Fig. 1. Horsts are blocks of more or less intact clay having sharp tips pointing upward. Their sides are generally inclined to about 60° with the horizontal (Fig. 1). Grabens are blocks of more or less intact soil having flat horizontal tops with trees that can still stand straight after the movement. The failure surface for the spreads studied was found to be almost horizontal and located generally at the elevation of the toe of the slope, or 1 to 2.5 m above or below it. No weak zone seems to be controlling the failure surface location. These observations enabled to conclude that horsts and grabens are the results of dislocation, translation and subsidence of the soil mass above the failure surface with no or very little rotation. It is also believed that these blocks are formed in one large continuous movement and not by the movement of individual horsts and grabens that would slide and translate on after the other. Recent investigations indicate that the failure surface can develop on more than one level, as is seen in the 1971 Casselman case (Durand, 2016) and the 2010 Saint-Jude spread (P. Locat et al. 2011), and reveal that spreads can be complex and need detailed investigations in order to understand the kinematic involved during failure.

When studying the geotechnical properties of the soil involved in the various spreads studied, it can be seen that most spreads occurred in silty clays ($< 2 \mu\text{m}$ between 27 to 87%) having plasticity index varying from 3 to 40% and liquidity index (I_L) varying from 1.0 to 5.0. Remoulded shear strength (Su_r) is consistent with I_L values and can be lower than 0.07 kPa. Most of the spreads studied occurred in nearly normally consolidated soft clays ($10 \text{ kPa} < Su < 35 \text{ kPa}$ and overconsolidation ratio ≈ 1.1). Sensitive clay flowslides tend to occur in clays having Su_r lower than 0.8 kPa and I_L larger than 1.5 (Demers et al. 2014). Contrarily to flowslides, spreads can occur in clays having lower liquidity index and larger remoulded shear strength than what is generally observed for flowslides. As an example, the spread that occurred at Saint-Barnabé involved soil with average liquidity index around 1.1 (A. Locat et al. 2017). During undrained shear, strain-softening behaviour has been observed through triaxial tests, DSS tests, DS tests and RS tests.

APPLICATION OF PROGRESSIVE FAILURE TO SPREADS

The implication of the strain-softening behaviour of sensitive clays on the failure mechanism of spreads, suggest that progressive failure is involved in these landslides. Skempton (1964) described the failure mode occurring during progressive failure with the following statement:

“[...] if for any reason a clay is forced to pass the peak at some particular point within its mass, the strength at that point will decrease. This action will throw additional stress on the clay at some other point, causing the peak to be passed at that point also. In this way a progressive failure can be initiated and, in the limit, the strength along the entire length of a critical slip surface will fall to the residual value.” Bjerrum (1967) also presented the idea that progressive failure could explain how failures propagating upslope can be initiated in intact slopes consisting of overconsolidated plastic clays and clay shales. He applied this idea to large retrogressive landslides as a drained or effective stress phenomenon. A. Locat et al. (2011, 2013 and 2015) suggested that spreads may be explained by upward progressive failure. This mechanism could physically explain how a failure can be triggered at the toe of a slope, how it can propagate in a homogeneous deposit, and finally why the soil mass above this failure surface dislocates in active failure, forming horsts and grabens typical of spreads.

A numerical method was developed at Université Laval with the collaboration of the Norwegian Geotechnical Institute (NGI) in order to apply the progressive failure concept to spreads in Canadian sensitive clays (A. Locat et al. 2013). The method uses the finite elements software Plaxis 2D to define the initial stress conditions in a naturel slope and Bifurc, a finite element model developed at NGI, to model the progressive failure along a potential failure surface. This method allows for the determination of the susceptibility of a slope to progressive failure by estimation of the magnitude of the disturbance needed to initiate failure and the estimation of the final extent of the failure surface, once the failure is initiated. For now, this method has been applied to 4 different spreads: the 1994 Sainte-Monique spread (A. Locat et al. 2015), the 2005 Saint-Barnabé spread (A. Locat et al. 2017), the 1971 Casselman spread and the 1986 Saint-Luc-de-Vincennes spread (Durand 2016).

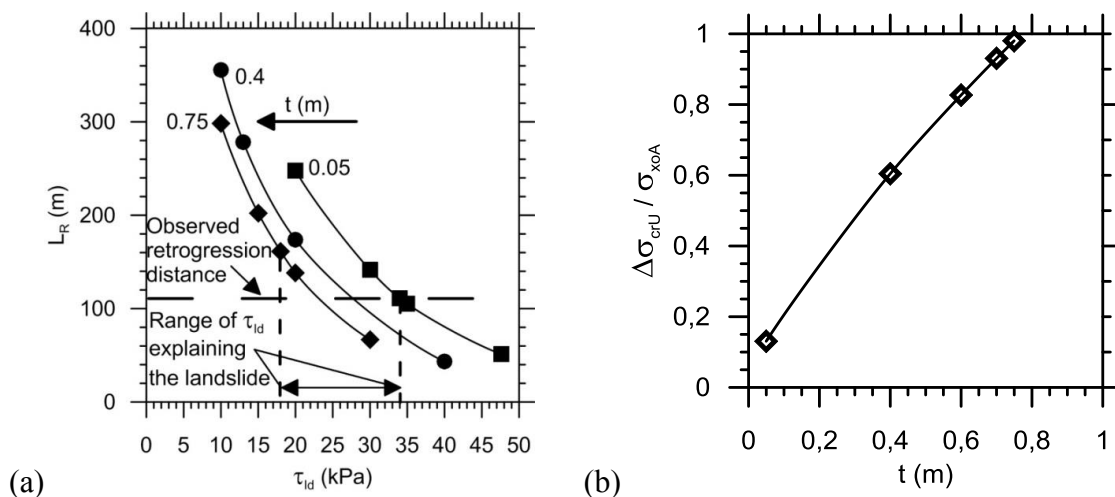


Fig. 2 (a) Retrogression distance (L_R) of the landslide as a function of large-deformation shear strength (τ_{id}) for various shear zone thicknesses (t) for the 2005 Saint-Barnabé-Nord spreads. (b) Unloading ratio ($\Delta\sigma_{crU} / \sigma_{xoA}$, for which 1 = total unloading of the toe of the slope and 0.5 = 50% of unloading of the toe of the slope) as a function of shear zone thickness for a large deformation shear strength of 20 kPa for the 2005 Saint-Barnabé-Nord spreads (A. Locat et al. 2017).

What was learned from these first applications of progressive failure to these case studies is that before failure, the initial shear stress along a potential horizontal failure surface was unevenly distributed with, in certain cases, a maximum close to the intact shear strength of the soil. All other parameters considered the same, larger sensitivity (lower large deformation shear strength) leads to larger retrogression distance of the failure surface (Fig. 2a). When thin shear

zones are formed, soils exhibit more brittle shear behaviour, defined here as a rapid decrease of strength beyond the peak shear strength, and the susceptibility to progressive failure is increased, as less unloading of the toe of the slope is needed to initiate the landslide (Fig. 2b). Also, the stress–strain behaviour of the soil needed to back-calculate the failure is generally much more brittle than the one measured in triaxial compression or DSS tests, with lower large deformation shear strength. RS tests enabling larger shear strain are therefore being used to measure the actual large-deformation shear strength of the soil. In addition, the reduction of the horizontal stress during failure propagation seems large enough to explain the formation of horsts and grabens by active failure of the soil mass.

CONCLUSION

The next step is now to model in two dimensions, in a similar way as Dey et al. 2015, additional cases of detailed spreads in sensitive clays. Additional testing is also needed with the RS tests in order to see if the measured undrained soil behaviour in the laboratory may give appropriate results for the modeled spreads. Additional back calculated cases of spreads will confidently lead to the determination of appropriate parameters to determine conditions in which spreads occurred and how to prevent them.

REFERENCES

- Bjerrum L (1967) Progressive failure in slopes in overconsolidated plastic clay and clay shales. Terzaghi Lecture, *Journal of Soil Mechanics and Foundations Division*, ASCE. 93(5): 3-49.
- Demers D, Robitaille D, Locat P & Potvin J (2014) Inventory of large landslides in sensitive clays in the Province of Québec, Canada: preliminary analysis. In *Landslides in Sensitive Clays: From Geosciences to Risk Management, Advances in Natural and Technological Hazards Research 36*, L'Heureux JS et al. (eds.), Springer, pp. 77-89.
- Dey R, Hawlader B, Phillips R & Soga K (2015) Large deformation finite-element modelling of progressive failure leading to spread in sensitive clays slopes. *Géotechnique*. 65(8): 657-668.
- Durand A (2016) Contribution à l'étude des étalements dans les argiles sensibles de la mer de Champlain, Étude des étalements de Casselman (1971) et de Saint-Luc-de-Vincennes (1986). M.Sc. Thesis, Département de génie civil et de génie des eaux, Université Laval, Québec.
- Locat A, Leroueil S, Demers D & Locat J (2017) The Saint-Barnabé case study. *Understanding landslides through case studies*. Leroueil S & Picarelli L (eds.) Taylor & Francis Group. Accepted
- Locat A, Demers D & Leroueil S (2016) Spreads in Canadian sensitive clays. *Landslides and Engineered Slopes – Experience, Theory and Practice*. Aversa S et al. (eds.) Proceedings of the 12th International Symposium On Landslides. 12-19 Juin 2016. Naples, Italie. Taylor & Francis Group. pp. 1295-1304.
- Locat A, Leroueil S, Fortin A, Demers D & Jostad HP (2015) The 1994 landslide at Saint-Monique, Quebec : Geotechnical investigation and application of progressive failure analysis. *Canadian Geotechnical Journal*. 52(4) : 490-504.
- Locat A, Jostad HP & Leroueil S (2013) Numerical modeling of progressive failure in sensitive clays. *Canadian Geotechnical Journal*, 50(9) :961-978.
- Locat A, Leroueil S, Bernander S, Demers D, Jostad HP & Ouehb L (2011) Progressive failures in Eastern Canadian and Scandinavian sensitive clays. *Canadian Geotechnical Journal*, 48(11): 1696-1712.
- Locat P, Fournier T, Robitaille D & Locat A (2011) Glissement de terrain du 10 mai 2010, Saint-Jude, Montérégie, Rapport sur les caractéristiques et les causes. Rapport MT11-01. Section des mouvements de terrain, Services de la géotechnique et de la géologie, Ministère des transports du Québec. Bibliothèque et Archives nationales du Québec, Gouvernement du Québec. 101 p.
- Skempton AW (1964) 4th Rankine Lecture : Long-term stability of clay slopes. *Géotechnique*, 14(2): 77-102.

TWENTY YEARS OF CONTINUOUS MONITORING OF THE VALLCEBRE LANDSLIDE (EASTERN PYRENEES): LESSONS LEARNED

J. Moya*, J. Corominas*, J.A. Gili*, A. Ledesma*, A. Lloret*

* Division of Geotechnical Engineering and Geosciences,

Universitat Politècnica de Catalunya UPC - BarcelonaTech, Barcelona, Spain

The Vallcebre landslide has been monitored for displacements and groundwater level fluctuations since 1996, showing a fast response to rainfall and groundwater changes. Its overall evolution in terms of displacements can be simulated by means of simple models including a viscous component. However, to reproduce local details of the movement, more sophisticated models involving alternative mechanisms of the basal shear band are required.

Keywords: Vallcebre, landslide, slow-moving, long-term monitoring, modelling.

INTRODUCTION

The Vallcebre landslide is a large ($> 20 \text{ Mm}^3$) slow-moving translational slide, located in the South Eastern Pyrenees, which is regarded as a natural laboratory. A monitoring network consisting of 8 inclinometers, 14 piezometers and 8 in-hole wire extensometers, were set up since 1996. Readings in piezometers and extensometers were taken each 20 min. It allowed a high-frequency and a long-term recording of the landslide behaviour along 20 years. A complete description of the network can be found in previous works [1, 2, 3].

This contribution summarizes the main geological characteristics of the landslide and the lessons on its hydro-mechanical behaviour learned along these years. In addition, some key observations that help to understand this behaviour are presented.

LANDSLIDE MATERIALS AND GEOMETRY

The slide develops in a gentle (7°) slope consisting on tectonised Palaeocene clayey siltstones, which are underlayed by a limestone formation (Fig. 1). The landslide is formed by three main units that are separated by scarps and grabens showing tension cracks [1]. Most of the monitored points were located at the lower unit, because its higher activity.

Wire extensometers have shown that the movement in the landslide mass occurs in a thin basal shear band 20 to 35 cm thick [2]. The band is developed within a stiff and overconsolidated siltstone shale layer showing a dense network of microfaults. Lab shear tests gave nil cohesion and 11.8° for the minimum effective friction angle (ϕ') of this material.

A $\phi=7.8^\circ$ was assessed for the slickensided surfaces by means direct shear tests [1].

The basal shear is 15 and 42 m deep on average, respectively in the lower and intermediate unit, and it is quite planar (Fig. 1). Both the ground surface and the shear band dip upslope at the foot which, consequently, acts as a buttress that opposes to the movement (Fig. 1). Here local failures transfer the mass to a small torrent (Vallcebre torrent in Fig. 1), where the material is eroded episodically by floods.

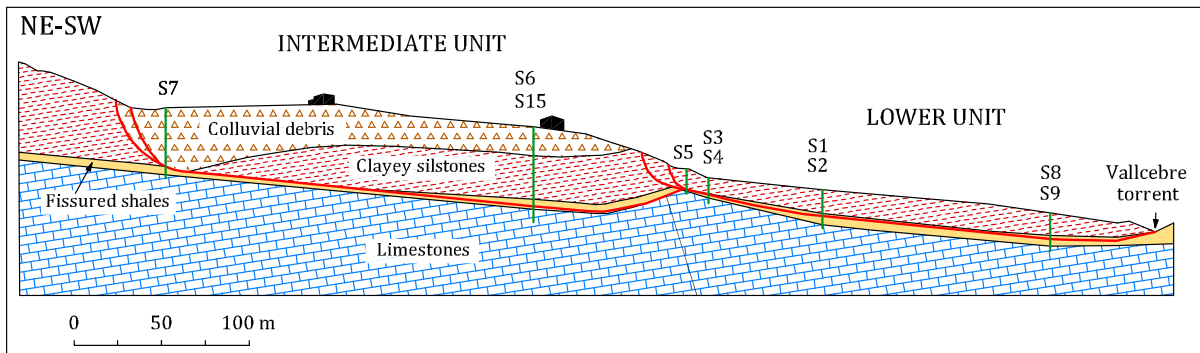


Fig 1. Geological cross-section of the Vallcebre landslide. Red line: basal shear, vertical green line: borehole.

LANDSLIDE MOVEMENT AND RESPONSE TO GROUNDWATER CHANGES

The slide units show a relative movement. The upper unit is inactive and the intermediate unit is a third slower than the lower one. This latter was always moving from July 1996 to December 2015 at a rate of 252 mm/year on average and displaced 4.9 m in borehole S2 (Fig. 2).

The landslide is very sensitive to rainfall and groundwater fluctuations (Fig. 2), showing that water infiltration is governed by ground fissures and tension cracks rather than by matric soil porosity of the clayey landslide materials [1]. On the other hand, groundwater level (GWL) stabilizes at a certain depth during dry periods (i.e. 6.2 m in borehole S2) when the slide moves at a constant and very small velocity (boreholes S4 and S2). Near the foot (in the borehole S9), sliding stops for GWL deeper than 4.5 m. This occurred from July to October or November in five of the nine years in which the wire extensometer worked in this borehole (see Fig. 2). This indicates that the foot but also the lower part of this slide unit is contributing to slow down the movement during dry periods.

Pseudo-static analysis

The steady conditions reached during dry periods, when the slide is close to stop, were analysed for the lower landslide unit. An upper value of $\phi_{res}=14^\circ$ was obtained by using limit equilibrium (LE) back-analysis, and considering a safety factor equal to one, null cohesion and the lowest GWL observed. It is worth noting that, in any case, ϕ_{res} is greater than the dip (β) of the failure surface ($\beta \approx 6 - 7^\circ$) for the most part of the landslide. The same is observed in many slow-moving large landslides [4].

Nevertheless, if the ϕ_{res} lab value for the fissured shales (7.8°) and the lowest GWL scenario are used in LE analysis, the safety factor obtained is very low ($F=0.79$), which seems not compatible with the almost imperceptible velocity observed in the borehole S2 (0.3 mm/day) and nil in the borehole S9. This suggests that, in addition to frictional forces, viscous forces may play a role in the movement.

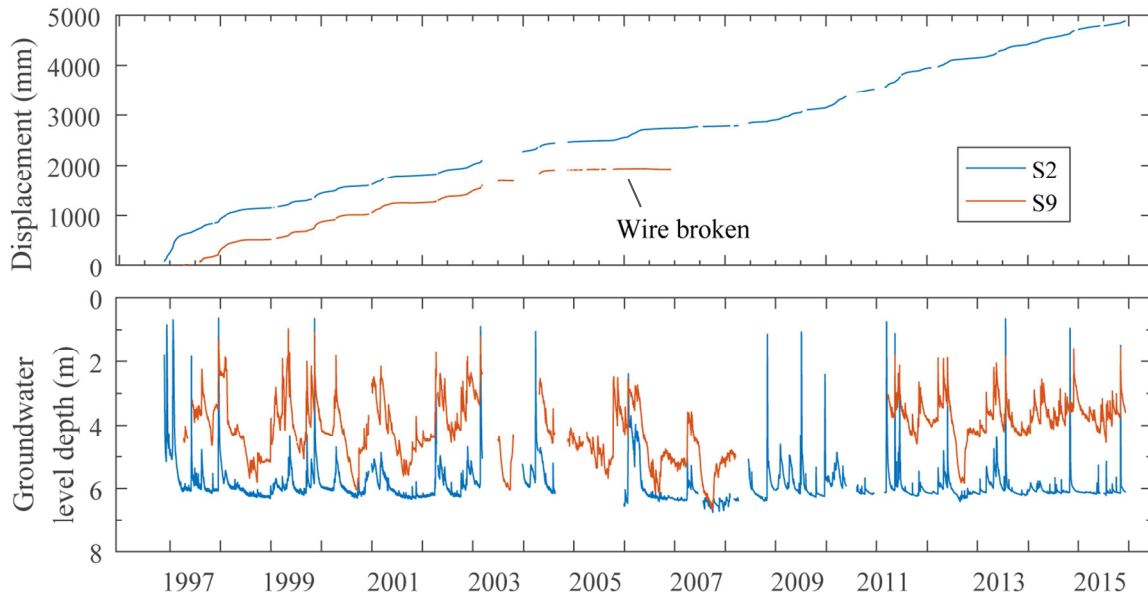


Fig 2. Displacement and groundwater level measured in boreholes S2 and S9 from Nov-1996 to Dec- 2015.

Dynamic analysis

Slow-moving landslides are usually analysed considering a viscous term. In a quasi-static approach, a perfect viscous material would show a constant strain rate when keeping all the driving forces and boundary conditions constant. In Vallcebre, such relationship between GWL and local velocity is observed in dry periods in the borehole S2. This fact suggested the existence of a viscous component in the landslide. Adding a viscous term to the linear momentum equation, assuming infinite slope conditions, and using a viscosity parameter back-analysed from monitoring data, it was possible to reproduce satisfactorily displacements and velocities for the borehole S2 [1], though the predictions were not so good for other ones (S9 and S5). The borehole S5 is near to the head of the lower unit of the landslide and the borehole S9 is close to the foot. The failure surface shows a marked curvature in both sites, and assumption of infinite slope does not hold.

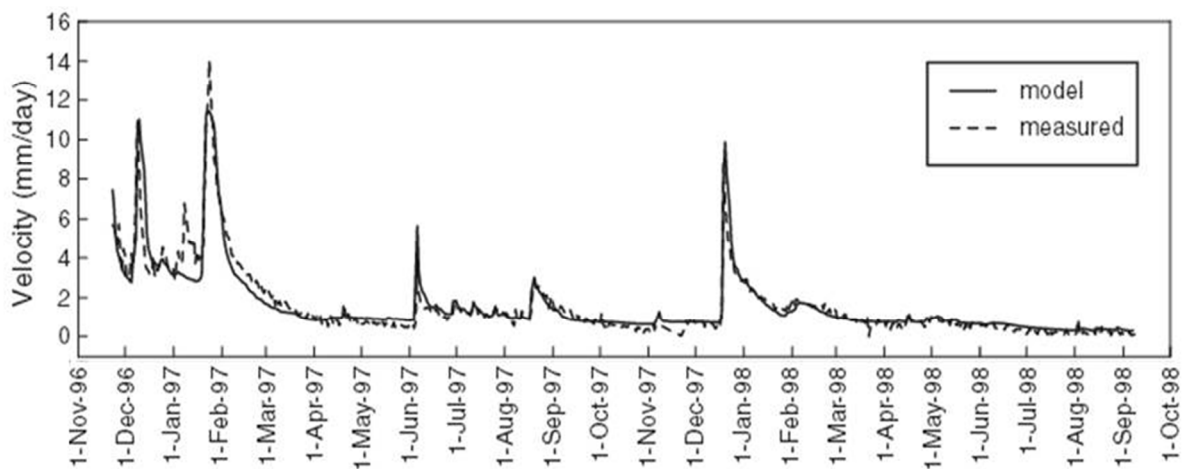


Fig 3. Measured predicted velocities at borehole S2 a using two interacting sliding blocks with different dip and Bingham viscous component (modified from [5]).

Two interacting blocks sliding on two different planes were used in [5] to model the influence of the accumulation for erosion at the toe on the behaviour of the Vallcebre landslide. The model also includes a viscous term. This is a more realistic approach to the actual geometry of the failure surface. The results obtained fit well the velocity observed in borehole S2 (Fig. 3). The model predicts that mass accumulation at the foot progressively reduces the sensitivity of the landslide behaviour to groundwater level fluctuations and that erosion has the opposite effect, as it can be expected.

This model also predicts a linear relationship between the velocity and the GWL, what does not agree the hysteresis observed in several events. The lack of hysteresis in the model results has been considered due to the small quantity of mass transferred towards the foot during the considered period (Dec-1996 to Oct-1998) [5]. Nevertheless, the displacement recorded during the last 20 years in the landslide reached less than 5 m.

CONCLUSIONS

The continuous record of both the groundwater levels and landslide displacements has shown some characteristics of the landslide behaviour that otherwise would have been missed.

The landslide shows a fast response to groundwater level changes. For steady groundwater conditions the constant velocity can be explained with a simple model including a viscous component. A hysteretic response of movement to groundwater level fluctuations has been observed in several events. That may be due to a non-constant value of the viscosity or to changes in the conditions on the landslide due to this movement; however, transfer of landslide mass towards the toe is very limited because its very slow velocity.

Mechanisms of deformation within the basal shear band alternative to viscous deformation and non-parallel groundwater flow are being considered in our current research, which require more advanced (numerical) modelling approaches.

ACKNOWLEDGEMENTS

This work has been partially carried out by the PyrMove research network, funded by the Government of Catalonia (grant AGAUR 2014CTP00051) in the framework of the Working Community of the Pyrenees. We acknowledge the essential contribution of Tomás Pérez (extensometer design), Joan Rius and David González (maintenance of the system).

REFERENCES

- [1] Corominas, J., Moya, J., Ledesma, A., Lloret, A., Gili, J.A. (2005) Prediction of ground displacements and velocities from groundwater level changes at the Vallcebre landslide (Eastern Pyrenees). *Landslides* 2, 83–96.
- [2] Corominas, J., Moya, J., Lloret, A., Gili, J.A., Angeli, M.G., Pasuto, A., Silvano, S. (2000) Measurement of landslide displacements using a wire extensometer. *Engineering Geology* 55, 149–166.
- [3] Gili, J.A., Moya, J., Corominas, J., Crosetto, M., Monserrat, O., Luzi, G. (2016) Twenty-five years of Vallcebre landslide monitoring: from theodolite to Radar. 1st IMEKO TC-4 International Workshop on Metrology for Geotechnics. Benevento, Italy, March 17–18, 2016.
- [4] Glastonbury, J., Fell, R. (2008) Geotechnical characteristics of large slow, very slow and extremely slow landslides. *Can. Geotech. J.* 45, 984–1005.
- [5] Ferrari, A., Ledesma, A., González, D.A., Corominas, J. (2011) Effects of the foot evolution on the behaviour of slow-moving landslides. *Engineering Geology* 117, 217–228.

IN-SITU MONITORING OF SLOPE MASS-WASTING. EXAMPLES FROM THE PYRENEES

Raül Oorthuis*, Marcel Hürlimann*, Jose Moya*, Jean Vaunat*

* Department of Civil and Environmental Engineering, UPC BarcelonaTECH, Spain

Slope mass-wasting triggered by rainfall is a complex phenomenon and represents an important hazard in most mountainous regions. In-situ monitoring of the involved processes is difficult due to harsh environmental conditions and the fact of remote monitoring sites. The present work shows examples of monitoring data gathered in two test sites, where shallow landslides and torrential processes produce slope mass-wasting.

Keywords: slope-mass-wasting, in-situ monitoring, Pyrenees

INTRODUCTION

Mass wasting due to shallow slope failures represents the most important erosional process in many mountainous regions and may also be the most dangerous (Hovius et al., 1997). Slope mass-wasting induced by rainfall and associated downslope/downstream sediment transfer due to debris flows and debris floods can have manifold direct and indirect consequences such as damages of infrastructure and buildings, injured persons and fatalities, soil degradation due to loss of agriculture or forested areas and volume reduction of water reservoirs.

The in-situ monitoring of rainfall-triggered mass movements is generally focusing on the hydrologic response of the natural slopes (e.g. Fannin et al., 2000; Huang et al., 2008). Very few studies have combined a sensor network recording (pre-)failure and post-failure behavior. Most of them have only been installed temporally and the failure has been triggered by artificial rainfall (e.g. Ng et al., 2008). In contrast, an interesting and exceptional case is described in Godt et al. (2009), who could monitor a rainfall-induced shallow slope failure for the first time under natural conditions.

The in-situ monitoring of slope mass-wasting in natural slopes and catchments, which will be presented in the following, is incorporated in a multidisciplinary Spanish research project called “SMuCPhy” (<http://smucphy.upc.edu>). This project focuses on the analysis of slope mass-wasting at three different scales: regional, catchment and individual slope. A main goal of the project is the investigation of future global changes (temperature, precipitation, vegetation etc.) on the rate of slope mass-wasting.

DESCRIPTION OF IN-SITU MONITORING

The two monitoring sites selected in this work are Rebaixader and Cercs, both located in the Catalan Pyrenees (Fig. 1a). The Rebaixader catchment is a typical old high-mountain glacial basin, in which slope and torrential processes are nowadays dominant. The drainage area covers 0.7 km² with altitudes between 1425 and 2475 m a.s.l. The slope mass-wasting under consideration at this site include different torrential processes like shallow slides, debris flows, debris floods, surficial sediment erosion, rockfalls etc. The in-situ monitoring was started in 2009 and consists nowadays of different wired and wireless stations (Tab. 1), which analyze the rainfall infiltration in the soil layer inside the headwater and detect the torrential processes in the downstream channel reach. Details on the monitoring system and preliminary results can be found in Hürlimann et al. (2014).

The Cercs monitoring system is installed in a shallow slope failure developed in weathered claystones of the Garumnian Facies (Upper Cretaceous-Paleocene), located in the Pre-Pyrenees (Fig 1a). The wireless monitoring consists of a set-up, which includes a meteorological station, different sensors to register the rainfall infiltration and also a wire extensometer (Tab. 1). The sensors are installed both in the weathered claystone and in the overlaying clayey colluvium.

Tab. 1 List of the sensors installed at Rebaixader and Cercs, which focus on the rainfall infiltration.

Sensor	Rebaixader	Cercs
rain gauge	1	1
air temperature sensor	2	1
relative air humidity sensor	1	1
snow height sensor	1	0
soil moisture sensor	10	3
water potential sensor	4	2
soil temperature sensor	4	2
piezometer	2	1

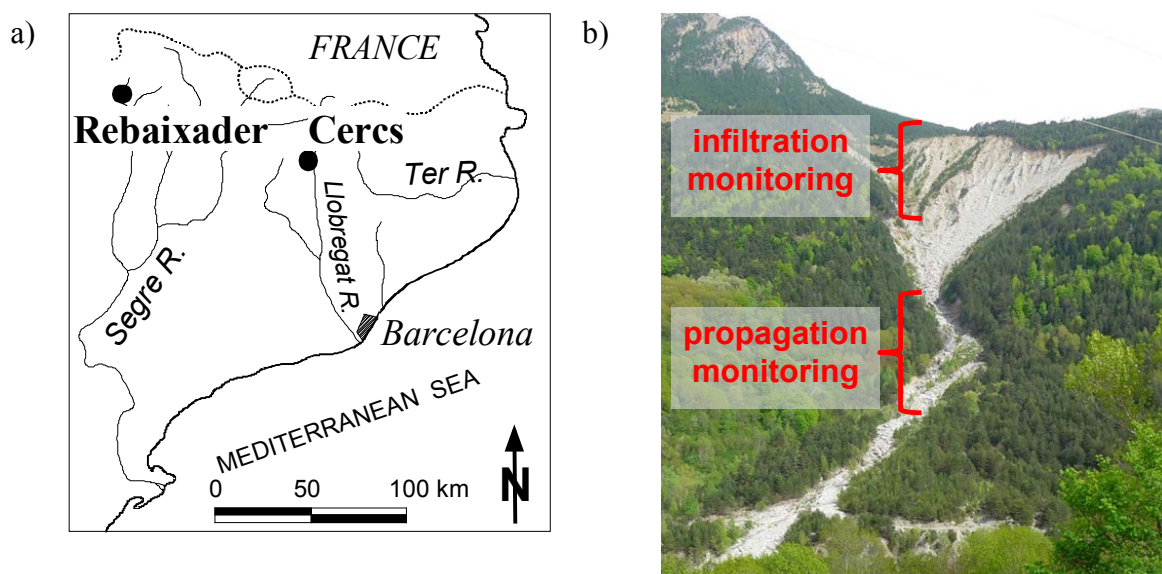


Fig. 1 a) Location of the two monitoring sites. b) General view of the Rebaixader monitoring site indicating the two principal areas of monitoring.

RESULTS

Some results on the response of the unsaturated soils in relation with precipitation are presented. Fig. 2 shows the data recorded on the rainfall infiltration in Cercs slide during 2015. The daily precipitation measurements are compared with the water potential and volumetric water content at two different depths. The data show a clear correlation between the rainfall intensity and the hydrologic regime in the unsaturated soil layer.

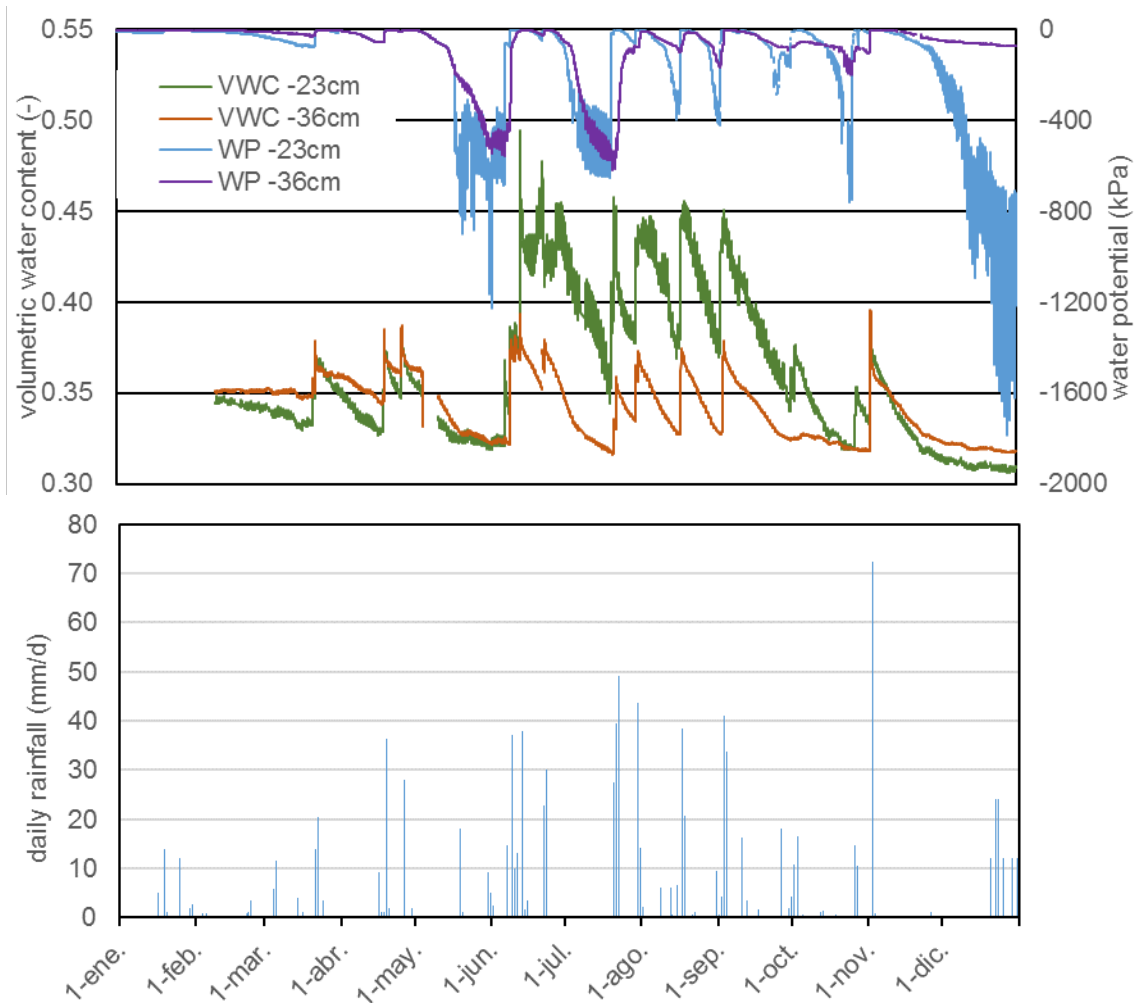


Fig. 2 Data of in-situ monitoring in Cercs gathered during 2015. The daily rainfall (below) and the response of the soil by volumetric water content and water potential (above).

The second example shows interesting data gathered at Rebaixader test site during a rainstorm on July 7th 2013. This typical summer rainstorm triggered an important debris flow in the catchment. The monitoring data reveal a clear relationship between the timing of the rainfall, the infiltration of water in the soil and the subsequent torrential process (Fig. 3). Due to the characteristics of the soil, which is formed by a glacial deposit mainly consisting of gravel and sand, the increase of water content is almost immediately.

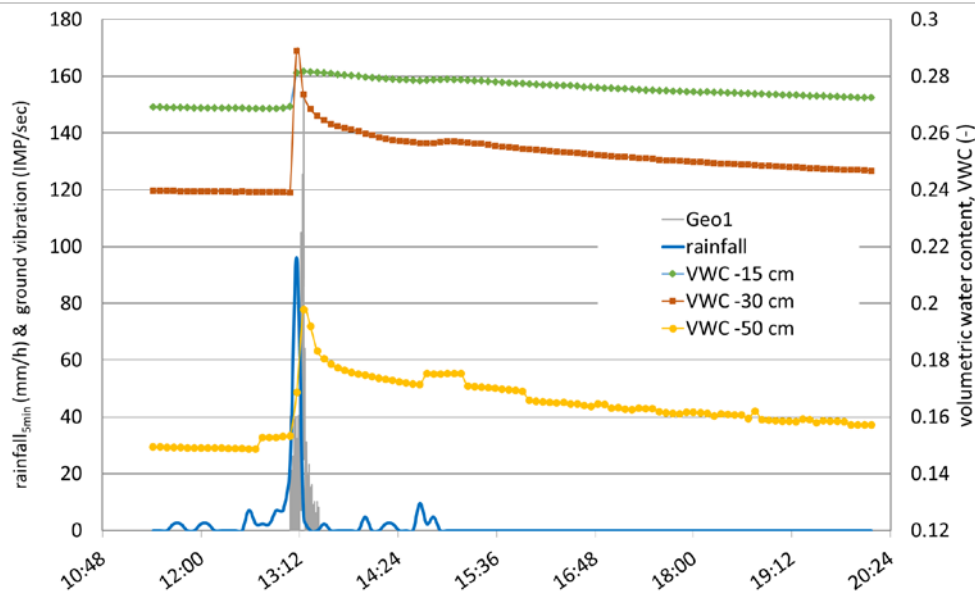


Fig. 3 Data registered at Rebaixader during a rainfall episode in July 2013 that triggered a debris flow in the catchment. The rainfall and volumetric water content are compared with the ground vibration measured at geophone Geo1.

CONCLUDING REMARKS

In-situ monitoring provides essential data for the understanding of mechanisms related to rainfall infiltration into unsaturated soils. In addition, the registered data offer necessary inputs for numerical models. Our experience shows that monitoring of slope mass-wasting is a difficult task due to harsh environmental conditions and associated technical issues. Moreover, the registered data strongly depend on the adequate installation and maintenance of the sensor system. Special focus should be taken on the accurate lithological and geotechnical understanding of the soil layer, where sensors are installed, in order to correctly interpret the gathered data.

ACKNOWLEDGEMENTS

The SMuCPHY project is funded by the Ministry of Economy and Competitiveness of Spain, with project reference number BIA 2015-67500-R.

REFERENCES

- Fannin RJ, Jaakkola J, Wilkinson JMT, Hetherington ED (2000) Hydrologic response of soils to precipitation at Carnation Creek, British Columbia, Canada. *Water Resour. Res.* 36, 1481–1494.
- Hovius N, Stark C, Allen P (1997) Sediment flux from a mountain belt derived by landslide mapping. *Geology* 25, 231–234.
- Huang C-C, Lo C-L, Jang J-S, Hwu L-K (2008) Internal soil moisture response to rainfall-induced slope failures and debris discharge. *Eng. Geol.* 101, 134–145.
- Hürlimann M, Abancó C, Moya J & Vilajosana I (2014) Results and experiences gathered at the Rebaixader debris-flow monitoring site, Central Pyrenees, Spain. *Landslides*.11(6), 939-953.
- Ng C, Springman S, Alonso E (2008) Monitoring the Performance of Unsaturated Soil Slopes. *Geotech. Geol. Eng.* 26, 799–816.

PRELIMINARY ESTIMATION OF AUBETA DEBRIS FLOW DEPOSITION AND EROSION VOLUMES USING LIDAR DATA.

J. Pinyol, M. González, M. Moysset

Cartographic and Geological Survey of Catalonia (ICGC), Parc de Montjuïc s/n, 08038 Barcelona

During the 17th and 18th June 2013 catastrophic rainfall event, a significant debris flow occurred in a torrent of the Pyrenees. Orthophotos and digital terrain models made periodically by the Cartographic and Geological Survey of Catalonia (ICGC) together work field have been used to map the debris flow area and calculate the sediment budget. The analysis of the mass balance showed that approximately 104.000 m³ was mobilized in the debris flow area, of which 71.000 m³ settled there. This implies that 33.000 m³ of sediments were incorporated into the river Valarties.

Keywords: Debris flow, LiDAR, Volumetric Sediment Budget

INTRODUCTION

In Catalonia, torrential flows are a frequent process mainly presents in two areas: the Pyrenees and the Pyrenean foothills, and the coast and the pre-coastal area of Catalonia. In the past, many significant rainfall episodes with catastrophic consequences have been inventoried. During the 20th century the most important, due to their catastrophic effect, occurred in 1907, 1937 and 1982, causing floods, deposition of sediments and damages in the infrastructures (Balasch et al., 2008). More recently, at the beginning of this century, intense rainfalls have also caused significant damage. Of note are the episodes of August 2008 in the Runer river located on the Andorra-Catalonia border (Hürlimann et al., 2011), and the recent intense torrential activity presented between 2006 and 2015 in Port-Ainé torrent (Pinyol et al., 2017).

In 2013, during the 17th and 18th of June there were a significant rainfall in the Central Pyrenees, which caused an exceptional flood of the Garonne and Noguera Pallaresa river (Oller et al., 2013). These events produced significant alterations to the river area, as well as important damage in different infrastructures. The material losses insured were estimated at 19,60 million euros according to the Insurance Compensation Consortium (2013). The causes of the flood of the Garonne were due to the coincidence of two exceptional events, a severe rainfall (124,7 mm, 101,2 mm of which corresponds to June 18) and important meltwater, due to an exceptional snow thickness. On 17th of June the flow of the Garonne river was also very high due to snow melting (125 m³/s) and suddenly the peak value increase until 280 m³/s, in Bost, the highest value since 1937 (Pineda et al., 2013).

One of the most important events inventoried by its dimensions and its effects on the environment and in the infrastructure has been the debris flow in Aubeta torrent. In this paper we present a mobilized material preliminary estimation made by space-time comparison of Digital Terrain Models (DTM) obtained from data LiDAR (Light Detection and Ranging).

STUDY SITE

The Aubeta torrent (ETRS89: 42.6587 N/ 0.8585 E) is located in the Central Pyrenees at the north side of the Aigüestortes and Estany de Sant Maurici National Park (Val d'Aran County, Spain). The Aubeta basin covers a total drainage area of 2,08 km² and its altitude ranges from 1375 m to 2502,5 m. a.s.l. (Pujalbo peak). The basin drains towards the East and ends in the Valarties River. The Melton ratio is 0,50 and the Relief ratio 1,05. The analysis of the morphometric parameters of the catchment indicates that the Aubeta basin is susceptible of generating hyperconcentrated flows (Wilford et al. 2004). From a geological point of view, the Aubeta stream is located in the Pyrenean Axial Zone, and is part of a Hercynian WNW-ESE oriented thrust fault structure. The bedrock is formed by Paleozoic materials, Cambro-Ordovician sandstone, Siluric metapelite and black shales and Devonian and Carboniferous limestones. The bedrock is in a great part covered by Quaternary glacial deposits.

DATA SET

Analyses were performed on aerial images and airborne LiDAR datasets obtained before and after the debris flow event. For the geomorphological cartography 3 sets of aerial images (orthophotos) have been used: 2011, 2013 (a month after the event) and 2015. For the quantitative analyses, the work method consists in the space-time comparison of DTMs obtained from data LiDAR, acquired in 2011 and 2016.

Data collection was carried out with the CARAVAN aircraft, owned by the ICGC, and the topographical LiDAR sensor Leica ALS50-II. The average density obtained per block is 1,928 pt/m² for 2011 and 1,577 pt/m² for 2016. For the orientation, the 3D coordinates of the laser points were obtained from the calculation of the trajectory of the airplane in the ETRS89 reference system and with point cloud adjustment obtained the dz, roll, pitch and heading corrections. The altimetry requires control points measured directly in the field with GPS. After the adjustment, an automatic points ground classification was obtained and after that it was reviewed by an expert operator. The altitudes are referred to geoid EGM08D595. For the filtering, the TerraScan module of TerraSolid software has been used. The altimetric accuracy is estimated between 15 and 50 cm depending on the slope.

For the comparative analysis between the data of 2011 and 2016, two DTM of both years were obtained from the points classified as terrain. These were obtained by the linear triangulation interpolation method, establishing a cell size of 2 x 2m. Through the subtraction between the two MDTs a difference model has been made, which allows the detection of preferential erosion and accumulation zones. The calculation of volumes of eroded and accumulated material was done with the "Cut Fill" tools of ArcGIS, which consists of a cut and fill operation and calculation of the difference in surface elevation of the MDT for each cell. With these results we obtained the sediment balance between the total volume of material loss (erosion) and increase of material (accumulation).

GEOMORPHOLOGICAL CARTOGRAPHY

Mapping of debris flow (see Fig. 1) was carried out from the helicopter inspection on 20th June 2013, from the orthophotos taken by ICGC, especially the July 2013 orthophoto, and from

the 2016 field observations. From the erosive point of view, the debris flow started in the channel itself, at the 2080 m. a.s.l. Nevertheless, a significant lateral scar of 5.250 m² was identified at 1907 m. a.s.l., which undoubtedly incorporated a great amount of sediments to flow. The debris flow traveled 1.960 meters to the Valarties river, eroding importantly the bed and lateral margins, but also depositing in elevated areas, waters behind the dike of the 1539 m. a.s.l. and above all, in the cone of dejection. From all these observations, the cartography of the area affected by the debris flow was carried out. This area was used as an area of analysis for the comparison of MDTs.



Fig. 1 Orthophotos before and after the debris flow. At top, 2011 orthophoto shows the parking in the dejection cone. At bottom, 2013 orthophoto with delimited debris flow area (in red).

VOLUME CALCULATION RESULTS

By comparing the MDTs, accumulations of up to 8,6 meters and erosions of up to 14,7 meters have been observed (see Fig 2). The maximum accumulations have occurred in the dejection cone, in the area that was lowered for use as parking. The maximum erosions have occurred in the lateral scar. The total debris flow mass balance calculation showed that 104.000 m³ was mobilized in the debris flow area, of which 71.000 m³ settled there. This implies that 33.000 m³ of sediments were incorporated into the river Valarties. It is worth noting that the MDT of 2016 includes several anthropic modifications made in the dejection cone due to tourist interest. However, it has been considered that the sediment was not transported outside the study area.

CONCLUSIONS

This paper presented a methodology for analyses of debris flow using space-time comparison of Digital Terrain Models (DTM) obtained from data LiDAR (Light Detection and Ranging), acquired in 2011 and 2016. The following summarizes the conclusions:

The Aubeta catchment basin is characterized by the following morphometric parameters: its area are 2,08 km², the Melton ratio is 0,50 and the Relief ratio 1,05. The analysis of these parameters indicates that the Aubeta basin is susceptible of generating hyperconcentrated flows.

The maximum accumulations have occurred in the dejection cone, in the area that was lowered for use as parking. The maximum erosions have occurred in the lateral scar. The total debris flow mass balance calculation showed that 104.000 m³ was mobilised in the debris flow area, of which 71.000 m³ settled there. This implies that 33.000 m³ of sediments were incorporated into the river Valarties.

The methods proposed are recommended for quickly and accurately estimation of the mobilized material. Nevertheless, we would like recommend the importance of carrying out the LiDAR flight immediately after of the occurrence of the event, before that anthropic action modified the mobilized material.

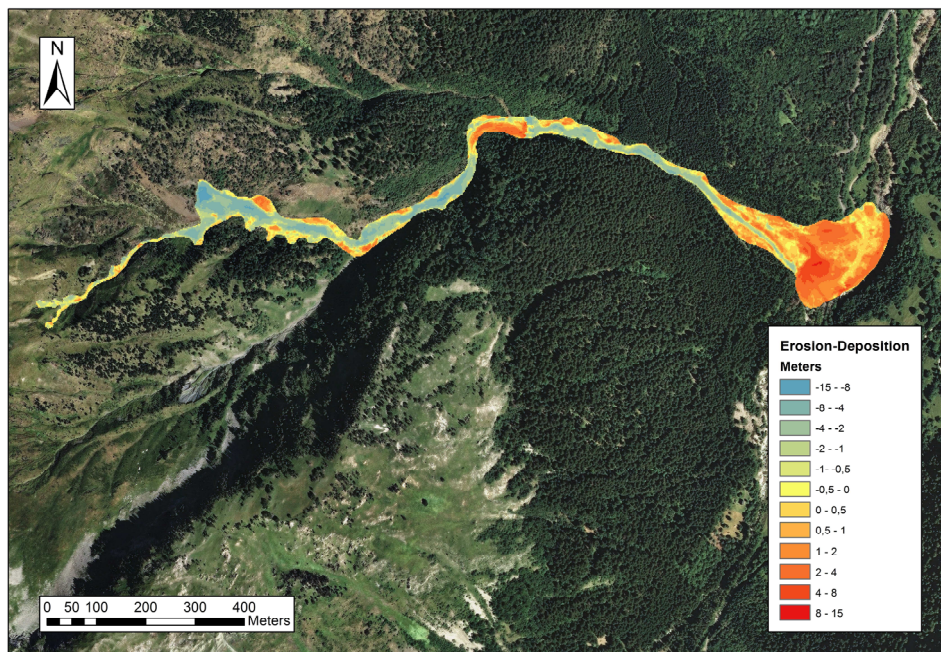


Fig. 2 Results of the difference model between the two MDTs (2011-2016).

REFERENCES

- Balasc C, Becat J, Marugán CM, Nadal A, Rapalino V & Remacha R (2008) Les riuades del segle XX al Pallars Sobirà: 1907, 1937 i 1982. Arxius i societat, Quaderns de divulgació històrica, Núm 2. Departament de Cultura i Mitjans de comunicació, Generalitat de Catalunya. 239p.
- Hürlimann M, Abancó C, Moya J, Raïmat, C & Luis-Fonseca R (2011) Debris-flow monitoring stations in the eastern Pyrenees. Description of instrumentation, first experiences and preliminary results. Italian Journal of Engineering Geology and Environment - Book. Casa Editrice Università La Sapienza, 2011. DOI: 10.4408/IJEGE.2011-03.B-061, pp. 553-562.
- Oller P, Pinyol J, González M, Ripoll J & Micheo M^aJ (2013) Efectes geomorfològics de l'aiguat i riuada del 18 de juny de 2013. *Proceedings of the conferences La gestió de les inundacions*, November 27 and 28, 2013.
- Pineda N, Prohom M, Serra A, Martí G, Garcia C, Velasco E & Gracia A (2013) Efectes geomorfològics de l'aiguat i riuada del 18 de juny de 2013. *Proceedings of the conferences La gestió de les inundacions*, November 27 and 28, 2013.
- Pinyol J, Hürlimann M, Furdada G, Moysset M, Palau RM^a, Victoriano A, Gonzalez M, Moya J, Guinau M, Raïmat C & Fañanás C (2017) El barranco de Portainé (Pirineo Central): Un laboratorio in situ completo para el estudio de la actividad torrencial. Abstract accepted in IX Simposio Nacional sobre Taludes y Laderas Inestables, June 27-30, 2017.
- Wilford DJ, Sakals ME, Innes JL, Sidle RC & Bergerud WA (2004) Recognition of debris flow, debris flood and flood hazard through watershed morphometrics. *Landslides (2004) 1*: DOI 10.1007/s10346-003-0002-0. Published online: 5 March 2004, Springer-Verlag, pp. 61-66.

STABILITY OF RESIDUAL SOIL SLOPES BASED ON SPATIAL DISTRIBUTION OF SOIL PROPERTIES

Harianto Rahardjo*, Alfrendo Satyanaga[†]

* Professor, School of Civil and Environmental Engineering, Nanyang Technological University, Singapore, chahardjo@ntu.edu.sg

[†] Research Fellow, School of Civil and Environmental Engineering, Nanyang Technological University, Singapore, alfrendo@ntu.edu.sg

Residual soils are highly heterogeneous with highly variable properties in nature due to the spatial variation of degrees of weathering. In this study, the geostatistical method was used as a preliminary attempt to model the spatial distribution of residual soils in Singapore. The stability analyses were carried out to understand the variations of factor of safety within several zones of residual soils from three different rock formations in Singapore.

Keywords: residual soil, geostatistical method, factor of safety, spatial distribution

INTRODUCTION

Residual soils are formed by the in situ weathering of rocks (Wesley, 1990) and they can be found in large areas of the world. Residual soil slopes are commonly unsaturated since water table in the residual soil is generally quite deep (Rahardjo et al., 2004). The negative pore-water pressure or matric suction of the unsaturated soil contributes to the shear strength and overall stability of the slope (Fredlund and Rahardjo, 1993). The infiltration of rainwater into residual soil slopes causes the changes in negative pore-water pressure and consequently in the shear strength of unsaturated soil and the stability of the residual soil slope during rainfall (Rahardjo et al., 2008; Fredlund et al., 2012). The problems associated with infiltration and slope stability variation during rainfall are complex due to the highly non-linear analyses involving unsaturated soil properties (Ng et al., 2001; Rahardjo et al., 2013). In addition, the variability in degree of weathering contributes to the non-homogeneity of residual soil and the spatial distribution of its properties. As a result, the stability analyses of residual soil slopes can be quite complex. Classic statistical methods may be inadequate for interpolation of spatially dependent variables since these methods assume random variation and do not consider spatial correlation and relative locations of soil samples. Geostatistical analyses recognize these difficulties and provide tools to facilitate the spatial distribution of residual soil properties. The objective of this study is to perform geostatistical analyses for the development of soil property and factor of safety zonation map for Singapore.

METHODOLOGY

The study consisted of four stages of research works. In the first part of the study, the characteristics of residual soil properties from different locations within a selected zone were inves-

tigated through saturated and unsaturated laboratory tests. In the second part of the study, geostatistical analyses were carried out using Kriging method to estimate the spatial distribution of residual soil properties. As a result, the appropriate boundary of the selected zone could be established. In the third part of the study, stability analyses were conducted using typical saturated and unsaturated shear strength data to generate variations of factor of safety within each of the established zones. In the fourth part of the study, analytical hierarchy process was performed to determine the weight value of each factor contributing to slope stability. Thereafter, the spatial analyses were carried out to generate the preliminary slope susceptibility map of Singapore.

SOIL CHARACTERIZATION

Forty-four slopes in Singapore were selected for site investigations which are located in the residual soils from the sedimentary Jurong Formation (JF), Bukit Timah Granite (BTG) and Old Alluvium (OA) (see Fig. 1). Laboratory tests were performed on the undisturbed soil samples obtained from site investigations of the forty-four slopes. The laboratory tests comprised of index properties tests, saturated permeability, soil-water characteristic curves (SWCC), saturated and unsaturated triaxial tests. The soil samples were classified under the Unified Soil Classification System (USCS) using the information from the index properties tests (ASTM D2487-10). SWCC was obtained from combination of three different tests using Tempe cell and pressure plate following procedures explained in Fredlund et al. (2012). Saturated permeability was measured using a triaxial permeameter with two back-pressure systems as described by Head (1986). Saturated shear strength parameters (i.e. c' and ϕ') were obtained from consolidated undrained triaxial tests with pore-water pressure measurements (ASTM D4767-04) whereas unsaturated shear strength parameter ϕ^b was obtained from consolidated drained triaxial tests using a modified triaxial apparatus (Fredlund and Rahardjo, 1993).

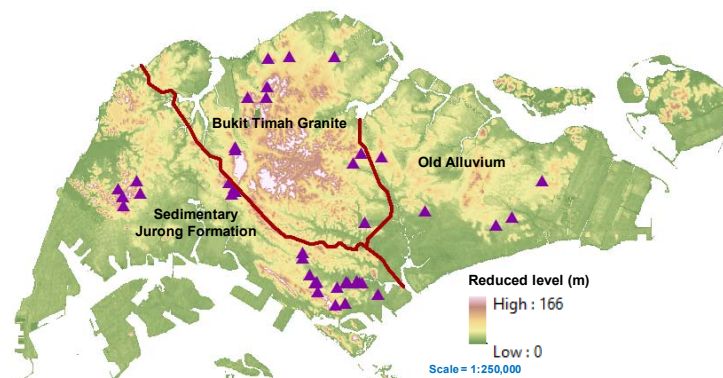


Fig. 1 Location of soil investigations in Singapore

SPATIAL DISTRIBUTION OF SOIL PROPERTIES

Geostatistical analyses were carried out using Ordinary Kriging method to create the spatial variations of soil properties (digital soil mapping) in Singapore. R software package (RStudio v0.98.1102) was used for statistical computation in this study since this software is commonly used for sophisticated spatial data analyses (Brundson and Comber, 2015; Bivand et al.,

2013). Ordinary Kriging was used in the analyses since it is the simplest form of Kriging, but it is also the most robust (Li and Heap, 2014). The spatial analyses results from R software were exported into Quantum Geographical Information System (QGIS v2.10 Pisa) for data viewing and analysis. The input for the spatial analyses consisted of basic map of Singapore and the soil properties data which included variables of SWCC (i.e. air-entry value), Fredlund and Xing (1994) fitting parameter (i.e. a , n and m), shear strength parameters (i.e. c' , ϕ' and ϕ^b). Study by Zhai et al. (2016) showed that the upper and the lower bounds of the saturated permeability (k_s) and the saturated volumetric water content (θ_s) were found to be in the narrow band. Therefore, the envelopes of k_s and θ_s for the JF, BTG and OA residual soils were assigned to all zones of JF, BTG and OA, respectively in Fig 3. Georeferenced map used in this study was based on a coordinate reference system. Based on the spatial distributions of air-entry value, effective cohesion (c'), effective friction angle (ϕ') and ϕ^b angle, the preliminary zonation of soil properties in Singapore was established (see Fig. 3). Figs. 2a to 2c present the results of the Ordinary Kriging analyses on the shear strength parameters, c' , ϕ' and ϕ^b .

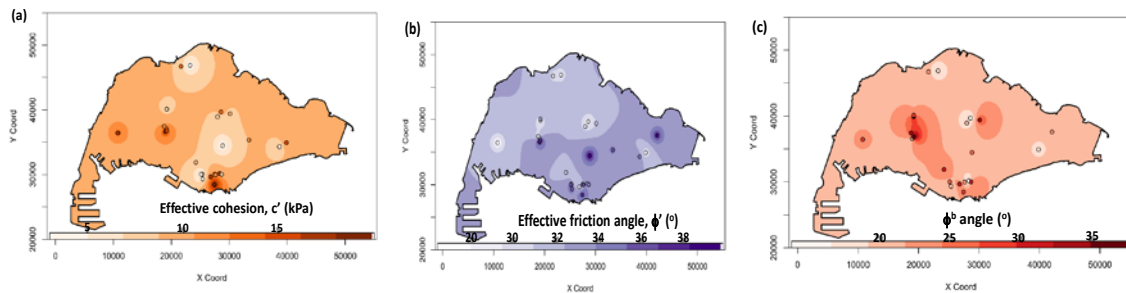


Fig. 2 Spatial distribution of (a) effective cohesion, (b) effective friction angle and (c) ϕ^b angle in Singapore

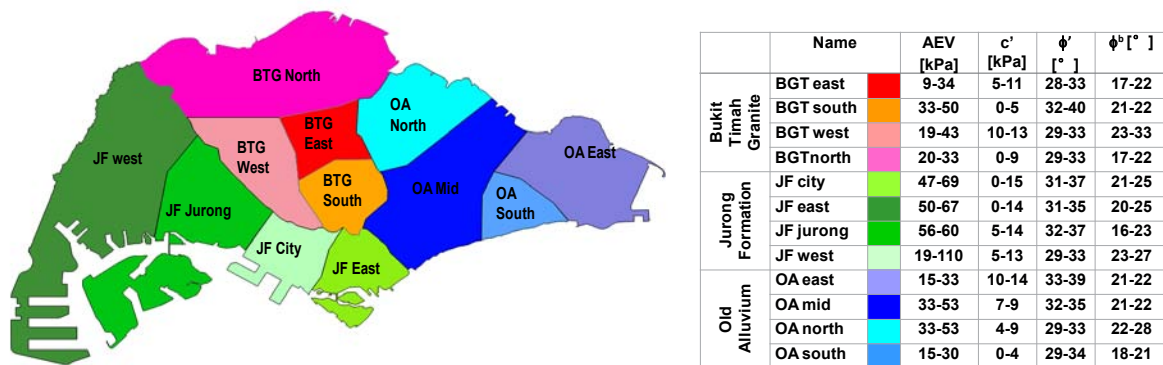


Fig. 3 Preliminary digital soil mapping of Singapore

SLOPE STABILITY ANALYSES

Seepage analyses were conducted using Seep/W (Geoslope, 2012a) to obtain variations of pore-water pressures under dry and rainy periods for different soil zonations in Singapore. The upper and lower bounds of air-entry value as well as Fredlund and Xing (1993) fitting parameters a , n and m were used to generate upper and lower bounds of SWCC for each zonation in Fig. 3. The upper and lower bounds of saturated permeability and SWCC were used to

generate the unsaturated permeability for each zonation. Then, these soil properties were incorporated in the seepage analyses under an extreme rainfall of 22 mm/h for 24 hours. Typical groundwater table position and geometry of residual soil slope in Singapore (see Fig. 4) were used in the analyses. The results from seepage analyses were exported to Slope/W (Geoslope, 2012b) for slope stability analyses. The upper and lower bounds of shear strength parameters were used in these analyses to establish the upper and lower bounds of the variations in factor of safety, respectively for different zonations in Singapore. The results from slope stability analyses of slope at BTG North are presented in Fig. 5.

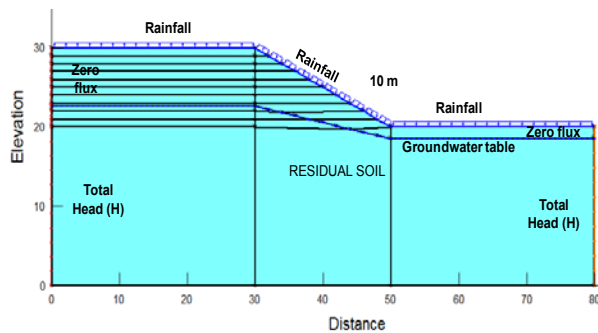


Fig. 4 Slope model for stability analyses

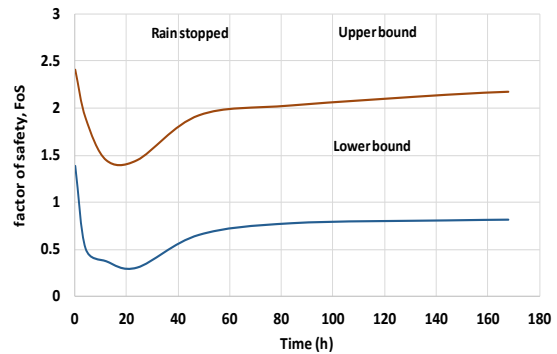


Fig 5. Upper and lower bounds of variations of factor of safety for BTG North

SLOPE SUSCEPTIBILITY MAP

The upper and the lower bounds of the initial and the minimum factor of safety as well as the differences between the initial and the minimum factor of safety were used as the main factors in the development of slope susceptibility map. The other factors were the gradient and the elevation of the slope. Analytical hierarchy process (AHP) developed by Satty (1980) was used in generating the hierarchical structure of these 8 factors. While applying AHP, factors are compared with each other to determine the relative preference of each factor in accomplishing the overall goal. Numerical values are assigned to each pair of the factors using the guidelines established in Fundamental Satty’s Scale (Satty, 1980). The calculated weighted values were as follows: 2.4 % for slope gradient, 2.4 % for slope elevation, 7.6 % for the lower bound of the initial factor of safety, 6.8 % for the upper bound of the initial factor of safety, 87.4 % for the lower bound of the minimum factor of safety, 22.2 % for the upper bound of the minimum factor of safety, 11.8 % for the lower bound of the differences in the factor of safety and 10.8 % for the upper bound of the differences in the factor of safety. After assigning the weight values to these main factors, the cumulative weight value for each grid in the slope susceptibility map was calculated using the landslide hazard zonation model developed by Esmali (2003). Figure 6 presents the preliminary slope susceptibility map of Singapore. It shows that the majority of very high risk areas are located in the west-north location of Singapore. This result is in agreement with the locations of slope failures in Singapore which occurred during periods of heavy rainfalls in December 2006 and January 2007 by Rahardjo et al. (2007) (see Fig. 6).

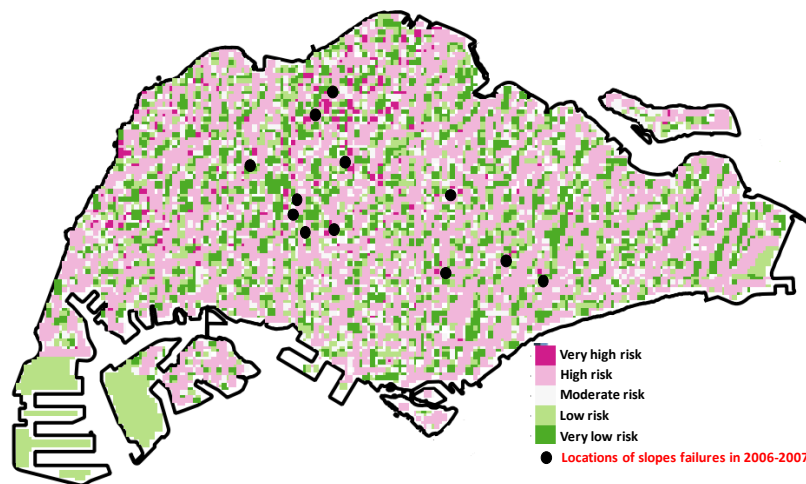


Fig. 6 Preliminary slope susceptibility map with location of previous slope failures in Singapore

REFERENCES

- ASTM D2487-10 (2010) Standard practice for classification of soils for engineering purposes (Unified Soil Classification System). *Annual Book of ASTM Standards*, Vol. 04.08, ASTM International, West Conshohocken, PA.
- ASTM D4767-04 (2004) Standard test method for consolidated undrained triaxial compression test for cohesive soils. *Annual Book of ASTM Standards*, Vol. 04.08, ASTM International, West Conshohocken, PA.
- Bivand R, Pebesma E & Gomez-Rubio V (2013) Applied Spatial Data Analysis with R, Springer.
- Brundson C & Comber L (2015) An Introduction to R for spatial analysis & mapping, SAGE.
- Esmali A (2003) Using GIS & RS in Mass Movements Hazard Zonation - A Case Study in Germichay Watershed, Ardebil, Iran, Ph. D. Thesis, Tehran University, Karaj, Iran.
- Fredlund D G & Xing A (1994) Equations for the soil-water characteristic curve. *Canadian Geotechnical Journal* 31, 521-532.
- Fredlund D G, Rahardjo H & Fredlund MD (2012) Unsaturated soil mechanics in engineering practice. New York: John Wiley & Sons, Inc., pp. 926 (ISBN 978-1-118-13359-0).
- Geoslope International Pte Ltd (2012a) SEEP/W for Seepage Analysis. Geoslope International Ltd., Canada.
- Geo-Slope International Pte Ltd (2012b) SLOPE/W for Slope Stability Analysis. Geo-slope International Ltd., Canada.
- Head KH (1986) Manual of Soil Laboratory Testing. Vol. 2, 1st ed., ELE International Ltd.
- Li J & Heap AD (2014) Spatial interpolation methods applied in the environmental sciences: A review. *Environmental Modelling & Software*, 53, 173 -189.
- Ng CWW, Wang B & Tung YK (2001) Three-dimensional numerical investigations of groundwater responses in an unsaturated slope subjected to various rainfall patterns. *Canadian Geotechnical Journal*, 38, 1049–1062.
- Rahardjo H, Aung KK, Leong EC & Rezaur RB (2004) Characteristics of residual soils in Singapore as formed by weathering. *Engineering Geology* 73, 157-169.
- Rahardjo H, Satyanaga A, Leong EC, Ng YS, Foo MD & Wang CL (2007) Slope failures in Singapore due to rainfall. *Proceedings of 10th Australia New Zealand Conference on Geomechanics "Common Ground"*. Brisbane, Australia, 21-24 October, 2, 704 – 709.
- Rahardjo H, Rezaur RB, Leong EC, Alonso EE, Lloret A & Gens A (2008) Monitoring and modeling of slope response to climate changes. KEYNOTE LECTURE. *Proceedings of the 10th International Symposium on Landslides and Engineered Slopes*. Chinese Institution of Soil Mechanics and Geotechnical Engineering – Geotechnical Division of the Hong Kong Institution of Engineers, Xi'an, China, 30 June – 4 July, 1, 67-84.
- Rahardjo H, Satyanaga A & Leong EC (2013) Effects of flux boundary conditions on pore-water pressure distribution in slope. *Journal of Engineering Geology, Special Issue on Unsaturated Soils: Theory and Applications*, 165, 133-142.
- Zhai Q, Rahardjo H & Satyanaga A (2016) Variability in unsaturated hydraulic properties of residual soil in Singapore. *Engineering Geology* (Accepted April 2016).
- Saaty TL (1980) The analytical hierarchy process, McGraw Hill, New York.
- Wesley LD (1990) Influence of structure and composition on residual soils. *Journal of Geotechnical Engineering*, 589-603.

THE USE OF INSAR IN LANDSLIDE MONITORING

Josep Raventós*, Marcos Arroyo†

* TRE ALTAMIRA, Carrer Còrsega 381-387. 08037 BARCELONA, SPAIN. josep.raventos@tre-altamira.com

† DECA- UPC, BARCELONA, SPAIN

InSAR (acronym for Interferometry of Synthetic Aperture Radar) uses the electromagnetic wave signal emitted by radars shipped in satellites orbiting in quasi polar orbits to measure with millimetric accuracy displacements of the Earth's surface or objects on it. The first SAR sensors were shipped in the early 1990s providing the possibility to process data from the past. Together with the schedule of new satellite acquisitions it allows investigations on slope stability before the start of the project, during construction and for the maintenance of the infrastructure.

The paper describes the use of this microwave remote sensing technique to monitor ground displacement over a site where landslides occur in different contexts: the case study describes the use to monitor slopes surrounding water reservoirs in the hydropower generation sector.

Keywords: monitoring, InSAR, Remote Sensing, Satellite, Radar, electromagnetic Pulse, PSI, measurement point

INTRODUCTION

Interferometric Synthetic Aperture Radar (InSAR) technology is a well consolidated operational tool used worldwide for measuring and monitoring ground motion. Compared to other surveying techniques, InSAR has the advantage of offering a high density of measurement points over large areas, including areas that are dangerous or difficult to access. Advanced InSAR techniques, such as PSInSAR and SqueeSAR, developed in the last decade, provide high precision time series of movement that allow typical displacement patterns, such as changes in ground movement over time as well as seasonal uplift/subsidence cycles, to be highlighted. Additionally an archive historical of SAR data acquired from 1992 is available and can be used to analyze the ground movements happened in the past.

The main objective of this study is to show the application of methodologies based on SAR satellites to detect and monitor ground motion related to landslides. The case study presented in this paper focuses on the application of advanced Persistent Scatterer Interferometry (PSI) technique to monitor both past and present ground movements over all the slopes draining to a water reservoir in Spain.

TECHNICAL BASIS OF DINSAR

Differential Aperture Synthetic radar interferometry (DInSAR) is a remote sensing technique able to measure surface deformation on the ground using complex satellite radar image datasets. The main information used by DInSAR analysis corresponds to the interferometric phase obtained by the computation of the phase difference between a pair of SAR images, the interferogram. The phase information coming from an interferogram is the sum of the ground displacement but it also contains other components that must be retrieved to achieve millimetric accuracy (phase noise related with the scatter quality; atmospheric noise related with the signal distortions due to the propagation through the atmosphere; topographic error related on the difference between real topography and model topography). These three components not related with ground motion can be retrieved by using a high quality Digital Elevation Model (DEM) in the case of the topographic part, and the use of advanced DInSAR techniques (Ferretti et al., (2001); Lanari et al., (2004)).

The displacement estimation in DInSAR techniques is based on the phase unwrapping, which is the most critical process in the processing chain. To perform the unwrapping properly, the gradient of displacement must accomplish two conditions, one related with time and other with space. In space, the phase gradient between close pixels cannot be greater than π , otherwise it is not possible to follow spatially the real displacement. Similarly, in time the velocity of displacement cannot be greater than a quarter of the wavelength between acquisitions. The latter can be achieved acquiring images at the greater rate of acquisition over long periods of times which, moreover, allows redundant information to be obtained. This information helps the noise derived by atmospheric artifacts to be reduced and accuracy to be improved. This later issue was developed in some advanced DInSAR techniques, including Permanent Scatterers (Ferretti et al., 2000) and the Small Baseline Subset (Berardino et al., 2002; Lanari et al., 2004). Other interesting approaches can be found in Werner et al., 2003, Mora et al., 2003 and Hooper et al., 2004. In the best-case velocity precision may be below 1 mm/year as described in Colesanti et al., 2003.

Since the first description of DInSAR technique using SEASAT SAR data by Gabriel et al., 1989, DInSAR techniques were applied in a wide range of applications as landslides (Tamburini et al., 2013), seismology (Massonet et al., 1993), volcanology (Amelung et al., 2000), glaciology (Goldstein et al., 1993), terrain subsidence (Galloway et al., 1998), etc. Further details on the applications of advance DInSAR techniques can be found in Rosen et al., (2000), Hanssen (2001) and Ferretti (2014).

PSI TECHNIQUES AND SQUEESARTM MILLIMETRIC MOTION ESTIMATION

During years, InSAR analysis was performed on the basis of analyzing the position and control of very coherent radar reflectors - called Permanent Scatterers (PS) - that can be detected in the whole dataset. This so called PS-InSAR application (Ferretti et al., 2000) was able to achieve millimetric accuracies in motion estimation with very good results and significant density of measurement points where natural reflectors are found (urban areas, areas with infrastructure concentration and/or rocky outcrops, etc) . In order to improve point density in the other areas also reflectors known as Distributed Scatterers (DS) were took into account. The DS measurement point corresponds to areas showing similar SAR signals. The size of the area is dependent on the pixel size and the number of adjacent pixels showing the same SAR signal.

SqueeSAR (Ferretti et al, 2001) is one of the advanced processing techniques that uses both PS and DS that preserves the PS-InSAR accuracy while expanding the use of the technique to more challenging sites where no significant natural reflectors density are expected. The SqueeSAR algorithm also produces improvements in the quality of the displacement time series. The single time series attributed to each DS is estimated by averaging the time series of all pixels within the DS, effectively reducing noise in the data.

CASE STUDY

One of the studies presented is in the context of a dam built in 1950s and located on a subsidiary river of Ebro. Due to its installed capacity, this dam plays a major role in the Southeastern hydropower system of the river. It’s a gravity dam of 140m height and 200m length in coronation. The reservoir capacity is 912.6hm³ and its surface about 1800ha. The installed capacity is of 108MW.

Two different studies regarding the slope stability of the reservoir are performed. The first, an historical study in both geometries of acquisition with c band sensor ENVISAT from 2003 to 2010 and a monitoring study with another c band sensor called Sentinel from October 2014 to the end of 2016.

Figure 1 shows the point density obtained with Sentinel. Table 1 shows the time coverage and the number of images used in both studies.

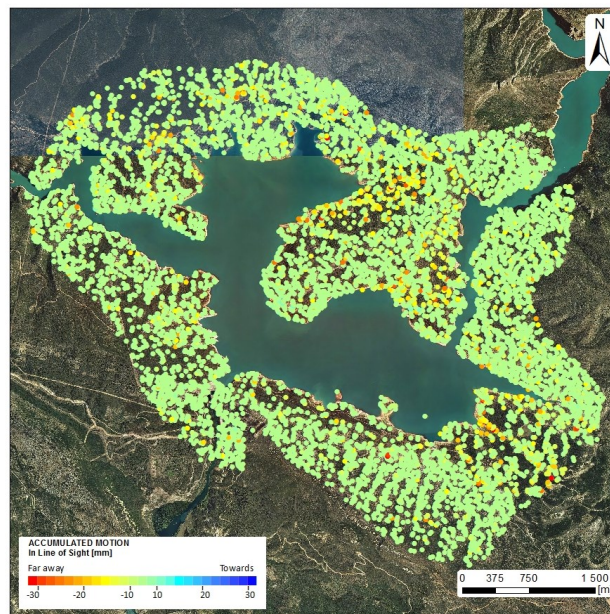


Figure 1. Measurement points density with a single geometry of acquisition with Sentinel from 2014 to 2016.

Table 1. Dataset and geometry of acquisition

Satellite	Geometry	# of images	Time spam	LOS angle
Envisat	Ascending	27	14/01/2003-10/08/2010	20.79°
Envisat	Descending	29	14/01/2003-10/08/2010	19.78°
Sentinel	Ascending	45	28/02/2015-26/09/2016	44.22°

REFERENCES

- Amelung, F., Jonson, S., Zebker, H.A., Segall, P. (2000). “Widespread uplift and 'trapdoor' faulting on Galápagos volcanoes observed with radar interferometry”. *Nature*, 407, 993-996.
- Berardino, P., Fornaro, G., Lanari, R., Sansosti, E. (2002). “A new algorithm for surface deformation monitoring based on small baseline differential SAR interferograms”. *IEEE Transactions on Geoscience and Remote Sensing*, 40(11), 2375-2383.
- Colesanti, C., A. Ferretti, C. Prati, C. and F. Rocca. 2003, Monitoring landslides and tectonic motions with the Permanent Scatterers Technique. *Engineering Geology*. 68: 3–14.
- Ferretti, A., Prati, C., and Rocca, F. 2000, Nonlinear subsidence rate estimations using permanent scatterers in differential sar interferometry. *IEEE Transactions on Geoscience and Remote Sensing*, 38(5):2202–2212
- Ferretti, A., C. Prati, and F. Rocca. 2001, Permanent scatterers in SAR interferometry. *IEEE Trans. Geosci. Remote Sens.* 39(1): 8–20.
- Ferreti, A. (2014). “Satellite InSAR Data. Reservoir Monitoring from Space”. EAGE Publications.
- Gabriel, A.K., Goldstein, R.M., Zebker, H.A. (1989). “Mapping small elevation changes over large areas: differential radar interferometry”. *J. Geophys. Res.*, 94 (B7), 9183-9191.
- Galloway, D.L., Hudnut, K.W., Ingebritsen, S.E., Phillips, S.P., Peltzer, G., Rogez, F., Rosen, P.A. (1998). “Detection of aquifer system compaction and land subsidence using interferometric synthetic aperture radar, Antelope Valley, Mojave Desert, California”. *Water Resources Research*, 34 (10), 2573-2585.
- Goldstein, R.M., Englehardt, H., Kamb, B., Frolich, R.M. (1993). “Satellite radar interferometry for monitoring ice sheet motion: application to an Antarctic ice stream”. *Science*, 262, 1525-1530.
- Hanssen, R. (2001). “Radar interferometry”. Kluwer Academic Publishers, Dordrecht, The Netherlands.
- Hooper, A., Zebker, H., Segall, P., Kampes, B. (2004). “A new method for measuring deformation on volcanoes and other natural terrains using InSAR Persistent Scatterers”. *Geophysical Research Letters*, 31, L23611, doi:10.1029/2004GL021737.
- Lanari, R., Mora, O., Manunta, M., Mallorquí, J.J., Berardino, P., Sansosti, E. (2004). “A small-baseline approach for investigating deformations on full-resolution differential SAR interferograms”. *IEEE Transactions on Geosciences and Remote Sensing*, 42(7), 1377-1386.
- Massonnet, D., M. Rossi, C. Carmona, F. Adragna, G. Peltzer, K. Feigl, and T. Rabaute. 1993, The displacement field of the Landers earthquake mapped by radar interferometry. *Nature*. 364: 138–142.
- Mora, O., Mallorquí, J.J., Broquetas, A. (2003). “Linear and nonlinear terrain deformation maps from a reduced set of interferometric SAR images”. *IEEE Transactions on Geosciences and Remote Sensing*, 41(10), 2243 –2253.
- Rosen, P.A., Hensley, S., Joughin, I.R., Li, F.K., Madsen, S.N., Rodríguez, E., Goldstein, R.M. (2000). “Synthetic Aperture Radar Interferometry”. *Proc. of the IEEE*, 88 (3), 333-382.
- Tamburini, A., S. Del Conte, G. Larini, L. Lopardo, C. Malaguti and P. Vescovi. 2013, Application of SqueeSAR™ to the characterization of deep seated gravitational slope deformation: the Berceto case study (Parma, Italy). In *Landslide Science and Practice*, eds. C. Margottini, P. Canuti, K. Sassa, Springer, 437-443.
- Werner, C., Wegmüller, U., Strozzi, T., Wiesmann, A. (2003). “Interferometric point target analysis for deformation mapping”. *Proceedings of IGARSS 2003*, 4362-4364.

WETTING COLLAPSE AND FAILURE OF AN SLOPE TESTED IN CENTRIFUGE MACHINE

Álvaro Ruiz*, Mauricio Alvarado*[†], Núria M. Pinyol*[†], Bernardo Caicedo[#]

* Centre Internacional de Metodes Numerics en Enginyeria (CIMNE), Barcelona, Spain

[†] Universidad Politécnica de Catalunya (UPC). Barcelona, Spain

[#] Universidad de los Andes, Bogotá, Colombia

This paper presents a centrifuge model of a silty clay slope. The increase of the gravity acceleration is applied to the slope under unsaturated conditions. The slope is wetted in flight by means of water injection from the bottom. The deformation of the slope and the subsequent failure is analyzed. In order to avoid difficulties in the installation of sensors in the prototype, the model was built in a box of transparent walls and the slope behavior during the flight was recorded using a digital camera. The images were analyzed using the PIV method (Particle Image Velocimetry) and processed by means of the methodology called PIV-NP with the aim of obtaining accumulated displacements and strains. This methodology is able to provide the strains from PIV measurements following an Eulerian scheme even in case of large deformations. The experimental results indicate that the wetting-induced volumetric strains (collapse) occurred in the wetting front and the soil located above settled as a rigid block. The slope failure was observed at a certain time before the wetting front reached the slope surface and the failure surface was located close to the wetting front.

TEST DESCRIPTION AND PIV ANALYSIS

The slope model was carried out in the centrifuge of the geotechnical laboratory of the Universidad de los Andes in Bogotá (Colombia) (Fig. 1a). The prototype of the slope was built in the transparent box shown in Figure 1b. Dimensions of the slope are indicated in the figure. The slope inclination is 50°. The tested soil was a silty clay of low plasticity ($w_L=33\%$, $IP=18\%$) used in the construction of a dam core (Albagés dam, Spain). Initially, the soil exhibited an average water content of 10% and an average dry density of 1.5 kg/m^3 ($e = 0.8$). A column of gravel was built on the right side of the slope in the contact between the soil and the lateral wall of the box to facilitate the lateral inflow of water towards the slope.

After slope construction, the centrifuge flight started by increasing the gravity until 50g which corresponds to an increase of the scale of the prototype equal to 50 times. Therefore, the 15 cm high of the slope are equivalent to 7.5 m. During the centrifuge flight water injection from the box base was imposed.

The entire experiment was recorded by capturing images at 60 frames per second (fps) with a digital camera GoPro with 1440 pixels of resolution. The images were analyzed using the particle image velocimetry technique (PIV) (Adrian, 1991). This technique allows the non-invasive measurement of displacements occurred in the time elapsed between captured images. The digital images taken before and after the deformation of the object are compared at the

scale of regions of pixels (called subsets) and the displacements are defined as the difference between the position of the reference subset centre and the corresponding subset centre in the deformed image.

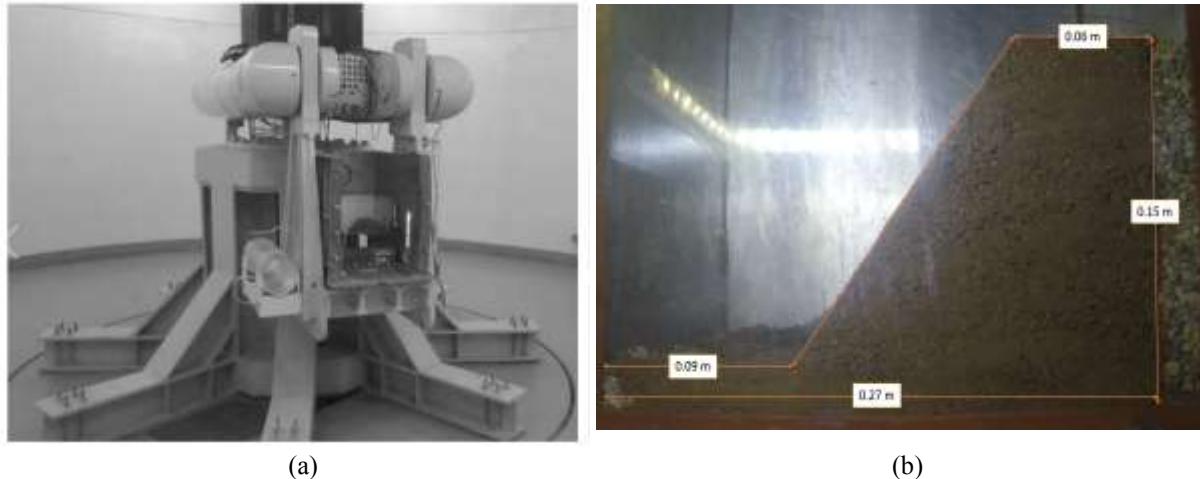


Fig. 1 (a) Centrifuge machine; (b) Silty clay slope after construction in the transparent box.

In this paper, the images were analyzed by means of the free software PIVLab (Thielicke et al., 2014). This program follows a Eulerian approach and the displacements occurred between subsequent images are measured in points fixed in the space. Consequently, the track of the particles located at different subsets during the motion is not directly provided by the method. The methodology called PIV-NP proposed by Pinyol and Alvarado (2017) was used in the analysis of the centrifuge experiment to postprocess the PIV measurements. Starting from measurements of displacement following Eulerian approach, PIV-NP provides the accumulated displacements and the strains associated with points (Numerical Particles) representing physical particles of the deformable soil. The methodology is specially well suited to interpret large strains. In the analysis performed here, interrogation areas of 100x100 pixels were selected and 9 numerical particles per element were used.

The experiment shows the settlement of the slope when gravity increases. During wetting, water went up through the soil and, more quickly, through the sandy column. This wetting induces the settlement of the slope due to soil collapse. At a certain time, the failure of the slope took place and the final inclination of the failed saturated slope was equal to 28°.

ANALYSIS OF EXPERIMENTAL RESULTS

Three stages of the motion of the slope were identified by the PIV analysis. Firstly, the slope settled due to the increase of gravity till 50g. Figure 2 shows the displacement and strains occurred during this first stage of loading. The incremental displacements measured by comparing two images captured at the end of the loading stage, obtained directly by PIV, are shown in Figure 2a. The accumulated displacements, obtained by means of PIV-NP, are plotted in Figure 2b. The displacements were larger in the zone where the slope is higher. A maximum displacement of 5 cm was measured. A well-defined shear zone was observed in the middle of the slope due to the different settlements between the toe and the crest. Maximum volumetric strains were measured in the deepest zone of the slope, where mean stresses reach the highest values.

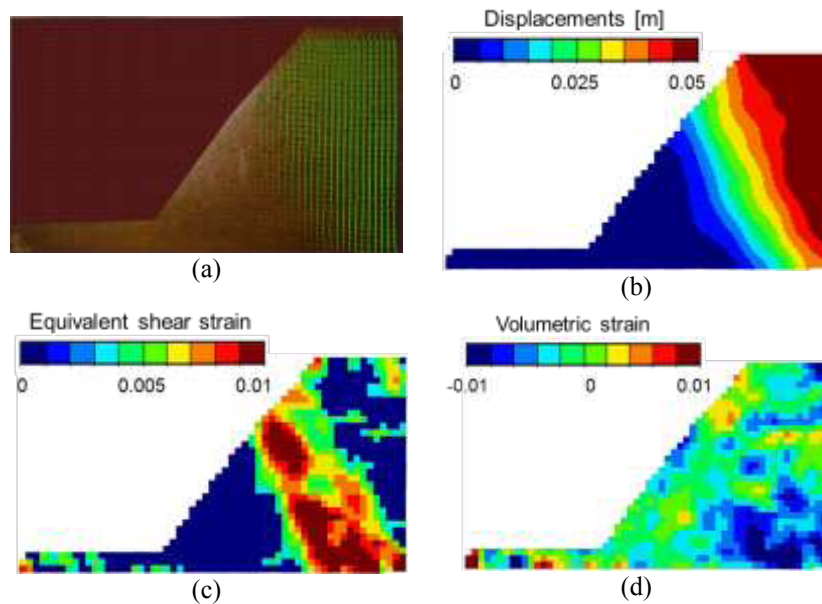


Fig. 2 Measurements at the end of the gravity increase stage ($t = 10s$). (a) Incremental PIV displacements vectors occurred during 2 seconds; (b) Accumulated displacement; (c) Accumulated equivalent shear strain; (d) Accumulated volumetric strain.

During the wetting process, water injected from the bottom of the slope went up through the silty soil and through the gravel column. A horizontal flow from the gravel column (quickly saturated) into the soil was observed. The evolution of the wetting front in time could be clearly distinguished because of the change in the colour of the sand between unsaturated and saturated states. The wetting-induced slope deformation is shown in Figure 3. The volumetric compression strains due to the wetting collapse were concentrated in the wetting front where the soil becomes saturated. Displacements were mainly observed above the wetting front where the soil settled as a rigid block.

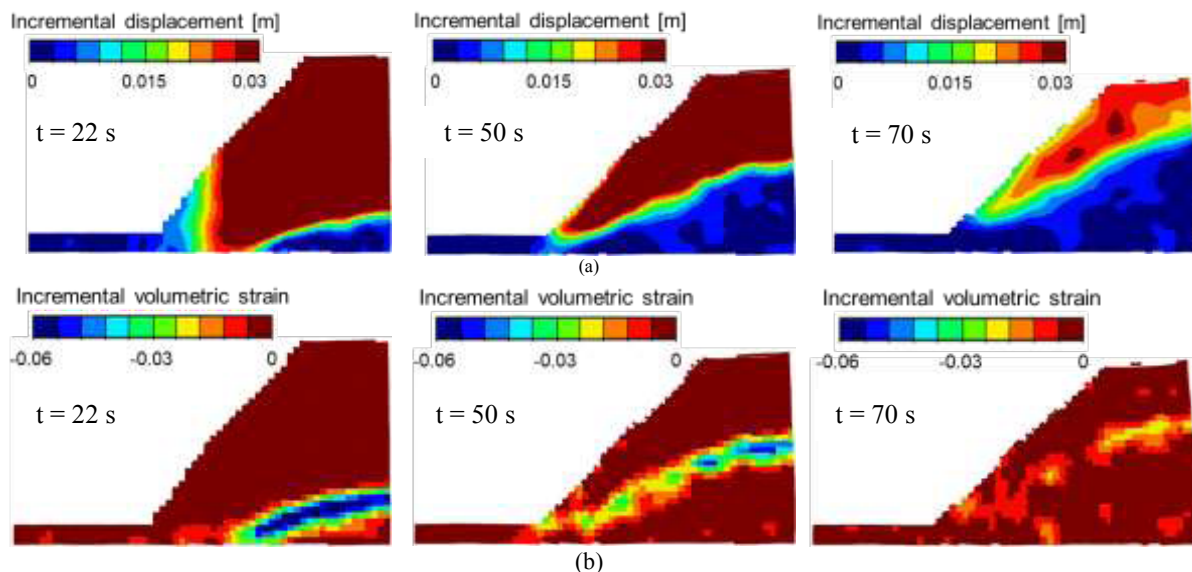


Fig. 3 Wetting stage. (a) Postprocessed incremental displacements; (b) Incremental volumetric strains.

Finally, the imposed wetting induced the failure of the slope (Fig. 4) due to the loss of suction. At this stage, collapse and shear deformation occurred at the same time. During wetting, shear

strains localized in the wetting front and at certain time ($t=140$ s) a catastrophic shallow sliding was observed.

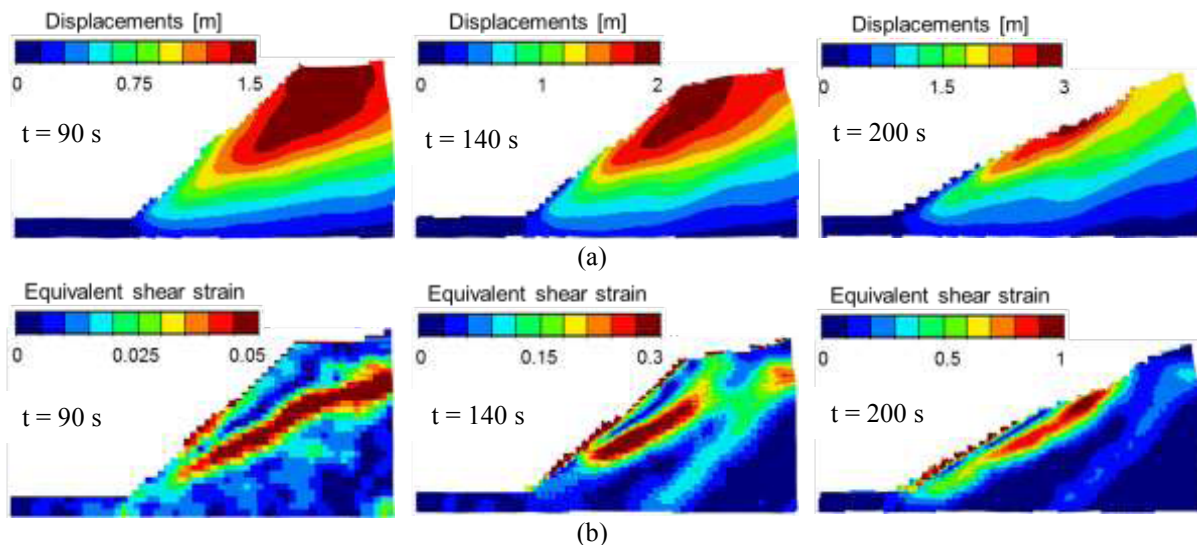


Fig. 4 Failure stage. (a) Accumulated displacements; (b) Equivalent shear strain.

CONCLUSIONS

A novel PIV interpretation technique, recently developed, provided an accurate estimation of the deformations observed in a wetted steep unsaturated slope in a low density silty soil. Initial stages of wetting from a lower boundary resulted in a progressive collapse strains of the soil, concentrated in the upward moving wetting front. This deformation mode evolved into a well-defined shallow sliding failure when the wetting front approaches the slope surface. The detailed information provided by this experiment constitutes a good benchmark to check the capabilities of available models for the analysis of slides in unsaturated soils subjected to wetting.

ACKNOWLEDGMENTS

The authors acknowledge the financial support to CIMNE via the CERCA Programme/ Generalitat de Catalunya and to the Spanish Government for the research fellowships awarded to the second and third authors.

REFERENCES

- Adrian RJ (1991) Particle-Imaging Techniques for Experimental Fluid Mechanics. *Annual Review of Fluid Mechanics* 23, 261–304.
- Pinyol NM, Alvarado M (2017) Novel PIV-based analysis for large strains. *Canadian Geotechnical Journal*. Accepted.
- Take WA (2003) Soil deformation measurement using particle image velocimetry (PIV) and photogrammetry. *Geotechnique* 53(7), 619–631.
- Take WA (2015) Thirty-Sixth Canadian Geotechnical Colloquium: Advances in visualization of geotechnical processes through digital image correlation. *Canadian Geotechnical Journal* 52(9), 1199–1220.
- White DJ & Bolton MD (2004) Displacement and strain paths during plane-strain model pile installation in sand. *Geotechnique* 54(6), 375–397.
- Thielicke W & Stamhuis EJ (2014) PIVlab – Towards User-friendly, Affordable and Accurate Digital Particle Image Velocimetry in MATLAB. *Journal of Open Research Software* 2(1):e30.

LANDSLIDES AND ITS RELATION WITH FAULTS AND HIDDEN FRACTURES ZONES – RESULTS FROM THE LIDAR-BASED DEM AND STRUCTURAL ANALYSIS (SILESIAN BESKID, OUTER CARPATHIANS).

Rafał Sikora*

* Polish Geological Institute – NRI, Geohazards Program, Cracow, Poland

Due to geological structure (flysch rocks) and morphology, landslides are one of the major natural hazards in the Outer Carpathian Mountains. The application of the method that integrates the structural research and LiDAR-based DEM lineaments analysis enable the identification of faults and hidden fractures zones in Silesian Beskid (Outer Carpathians). The comparison of that research with landslides map show the relationship between the structure of basement rocks and the landslide distribution. Size and scale of the landslides may relate their development with the historical seismic events.

Keywords: landslides, LiDAR, lineaments, structural research, Silesian Beskid.

INTRODUCTION

In the Polish part of the Outer Carpathians, the Landslide Counteracting System (SOPO) is realized since 2008. The project's main goals are: recognize and register landslides, understand what causes landslides and to prepare the scenario for extreme landslide events. Until today, more than 56000 landslides were described. The key to understand the nature of the mass movements in the Polish Outer Carpathians is to study the relation between landslides and geological structure. In this paper, some results of integrated DEM and structural analysis in landslides study are presented.

GEOLOGICAL SETTINGS

The study area (more than 62 km²) is located in the Vistula River source area (Fig. 1) on the western slopes of the Barania Góra Mountain ridge (Silesian Beskid, Outer Carpathians). The Outer Carpathians geological structure is typical for a fold-and-thrust belt build of flysch sediments (intercalated layers of sandstones and shales). They were formed during the Alpine orogeny. In the study area basement is built by Upper Cretaceous flysch rock of the Silesian Nappe and its can be divided into two areas. The northern part is dominated by medium to thick-bedded sandstones of the Upper Godula Beds that are interbedded by shales and in upper part by thin-bedded Malinów Conglomerate. In the southern part the Upper Godula Beds are overlain by thin-bedded, coarse grained sandstones of the Lower Istebna Beds. Structurally study area is a part of the southern limb of the Szczyrk Anticline. All rocks in this area are

dipping 10-30° to the SW or S . The study area is situated in the high level part of the macro-seismic zones of Outer Carpathians (Schenk at al., 2001).

In the area of research during the landslides mapping at 1:10 000 scale (part of the Landslide Counteracting System project) more than 170 landslides was recognized and registered in database. Most of them are larger than 20 hectares and is classified as compound landslide (Sikora & Piotrowski, 2013).

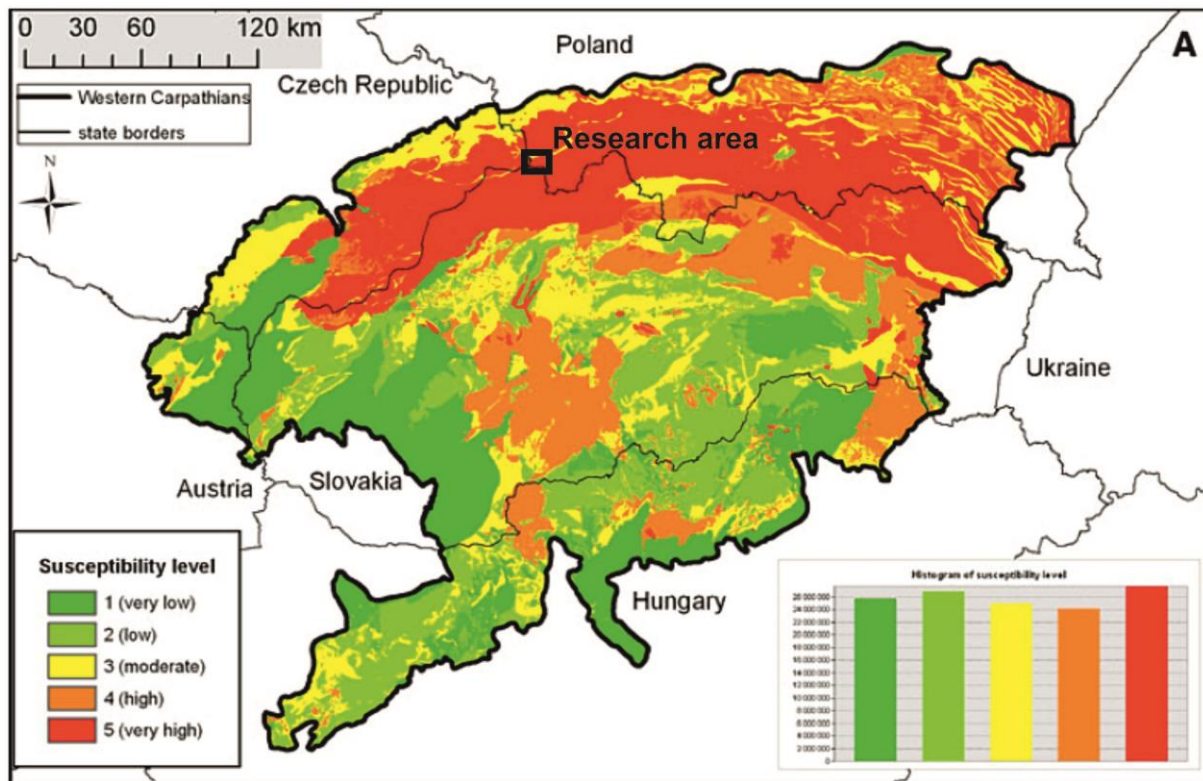


Fig. 1 Location study area on the landslide susceptibility map of the Carpathian Mts after Holec at al., 2013.

METHODOLOGY

Methodology that was used to analyze the relation between landslide distribution and chosen structural parameters in the Silesian Nappe is presented on Fig. 2. On the first stage, the data was gathered in two independent ways – the LIDAR-based DEM analysis and the field work. In this phase the lineaments was identified (by manual method) on the DEM. This set of lineaments was used to create a density map (LDM). The high density zones on LDM were selected for a detailed field work. The structural analysis supplied with fracture density was carried out in the selected outcrops. The comparison between the lineaments analysis and field based structural analysis allows the identification of faults and hidden fracture zones.

RESULTS

The areas with the highest density of lineaments overlaps with landslides which confirms their relationships with structure of basement (Fig. 3). These areas related to the clearly visible fault zones and hidden fracture zones. The hidden fracture zones are very important in landslides development. These zones were not identify before in the study area. Structural interpretation prove that orientation of landslide scarps and accompanying extensional cracks

corresponds to distinguished systems of joints and lineaments. Main and minor landslide scarps developed along faults and longitudinal L, L', L'' (ENE – WSW) and transversal T (NW – SE) set of orthogonal joint system (Sikora, 2014). Described relation determines formation of large, compound landslides and landslide complexes. It is most visible within the Biała Wiselka Landslide Complex and Czarna Wiselka Landslide Complex.

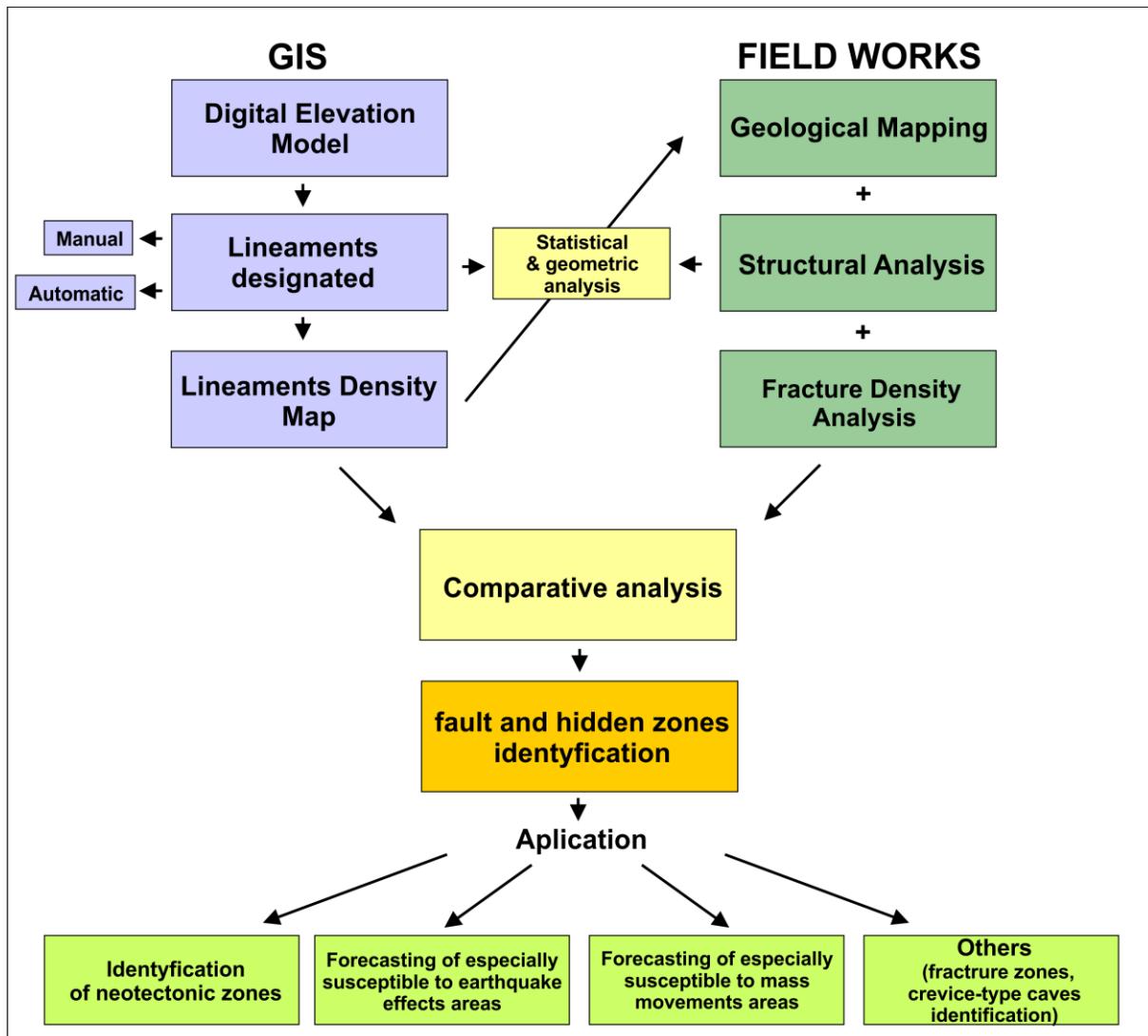


Fig. 2 The scheme of the methodology of integrated research for landslides, faults and hidden fracture zones identification.

CONCLUSION

Methodology proposed in this study enabled investigate relationships between structure of basement rocks and development of landslides on the Silesian Nappe in the Outer Carpathians. It demonstrate the clear relations between geologic structures, morphology and landslides which is a result of massif elevation and relaxation. The significant number of landslides and they large area can be joined with seismic activity of this region in historical time. The seismicity of this region can be confirmed for example by an earthquake which took place in XVIII century with 6-7 level of intensity in EMS scale. In the researched area seismic disruption could achieve $M > 4,3 \pm 0,4$ (Pagaczewski, 1972; Guterch, 2009). Proposed meth-

odology allows identifying areas which are exposed to the landslide risk and can be more affected during future earthquakes. It can be also used to identify of the neotectonic zones or crevice-type caves (Sikora, 2015).

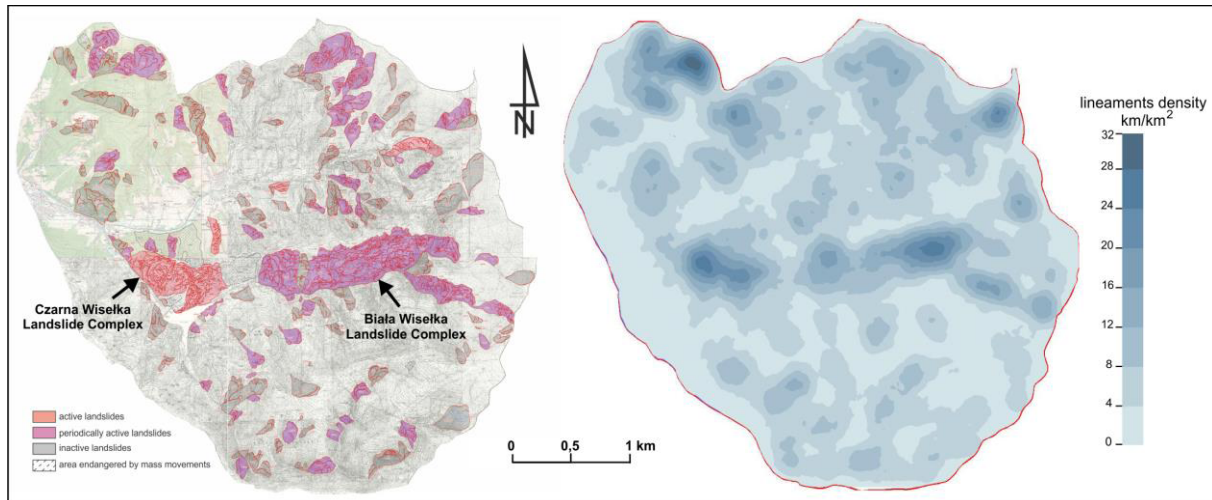


Fig. 3 The comparison of landslide map (Sikora & Piotrowski, 2013) with lineament density map (LDM).

REFERENCES

- Guterch B (2009) Seismicity in Poland in the light of historical records. *Prz. Geol.* 57, 513–520.
- Holec J, Bednarik M, Šabo M, Minař J, Yilmaz I, Marschalko M (2013) A small-scale landslide susceptibility assessment for the territory of Western Carpathians. *Nat Hazards* 69, 1081–1107.
- Pagaczewski J (1972) Catalogue of earthquakes in Poland in 1000–1970 years. *Publs. Inst. Geoph. Pol. Acad. Sc.* 51, 3–36.
- Schenk V, Schenková Z, Kottbauer P, Guterch B & Labák P (2001) Earthquake hazards maps for the Czech Republic, Poland and Slovakia. *Acta Geoph. Pol.* 49 (3), 287–302.
- Sikora R (2014) Structural origin of landslide in the Vistula River source area (Silesian Beskid, Outer Carpathian, Poland). *Proceedings XX Congress of the Carpathian – Balkan Geological Association, Tirana*. Begiraj A, Ionescu C., Christofides G., Uta A., Begiraj Goga E., Marku S. (eds.). *Biuletini I Shkencave Gjeologjike, Special Issue I*, (1), 470.
- Sikora R, Piotrowski A (2013) Maps of landslides and mass movement hazard areas 1:10 000, Wisła Commune. NAG, Warsaw (in Polish).
- Sikora R (2015) Structural and morphological markers for neotectonic dynamics of the Vistula river source area. *16th Workshop On Recent Geodynamics of the Sudety Mts. and Adjacent Areas*. Srebrna Góra 05-07.11.2015. Abstracts, pp. 52.
- Sikora R (2016) Identifications of hidden faults and fracture zones in the Silesian Beskid (Carpathians) on the basis of structural study, analysis of lineaments and DEM (from LiDAR data). *III Polish Geological Congress*, J. Wojewoda (eds.). Wrocław. Polish Geological Society, pp. 348–350.

BIPARTITE ROCKSLIDES: GEOMORPHIC EVIDENCE OF PARTIAL EXTREME MOBILITY

Alexander L. Strom*

* Geodynamics Research Center – branch of JSC "Hydroproject Institute", Moscow, Russia

Several typical examples of large-scale rockslides from the Central Asia region with bipartite deposits that have compact proximal and highly mobile avalanche-like distal parts are described. Such case studies illustrate partial involvement of rockslide debris in accelerated motion resulting in its extra-mobility. Besides long runout many of them are characterized by the abrupt change of the direction of rock avalanche motion relative to the direction of the initial slope failure, so that they can affect areas that otherwise would be considered as safe. It is hypothesized that such bipartition is caused by the fluidization of the frontal part of rockslide body that reaches the valley bottom first or by the momentum transfer from the entire collapsed rock mass to its portion retaining possibility of further motion after its collision with an obstacle or after entering sharp valley constriction.

Keywords: rockslide, rock avalanche, bipartition, fluidization, momentum transfer, mobility

INTRODUCTION

Large-scale bedrock landslides (rockslides) often convert into highly mobile rock avalanches that pose an exceptional threat, affecting vast areas extending up to 30-40 kilometers from the collapsing slopes (Kurdiukov, 1950; Crosta et al., 2015; Resnichenko, 2015; Robinson et al., 2015). Prediction of the reach of future slope failures that will occur in mountainous areas inevitably requires better understanding of motion mechanism(s) of such rock avalanches and of factors governing their origin and mobility. Two main approaches to reveal these regularities can be utilized. One of them is based on the statistical analysis of various quantitative parameters such as rockslide volume, runout, affected area, drop height, fahrböschung (Sheiddegger, 1973; Li, 1983; Shaller, 1991; Kilburn & Sørensen, 1998; Legros, 2002). Another approach requires detailed case-by-case description of morphological and sedimentological peculiarities of highly mobile rock avalanches, both historical and prehistoric, their classification and identifying of factors predetermining such an abnormal behavior. Combination of both approaches allows statistical analysis of case studies featuring similar style of formation and motion that provides more rigorous quantitative relationships (Shaller, 1991).

Compiling the rockslides database of the Central Asia region, which arid climate and lack of vegetation provide excellent morphological expressiveness of rockslide and rock avalanche bodies, we identified numerous case studies with distinct bipartition of the deposits that have compact and long runout (avalanche-like) parts. Study of their morphological peculiarities provides additional information on the processes evolving in catastrophic large-scale rock slope failures and governing their mobility. Several typical case studies classified as Jumping

and Secondary rock avalanches (Strom, 2006, 2010) demonstrating different types of such slope failures are presented and analysed in brief.

MORPHOLOGICAL TYPES OF BIPARTITE ROCKSLIDES

Jumping rock avalanches originate when the sliding surface daylight well above the slope base so that its debris really jumps and then fell nearly vertically colliding with valley bottom almost at a right angle. Such rockslides form thick proximal accumulation with convex slopes and gradually thinning avalanche-like part. Besides several Central Asian case studies one of which is shown on Fig. 1, such morphology characterizes famous 1881 Elm rock avalanche originated on the slope undercut by slate quarry (Heim, 1882; Hsü, 1978).

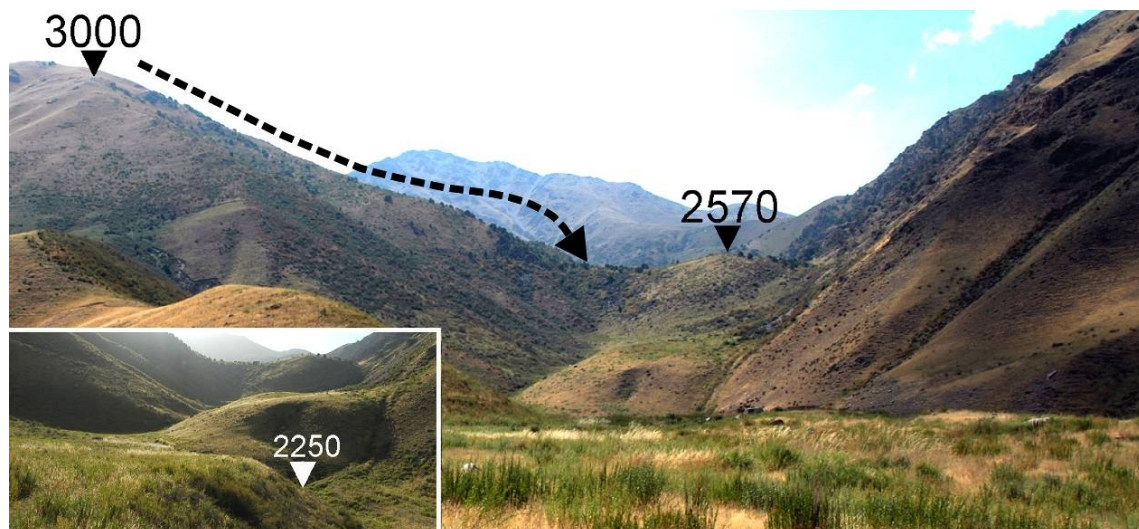


Fig. 1. Overview of the Northern Karakungey rockslide of the Jumping type in Central Tien Shan, Kyrgyzstan. It caved from the true right slope of the valley composed of granites (direction of motion is shown by the dashed arrow). Filling of the stream by avalanche-like portion of debris is shown in the inset

The most hazardous highly mobile Secondary rock avalanches originate when rapidly moving rockslide that gained its momentum during initial descend, either strikes with the slope base (not at an almost right angle as in the Jumping case) or with an opposite slope of the valley or enters sharp valley constriction, after which part of debris moves further demonstrating abnormally high mobility. The characteristic features of the Secondary rock avalanches are a concave slope of the compact part above the avalanche-like part – the so-called "secondary scar", accumulation of large portion of mobile debris at its distal part – opposite to the along-way debris distribution of the Jumping cases, and more pronounced flow-like style of the avalanche debris motion (Figs. 2, 3).

Rock avalanches of both Jumping and Secondary types can move either in the same direction as the initial slope failure or turn, practically up to the right angle. Thus they can affect areas that otherwise would be considered as safe even if we anticipate large scale slope failure from the source zone. While identified case studies of the Jumping type have relatively short mobile parts (the 2 km long 1881 Elm rock avalanche seems to be one of the longest) some of the Secondary rock avalanches demonstrate extreme mobility, often being 5-7 km long. Even length of the deflected cases that moved at a right angle to the direction of the initial debris

motion can exceed 4 km. Sometimes one can identify several successive secondary scars reflecting multistage interruption of debris motion (see Fig. 3).



Fig. 2. The Karasu Lake rockslide (Central Tien Shan, Kyrgyzstan) accompanied by the deflected secondary rock avalanche that involved ~10% of the entire rockslide and moved 1.4 km down-valley at a right angle to the direction of the initial slope failure. Its well pronounced secondary scar is marked by yellow triangles. T – the distinct right-side trimline. 3D Google Earth view

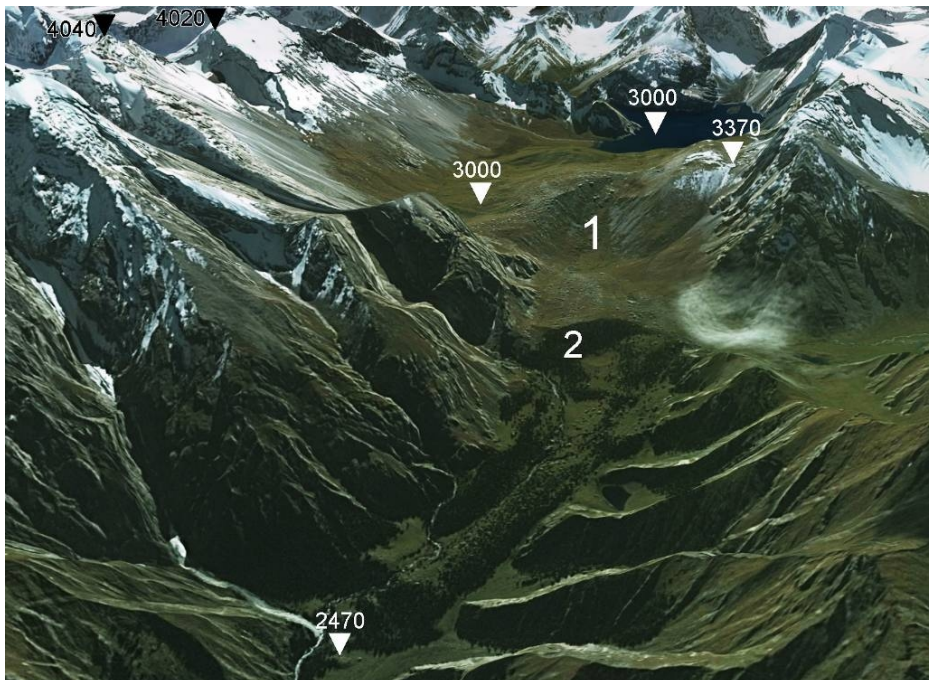


Fig. 3. The Big Dragon Lake rockslide about 2 km³ in volume (Eastern Tien Shan, China) with 370 m runup of its frontal part accompanied by the 4.3 km long deflected Secondary rock avalanche that originated from the secondary scar # 1 and moved up to 2470 m a.s.l. with an intermediate secondary scar #2. 3D Google Earth view

ASSUMED BIPARTITION MECHANISMS

The bipartition of Jumping rock avalanches can be explained as follows. When the frontal part of sliding block had jumped and fallen down on the valley bottom, its following sections that originate from top of the ridge and, thus, have larger unit potential energy, are still sliding down and after jumping they fall down on top of debris that is already at place, compressing it. Moreover, such compression is not just static loading, but highly dynamic process that, considering giant dimensions of the study features, could fluidize the basal debris units extruding them from under accumulating tailing portion. This fluidized material flows downstream as a dry viscous granular flow forming the avalanche-like part.

Mechanism of the Secondary rock avalanches bipartition seems to be different. Rock mass collapsing catastrophically from the high slope gains enormous momentum. When it meets any obstacle it stops, but if some part of debris has "free face" it retains possibility of further motion. It is hypothesized that debris colliding with an obstacle deforms elastically and part of the overall momentum transfers to its portion that accelerates and ejects from the "free face" forming long runout rock avalanche. These phenomena can repeat several times as it can be seen on Fig. 3.

REFERENCES

- Crosta GB, Frattini P, Valbuzzi E, and Hermanns RL (2015) The Cerro Caquilluco–Cerrillos Negros Giant Rock Avalanches (Tacna, Peru). *Engineering Geology for Society and Territory – Volume 2*. G. Lollino, D. Giordan, G.B. Crosta, J. Corominas, R. Azzam, J. Wasowski, N. Sciarra. (eds.), Springer International Publishing Switzerland, pp. 921-924.
- Heim, A. (1882) Der Eergsturz von Elm. *Z der Deutschen Geologischen Gesellschaft* 134, 74-115.
- Hsü, K.J. (1978) Alberl Heim: observations on landslides and relevance to modern interpretations, in E. Voight (Ed). *Rockslides and Avalanches. V. I. Natural Phenomena* Amsterdam: Elsevier, 71-93.
- Kilburn, C.R.J., Sørensen, S-A. (1998) Runout length of sturzstroms: the control of initial conditions and of fragment dynamics, *J. Geophys. Res.* I03: No EB. I7877-17884.
- Kurdiukov KV (1950) Ancient rockfalls in the Alay Range valleys. *Problems of Geography*, 21, 191-204. (in Russian).
- Legros, F. (2002) The mobility of long-runout landslides, *Engineering Geology* 63, 301-331.
- Li. Tianchi (1983) A mathematical model for predicting the extent of a major rockfall, *Z- fur Geomorphologie N.F.* 27,473-IB2.
- Reznichenko N & Davies T (2015) The Gigantic Komansu rock avalanche deposit in the glaciated Alai Valley, Northern Pamir of Central Asia. *Engineering Geology for Society and Territory – Volume 2*. G. Lollino, D. Giordan, G.B. Crosta, J. Corominas, R. Azzam, J. Wasowski, N. Sciarra. (eds.), Springer International Publishing Switzerland, pp. 895-898.
- Robinson TR, Davies TRH, Reznichenko N & De Pascale GP (2015) The extremely long runout Komansu rock avalanche in the Trans Alay range, Pamir Mountains. Southern Kyrgyzstan. *Landslides*, 12, 523-535.
- Shaller, P.J. (1991) Analysis and implications of large Martian and Terrestrial landslides... Ph.D. Thesis, ("Alilomia Institute of Technology).
- Sheidigger, A.E. (1973) On the prediction of the reach and velocity of catastrophic landslides. *Rock Mechanics* 5,231 -236.
- Strom, A.L. (2006). Morphology and internal structure of rockslides and rock avalanches: grounds and constraints for their modelling. In: Evans, S.G.; Scarascia Mugnozza, G.; Strom, A.; Hermanns, R.L. (Eds.) *Landslides from Massive Rock Slope Failure*. NATO Science Series: IV: Earth and Environmental Sciences, Vol. 49, 305-328.
- Strom, A.L. (2010) Evidence of momentum transfer during large-scale rockslides' motion. In: Williams AL, Pinches GM, Chin CY, McMorran TG, Massei CI (eds.) *Geologically Active*. Proc. of the 11th IAEG Congress, Auckland, New Zealand, 5-10 September 2010, Taylor & Francis Group, London, 73-86.

LONG-TERM SLOPE INSTABILITY AFTER GIGANTIC EARTHQUAKES AND THEIR CAUSES WITH EMPHASIS ON ROCK FRACTURING

Ikuo Towhata*, Keigo Gunji†

* Professor Emeritus, University of Tokyo, Tokyo, Japan

† Former graduate student, University of Tokyo, Japan

The earthquake-induced landslide is attracting engineering concerns internationally. One of its effects is that slope stability continues for a long time such as years or even centuries. The causes of this long-term effect are open cracks in the slope surface, sediment deposits in the valley bottom and mechanical deterioration such as micro fractures in the vicinity of a fault plane. After introducing examples of the long-term instability, the present paper addresses laboratory tests which aimed to reproduce the effects of earthquake stress history and creep deformation on mechanical properties of artificial rock specimens. It is shown that both earthquake stress history and creep equivalently deteriorate the mechanical strength of rock.

Keywords: earthquake, long-term slope instability, laboratory test, creep, deterioration

INTRODUCTION

Failure of mountain slopes is one of the natural disasters that occur at many places in the world and earthquake shaking is its important causative mechanism. The conventional studies and engineering practices have addressed the risk evaluation, assessment of instability and damage mitigation. In spite of their profound effects on the affected communities, the earthquake-induced landslides have not been studied in details. After visiting the sites of such landslides after the 1999 Chi-Chi earthquake in Taiwan, the 2005 earthquake in Northern Pakistan and the 2008 Wenchuan earthquake in Southwest China, the authors started to pay attention to the long-term instabilities after the earthquake events. They found that many slopes in the affected area started to move after earthquakes although they had been stable for a long time. Because precipitation increase after those earthquakes is unlikely, there should be some instability mechanisms that are particular to the local seismic activities. It is further interesting to find that Ohya landslide slope in Japan has been unstable for at least 300 years after a previous gigantic earthquake. To shed light on such events, the authors conducted laboratory tests on rock specimens by which the effects of cyclic (earthquake) loading is reproduced. The following chapters will introduce the output and conclusions of their study.

SLOPE DISASTERS AFTER PAST BIG EARTHQUAKES

There are several examples where slope disasters were caused by big earthquakes and were followed by long-term slope instabilities. The 1999 Chi Chi earthquake of $M_w=7.6$ in Taiwan caused many slope failures along the causative Chelungpu Fault that was as long as 100 km (Shishikura et al., 2002). In addition to many big slope failures, there were also unaccountable

number of surface fallings; see Fig. 1. During the years after this earthquake, many debris flows occurred in Taiwan (Lin et al., 2010).



Fig. 1 Slope failures caused by the 1999 Chi Chi earthquake in Taiwan



Fig. 2 Repeated debris flows during heavy rains after the 2008 Wenchuan earthquake in China

The second important example of long-term instability is found in the Sichuan Province of China where the 2008 Wenchuan earthquake of $M_w=7.9$ caused many landslides in the mountainous region. The site in Fig. 2 had been a summer resort with many hotels and other facilities. After the earthquake, debris flow started to affect this site upon heavy rains and destroyed the community. It is interesting that the mountain slope behind this site was substantially disturbed during the earthquake and became the source of debris (Fig. 3). Note in Fig. 3 that the valley bottom is filled with debris deposit. The length of the causative Longmenshan Fault was 300 km.



Fig. 3 Disturbed mountain slope vulnerable to rainfall-induced slope disaster



Fig. 4 Site of debris flow in August, 2010, in Sichuan Province of China

Pakistan experienced a devastating earthquake in its northern part in 2005. This event with $M_w=7.6$ caused a similar situation in mountain slopes. Fig. 5 illustrates a damaged slope immediately after the disaster. Located along the causative Muzaffarabad fault, this slope appears very similar to those in Fig. 1; slope surface being covered by many slides. It is important that this situation was not the end of the disaster but the beginning. Fig. 6 shows a continued instability of the slope behind the city of Muzaffarabad. This slope remained green after the earthquake but gradually became unstable with time. The causative fault of this earthquake was at least 75 km in length according to the surface rupture trace (Avouac, 2006).

The 1707 Hiei earthquake of $M_w=8.7$ or greater in Japan triggered a gigantic Ohya landslide (Fig. 7). It is supposed that the total volume of this landslide was approximately 120 million cubic meters (Takeuchi and Tsutsumi, 1985). After this event, the Ohya slope has been falling upon many heavy rains. Consequently, the river bed in the downstream area is filled with debris deposit now. Note the similarity with Figs. 3 and 4.



Fig. 5 Slope failures near Balakot after the 2005 earthquake in Pakistan



Fig. 6 Post-earthquake instability of slope behind Muzaffarabad after the earthquake



Fig. 7 Present appearance of unstable Ohya landslide



Fig. 8 Location of Ohya landslide with the location of Itoigawa-Shizuoka Tectonic Line

The Ohya site is located near or within what is called Fossa Magna depression that consists of many faults, inclusive of the Itoigawa-Shizuoka tectonic line of approximately 150 km in length (Fig. 8). It is interesting that there are many big unstable sites along this tectonic line and one of the biggest of them is the Shichimen-Zan landslide which has been failing since 13th Century or older. (Figs. 8).

CAUSATIVE MECHANISMS OF LONG-TERM SLOPE INSTABILITY

Earthquake-induced cracks is obviously one of the causes of slope instability after an earthquake. Rain water can come into the slope and reduces the stability. However, this alone cannot account for the very long duration of instability for decades or centuries. In this regard, the deterioration of material properties caused by earthquake cyclic stress was investigated by running unconfined compression tests. The tests were run on artificially prepared (rock) samples (mixture of gypsum and silica sand together with water) that had uniform material properties so that test results from respective samples might be compared. Without cyclic loading, this sample showed the unconfined compression strength (q_u) of 4425 kPa. In contrast, the test in Fig. 9 exhibits that q_u was reduced to 3480 kPa after the significant cyclic loading. By repeating similar tests, the obtained peak strength points were connected to draw a curve that is “assumed” to represent the post-earthquake strength (Fig. 10).

Rock mass near a fault is often subject to creep deformation. Thus, tests were also run on effects of creep on strength of artificial rock specimens. Fig. 11 plots the obtained stress-strain as well as the strain-rate curves. Under the constant axial stress of 3600-3800 kPa, the strain

rate suddenly increased when the accumulated stress approached the above-mentioned “assumed” “fundamental” curve. In this regard, both cyclically-induced and creep-induced failures of the material are equivalent with each other.

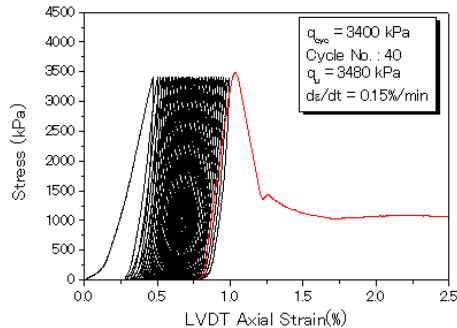


Fig. 9 Test results with more significant cyclic loading

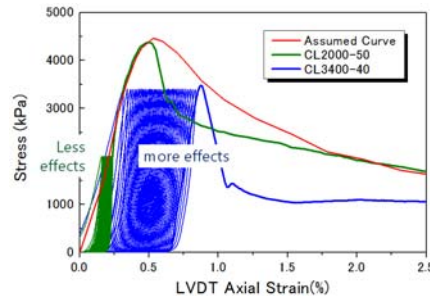


Fig. 10 Cyclic loading towards post-peak softening stage of monotonic loading

All the aforementioned examples of long-term instability occurred near big faults. In this context, the test results suggest that rock mass along faults are deteriorated either by repeated earthquake stress history or by creep. “Process Zone” discussed by Vermilye and Scholz (1998) seems meaningful. This zone consists of many fissures and is of reduced material strength. They proposed that the range of fissures reaches 1% of the fault length. The length of faults as introduced in this paper suggests that the width of the process zone is of the order of km or more that is consistent with the size of areas of experienced slope instabilities.

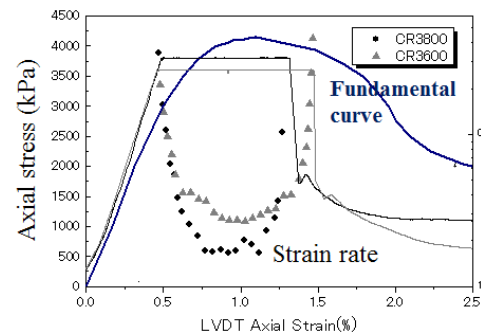


Figure 11 Creep-induced failure of sample

CONCLUSION

The present paper concerned the long-term slope instability that is triggered by big earthquakes. After addressing many examples, laboratory tests were carried out on one of the mechanisms of long-term instability. It is concluded that the long-term instability are caused by surface cracks, sediment deposit in valleys and cyclic or creep deterioration of rocks. The last mechanism is related with the concept of process zone as proposed by Vermilye and Scholz (1998).

REFERENCES

- Avouac, J.-P. et al. (2006) The 2005, Mw 7.6 Kashmir earthquake: Sub-pixel correlation of ASTER images and seismic waveforms analysis, *Earth and Planetary Science Letters* 249, 514–528.
- Lin, M.L. et al. (2010) Debris flow hazard and mitigation in Taiwan following Chi-Chi earthquake, 1999, *Proc. 17th Southeast Asian Geotechnical Conference, Taipei*, 123-126.
- Shishikura, M. et al. (2002) Paleoseismological study at Fengyuan site on the northern part of the Chelungpu Fault, central Taiwan, *Annual Report on Active Fault and Paleoseismic Researches 2*, 279-289 (in Japanese).
- Takeuchi, T. and Tsutsumi, H. (1985) Ohya landslide, Shin-Sabo, *Magazine of the Japan Society of Erosion Control Engineering* 38(3), 20-22 (in Japanese).
- Vermilye, J.M. and Scholz, C.H. (1998) The process zone: a microstructural view of fault growth, *Journal of Geophysical Research* 103(B6), 12223-12237.

ANALYSIS, EVALUATION AND ZONING OF THE SUSCEPTIBILITY DUE TO LANDSLIDES IN THE ALOAG - SANTO DOMINGO ROAD (ECUADOR)

Francisco J. Torrijo*, Julio Garzón-Roca*, Vicente Capa*

* Geotechnical Engineering Department, Universidad Politécnica de Valencia, Valencia, Spain

This article presents a summary of the analysis, evaluation and zoning of susceptibility due to landslides, on a regional scale, in the zone of *Via Aloag Santo Domingo Km 11 + 500 to Km 77 + 000* of Ecuador. This type of zoning is generally used for information purposes and for giving general recommendations for regional development, so zoning level corresponds to a preliminary level with a depth of a basic study. Assessment can be qualitative or quantitative with an inventory type analysis (distribution analysis, density, activity) and a heuristic one (geomorphological, parameter weighting), with map scales of 1:10,000.

Keywords: evaluation, susceptibility, landslides, photointerpretation

Sometimes problems arising from the interaction between the geological environment and road infrastructures make it necessary to propose suitable actions to achieve a balance between natural conditions and the operation of the road network. In such cases, implantation of infrastructures in a territory requires incorporate methods of risk prevention and assessment. An example of this is the region where the road from Aloag to Santo Domingo is located. That region presents a high complexity from the geotechnical point of view, giving problems basically associated with slopes and streams.

This article presents a summary of the analysis, evaluation and zoning of susceptibility due to landslides, on a regional scale, in the zone of *Via Aloag Santo Domingo Km 11 + 500 to Km 77 + 000* of Ecuador. This type of zoning is generally used for information purposes and for giving general recommendations for regional development, so zoning level corresponds to a preliminary level with a depth of a basic study. Assessment can be qualitative or quantitative with an inventory type analysis (distribution analysis, density, activity) and a heuristic one (geomorphological, parameter weighting), with map scales of 1:10,000.

The method used to elaborate the inventory and the characterization of mass movements combined photointerpretation of aerial photos and field verification. In this way the landslides and their characteristics were identified by photointerpretation, then they were confirmed and described in field, and later photointerpretation was used again to suitably introduce them in the inventory map and in the database. Identification, mapping and analysis of mass movement during fieldwork is very important for the inventory and to obtain a three-dimensional view of the phenomenon, its mechanism of movement and causes, and thus design possible

control measures and further studies. In the study area numerous landslides were identified, being represented as polygons at a scale of 1:10,000. Those polygons represented sites of mass movements that were approximately 5 mm in the scale of the map, therefore these areas assumed a dimension in the field of approximately 50 m.

Risk level of the different instabilities detected was comparatively assessed by homogeneous criteria, so that risk levels at each point were analyzed in an integrated and uniform way. Methodological tests performed were based on heuristic and statistical analyses, such as Brabb, Mora-Vahrson and other statistical methods. According to local experience and partly determined by the method of analysis, the following parameters were chosen for analysis and evaluation: lithology, terrain slope, geomorphology, precipitation, seismicity, soil use and vegetation cover.

Factors selected for analysis and evaluation of susceptibility were characterized according to the methods of analysis and / or availability of information. However some of those factors (such as lithology, geomorphology) were not easy to obtain at work scale and others (like seismicity, moisture and rainfall) in the area did not have a good density of information.

The analyses were carried out without differentiating the types of movements and considering that landslides represent the majority of mass movements mapped in the area (98%) and therefore they are the most representative in terms of planning, territorial organization and risk management, at a regional level. It was not possible to test an analysis and evaluation of the vulnerability during this work, but an evaluation of the susceptibility, because it is difficult to determine, with the information obtained, the date of occurrence, frequency or return period of mass movements, as well as their speed and displacement.

It was concluded that there were several active unstable areas with large volume, which would pose a significant risk to people who lives in the region, such as in *Unión del Toachi* and *Alluriquin*, and to a lesser extent in *Tandapi*. Furthermore, the most favorable inclination of the slope for the occurrence of the type of mass movements identified in the area corresponded to angles between 20 and 35 degrees. Likewise, more than a 70% of the geomorphological units of the area under study were classified as high susceptibility. These units were grouped in zones and not as isolated streams or slopes.

The result of the Mora-Vahrson method was chosen to represent the susceptibility zoning by landslides in the Aloag-Santo Domingo road, since it better represented the criteria chosen to identify the susceptibility of the zone, according to the comparative analysis and the images of the susceptibility classes distribution.

The elaboration of the susceptibility and hazards by mass movements zoning map, at a scale of 1:10,000, for the area *Via Aloag Santo Domingo Km 11 + 500 to Km 77 + 000* (Ecuador) by means of several methods of analysis and the evaluation of susceptibility by mass movements, at regional level, for being used in regional territorial planning and geological risk management, also resulted in defining a series of stabilization actions required and their priority based on the severity of the risk level.

Based on the results obtained in the susceptibility mapping, a brief geotechnical analysis was carried out on the most unstable slopes. On these areas, it was necessary to act immediately to prevent future mass movements. Preliminary design recommendations were also proposed, which should be later confirmed with a detailed study for the final designs. From this work

the following conclusions were obtained:

- The studied slopes, obtained from the susceptibility analysis conducted, are in the process of weathering due to the effects of the climate and water courses and they require urgent control measures.
- At the top of the slopes of the current road it is recommended to avoid saturation by drainage. This drainage should be directed to culverts and water courses that do not affect the stability of the slopes.
- In the upper part of the slopes formed by loose or colluvial soils, it is necessary to have a terrace and protection with berms for the possible fall of blocks.
- In places where loose blocks are present or to be detached, it is recommended to construct protective meshes to prevent the blocks from falling on the road.
- It is recommended to use self-sustaining measures, such as shotcrete, anchors or injections, depending on the characteristics presented in the final design stage.
- In ravines or slopes where loose materials have been detected, it is recommended to evacuate them as a first step before the rainy season. This would avoid subsequent catastrophic processes associated with earth flows.
- It should be noted that since the existing surface and groundwater flow levels are not known, slope stability analysis was performed under dry conditions, i.e. without considering the presence of surface water and groundwater. Those conditions may have a significant influence in the risk of failure of each location studied.

REFERENCES

- INGEOMINAS (2001). Evaluación del Riesgo por Fenómenos de Remoción en Masa, Guía Metodológica. Primera Edición, Bogotá, 166 pp.
- JTC-1. Joint Technical Committee on Landslides and Engineered Slope (2008). Guidelines for landslide susceptibility, hazard and risk zoning for use planning. *Engineering Geology*, 102: 83-84.
- Mora, S. and Vahrson, W.G. (1993). Manual for Zonation on Seismic Geotechnical Hazard. The Japanese Society of Soil Mechanics and Foundations Engineering. Tokyo, Japan, pp 56-60.
- Mora, S. and Vahrson, W.G. (1994a). Macrozonation Methodology for Landslide Hazard Determination. *Association of Engineering Geologists Bulletin*, 31 (1): 49-58.
- Mora, S. and Vahrson, W.G. (1994b). Macrozonation Methodology for Landslide Hazard Determination. I Simposio Panamericano de Deslizamientos de Tierra. Sociedad Ecuatoriana de Mecánica de Suelos y Rocas. Guayaquil – Ecuador. pp. 406 – 431.
- Plaza, G. (1996). La amenaza y vulnerabilidad por deslizamientos en la región andina del Ecuador. 7º Congreso Ecuatoriano de Geología, Minas, Petróleos y Medio Ambiente. CIGMYP, Quito – Ecuador. Tomo II, pp. 513 – 526.
- Proyecto Multinacional Andino, PMA: GCA (2007). Movimientos en Masa en la Región Andina, una Guía para la Evaluación de Amenazas. Ingemmet, 432 pp.
- Technical Comitee for Earthquake Geotechnical Engineering, TC- 4, ISSMFE (1993). Manual for Zonation on Seismic Geotechnical Hazard. The Japanese Society of Soil Mechanics and Foundations Engineering. Tokyo, Japan, 149 pp.
- Varnes, D. (1984). Landslide Hazard Zonation: A review of principles and practice, UNESCO, 63 pp.

COUPLED DISTINCT ELEMENT METHOD COMPUTATIONAL FLUID DYNAMICS ANALYSES FOR RESERVOIR LANDSLIDE MOD- ELLING

S. Utili*, T. Zhao†

* School of Civil Engineering and Geosciences, Newcastle University, Newcastle upon Tyne,
United Kingdom

† College of Water Resource and Hydropower, Sichuan University, Chengdu, China

The Vajont landslide involved a large mass of rock splashing at high speed into the reservoir which in turn generated a high impulse water that overtopped the dam and swept away the downstream village. In several cases of reservoir landslide, albeit the flood defence structures may remain intact, a catastrophe still occur due to the generation of a ‘tsunami’ wave. Since the features of the tsunami wave strongly depend on the physics of the rock splashing and the subsequent rock – water interaction, a numerical tool accounting for such physics is required for predictions to be reliable.

Here, the formulation of a coupled 3D Distinct Element Method (DEM) – Computational Fluid Dynamics (CFD) code used to simulate the rock slide from onset to impact with the reservoir and the subsequent generation of the impulse wave, is presented. To run realistic simulations in an affordable runtime, coarse graining is employed. The main results of quasi 3D analyses in plane strain along two cross-sections representative of the eastern and western slope sectors are presented. The results show to be in broad agreement with the available recorded observations.

Keywords: Vajont landslide, impulse wave, rapid rockslide, coupled DEM-CFD

INTRODUCTION

The Vajont rockslide (Semenza and Ghirotti 2000) in October 1963 involved approximately 270 million m³ of rock and generated water waves probably averaging 90 m above the dam crest. 100 and 200 metres high water wave traces were observed along the left and right valley flanks, respectively (Chowdhury 1978). The displaced water initially raised along the opposite valley flank and then overtopped the dam flooding successively the downstream village of Longarone, along the Piave river valley, causing more than 2,000 casualties.

Even though parallel computation techniques have been developed, the number of particles which can be simulated on PCs or PC clusters is still far smaller than that typical of real slopes (*e.g.* thousands of billions of grains). To overcome this problem, coarse graining (Sakai et al. 2012) is employed. In this technique, a coarse particle represents a collection of real fine particles. As a result, a large-scale DEM simulation of granular flow can be performed using a relatively small number of calculated particles (Sakai et al. 2012).

The theory and methodology of the DEM-CFD coupling model are introduced in the next section together with the governing equations for particle motion, particle-fluid interaction and fluid flow. In the following section, the coarse graining technique is described. Finally, the main results of the simulations of the reservoir landslides are summarised.

THEORY AND METHODOLOGY

The DEM code ESyS-Particle (Abe et al., 2004) and the CFD code OpenFOAM (OpenCFD, 2004) were employed for the simulations presented here. The coupling algorithm originally written in YADE (Chen et al., 2011) was implemented in ESyS-Particle by the authors (Zhao et al., 2014). The mechanical contact law between solid particles is based on linear springs and frictional tangential sliders plus rolling resistance (Jiang et al., 2005).

The fluid–particle interaction force consists of two parts: hydrostatic and hydrodynamic forces. The hydrostatic force acting on a single particle, i , accounts for the influence of fluid pressure gradient around the particle, i.e. buoyancy (Kafui et al., 2011). The hydrodynamic forces acting on a particle are the drag, lift and virtual mass forces; the latter two forces being neglected. The drag force acting on an individual solid particle is here calculated using the empirical correlation proposed by Di Felice (1994). The drag force coefficient is defined according to the correlation proposed by Brown and Lawler (2003).

The governing equations of fluid flow in a fluid–solid mixture system can be derived from the theory of multi-phase flow (Brennen, 2005), in which the free surface condition is resolved by the Volume of Fluid method (Hirt & Nichols, 1981). In our numerical simulations, the fluid domain is initially discretized into a series of mesh cells, in which the solid particles may be dispersed. In each fluid mesh cell, the volume fraction of the summation of fluid phases is n (i.e. porosity), for which, the volume fraction occupied by the fluid phase 1 (e.g. water) is β ($0 \leq \beta \leq 1$), while it is $1 - \beta$ for the other phase.

COARSE GRAINING TECHNIQUE

We assume that: (1) one large particle represents a clump of real sized sand grains (see Fig. 1); (2) the fine grains are bonded together, so that they can move as a whole; (3) the translational and rotational motion of the coarse grain and the clump of fines grains are the same; (4) the contact forces acting on the coarse grains are the summation of contact forces acting on this clump of real grains by the neighbouring grains. The fluid viscous drag force acting on the coarse particle is calculated by balancing the coarse particle and a clump of real particles. This particle scale up method is called a “coarse grain model” in the literature (Sakai et al. 2012).

Denoting the sizes of the coarse grain particle and original real sand particle as D and d respectively, the number of particles (N) in the clump can be approximated as: $N = D^3/d^3$. The drag force acting on the clump is the summation of the drag forces acting on all the grains. Thus, the drag force on a scaled particle in the CFD-DEM code should be scaled up by a factor α with $\alpha = F_d/F'_d$, F_d the drag force acting on the clump and the drag force acting on the scaled particle. By setting the Reynolds numbers the same, the values of the drag force coefficient are the same for both the real fluid flow and the numerical models, so $\alpha = D/d$. Simulations were run for different values of α . As shown in Table 1, α was set to 1, 5 and 10, so that one large particle in the DEM can represent a clump of fine grains ranging in number from 1 to 10^3 . The hydrostatic forces acting on a coarse particle and a clump of fine grains are the same, because it is determined only by the volume of solid materials. It is also noted that other parameters for the coarse and real particles are the same, so that realistic soil properties can be modelled in numerical simulations.

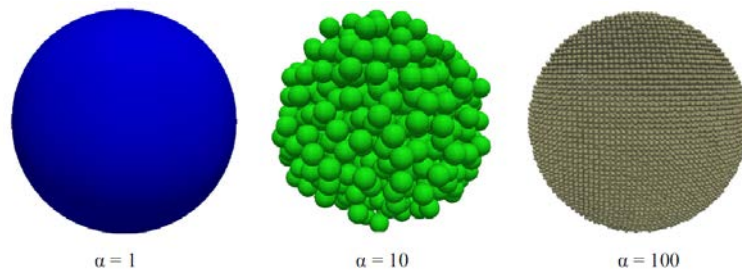


Fig. 1 Schematic view of the scaling law used in the DEM, α is the scaling factor.

RESULTS OF THE NUMERICAL SIMULATIONS

A plan view of the Vajont rockslide is shown in Fig. 2a, together with the traces of the two cross sections A–A and B–B, representative of the eastern and western sectors of the slide, and herein analysed. The profiles along these cross sections are illustrated in Fig. 2b and 2c. Details of the generation procedure of the slope mass are given in (Zhao et al., 2016).

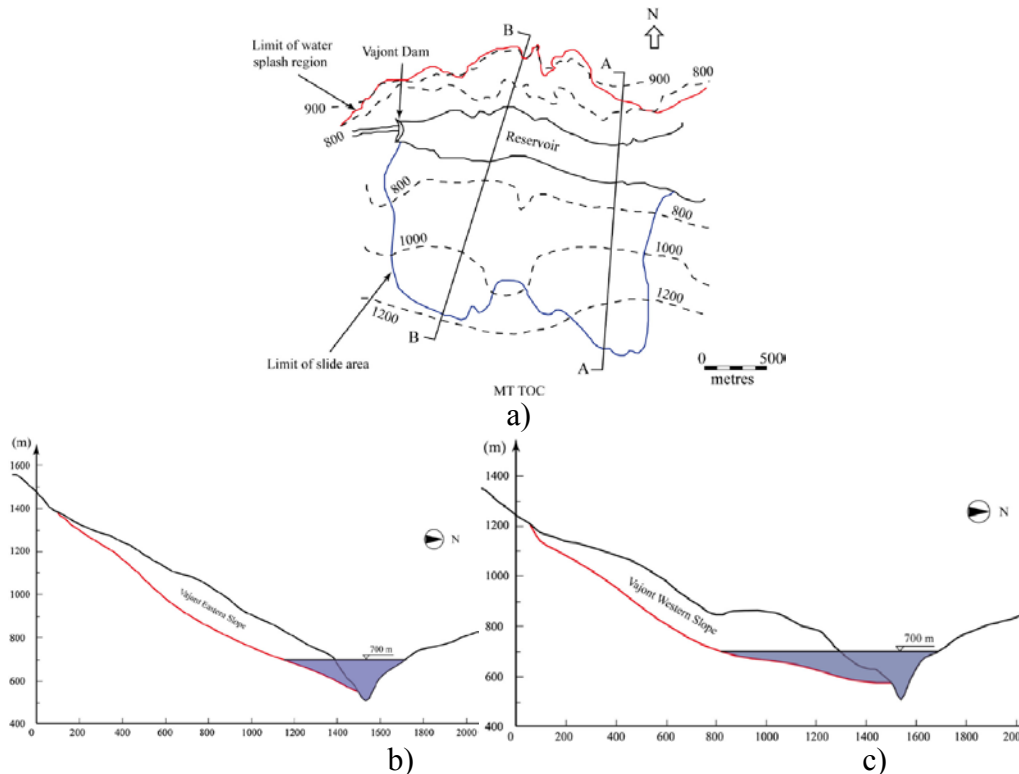


Fig. 2 a) Plan view of the Vajont rockslide with the straight lines indicating the cross sections A–A and B–B corresponding to the eastern and western slopes of the Vajont valley respectively; b) profile of the eastern slope; c) profile of the western slope. The water reservoir is in blue.

Figure 3 illustrates the evolution of slope deformation and the motion of water wave during the sliding of Vajont eastern slope (section A–A in Fig. 2b). The slope mass is initially coloured grey and green at different parallel layers, so that its deformation can be clearly identified during the rocksliding. It can be observed that at the beginning of the slide, the slope mass moves as a whole on the failure surface and quickly slides into the reservoir with a slight rotational component of motion, generating water waves. The water wave moves in the sliding direction and splashes onto the northern bank of the Vajont valley. Near the flow front, the CFD mesh

cells are filled with both water and air, thus, the colour representing the water phase is less intense.

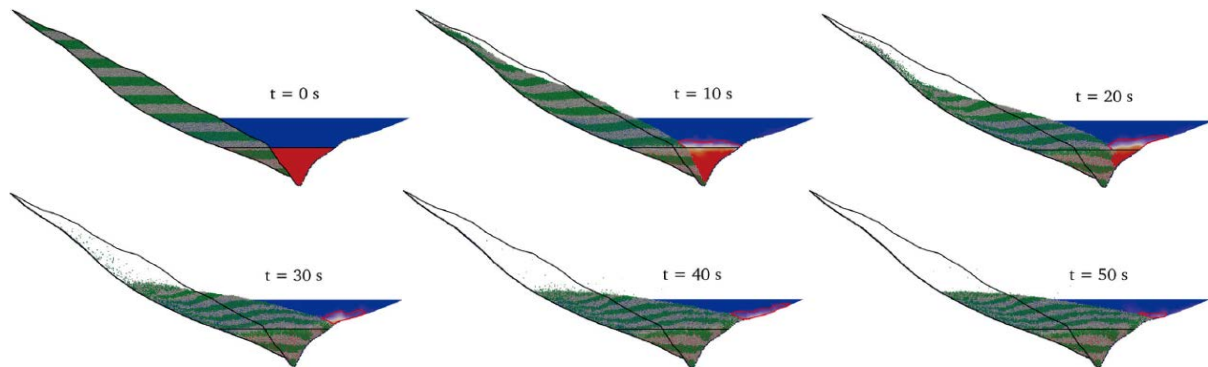


Fig. 3 Evolution of slope section A-A. The granular mass is initially coloured in horizontal stripes to follow the internal deformation. For the fluid domain, red and blue represent water and air respectively with the smear colour representing the air-water mixture. The splashed water wave is represented by regions enclosed by red curves.

CONCLUSIONS

The average slope velocity for the slopes and the corresponding water wave velocities together with the maximum height of the wave runup on the opposite valley flank for both slopes turn out to be in very close to the field observations at the same spots.

ACKNOWLEDGMENTS

This project has received funding from the European Union's Horizon 2020 research and innovation programme under the Marie Skłodowska-Curie grant agreement No 645665.

REFERENCES

- Semenza E, Ghirotti M (2000) History of the 1963 Vaiont slide: the importance of geological factors. *Bull Eng. Geol Env*, 59: 87-97.
- Chowdhury R (1978) Analysis of the Vajont slide—new approach. *Rock Mechanics* 11(1): 29–38.
- Sakai M, Takahashi H, Pain CC, Latham J-P, Xiang J (2012) Study on a large-scale discrete element model for fine particles in a fluidized bed. *Adv Powder Technol* 23(5): 673–681
- Abe S, Place D, Mora P (2004) A parallel implementation of the lattice solid model for the simulation of rock mechanics and earthquake dynamics. *Pure appl Geophys* 161(11–12):2265–2277.
- OpenCFD (2004) OpenFOAM—The open source CFD toolbox, <http://www.openfoam.com/>
- Chen F, Drumm EC, Guiochon G (2011) Coupled discrete element and finite volume solution of two classical soil mechanics problems. *Comput Geotech* 38(5): 638–647.
- Jiang MJ, Yu HS, Harris D (2005) A novel discrete model for granular material incorporating rolling resistance. *Comput Geotech* 32(5): 340–357.
- Kafui KD, Thornton C, Adams MJ (2002) Discrete particle- continuum fluid modelling of gas–solid fluidised beds. *Chem Eng Sci.*, 57(13):2395–2410
- Di Felice R (1994) The voidage function for fluid–particle interaction systems. *Int J Mult. Flow* 20(1): 153–159.
- Brown P, Lawler D (2003) Sphere drag and settling velocity revisited. *J Environ Eng* 129(3): 222–231.
- Brennen CE (2005) *Fundamentals of multiphase flow*. Cambridge University Press, Cambridge.
- Hirt CW, Nichols BD (1981) Volume of fluid (Vof) method for the dynamics of free boundaries. *J Comput Phys*, 39(1): 201–225.
- Zhao T., Houlsby GT, Utili S. (2014). Investigation of granular batch sedimentation via DEM-CFD coupling. *Granular matter*, 16(6): 921-932.
- Zhao T, Utili S, Crosta GB (2016) Rockslide and impulse wave modelling in the Vajont reservoir by DEM-CFD analyses. *Rock Mech Rock Eng* 49: 2437-2456.

THREE-DIMENSIONAL SIMULATION OF THE HONGSHIYAN LANDSLIDE WITH THE MATERIAL POINT METHOD

Xiaorong Xu^{*†}, Qicheng Sun^{*}, Feng Jin^{*}, Kenichi Soga[†]

^{*} State Key Laboratory of Hydrosience and Engineering, Tsinghua University, Beijing, China

[†] Department of Civil and Environmental Engineering, University of California, Berkeley, USA

In mountainous areas of Southwestern China, landslides often take place. They are highly dynamic accompanied with large deformation and are inherently difficult-to-predict due to complicated topography. In this study, a coupling approach of the material point method (MPM) and ArcGIS terrain data is developed for the three-dimensional modelling of landslides. MPM is a continuum-based particle method, which is convenient to implement various boundary conditions and constitutive laws. The real terrain data extracted and pre-processed from ArcGIS software are used to model the foundation boundary and the sliding body. The Hongshiyang landslide, which occurred in August, 2014 in Yunnan Province, China, was chosen for the simulation of its sliding process with the approach proposed in this work.

Keywords: landslide; material point method; ArcGIS; rheological relation

INTRODUCTION

Estimation of the initiation and runout process of a landslide is of great importance in the prevention of natural disasters and reduction of risks to local residents and infrastructures (Xu et al., 2016). Traditional geotechnical research of landslides focused on failure prediction and factor of safety based design, which have difficulties in describing the post-failure behaviors with large deformation (Soga et al., 2016). Considering that the discrete element method (DEM) has limitations to simulate large mass of soil and that the finite element method (FEM) has problems of mesh distortion, meshfree methods within the framework of continuum mechanics (e.g. smoothed particle hydrodynamics (SPH) and MPM) are now being the popular choice for large deformation problems. SPH is a fully Lagrangian method and is widely applied to flow-like landslides, but it exhibits spatial instabilities and consumes time to search for the neighbouring particles (Bandara and Soga, 2015). MPM is a hybrid Eulerian-Lagrangian approach. By incorporating advanced constitutive models of soil or granular materials, it can analyze landslides from the pre-failure stage with small strains to the post-rupture phase involving large deformation (Alonso et al., 2015). Recent works on MPM for slope stability problems include retrogressive and progressive slope failure, slope seismic response (Bhandari et al., 2016), slope failure with weak layers, rainfall-infiltration-induced landslides, interaction between the flow-like landslides and rigid structures and post-failure runout processes of the Wangjiayan landslide (Li et al., 2016). Most landslide simulations using meshfree methods are two-dimensional or depth-averaged, while there are still limited reported cases for modelling real three-dimensional landslides.

MPM can adopt complex boundaries with background mesh, and calculate arbitrary-shaped objects with material points discretization. ArcGIS is an efficient geography tool for spatial data management. Therefore, this paper reports the work of coupling MPM with ArcGIS terrain

data for modelling the three-dimensional movement of a landslide. The flow process of a landslide is often accompanied by a transitional behavior from solid-like to fluid-like states and this brings difficulties in proposing a unified phenomenological constitutive model. Recently two continuum constitutive models are developed for multi-states granular flows based on the MiDi rheological relations (Dunatunga and Kamrin, 2015, Fei et al., 2016). Although the performance of such models have been verified for simple cases, but they are yet to be applied to real landslide simulations.

This paper is organized as follows: the section of methodology presents the modelling scheme of MPM coupled with ArcGIS terrain data, and the constitutive law of multi-phase granular flows. A simulated example of the Hongshiyuan landslide is given in the result section. The findings from the work are summarized in the conclusion section.

METHODOLOGY

Disaggregated landslides can be deemed as granular flows composed of coarse individual particles. Within the continuum mechanics of MPM, they are treated as a continuum body, which is further divided into a set of material points (Fig.1(a1-a4)). Each material point (MP) storing all the physical variables of its representative area, such as mass and momentum, are linked to the background grid nodes (GN). A calculation cycle contains: (b1) mapping MP information to GN, (b2) solving momentum equations on GN and update their positions and kinetics, (b3) mapping updated information of GN back to MP, (b4) updating the positions and kinetics of MP, (b5) resetting deformed grids (Fig.1(b1-b5)). Particle domain of material points is in Lagrangian description allowing an arbitrary movement, while the grid view is in Eulerian description with background mesh actually keeping still after each step (Fig.1(c1-c4)).

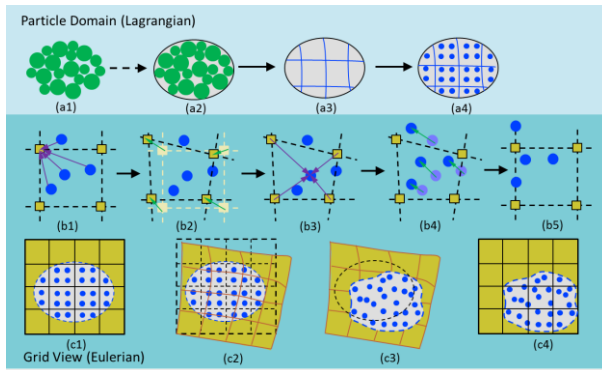


Fig.1 The calculation scheme of MPM

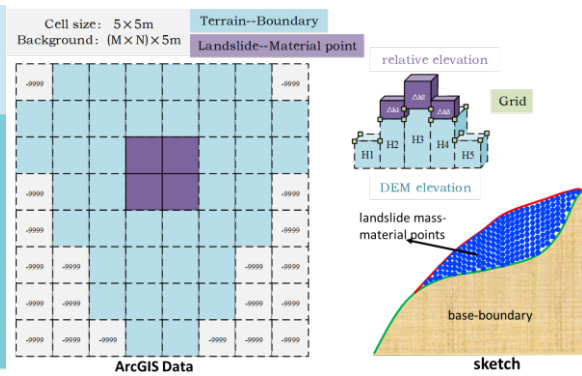


Fig.2 The coupling sketch of MPM and ArcGIS data

The motion of a material point is mainly governed by the balance of momentum

$$\rho \dot{\mathbf{v}} = \nabla \cdot \boldsymbol{\sigma} + \rho \mathbf{b} \quad (1)$$

where ρ is the density, $\dot{\mathbf{v}}$ is the acceleration vector, $\nabla \cdot \boldsymbol{\sigma}$ is the spatial gradient of stress tensor, and \mathbf{b} is the specific body force. With the shape function $N_{lp} = N_l(x_p)$ of grid node l on material point p , it is solved on the background mesh according to the Newton's second law

$$\dot{p}_{il}^n = f_{il}^{\text{int},n} + f_{il}^{\text{ext}} \quad p_{il}^{n+1} = p_{il}^n + (f_{il}^{\text{int},n} + f_{il}^{\text{ext},n}) \Delta t \quad (2)$$

where the the material point quantities (mass m , momentum p , internal force f_{il}^{int} and external force f_{il}^{ext}) are all mapped to the grid nodes

$$\begin{aligned} m_l^n &= \sum_{p=1}^{n_p} m_p N_{lp} & p_{il}^n &= \sum_{p=1}^{n_p} m_p v_i^n N_{lp} \\ f_{il}^{\text{int},n} &= -\sum_{p=1}^{n_p} N_{lp,j} \sigma_{ijp} m_p / \rho_p & f_{il}^{\text{ext},n} &= \sum_{p=1}^{n_p} m_p N_{lp} b_{ip} + \sum_{p=1}^{n_p} N_{lp} \tau_i dS \end{aligned} \quad (3)$$

The motion of grid nodes leads to the deformation of cells $\Delta\varepsilon_{pji}^{n+1}$, according to which the constitutive law of material is applied to update the stress of MP. In this paper, the total stress σ is divided into two terms, the rate-independent stress $\sigma^0(\varepsilon)$ and the rate-dependent kinetic stress $\sigma^k(\dot{\varepsilon})$. The former term is calculated by Drucker-Prager elastoplastic model, while the latter one by $\mu(I)$ rheological relation, which emphasizes the energy dissipation nature.

$$\sigma = \sigma^0(\varepsilon) + \sigma^k(\dot{\varepsilon}) \quad (4)$$

$$d\sigma_y^0 = C_{ijkl}(d\varepsilon_{kl} - d\varepsilon_{kl}^p) \quad \sigma_y^k = -aI^b \sigma_m^e D_{ij} \quad (5)$$

Here, C_{ijkl} is the elastic stiffness tensor, $d\varepsilon_{kl}$ is the total strain increment and $d\varepsilon_{kl}^p$ is the plastic component; $D_{ij} = \frac{\dot{\gamma}_{ij} - \delta_{ij}\dot{\gamma}_{kk}/3}{\sqrt{\dot{\gamma}_{ij}\dot{\gamma}_{ji}/2}}$, $\dot{\gamma}_{ij} = d\varepsilon_{ij}/dt$ is the shear rate; $I = \frac{\dot{\gamma}d}{\sqrt{\sigma_m^e/\rho}}$ is the inertial number, $\dot{\gamma} = \sqrt{\dot{\gamma}_{ij}\dot{\gamma}_{ji}/2}$, σ_m^e is the spheric stress; a and b are experimental parameters of material properties (Dunatunga and Kamrin, 2015, Fei et al., 2016).

As shown in Fig.2, the ArcGIS terrain data downloaded from Geospatial Data Clouds are preprocessed in a format of $M \times N$ square rasters and interpolated into higher resolutions. Where there is no terrain, a null value of -9999 is set. Each raster carries its DEM (digital elevation model) elevation, which can be divided into the height of foundation boundary $H_i (i=1,2,...)$ and the relative elevation $\Delta H_i (i=1,2,...)$ of the sliding body. To import the special data into MPM, we use a cubic cell of eight nodes in a Cartesian background mesh. The shape function can be written as $N_{lp} = (1 + \xi\xi_l)(1 + \eta\eta_l)(1 + \zeta\zeta_l)/8$. The sliding mass of landslide is discretized into material points carrying the position and mass of its representative area. The base boundary is fixed with zero displacement on the grid nodes. Before the runout process, the initial stress is generated using gravity loading by increasing the strength of the sliding body in an elastic constitutive model.

RESULTS

The Hongshiyuan landslide was triggered by the Ludian earthquake, which took place in Yunnan province, China on August 3, 2014. The avalanche body of about 17.0 million m^3 in volume rushed into the Niulan River and formed a dammed lake. The before- and after-earthquake topography data were obtained from on-site geological survey. We chose an area of $x \times y = 1800 \times 1320m$ as the computational domain with the elevation $z = 1000-2000m$.

Firstly, a validation case of granular column collapse was conducted in comparison with the experimental results (Xu et al., 2016) and it exhibited a good match. Then the numerical model of the Hongshiyuan landslide was constructed three-dimensionally with 5m resolution. The size of the background cell was 5m and the cell contained four material points initially. The time step was automatically calculated as $\Delta t \approx 4.5 \times 10^{-4}s$, and the total calculation time was 100s. The material parameters of $E = 10MPa$, $\nu = 0.4$, $\rho = 1700kg/m^3$, $\varphi = 26^\circ$, $c = 0kPa$ were the young modulus, the poisson's ratio, the absolute density, the friction angle and the cohesion coefficient, respectively. In Eq. (5), the $\mu(I)$ rheological parameters of $a = 25$ and $b = 1.0$ were estimated from the maximum speed of granular flows along the inclined slope.

Figure 3 shows the deposit thickness of material points above the initial foundation boundary during the dynamic movement of the Hongshiyuan landslide. The simulation was activated at $t = 0s$ by gravity driving. The weak soil then began to slide down the slope in an inclination angle of approximate 45° , with the velocity increasing rapidly. The avalanche body was disaggregated and collapsed to rush into the Niulan river. During the conversion of gravitational potential energy to kinetic energy, the front of the sliding body reached a

maximum velocity of about 60m/s at $t = 30s$. After that, the velocity began to decrease and the deposit became larger and larger. At about $t = 50s$ the thickness of the deposit peak reached the maximum of 120m, but the soil on the two sides was still creeping along the horizontal channel balanced by the force of friction and the moment of inertia. The simulation lasted about 80s and the final configuration of deposit is shown in Fig. 3, which is very close to the realistic result.

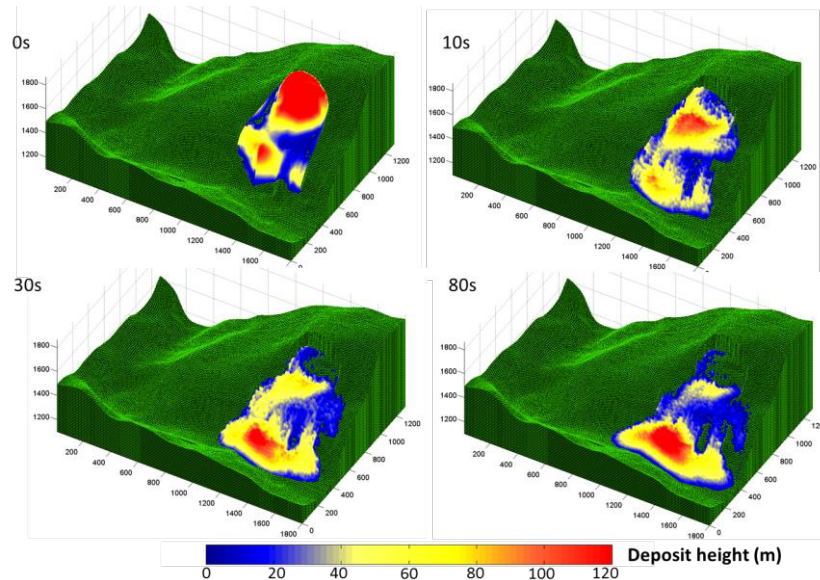


Fig.3 MPM simulation results of Hongshiyuan landslide in Yunnan, China

CONCLUSION

This work reports a three-dimensional modelling scheme for landslides. MPM is a suitable continuum method for large deformation problems, and is convenient to implement the boundary conditions of complicated topography. ArcGIS terrain data is pre-processed and used to model the foundation boundary and the avalanche body. Meanwhile by adopting $\mu(I)$ rheological relation, the developed approach shows great potentials to study the mechanics of multiple mechanical phases of disaggregated landslides.

REFERENCES

- Alonso EE, Yerro A & Pinyol NM (2015) Recent developments of the Material Point Method for the simulation of landslides. *IOP Conference Series: Earth and Environmental Science* 26, 012003.
- Bandara S & Soga K (2015) Coupling of soil deformation and pore fluid flow using material point method. *Computers and Geotechnics* 63, 199-214.
- Bhandari T, Hamad F, Moormann C, Sharma KG & Westrich B (2016) Numerical modelling of seismic slope failure using MPM. *Computers and Geotechnics* 75, 126-134.
- Dunatunga S & Kamrin K (2015) Continuum modeling and simulation of granular flows through their many phases. *J. Fluid Mech* 779, 483-513.
- Fei ML, Sun QC, Xu XR, Jin F & Zhou GGD (2016) Simulations of multi-states properties of granular materials based on non-linear granular elasticity and the MiDi rheological relation. *Powder Technology* 301, 1092-1102.
- Li XP, Wu Y, He SM & Su LJ (2016) Application of the material point method to simulate the post-failure runoff processes of the Wangjiayan landslide. *Engineering Geology* 212, 1-9.
- Soga K, Alonso EE, Yerro A, Kumar K & Bandara S (2016) Trends in large-deformation analysis of landslide mass movements with particular emphasis on the material point method. *Géotechnique* 66, 248-273.
- Xu XR, Sun QC, Jin F & Chen YP (2016) Measurements of velocity and pressure of a collapsing granular pile. *Powder Technology* 303, 147-155.

RUNOUT EVALUATION OF THE OSO LANDSLIDE WITH THE MATERIAL POINT METHOD

A. Yerro*, K. Soga[†], J. Bray[†]

* Univ. of Cambridge, Department of Engineering, Cambridge, UK

[†] Univ. of California, Berkeley, Department of Civil & Environ. Engineering, Berkeley, USA

Landslides can cause significant damages around the world and represent one of the most important problems in geotechnical engineering. Understanding the mechanics of the slope deformation process is of particular importance for risk assessment and is challenging due to its complexities. This work examines the Oso Landslide, which occurred in the State of Washington, USA on 22 March 2014. The Oso Landslide is one of the worst landslide disasters in the history of USA with 43 fatalities. It appeared in multiple failure stages, travelled nearly 1 km over the floodplain involving several failure surfaces and significant soil softening. Despite it took place after a period of abnormal wet weather, real causes inducing the triggering are still under investigation. The material point method (MPM) is presented as a numerical tool capable of analysing this complex problem. The runout of the Oso Landslide is simulated, and several hypothetical scenarios are investigated.

Keywords: landslide, runout, material point method

INTRODUCTION

The Oso Landslide occurred on 22 March 2014, Washington, USA. Almost 8 millions of m³ of mud and debris flow travelled approximately 1 km and spread out all over the valley of North Fork of the Stillaguamish River covering a small neighbourhood. Although it occurred on a sunny day, the event was preceded by a three-week period of wet weather. With 43 casualties, this is one of the worst landslide catastrophes in US history. Before 2014, smaller parts of the same slope had failed on several occasions. Those movements showed a retrogressive behaviour although none of them exhibited extremely long runouts. The most recent landslide was in 2006, known as “Hazel Landslide”, which partially blocked the river located at the toe of the slope with debris material.

Field observations taken immediately after the Oso Landslide by the US National Science Foundation (NSF)-sponsored Geotechnical Extreme Events Reconnaissance (GEER) Association team (Keaton et al., 2014) support that the main event occurred essentially in two primary stages. Later in-depth studies by Pyles et al. (2016) shed additional insights. Stage 1 was interpreted as the remobilisation of the previous Hazel Landslide (referred in Fig. 1a as M1 and Debris mass units) and part of the mid-slope bench (M2 mass unit), which slid over an ancient failure surface. This material mobilised as a debris flow travelled rapidly across the valley causing most of the destruction. In Stage 2, a new rotational failure occurred forming a large scarp 90 m horizontally deeper in the slope. This second landslide (M3 mass unit) collided with the first one before coming to rest. The interpretations of seismic signals (Hibert et al., 2014;

Iverson et al., 2015) exhibit that the estimated duration of the main event was nearly 100 s and the peak velocity was 19 m/s.

Although primary causes of the Oso Landslide are still unclear, there are several hypotheses that could explain the long runout of the materials mobilized in Stage 1 (Keaton et al., 2014). These are a) the static liquefaction of the Debris deposits at the toe of the slope, b) the decrease of debris material strength due to the mixing with river water, and c) the fact that the mobilized materials in this case were higher on the slope, among others. The objectives of this work are to ascertain if the MPM can capture the runout distance travelled by the Oso Landslide, to investigate the effect of Stage 2 on the final runout, and to evaluate if liquefaction/softening of the 2006 Debris field and fluidization due to mixing with the river water significantly affected the behaviour of the landslide

METHODOLOGY

The MPM is a particle-based continuum method that was developed to simulate large deformations in history-dependent materials (Sulsky et al. 1994). It combines the advantages of Eulerian (i.e., fixed finite element grid) and Lagrangian (i.e., moving material points) approaches. Each material point represents and moves attached to a portion of the material while main governing equations are solved at a computational fixed mesh. Thus, mesh distortion problems, which are typically a major shortcoming in the use of conventional finite element methods, are eliminated. During the last decade, MPM has been used to analyse a number of landslides and slopes (Andersen & Andersen, 2010; Yerro et al., 2015; Soga et al., 2015; Yerro et al., 2016).

In this study, a series of plane strain analyses of a centred representative section is conducted using *Anura3D* (MPM software developed by the MPM Research Community). The advantages of performing plane strain analysis is that the computational cost is much lower than in 3D simulations. In this way, parametric analysis can be performed efficiently to gain a better understanding of the behaviour of the landslides.

NUMERICAL MODEL

The computational mesh of the plane strain Oso Landslide model is formed by linear tetrahedral elements. The thickness is one element and out-of-plane deformation is restricted to ensure plane strain conditions. The mesh is refined in the region where the mobilized mass will move to optimize the computational time and to obtain more accurate results. The minimum edge of the elements is 3 m. Initially, four material points are distributed within each element. Figure 1a shows the slope and material units.

The topography of the site is based on Lidar data sets of before and after failure. The stratigraphy (Fig. 1a), the surfaces of rupture geometry, and the engineering properties of materials involved in the landslide are estimated based on field and laboratory data (Rogers et al., 2016; Pyles et al., 2016). M1 and M2 are placed above the ancient landslide slip-surface identified during site investigation. M1 moved during the previous landslide that occurred in 2006, whereas M2 did not. M3 is placed above the new slip-line generated by the Oso Landslide,

which was determined from the site investigation and separate slope stability analysis. Undrained total stress analysis is performed, because the runout of the Oso Landslide occurred rapidly, and the constitutive model considered for all materials is the Tresca model.

The stresses are initialized under the condition of elastic gravity loading and the instability is triggered in two stages. In Stage 1, the undrained shear strength (c_u) of M1, M2 is set to 50 kPa, Debris is assumed liquefied ($c_u=2$ kPa), and the stability of M3 is maintained ($c_u=500$ kPa). After 25 seconds, Stage 2 is initiated by setting c_u of M3 equal to 250 kPa. The fluidisation effect of M1 and M2 due to the water supply from the river is considered by reducing their c_u to 5 and 10 kPa respectively when the material moves beyond the river location (indicated in Fig. 1b). The saturated unit weight of M1, M2, and Debris materials is 18.05 kN/m^3 , whereas that of M3 is 19.62 kN/m^3 . The model is designed so that the mobilised material can slide over a fixed predefined contact surface that is divided into different sections to simulate changes in lithology and surface type. Different undrained shear strengths are assigned to each section.

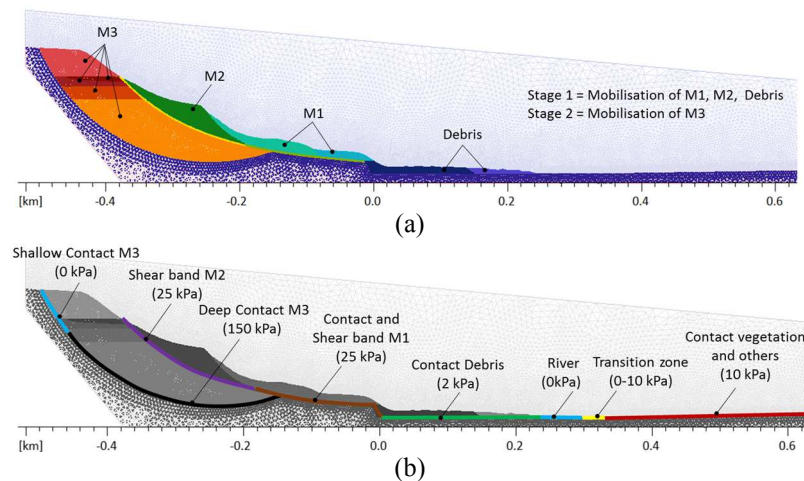


Fig. 1. Oso Landslide model. (a) Initial location of M1, M2, M3 and debris material. (b) Zones of the contact surface and shear bands with corresponding strengths.

RESULTS

Figure 2 shows the runout behaviour at different times of the Oso Landslide model. It can be seen that the leading edge of the landslide crosses the North Fork of the Stillaguamish River before Stage 2 is initiated ($t=25$ s). M1 and part of M2 move on top of the softened Debris unit and travel rapidly across the floodplain. After Stage 2 initiation, M1 and M2 are pushed by M3 and the runout distances increase. Finally, the computed runout distances of the different material units are similar to those observed in the field (indicated in Fig. 2, $t=100$ s). The duration of the whole event also coincides with interpretations of seismic records.

In addition, a parametric analysis was performed, and the following findings were observed: a) if the fluidisation effect from the river water to M1 and M2 is not considered (keeping the rest of the parameters the same) the final runout is similar; b) if the Debris material is not liquefied ($c_u=50$ kPa) but the fluidisation effect is considered, the final runout decreases slightly; c) if neither liquefaction nor fluidisation effects are considered, the runout is reduced considerably; and d) if M3 remains stable the movement of M2 is considerably more limited and final runout decreases slightly. In all cases, the leading edge of the landslide extends beyond the North Fork of the Stillaguamish River.

CONCLUSION

The MPM has been able to capture the general characteristics of the Oso Landslide. The combination effect of liquefaction of the Debris material and the decrease of strength due to the contribution of river water seem to play a key role in the large runout of the Oso Landslide.

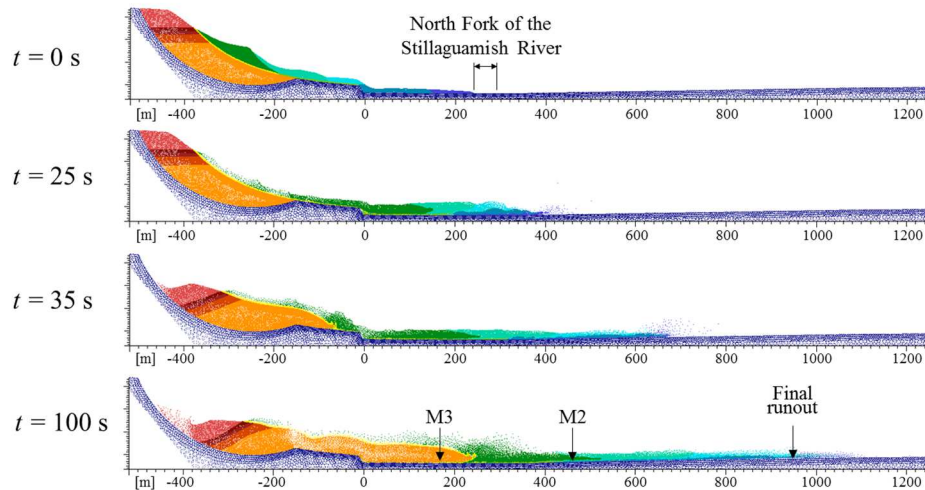


Fig. 2. MPM results of the Oso Landslide model at different moments of the simulation. The location of the North Fork of the Stillaguamish River and runouts of different units observed in the field are indicated.

ACKNOWLEDGEMENTS

This work was part of the effort by the State of Washington SR-530 landslide expert team. The critical contributions of Marv Pyles, David Rogers, Arne Skaugset, Rune Storesund, and Gunnar Schlieder are greatly acknowledged. We also appreciate the State of Washington support.

REFERENCES

- Andersen S & Andersen L (2010) Modelling of landslides with the material-point method. *Computational Geosciences* 14(1), 137–147.
- Hibert C, Stark CP & Ekström G (2014) Seismology of the Oso-Steelhead landslide. *Natural Hazards and Earth System Sciences. Discussions* 2, 7309–7327.
- Iverson RM, George DL, Allstadt K, Reid M E, Collins BD, Vallance JW & Bower JB (2015) Landslide mobility and hazards: Implications of the 2014 Oso disaster. *Earth and Planetary Science Letters* 412, 197–208.
- Keaton JR, Wartman J, Anderson S, Benoît J, DeLaChapelle J, Gilbert R & Montgomery DR (2014) The 22 March 2014 Oso Landslide, Snohomish County, Washington. *Turning Disaster into Knowledge. Geotechnical Extreme Events Reconnaissance*.
- Pyles MR, Rogers JD, Bray JD, Skaugset A, Storesund R & Schlieder G (2016) *Expert opinion report, Superior Court of Washington for King County. Case No. 14-2-18401-8 SEA, June 30*.
- Rogers JD, Pyles MR, Bray JD, Skaugset A, Storesund R & Schlieder G (2016) *Interim Expert Report, Superior Court of Washington for King County, No. 14-2-18401-8 SEA, January 22*.
- Soga K, Alonso E, Yerro A, Kumar K & Bandara S (2015) Trends in large-deformation analysis of landslide mass movements with particular emphasis on the material point method. *Géotechnique* 66(3), 248–273.
- Sulsky D, Chen Z & Schreyer HL (1994) A particle method for history-dependent materials. *Computer Methods in Applied Mechanics and Engineering* 118(1–2), 179–196.
- Yerro A, Alonso EE & Pinyol NM (2016) Run-out of landslides in brittle soils. *Computers and Geotechnics* 80 December 2016, 427–439.
- Yerro A, Alonso E & Pinyol N (2015) The material point method for unsaturated soils. *Géotechnique*, 65(3), 201–217.

JTC1 Workshop 2017

24 May 2017, Barcelona, Spain

FIELD TRIP PROGRAMME

VALLCEBRE LANDSLIDE



FIELD TRIP TO THE VALLCEBRE LANDSLIDE. EXPERIENCES ON LONG TERM MONITORING OF A SLOW-MOVING SLIDE. May 24th, 2017

Josep A. Gili and José Moya

Div. Geotechnical Engineering and Geosciences.
Dpt. Civil and Environmental Engineering
Universitat Politècnica de Catalunya, BarcelonaTech

In active landslides, the prediction of acceleration of movement is a crucial issue for the design and performance of warning systems. The Vallcebre landslide is a large ($> 20 \text{ Mm}^3$) slow-moving translational slide, located in the Pyrenees 150 km north of Barcelona. The overall geometry and geology of the slope is rather simple and the catchment basin is small. A few farm houses are located on the slide; however, the natural environmental conditions have been not modified by stabilization works. Due to this set of characteristics, Vallcebre landslide is regarded as a natural laboratory, in which the landslide behaviour has been investigated under a wide range of environmental conditions for the last 20 years.

Since 1996 several borehole drilling campaigns were carried out to assess properties of the landslide materials and the landslide geometry, and to monitor the movement of the slope and groundwater in a regular basis. The monitoring network consists of 14 piezometers, 8 inclinometers, 8 in-hole wire extensometers, 17 high-precision differential GPS targets, and temporally 14 InSAR satellite and terrestrial reflectors. Using complimentary techniques in the network allowed monitoring the landslide in a distributed way (DGPS and InSAR) in monthly to annual campaigns and also in continuous mode (every 20 minutes in wire extensometers and piezometers). The system remains partially operational nowadays after more than 20 years of operation.

The landslide has an almost immediate response to rainfall episodes and groundwater changes, due to the presence of preferential drainage ways. High-frequency displacement data revealed the presence of non-frictional (viscous) forces resisting the movement. On the other hand, the landslide foot dips upslope and acts as a buttress that opposes to the movement. Landslide displacements and velocities have been modelled considering both a viscous term and the stabilizing effect of the foot.

The field-trip will focus on the landslide geology and geomorphology and on the monitoring system. The experiences gained and lessons learned along 20 years of observations will be described and discussed in-situ at several key points of the landslide.

References

- Corominas, J., Moya, J., Lloret, A., Gili, J.A., Angeli, M.G., Pasuto, A., Silvano, S. (2000) Measurement of landslide displacements using a wire extensometer. *Engineering Geology* 55, 149-166.
- Corominas, J., Moya, J., Ledesma, A., Lloret, A., Gili, J.A. (2005) Prediction of ground displacements and velocities from groundwater level changes at the Vallcebre landslide (Eastern Pyrenees, Spain). *Landslides* 2, 83-96.

- Crosetto, M., Gili, J.A., Monserrat, O., Cuevas-González, M., Corominas, J., Serral, D. (2013) Interferometric SAR monitoring of the Vallcebre landslide (Spain) using corner reflectors. *Natural Hazards and Earth System Science* 13, 923-933.
- Ferrari, A., Ledesma, A., González, D.A., Corominas, J. (2011) Effects of the foot evolution on the behaviour of slow-moving landslides. *Engineering Geology* 117, 217-228.
- Gili, J.A., Corominas, J., Rius, J. (2000) Using Global Positioning System Techniques in landslide monitoring. *Engineering Geology* 55, 167-192.
- Gili, J.A., Moya, J., Corominas, J., Crosetto, M., Monserrat, O., Luzi, G. (2016) Twenty-five years of Vallcebre landslide monitoring: from theodolite to Radar. 1st IMEKO TC-4 International Workshop on Metrology for Geotechnics. Benevento, Italy, March 17-18, 2016
- Monserrat, O., Moya, J., Luzi, G., Crosetto, M., Gili, J.A., Corominas, J. (2013) Non-interferometric GB-SAR measurement: application to the Vallcebre landslide (eastern Pyrenees, Spain). *Natural Hazards and Earth System Science* 13, 1873-1877.
- Moya, J., Corominas, J., Gili, J.A., Ledesma, A., Lloret A. (2017) Twenty years of continuous monitoring of the Vallcebre landslide (eastern Pyrenees): lessons learned. JTC1 Workshop on Advances in Landslide Understanding. May 24-26, 2017, Barcelona, Spain.

Field trip schedule: from 8:00 a.m. to 6:00 p.m.

Meeting point (at 8:00 a.m.):

Western corner of the Campus Nord of UPC.

The bus will be waiting for us at the junction of "Sor Eulàlia d'Anzizu street" and "Gran Capità street"

(<https://goo.gl/maps/8begWcc14DE2>)

Approximate schedule:

08:15-10:00: Bus approach to Vallcebre.

10:00-11:00: Landslide explanation from the mirador (scenic view).

11:00-11:15: The bus will drop us at the Landslide toe.

11:15-13:30: Hike across the landslide. Explanations about the monitoring techniques in use.

13:30-14:00: Walk until the "Camping El Berguedà" where the bus will collect us.

14:00-14:15: Bus to the Restaurant.

14:15-16:15: Lunch (*).

16:15-18:00: Travel back to Barcelona.

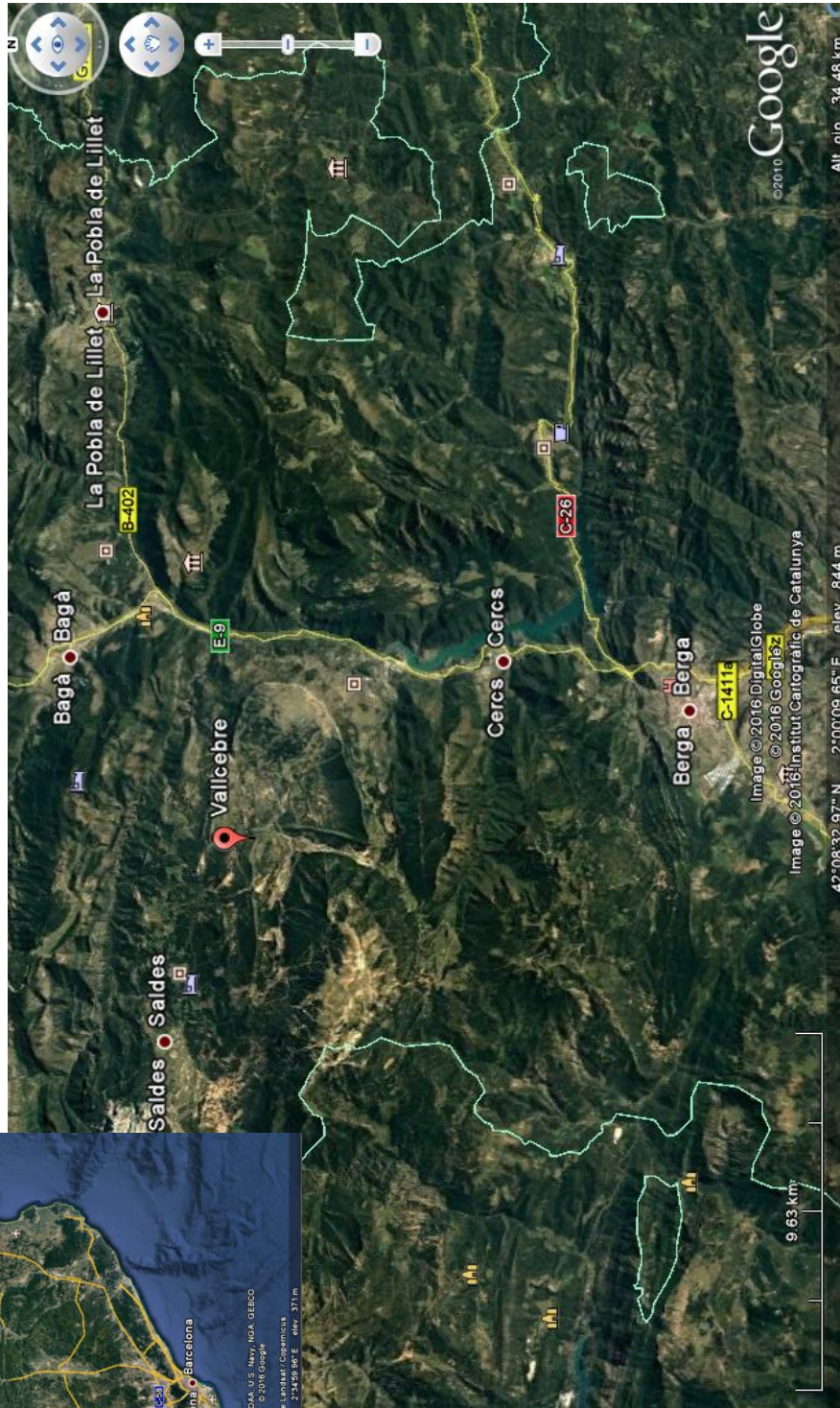
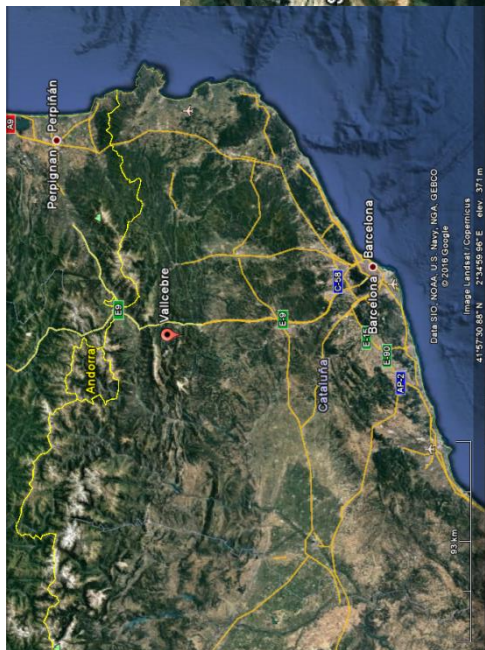
*: The lunch is included in the workshop fee, it will be provided in a typical catalan restaurant, the Hostal Pedraforca (Saldes), near the landslide.

After the lunch, we will travel back to Barcelona, where it is planned to arrive around 6 p.m. (same place as the meeting point).

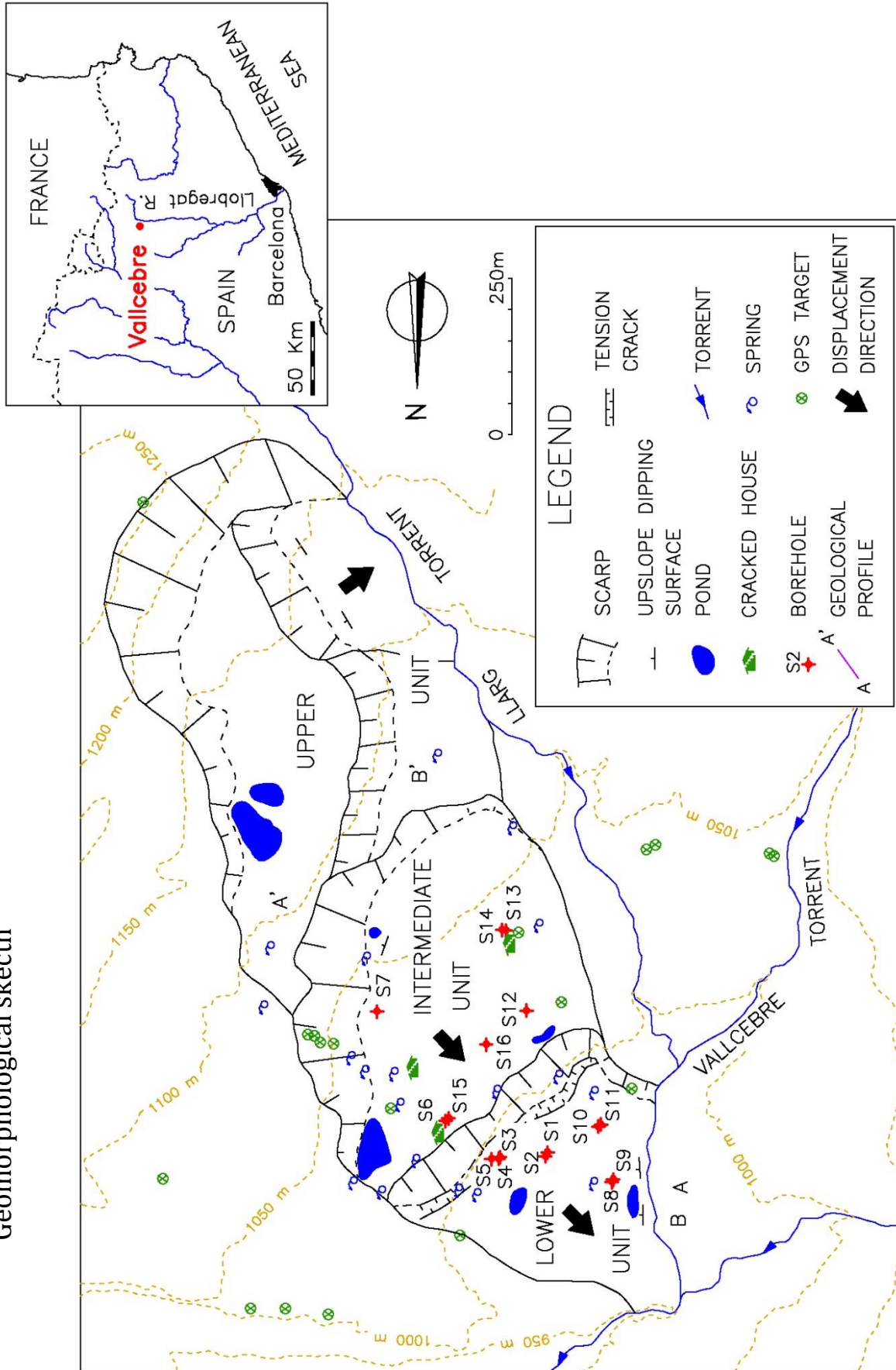
Other remarks:

- Please, wear shoes suitable for walking in the field. We will have a light hike across the landslide, but the ground is uneven, sometimes wet. Sneakers are enough, but bring your boots if you have it at hand.
- Hopping the best, prepared for the worst: The weather forecast for Wednesday is good by now. We expect a bright, sunny day. Bring protection against solar burning (UVA sunscreen and/or a cup). Some water will be also welcomed. Although the forecast is good, we cannot discard some showers, we will be in the Pyrenees mountains! Take your umbrella or anorak just in case...

Location map

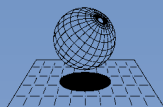


Geomorphological sketch



INDEX OF AUTHORS

Alberruche, M.E.	85	Navarro, V.	81
Alonso, E.E.	52	Ng, C.W.W.	13
Alvarado, M.	52, 122	Nicotera, M.	44
Arranz, J.C.	85	Oorthuis, R.	105
Arroyo, M.	118	Pagano, L.	24, 60
Asensio, L.	81	Pastor, M.	40
Balzano, B.	44	Pinyol, J.	109
Bray, J.	149	Pinyol, N.M.	52, 122
Caicedo, B.	122	Pirulli, M.	56
Calvello, M.	28	Puzrin, A.M.	21
Capa, V.	138	Rahardjo, H.	64, 113
Choi, C.E.	13	Raventós, J.	118
Choudhari, N.	77	Reder, A.	24, 60
Comegna, L.	60	Rianna, G.	24, 60
Corominas, J.	101	Rodríguez, R.	85
Dalvi, R.S.	77	Rodríguez, V.	85
Damiano, E.	9	Ruiz, A.	122
De Falco, M.	44	Ruiz, D.	48
De la Morena, G.	81	Saaltink, M.	48
Demers, D.	97	Samat, S.	48
Fernández, F.J.	85	Santo, A.	44
Forte, G.	44	Sarro, R.	85
Futai, M.M.	32	Satyanaga, A.	64, 113
Garzón, J.	138	Sikora, R.	126
Gili, J.A.	101	Soga, K.	145, 149
González, M.	109	Song, D.	13
Goto, S.	89	Stickle, M.	40
Gunji, K.	134	Strom, A.L.	130
Hamrouni, F.	93	Sun, Q.C.	145
Herrera, G.	85	Take, W.A.	69
Hürlimann, M.	105	Tarantino, A.	44
Istiyanti, M.L.	89	Torrijo, F.J.	138
Jamei, M.	93	Towhata, I.	134
Jin, F.	145	Trabelsi, H.	93
Kwan, J.S.H.	36	Utili, S.	141
Ledesma, A.	101	Vadillo, L.	85
Leroueil, S.	97	Vaunat, J.	48, 105
Lloret, A.	101	Virely, D.	48
Locat, A.	97	Wang, G.	73
Manzanal, D.G.	40	Xu, X.R.	145
Mateos, R.M.	85	Yague, A.	40
Moya, J.	101, 105	Yerro, A.	149
Moysset, M.	109	Zhao, T.	141
Mulligan, R.P.	69		



CIMNE

International Center
for Numerical Methods in Engineering